Charged Particle Interactions with Matter

7

Abstract In nuclear medicine, moving charged particles are released in tissue through either the radioactive decay processes of Chap. 4 or as a result of the photon–matter interactions of Chap. 6. Being charged, these particles interact significantly with the medium, transferring their kinetic energy resulting in an absorbed dose to the medium as they slow down to thermal energies. Hence, the study of charged particle interactions with matter is the fundamental core of ionizing radiation dosimetry. In this chapter, the two mechanisms of energy loss are presented. Collision energy losses between the particle and atomic electrons are derived through the Bohr classical and the Bethe quantum-mechanical means; hard collisions losses are derived independently from various quantum-mechanical results. Radiative energy losses resulting from *bremsstrahlung* are initially derived from classical theory which then progresses to the Bethe–Heitler quantum-mechanical theory. The polarization effects of a charged particle upon the medium will limit the collision energy losses and are derived. As energy loss is inherently stochastic, energy straggling models are also presented. In particular, the Vavilov theory of energy straggling is derived as are the Gaussian and Landau results which are treated limiting conditions to that theory. Multiple scatter strongly affects electrons and positrons and the Fermi–Eyges theory is derived as a means of justifying the Gaussian model. The Goudsmit–Saunderson and Moliére theories of multiple scattering are derived. Finally, the mechanisms through which a positron can annihilate on an electron are derived.

Contents

B.J. McParland, *Nuclear Medicine Radiation Dosimetry*,
DOI 10.1007/978-1-84882-126-2_7, © Springer-Verlag London Limited 2010

7.1 Introduction

It has been shown in Chaps. 4 and 6 that moving charged particles are products of radioactive decay and photon scattering. ^{4}He nuclei are emitted in α decay, moving electrons or positrons are created in β-decay and atomic electrons are ejected into the medium through internal conversion or atomic relaxation processes. Compton scatter sets electrons into motion and atomic electrons are ejected following photoelectron absorption. These moving charged particles slow down by transferring energy to the medium and, as this is the cause of the absorbed dose to tissue, charged particle–matter interactions with matter will be extensively reviewed.

Charged particles interact with the atoms in the medium they are traversing through the Coulomb component of the Lorentz force, $q(\mathbf{E} + \mathbf{v} \times \mathbf{B})$, by either transferring energy to (predominantly) the atomic electrons or else by being scattered by the nuclear and atomic electron Coulomb fields. These processes have markedly different consequences. In the former, a significant fraction of kinetic energy can be transferred to the atomic electron with, should the incident particle have a mass m much greater than that of the electron, negligible effect upon the projectile's trajectory. If the projectile is an electron or positron, the large mass differential between it and the nucleus can result in a significant deflection from its trajectory by the nuclear Coulomb field resulting in the emission of electromagnetic energy known as *bremsstrahlung* (braking radiation).

There are two fundamental differences between how photons and charged particles interact with matter that should be kept in mind. Being a boson, the photon interacts with matter through either direct absorption by a charged particle or through second-order effects such as Compton scatter. On the other hand, a charged particle will interact with other charged particles at extended distances through its surrounding Coulomb field (or, in another picture, the exchange of photons) resulting in the gradual transfer of energy to the medium and the eventual stopping of the particle. Thus, the cross section of the electromagnetic interaction between a charged particle and matter will be much greater than that for photons. This difference is made clearly evident by comparing the 10 cm mean free path of a 1 MeV photon in water with the few millimeter range of a 1 MeV electron in water.[1] The second fundamental difference between how photons and charged particles interact with matter is that, as a photon loses energy, its wavelength will increase and its frequency decrease but its speed remains constant.[2] Because a charged particle has mass, its speed is diminished through each instance of energy exchange to the medium until it reaches energies below the minimum ionization level and thus attains thermal equilibrium with the medium (although if the charged particle is a positron, it can annihilate with an electron either in-flight or once having been thermalized). Thus, unlike a photon, a charged particle will have a finite range.

[1] The photon mean free path is the reciprocal of the linear attenuation coefficient. The exact range of an electron in a medium is more difficult to define as, due to multiple scatter, its path will be tortuous.

[2] Assuming a constancy of photon speed ignores the frequency dependence of the medium's index of refraction. Such an effect, however, is negligible for photons with sufficient energy to ionize.

Should the charged particle be hadronic, additional energy loss channels become available as a result of the strong nuclear interaction between the projectile and the atomic nucleus. These include absorption, nuclear excitation, and even fragmentation of either the projectile or target nucleus. As previously discussed, the only hadron used in nuclear medicine is the α particle in therapy. α particles emitted in radioactive decay have kinetic energies of only a few MeV with the result that the α particle's penetration into tissue is small and its kinetic energy will be transferred to a very small volume leading to a high absorbed dose. The low kinetic energy will also mean that it is highly unlikely for the α particle to penetrate the nuclear Coulomb barrier in order to reach the ~1 fm separation from the nucleus in order to interact via the strong nuclear force and open up any nuclear energy loss channels.[3] Because there is no interest in nuclear interactions in clinical nuclear medicine, these will be neglected.

The mechanisms through which a moving charged particle loses energy in a medium through collisions can be broadly characterized in terms of the impact parameter, b, which is the perpendicular distance between the projectile's trajectory and a scattering center, such as an atom, as shown in Fig. 7.1 (in Bethe's theory, this categorization is in terms of the momentum transfer q which is approximately related to the impact parameter via $b \approx \hbar c/q$). For large impact parameters (i.e., b much greater than the atomic radius), the incident particle will interact with the atom as whole. The atom can be temporarily polarized (i.e., the electron cloud displaced from its equilibrium position) or atomic electrons excited into empty quantum states or, infrequently, into the continuum. As only small amounts of energy are transferred to the atom in such an encounter, it is described as a soft collision.

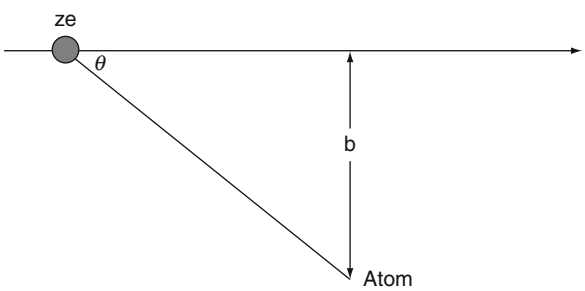

Fig. 7.1 Definition of the impact parameter b during an interaction between a passing charged particle and an atom

If b is comparable to atomic dimensions, the particle will interact with a single atomic electron rather than the entire ensemble. This knock on or hard collision can result in the transfer of substantial energy to the atomic electron which can be ejected, leading to the atom's ionization and subsequent relaxation processes. The ejected electron, also referred to as a δ ray, is capable of carrying energy a considerable distance away from the event site, a feature of considerable practical importance in dosimetry calculations. As the energy transfer in this collision type is high, the interaction can be well-approximated using the assumption that the atomic electron is unbound. Because it is more likely that a given charged particle will be at an extended distance from a given atom rather than in close proximity to it, the probability of a soft collision occurring is high and that of a hard collision will be much lower. However, the net energy transfers due to soft and hard collisions are roughly equal in that the cumulative energy transferred through high-probability low energy transfers is approximately equal to that for low-probability high-energy transfers.

If the impact parameter b is much smaller than atomic dimensions, the particle interacts with the nucleus rather than the atomic electrons. A light incident particle, such as an electron or positron, can be deflected violently from its trajectory by the nuclear Coulomb field. An accelerated electric charge will emit electromagnetic radiation. This radiation is known as *bremsstrahlung* with the kinetic energy lost by the projectile carried away by the photon (assuming negligible nuclear recoil). The *bremsstrahlung* energy spectrum is continuous and decreases with increasing photon energy, thus reflecting the higher probability of small deflections and a greater production yield of low energy (or "soft") photons. The maximum *bremsstrahlung* photon energy in the spectrum equals the kinetic energy of the incident charged particle and is the result of the stopping of the particle and the complete conversion of its kinetic energy to radiation (assuming, again, zero nuclear recoil).

An obvious metric of interest in describing the energy loss of a moving charged particle is the rate,

[3]Although it is possible for an α particle to penetrate the Coulomb barrier through quantum tunneling, but the likelihood of this occurring at kinetic energies of a few MeV typical of therapeutic nuclear medicine is extremely small.

averaged over many particles, at which energy is transferred to the medium per unit path length. This ratio is known as the linear stopping power.[4] So as to remove the influence of the medium's physical density, it is useful to define the mass stopping power as the linear stopping power normalized to the physical density of the medium. Stopping powers due to soft and hard collisions with atomic electrons are summed to yield the collision stopping power.[5] The radiative stopping power is a measure of the rate of energy loss due to *bremsstrahlung* alone and the total collision stopping power is given by the sum of the collision and radiative stopping powers. As alluded to above, a refinement to the collision stopping power of significant practical interest to radiation dosimetry considers only that energy deposited locally (i.e., neglecting the energy carried away by a δ ray). The restricted stopping power, or linear energy transfer, is that fraction of the collision stopping power in which the kinetic energy of the δ ray is less than a specified cut-off value Δ.

Because a charged particle loses energy as it penetrates a medium, it slows down and (excluding positron annihilation in-flight or the nuclear absorption of hadronic projectiles) is eventually stopped. The range of the charged particle can be calculated as the integral of the reciprocal of the linear stopping power between the limits of zero and its initial kinetic energy. This is known as the continuous slowing-down approximation (CSDA) range. There are other refinements of the particle range which reflect the stochastic nature of a large number of interactions and multiple scattering events and these will be discussed. Both the stopping power and CSDA range are mean quantities resulting from large numbers of individual interactions which involve the transfer of small amounts of energy and small angle.

As with the discussion of photon interactions with matter in the previous chapter, the quantitative examples of charged particle interactions provided will be those of carbon ($Z = 6$) and lead ($Z = 82$) media. Extension of these elemental results to compound media such as soft tissue and bone is provided through Bragg's additivity rule. As the charged particles of interest to nuclear medicine are electrons, positrons, and α particles, these will be emphasized in these discussions.[6]

7.2 Coulomb Scattering With no Energy Transfer to the Medium

7.2.1 Introduction

Interactions between a charged particle and matter are frequently categorized in terms of elasticity. Whether or not a given collision can be defined as being elastic or inelastic depends upon the number of degrees-of-freedom available to the system. For example, the Coulomb scatter of an electron by a free electron (Møller scatter) is elastic as the kinetic energy lost by the projectile electron is made manifest as the target electron's postcollision kinetic energy. Similarly, a charged particle, having been scattered from an infinitely-massive scattering center is considered to have been elastically scattered as it retains its kinetic energy. In both of these cases, the pre- and postcollision (or sum of postcollision) kinetic energies are equal. Despite both being elastic, Møller scatter results in the transfer of energy to the medium whereas Coulomb scatter from an infinitely-massive scattering center does not. On the other hand, if the target electron in Møller scatter is an atomic electron bound to a nucleus, additional energy channels of ionization or excitation will arise and not all of the lost incident energy will appear in the exiting electron's kinetic energy[7] and, as such, the scatter from an atomic electron is referred to as inelastic scatter. While inelastic scatter will always result in the transfer of energy to the medium, only some elastic scatters can (e.g., the projectile and target masses are comparable). Hence, for dosimetry purposes, it is more reasonable to characterize charged particle scattering processes in terms of whether or not they result in the transfer of energy to the medium rather than elasticity.

[4]It has been argued that this nomenclature incorrect as the ratio has the units of force (i.e., 1 N = 1 J/m) rather than power (i.e., 1 W = 1 J/s). While this proposal is dimensionally correct, it does not seem realistic to accept it given the decades-long use of the term stopping power in the context of a charged particle slowing down.

[5]Also called the electronic stopping power.

[6]Protons will also figure in these derivations due to their historical significance.

[7]While, strictly speaking, such an interaction would be considered inelastic, a hard collision can be modeled as being elastic if the projectile's incident kinetic energy sufficiently exceeds the electron binding energy such that the latter can be ignored.

7.2.2 Elastic Coulomb Scatter

7.2.2.1 Spin-0 Projectiles

Unscreened Potential (Rutherford Scatter)

This was previously studied to yield the differential cross sections of the Coulomb scatter of a spin-0 charged projectile from an infinitely-massive charged scattering center given by (3.61), (3.62), and (3.65).

Screened Potential

The elastic Coulomb scatter differential cross sections in solid angle of (3.61) and (3.62) for an unscreened Coulomb potential diverge as $\theta \to 0$. This problem can be managed by recalling that small scattering angles are associated with large impact parameters through the relationship $b \propto \cot\theta/2$. At large impact parameters, the projectile will find the nuclear Coulomb potential screened by the atomic electrons: the screening parameter κ used in the derivation of the scattering amplitude and appearing in the integral of (3.58) is nonzero. Repeating the derivation of (3.61) with $\kappa \neq 0$ results in,

$$\frac{d\sigma_{Ruth}}{d\Omega} = \frac{1}{4}\frac{\left(\frac{zZ\alpha\hbar c}{p\beta}\right)^2}{\left[\left(\frac{\hbar c\kappa}{2p}\right)^2 + \sin^2\frac{\theta}{2}\right]^2} = \frac{1}{4}\frac{\left(\frac{zZ\alpha\hbar c}{p\beta}\right)^2}{\left[\left(\frac{\lambda\!\!\!^{-}\kappa}{2}\right)^2 + \sin^2\frac{\theta}{2}\right]^2} \quad \text{Screened potential} \tag{7.1}$$

where $\lambda\!\!\!^{-} = \hbar c/p$ is the reduced de Broglie wavelength of the projectile. Equation (7.1) can, for later convenience in the discussion of multiple elastic Coulomb scatter, be rewritten in the form using the half-angle identity, $\sin\theta/2 = \sqrt{(1-\cos\theta)/2}$,

$$\frac{d\sigma_{Ruth}}{d\Omega} = \frac{\left(\frac{zZ\alpha\hbar c}{p\beta}\right)^2}{\left[\frac{\chi_o^2}{2} + 1 - \cos\theta\right]^2} \tag{7.2}$$

where the effect of screening is described by the dimensionless parameter, $\chi_0 = \lambda\!\!\!^{-}\kappa$, the nature of which can be identified by rewriting the differential cross section in the small-angle approximation,

$$\frac{d\sigma_{Ruth}}{d\Omega} = 4\frac{\left(\frac{zZ\alpha\hbar c}{p\beta}\right)^2}{\left(\chi_0^2 + \theta^2\right)^2} \quad \left(\text{Small - angle approximation, screened potential}\right). \tag{7.3}$$

χ_0 can be interpreted as a screening angle and represents a minimum scattering angle so that the differential cross section remains finite as the scattering angle $\theta \to 0$,

$$\frac{d\sigma_{Ruth}}{d\Omega} \to 4\frac{\left(\frac{zZ\alpha\hbar c}{p\beta}\right)^2}{\chi_0^4} \quad \text{as} \quad \theta \to 0 \tag{7.4}$$

as shown schematically in Fig. 7.2.

An expression for the screening angle χ_0 can be derived using the statistical Thomas–Fermi model of the atom by first equating κ to the reciprocal of that model's atomic radius which is,

$$R_{TF} = \frac{1}{2}\left(\frac{3\pi}{4}\right)^{2/3}\frac{r_\infty}{Z^{1/3}} \approx 0.885\frac{r_\infty}{Z^{1/3}}. \tag{7.5}$$

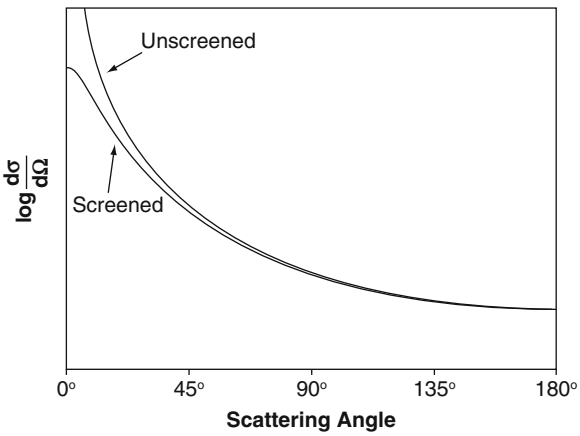

Fig. 7.2 Representative plot of screened and unscreened elastic Coulomb scatter differential cross section for spin-0 charged particles

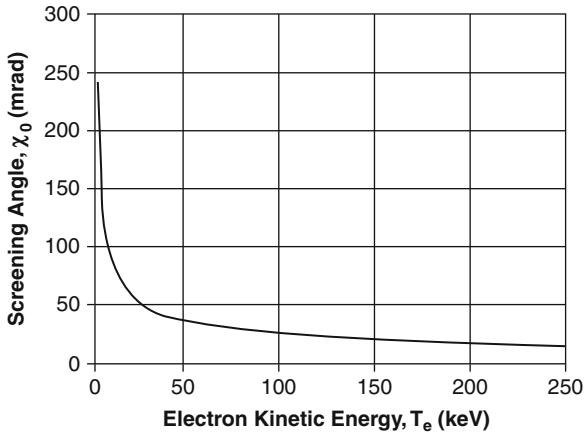

Fig. 7.3 Screening angle for electrons in carbon (neglecting spin)

From the definition of χ_0,

$$\begin{aligned}\chi_0 &= \hat{\lambda}\kappa \\ &= \frac{\hat{\lambda}}{R_{TF}} \\ &\approx 1.130\left(\frac{\hat{\lambda}}{a_\infty}\right)Z^{1/3}\end{aligned} \tag{7.6}$$

This expression for the screening angle χ_0 is plotted in Fig. 7.3 for electrons in carbon as a function of electron kinetic energy. The range of electron kinetic energies shown in this graph is typical of that following Compton scatter, photoelectric absorption, or β-decay in nuclear medicine applications. It can be seen that for electrons with a kinetic energy of 50 keV or higher, the screening angle is less than about 30 mrad.

Mean Free Path Between Elastic Scatters

Using the above results, it is possible to evaluate the mean free path between each elastic scatter. This quantity, which is also referred to as the macroscopic cross section, is of particular importance in that it is equal to the reciprocal of the probability of an elastic scatter occurring per unit pathlength, or,

$$\lambda_{Ruth} = \left(\frac{A}{\rho N_A \sigma_{Ruth}}\right) \tag{7.7}$$

where N_A is Avogadro's number, A is the atomic number of the medium and ρ is its physical density. The total Rutherford cross section is found by integrating the Rutherford cross section over a solid angle of 4π steradians,

$$\begin{aligned}\sigma_{Ruth} &= \int d\Omega \frac{d\sigma_{Ruth}}{d\Omega} \\ &= 2\pi\left(\frac{zZ\,\alpha\hbar c}{p\beta}\right)^2 \int_{-1}^{1} \frac{d(\cos\theta)}{\left[\frac{\chi_0^2}{2} + 1 - \cos\theta\right]^2}\end{aligned} \tag{7.8}$$

to give,

$$\sigma_{Ruth} = \left(\frac{zZ\,\alpha\hbar c}{p\beta}\right)^2 \frac{16\pi}{\chi_0^2(\chi_0^2+4)}. \tag{7.9}$$

Figure 7.4 shows the elastic scatter mean free path as a function of electron kinetic energy in a medium representative of carbon (i.e., Z = 6, A = 12 and ρ = 2 g/cm^3).

The combination of this small mean free path length and the θ^{-4} dependence of the Rutherford cross section leads to the dominance of forward-directed multiple elastic scattering of charged particles traversing a medium.

Elastic Scatter from an Atom

Instead of modeling the atom as a nucleus of infinite mass with the surrounding atomic electrons treated as a continuous screening function in radial distance through the use of a Yukawa-type potential, it is possible to explicitly calculate for the discrete contributions of the atomic electrons. Spin is still neglected. The combined interaction potential is the sum of the Coulomb potentials due to the nucleus and the individual atomic electrons,

$$U = z\,\alpha\hbar c\left[\frac{Z}{R} - \sum_{j=1}^{Z}\frac{1}{|\mathbf{R}-\mathbf{r}_j|}\right] \tag{7.10}$$

where $\mathbf{R}$ is the position vector of the projectile and $\mathbf{r}_j$ is that of the jth electron. The origin of the system is fixed at the center of the atomic nucleus and the overall system vector is $\mathbf{r} = (\mathbf{R},\mathbf{r}_1,\mathbf{r}_2 \ldots \mathbf{r}_Z)$. The pre- and

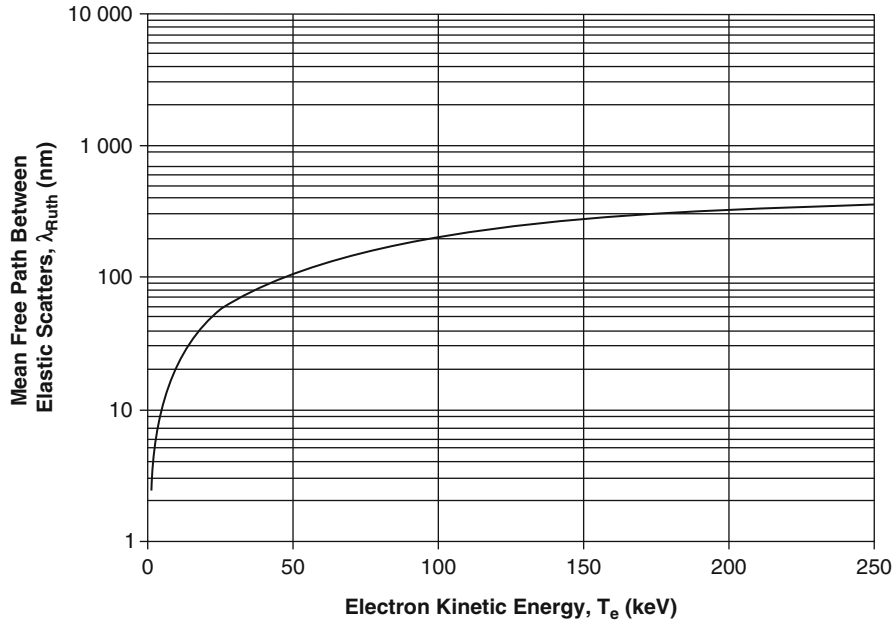

Fig. 7.4 Elastic Coulomb scatter mean free path for electrons in a medium representative of carbon (neglecting spin)

postscattering states of the projectile-atom system are, in bra-ket notation,

$$\begin{aligned}\langle \mathbf{r}|\mathbf{p},0\rangle &= \frac{1}{\sqrt{L^3}} e^{i\frac{\mathbf{p}\bullet\mathbf{R}}{\hbar c}}|0\rangle \\ &= \frac{1}{\sqrt{L^3}} e^{i\frac{\mathbf{p}\bullet\mathbf{R}}{\hbar c}}\psi_0(\mathbf{r}_1,\mathbf{r}_2,\ldots\mathbf{r}_Z)\end{aligned} \tag{7.11}$$

and

$$\langle \mathbf{r}|\mathbf{p}',0\rangle = \frac{1}{\sqrt{L^3}} e^{i\frac{\mathbf{p}'\bullet\mathbf{R}}{\hbar c}}\psi_0(\mathbf{r}_1,\mathbf{r}_2,\ldots\mathbf{r}_Z) \tag{7.12}$$

where $\psi_0(\mathbf{r}_1,\mathbf{r}_2,\ldots\mathbf{r}_Z)$ is the ground state atomic wavefunction and L^3 is the usual volume containing the system and which is to be used for normalization. As the scatter is elastic, the atomic ground state wavefunction appears in both initial and final system states. The differential cross section is obtained in the usual way from the transition rate given by Fermi's Golden Rule No. 2,

$$\lambda_{fi} = \frac{2\pi}{\hbar}|\langle \mathbf{p}',0|U|\mathbf{p},0\rangle|^2 \rho_f$$

where the phase space factor ρ_f is the density of final states per energy interval dT,

$$\rho_f\, dT' = \left(\frac{L}{2\pi\hbar c}\right)^3 d^3\mathbf{p}'. \tag{7.13}$$

By expanding the vector differential $d^3\mathbf{p}'$,

$$\begin{aligned}\rho_f\, dT' &= \left(\frac{L}{2\pi\hbar c}\right)^3 2\pi p'^2\, dp'\, d(\cos\theta) \\ &= \frac{1}{4\pi^2}\left(\frac{L}{\hbar c}\right)^3 p'^2\, dp'\, d(\cos\theta).\end{aligned} \tag{7.14}$$

The phase–space factor is,

$$\begin{aligned}\rho_f &= \frac{1}{4\pi^2}\left(\frac{L}{\hbar c}\right)^3 p'^2\left(\frac{dp'}{dT'}\right) d(\cos\theta) \\ &= \frac{1}{4\pi^2\,\beta'}\left(\frac{L}{\hbar c}\right)^3 p'^2 d(\cos\theta)\end{aligned} \tag{7.15}$$

where $\left(dp'/dT'\right) = 1/\beta'$ has been used. From Chap. 3, $|d(\cos\theta)| = q/p^2\, dq$, where q is the momentum transfer and the phase–space factor then becomes,

$$\begin{aligned}\rho_f &= \frac{1}{4\pi^2\,\beta'}\left(\frac{L}{\hbar c}\right)^3\left(\frac{p'}{p}\right)^2 q\, dq \\ &= \frac{1}{4\pi^2\,\beta}\left(\frac{L}{\hbar c}\right)^3 q\, dq\end{aligned} \tag{7.16}$$

where $\beta = \beta'$ and $p = p'$ due to the elasticity of the scatter and the negligible recoil of the scattering center.

The matrix element for both Coulomb interactions is next calculated for by separating the interactions into the projectile electron and projectile-nucleus components. The matrix element due to the Coulomb interaction between the projectile and the atomic electrons is found by expanding it in position space,[8]

$$\begin{aligned}\langle \mathbf{p}',0|\mathrm{U}|\mathbf{p},0\rangle &= \int \mathrm{d}^3\mathbf{r}\,\mathrm{d}^3\mathbf{r}'\langle \mathbf{p}',0|\mathbf{r}\rangle\langle \mathbf{r}|\mathrm{U}|\mathbf{r}'\rangle\langle \mathbf{r}'|\mathbf{p},0\rangle \\ &= \int \mathrm{d}^3\mathbf{r}\,\mathrm{d}^3\mathbf{r}'\langle \mathbf{p}',0|\mathbf{r}\rangle \mathrm{U}(\mathbf{r})\langle \mathbf{r}'|\mathbf{p},0\rangle \\ &= \frac{1}{\mathrm{L}^3}\int \mathrm{d}^3\mathbf{R}\,\mathrm{e}^{\mathrm{i}\frac{\mathbf{q}\bullet\mathbf{R}}{\hbar}}\prod_{\mathrm{j}=1}^{\mathrm{Z}} \\ &\quad \int \mathrm{d}^3\mathbf{r}_\mathrm{j}\,\psi_0^*(\mathbf{r}_1,\mathbf{r}_2\ldots\mathbf{r}_\mathrm{Z})\mathrm{U}(\mathbf{r}) \\ &\quad \times \psi_0(\mathbf{r}_1,\mathbf{r}_2\ldots\mathbf{r}_\mathrm{Z}) \\ &= -\frac{\mathrm{z}\alpha\hbar\mathrm{c}}{\mathrm{L}^3}\prod_{\mathrm{j}=1}^{\mathrm{Z}} \\ &\quad \int \mathrm{d}^3\mathbf{r}_\mathrm{j}\,\psi_0^*\left(\mathbf{r}_1,\mathbf{r}_2\ldots\mathbf{r}_\mathrm{Z}\right)\psi_0\left(\mathbf{r}_1,\mathbf{r}_2\ldots\mathbf{r}_\mathrm{Z}\right) \\ &\quad \times \int \mathrm{d}^3\mathbf{R}\,\frac{\mathrm{e}^{\mathrm{i}\frac{\mathbf{q}\bullet\mathbf{R}}{\hbar\mathrm{c}}}}{\left|\mathbf{R}-\mathbf{r}_\mathrm{j}\right|} \\ &= -\frac{\mathrm{z}\alpha\hbar\mathrm{c}}{\mathrm{L}^3}\prod_{\mathrm{j}=1}^{\mathrm{Z}} \\ &\quad \int \mathrm{d}^3\mathbf{r}_\mathrm{j}\,\psi_0^*\left(\mathbf{r}_1,\mathbf{r}_2\ldots\mathbf{r}_\mathrm{Z}\right)\psi_0\left(\mathbf{r}_1,\mathbf{r}_2\ldots\mathbf{r}_\mathrm{Z}\right) \\ &\quad \times \int \mathrm{d}^3\mathbf{R}'\,\frac{\mathrm{e}^{\mathrm{i}\frac{\mathbf{q}\bullet\left(\mathbf{R}'+\mathbf{r}_\mathrm{j}\right)}{\hbar\mathrm{c}}}}{\left|\mathbf{R}'\right|} \\ &= -\frac{\mathrm{z}\alpha\hbar\mathrm{c}}{\mathrm{L}^3}\prod_{\mathrm{j}=1}^{\mathrm{Z}} \\ &\quad \int \mathrm{d}^3\mathbf{r}_\mathrm{j}\,\psi_0^*\left(\mathbf{r}_1,\mathbf{r}_2\ldots\mathbf{r}_\mathrm{Z}\right)\psi_0\left(\mathbf{r}_1,\mathbf{r}_2\ldots\mathbf{r}_\mathrm{Z}\right) \\ &\quad \times \mathrm{e}^{\mathrm{i}\frac{\mathbf{q}\bullet\mathbf{r}_\mathrm{j}}{\hbar}}\int \mathrm{d}^3\mathbf{R}'\,\frac{\mathrm{e}^{\mathrm{i}\frac{\mathbf{q}\bullet\mathbf{R}'}{\hbar\mathrm{c}}}}{\left|\mathbf{R}'\right|} \end{aligned} \tag{7.17}$$

The solution to the integral was given by (3.59) and the matrix element is,

$$\begin{aligned}\langle \mathbf{p}',0|\mathrm{U}|\mathbf{p},0\rangle &= -4\pi\frac{\mathrm{z}\,\alpha\hbar\mathrm{c}}{\mathrm{L}^3}\left(\frac{\hbar\mathrm{c}}{\mathrm{q}}\right)^2\prod_{\mathrm{j}=1}^{\mathrm{Z}} \\ &\quad \int \mathrm{d}^3\mathbf{r}_\mathrm{j}\,\psi_0^*(\mathbf{r}_1,\mathbf{r}_2\ldots\mathbf{r}_\mathrm{Z}) \\ &\quad \times \mathrm{e}^{\mathrm{i}\frac{\mathbf{q}\bullet\mathbf{r}_\mathrm{j}}{\hbar\mathrm{c}}}\psi_0(\mathbf{r}_1,\mathbf{r}_2\ldots\mathbf{r}_\mathrm{Z}) \\ &= -4\pi\frac{\mathrm{z}\,\alpha\hbar\mathrm{c}}{\mathrm{L}^3}\left(\frac{\hbar\mathrm{c}}{\mathrm{q}}\right)^2\left\langle 0\left|\sum_{\mathrm{j}=1}^{\mathrm{Z}}\mathrm{e}^{\mathrm{i}\frac{\mathbf{q}\bullet\mathbf{r}_\mathrm{j}}{\hbar\mathrm{c}}}\right|0\right\rangle \\ &= -4\pi\frac{\mathrm{z}\,\alpha\hbar\mathrm{c}}{\mathrm{L}^3}\left(\frac{\hbar\mathrm{c}}{\mathrm{q}}\right)^2\mathrm{F}_0(\mathbf{q},\mathrm{Z}) \end{aligned} \tag{7.18}$$

where $\mathrm{F}_0(\mathbf{q},\mathrm{Z})$ is the elastic scattering form factor, which was seen before in the derivation of the photon coherent scatter cross section (and in a different guise in elastic scatter from the nucleus). Assuming a continuous electron spatial distribution rather than the discrete set of above, the form factor is the Fourier transform of the electron density. Here, the normalization of,

$$\begin{aligned}\mathrm{F}(0,\mathrm{Z}) &= \int \mathrm{d}^3\mathbf{r}\,\rho_\mathrm{e}(\mathrm{r}) \\ &= \mathrm{Z}\end{aligned} \tag{7.19}$$

will be imposed. As an example, following from the Yukawa approximation of the screened nuclear Coulomb potential, the atomic electron density can be modeled by,

$$\rho_\mathrm{e}(\mathrm{r}) = \Theta\,\mathrm{e}^{-\kappa\mathrm{r}} \tag{7.20}$$

where the normalization constant Θ is found via,

$$\begin{aligned}\int \mathrm{d}^3\mathbf{r}\,\rho_\mathrm{e}(\mathrm{r}) &= \Theta\int \mathrm{d}^3\mathbf{r}\,\mathrm{e}^{-\kappa\mathrm{r}} \\ &= 2\pi\,\Theta\int_0^\infty \mathrm{d}\mathrm{r}\,\mathrm{r}^2\,\mathrm{e}^{-\kappa\mathrm{r}} \\ &= 4\pi\frac{\Theta}{\kappa^3}.\end{aligned} \tag{7.21}$$

From these, $\Theta = \kappa^3\mathrm{Z}/4\pi$ and the electron density is now written in the form,

$$\rho_\mathrm{e}(\mathrm{r}) = \frac{\kappa^3\mathrm{Z}}{4\pi}\mathrm{e}^{-\kappa\mathrm{r}}. \tag{7.22}$$

[8] This implicitly neglects any electrostatic correlations between the atomic electrons.

The expression for the elastic scattering form factor is,

$$\begin{aligned} F(\mathbf{q},Z) &= \frac{\kappa^3 Z}{4\pi}\int d^3\mathbf{r}\, e^{-\left(\kappa r + i\frac{\mathbf{q}\bullet\mathbf{r}}{\hbar c}\right)} \\ &= \frac{\kappa^3 Z}{2}\int dr\, r^2\, e^{-\kappa r}\int d(\cos\theta) e^{-i\frac{qr\cos\theta}{\hbar c}} \\ &= \frac{\kappa^3 Z}{2}\frac{\hbar c}{q}\int dr\, r\, e^{-\kappa r}\sin\frac{qr}{\hbar c} \\ &= Z\frac{\kappa^4}{\left(\kappa^2+\left(\frac{q}{\hbar c}\right)^2\right)^2}. \end{aligned} \tag{7.23}$$

Using the momentum transfer expression of (3.52), the elastic form factor can be written in terms of the scattering angle as,

$$\begin{aligned} F_0(\theta,Z) &= Z\frac{\kappa^4}{\left(\kappa^2+\frac{4p^2}{(\hbar c)^2}\sin^2\frac{\theta}{2}\right)^2} \\ &= \frac{Z}{\left(1+\left(\frac{2p}{\hbar c\kappa}\sin\frac{\theta}{2}\right)^2\right)^2} \\ &= \frac{Z}{\left(1+\left(\frac{2}{\chi_0}\sin\frac{\theta}{2}\right)^2\right)^2}. \end{aligned} \tag{7.24}$$

Writing the form factor in this manner demonstrates that $F(\theta=0,Z)=Z$ at its maximum and decreases to $Z/\left(1+4/\chi_0^2\right)^2$ for $\theta=\pi$ (or to zero for the unscreened potential which corresponds to $\chi_0=0$). Now return to the evaluation the component of the matrix element due to the projectile-nuclear Coulomb potential,

$$\begin{aligned} \langle \mathbf{p}',0|U|\mathbf{p},0\rangle &= \int d^3\mathbf{r}\, d^3\mathbf{r}'\langle \mathbf{p}',0|\mathbf{r}\rangle\langle \mathbf{r}|U|\mathbf{r}'\rangle\langle \mathbf{r}'|\mathbf{p},0\rangle \\ &= \frac{zZ\,\alpha\hbar c}{L^3}\int d^3\mathbf{R}'\frac{e^{i\left(\frac{\mathbf{q}\bullet\mathbf{R}'}{\hbar c}\right)}}{R'}\prod_{j=1}^{Z} \\ &\quad \int d^3\mathbf{r}_j\,\psi_0^*(\mathbf{r}_1,\mathbf{r}_2\ldots\mathbf{r}_Z)\,\psi_0(\mathbf{r}_1,\mathbf{r}_2\ldots\mathbf{r}_Z) \\ &= \frac{zZ\,\alpha\hbar c}{L^3}\int d^3\mathbf{R}'\frac{e^{i\left(\frac{\mathbf{q}\bullet\mathbf{R}'}{\hbar c}\right)}}{R'} \\ &= 4\pi\frac{zZ\,\alpha\hbar c}{L^3}\left(\frac{\hbar c}{q}\right)^2 \end{aligned} \tag{7.25}$$

The complete matrix element is the sum of the projectile electron and projectile-nucleus components,

$$\langle \mathbf{p}',0|U|\mathbf{p},0\rangle = 4\pi\frac{z\,\alpha\hbar c}{L^3}\left(\frac{\hbar c}{q}\right)^2(Z-F_0(\mathbf{q},Z)). \tag{7.26}$$

The transition rate is,

$$\begin{aligned} \lambda_{fi} &= \frac{2\pi}{\hbar}|\langle \mathbf{p}',0|U|\mathbf{p},0\rangle|^2\rho_f \\ &= \frac{8\pi\, c}{\beta}\frac{(z\,\alpha\hbar c)^2}{q^3L^3}|Z-F_0(\mathbf{q},Z)|^2\,dq. \end{aligned} \tag{7.27}$$

The differential cross section in momentum transfer and scattered kinetic energy is obtained from the transition rate in the usual way by normalizing it to the incident particle flux,

$$d\sigma = \frac{L^3}{\beta\, c}\lambda_{fi} \tag{7.28}$$

leading to,

$$\frac{d\sigma}{dq} = \frac{8\pi}{q^3}\left(\frac{z\,\alpha\hbar c}{\beta}\right)^2|Z-F_0(\mathbf{q},Z)|^2 \tag{7.29}$$

A comparison of this result with the differential cross section in momentum transfer obtained previously for a single scattering center demonstrates that the Z^2 term for the unscreened potential has been replaced by $|Z-F_0(\mathbf{q},Z)|^2$. That is, the contributions of the atomic electrons, through interference as described by the elastic scattering form factor, lead to a reduction of the cross section and, in particular, the elastic scatter cross section is subject to the destructive interference between the nuclear and electronic amplitudes.

It has been seen that for zero momentum transfer (i.e., zero scattering angle), the elastic form factor is equal to Z. In the general case of small momentum transfer, the elastic form factor can be expanded to second order,

$$\begin{aligned} F(\mathbf{q},Z) &= \left\langle 0\left|\sum_{j=1}^{Z} e^{i\frac{\mathbf{q}\bullet\mathbf{r}_j}{\hbar c}}\right|0\right\rangle \\ &\approx \left\langle 0\left|\sum_{j=1}^{Z}\left(1+i\left(\frac{\mathbf{q}\bullet\mathbf{r}_j}{\hbar c}\right)-\frac{1}{2}\left(\frac{\mathbf{q}\bullet\mathbf{r}_j}{\hbar c}\right)^2\right)\right|0\right\rangle. \end{aligned} \tag{7.30}$$

As the momentum transfer is small, then $\cos\theta \approx 1$ so $\mathbf{q} \bullet \mathbf{r}_j \approx qr_j$. In addition, the matrix element of the first term of the expansion is equal to zero due to symmetry. Hence, for small q,

$$\begin{aligned} F(\mathbf{q}, Z) &\approx Z - \frac{1}{2}\left(\frac{q}{\hbar c}\right)^2 \sum_{j=1}^{Z} \langle 0|r_j^2|0\rangle \\ &\approx Z - \frac{1}{2}\left(\frac{q}{\hbar c}\right)^2 \overline{r^2} \end{aligned} \tag{7.31}$$

and the differential cross section in momentum transfer is,

$$\begin{aligned} \frac{d\sigma}{dq} &= \frac{8\pi}{q^3}\left(\frac{z\,\alpha\hbar c}{\beta}\right)^2 |Z - F_0(\mathbf{q}, Z)|^2 \\ &\approx 2\pi\left(\frac{z\,\alpha\hbar c}{\beta}\right)^2 \frac{q}{(\hbar c)^4}\left(\overline{r^2}\right)^2 \\ &\text{(small momentum transfer)}. \end{aligned} \tag{7.32}$$

The differential cross section with solid angle can next be derived in the usual way and by replacing $F_0(\mathbf{q}, Z)$ with the $F_0(\theta, Z)$ of,

$$\begin{aligned} \frac{d\sigma}{d\Omega} &= \frac{8\pi}{q^3}\frac{(z\,\alpha\hbar c)^2}{\beta}|Z - F_0(\theta, Z)|^2\left(\frac{p^2}{2\pi q}\right) \\ &= \frac{4p^2}{q^4}\frac{(z\alpha\hbar c)^2}{\beta}|Z - F_0(\theta, Z)|^2 \end{aligned} \tag{7.33}$$

As $q^4 = 16p^4 \sin^4\theta/2$ the differential cross section can be written in the form,

$$\frac{d\sigma}{d\Omega} = \frac{1}{4}\left(\frac{z\,\alpha\hbar c}{p\beta}\right)^2 \frac{|Z - F_0(\theta, Z)|^2}{\sin^4\theta/_2} \tag{7.34}$$

which is the analog to the point scattering center result.

Comparison of Atomic Scattering Results

In later consideration of charged particle transport, in particular multiple scattering, the elastic Coulomb scatter process will be significant. Hence, a review of the elastic Coulomb scatter differential cross sections calculated so far for an atomic target is now provided. Figure 7.5 shows the differential cross section in solid angle as a function of scattering angle for a 100-keV electron in carbon (the electron spin is, of course, neglected here but its effects will be considered explicitly in the next subsection). The two calculations are for the screened potential and the elastic form factor with the parameter κ defined as the reciprocal of the Thomas–Fermi atomic radius. For scattering angles exceeding about 3°, the two methods yield the same differential cross section, but diverge at smaller angles, both approaching approach a finite value at $\theta = 0$ due to screening. The differential cross section

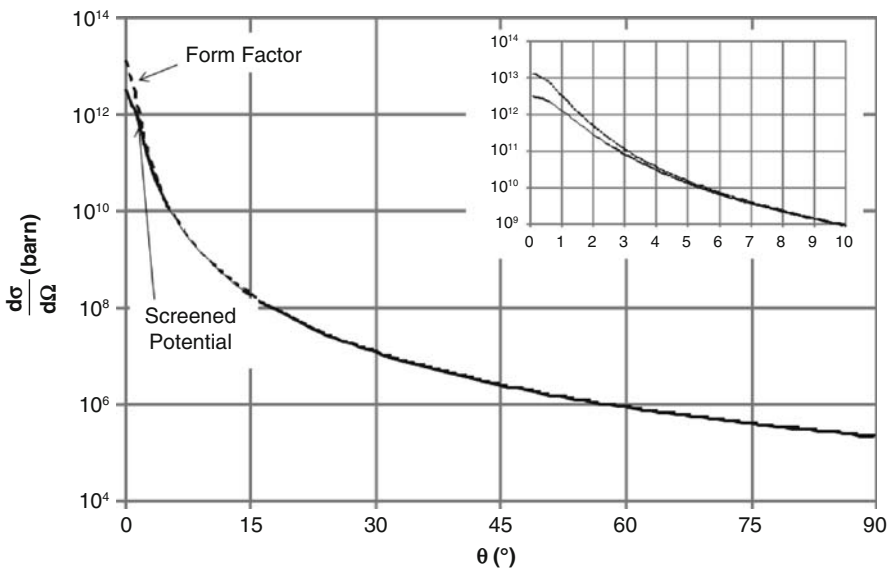

Fig. 7.5 Elastic Coulomb scatter differential cross sections for the screened nuclear Coulomb potential (*solid line*) and the discrete contributions of the atomic electrons (form factor*; dotted line*) as functions of the scattering angle for a 100 keV electron scattered from a carbon atom. Spin is neglected. The inset shows the differential cross sections for scattering angles below 10°

calculated by explicitly including the contributions of the individual atomic electrons only becomes significantly greater than that assuming a continuous screening of the potential for scattering angles of less than 3°. However, it is clear that elastic Coulomb scatter is highly forward directed with a very high differential cross section (exceeding 10^8 b for scattering angles of less than 1°). This feature is highly significant in describing the transport of charged particles in a medium. Charged particles will, as a result, undergo multiple scatters and result in a probability distribution describing both their spatial distribution and their angular direction. This will be discussed in detail later.

7.2.2.2 Spin-1/2 Projectiles

The Mott differential cross sections (Mott 1929, 1932) derived in Sect. 3.2.7 describes the interactions of a spin-1/2 projectile, such as an electron or positron, with a Coulomb field. The relevant expressions are given by (3.89) and (3.90).

7.3 Coulomb Scattering With Energy Transfer to the Medium

7.3.1 Introduction

While the results of the previous section are important input to charged particle transport calculations (through, e.g., evaluation of multiple scatter or range straggling), they do not lead to energy transfer. On the other hand, for example, following Møller scatter with an atomic electron, the atom is left in an excited or even ionized state. Energy is thus transferred to the medium. This section focuses on the inelastic collisions between a projectile and an atom (i.e., impact parameters comparable to or greater than atomic dimensions).

7.3.2 Rutherford Collision Formula

The initial derivation is of the classical formula describing the energy transfer to an electron via a Coulomb interaction with a moving heavy charged particle using the following assumptions:

- The energy loss is local (i.e., emission of electromagnetic energy is neglected).
- The particle is not deflected from its straight-line trajectory (i.e., the impulse approximation is used and multiple scatter is neglected).
- The ion is not "dressed" (i.e., it is completely stripped of electrons).[9]
- The speed of the particle is much higher than the orbital speed of any atomic electron (allowing the electron to be treated as being at rest) but is sufficiently low that nonrelativistic kinematics can be assumed.

Consider the passage of a particle with charge ze, speed v, and a mass $m \gg m_e$ in a medium with physical density ρ, atomic number Z, and atomic mass number A. It interacts with an electron through the Coulomb potential at an impact parameter b, as shown in Fig. 7.1. The force felt by the target electron is decomposed into two orthogonal components, one parallel, and the other perpendicular, to the particle's trajectory,

$$\mathbf{F} = -e\left(\mathbf{E}_{||} + \mathbf{E}_{\perp}\right) \tag{7.35}$$

where $\mathbf{E}_{||}$ and $\mathbf{E}_{\perp}$ are the two orthogonal electric field components at the position of the electron,[10]

$$\mathbf{E}_{||} = -\left(\frac{z\,(\alpha\hbar c)}{e}\right)\frac{\gamma v t}{\left[b^2 + (\gamma v t)^2\right]^{\frac{3}{2}}}\hat{\mathbf{v}}_{||} \tag{7.36}$$

$$\mathbf{E}_{\perp} = \left(\frac{z\,(\alpha\hbar c)}{e}\right)\frac{\gamma b}{\left[b^2 + (\gamma v t)^2\right]^{\frac{3}{2}}}\hat{\mathbf{v}}_{\perp} \tag{7.37}$$

[9]The presence of electrons in an ion projectile will have two effects upon the rate of energy loss. The first is that the effective charge will be reduced to the screening by these electrons. The second is that the excitation or ionization of the projectile itself will provide an additional energy loss channel.

[10]These transformed values of the electric field result from the Lorentz transformation corresponding to the boost along an axis with a speed βc for the particle in one reference frame to that containing the electron at rest. These are provided here without derivation, but one may refer to, for example, that provided by Jackson (1999).

$\hat{\mathbf{v}}_{||}$ and $\hat{\mathbf{v}}_{\perp}$ are the unit-vectors in the directions parallel and perpendicular to the projectile's trajectory. The magnitudes of these two electric field components are plotted in Fig. 7.6 as a function of time (weighted by $\gamma v/b$, which is a constant in this impulse approximation since the projectile speed is considered to be unaffected). The momentum transferred to the electron is given by the integral over all time of the force that the electron is subject to,

$$q_{||} = -e \int_{-\infty}^{\infty} dt\, E_{||} \tag{7.38}$$

$$q_{\perp} = -e \int_{-\infty}^{\infty} dt\, E_{\perp}. \tag{7.39}$$

It is clear from both the figure and the γvt multiplicative term in the expression for $\mathbf{E}_{||}$ that the net

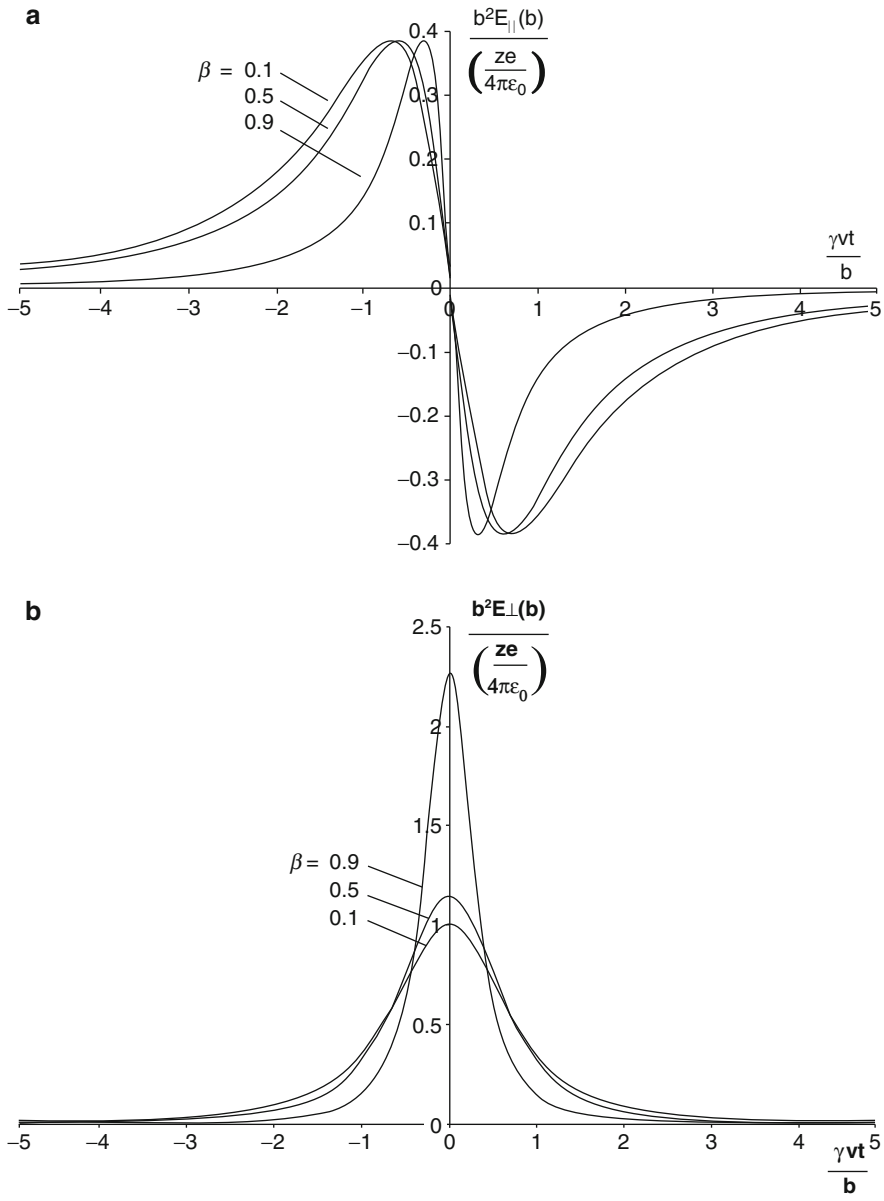

Fig. 7.6 Electric field components parallel and perpendicular to the charged-particle trajectory for different particle speeds

momentum component parallel to the particle trajectory is equal to zero and that the net non-zero momentum transfer will be that perpendicular to the particle's trajectory,

$$\begin{aligned} q &= q_\perp \\ &= -e \int_{-\infty}^{\infty} dt\, E_\perp \\ &= -(z\,\alpha\hbar c)\gamma b \int_{-\infty}^{\infty} \frac{dt}{\left[b^2 + (\gamma v t)^2\right]^{\frac{3}{2}}} \\ &= -(z\,\alpha\hbar c)\frac{\gamma}{b^2} \int_{-\infty}^{\infty} \frac{dt}{\left[1 + \left(\frac{\gamma v t}{b}\right)^2\right]^{\frac{3}{2}}} \\ &= -(z\,\alpha\hbar c)\frac{1}{bv} \int_{-\infty}^{\infty} \frac{dx}{\left[1 + x^2\right]^{\frac{3}{2}}} \\ &= -\frac{(2z\,\alpha\hbar c)}{bv} \end{aligned} \tag{7.40}$$

where the substitution of variables $x = \gamma v t/b$ has been used to solve the integral. As the recoil electron is treated as being nonrelativistic, the energy transferred to it is,

$$\begin{aligned} Q &= \frac{q^2}{2m_e} \\ &= \frac{(2z\,\alpha\hbar c)^2}{2m_e v^2 b^2} \\ &= 2m_e \left(\frac{z r_0}{\beta b}\right)^2. \end{aligned} \tag{7.41}$$

It can be immediately seen that the energy transfer decreases with $1/\beta^2$ (i.e., slower particles lose energy more rapidly) and with $1/b^2$ (i.e., energy loss decreases with increasing distance from the atom) and increases with z^2. This result can be used to demonstrate that collision energy losses will be dominated by the interactions of the projectile with atomic electrons rather than with the nucleus (whereas it is the converse with elastic scatter which is dominated by the interaction with the nucleus). The energy transfer to a nucleus of charge Ze and mass Am_N, where m_N is the nucleon mass, will scale from that to an electron by the ratio,

$$\frac{z^2 Z^2}{A m_N}\frac{m_e}{z^2} \approx \frac{Z}{2}\frac{m_e}{m_N} \approx \frac{Z}{3760}$$

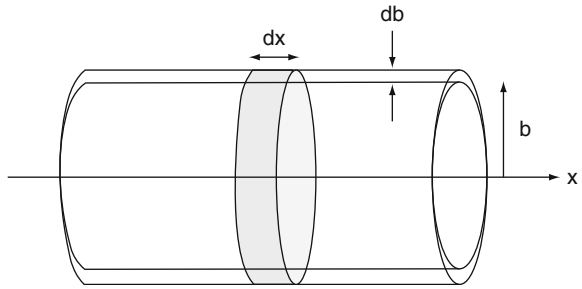

Fig. 7.7 Geometry for calculation of the Rutherford collision formula

As an example, the energy transferred to the nucleus of a carbon atom will be less than 0.2% of that transferred to an atomic electron. Nonradiative energy transfer is the result of an electromagnetic interaction with the nucleus will thus be neglected.

It is now necessary to move beyond consideration of the energy transfer to a single electron to the more realistic case of multiple energy transfers to an ensemble of electrons. Assume that the particle is moving through a sea of electrons and then isolate those electrons contained within a cylinder with its axis coincident with the particle's trajectory, as shown in Fig. 7.7. Because of the correspondence between the energy transfer and the impact parameter, the probability of an energy transfer between Q and Q + dQ to an electron occurring in a given differential pathlength dx of the traveling particle is equal to the probability of a collision with an impact parameter between b and b + db. This latter probability is equal to the number of electrons contained within the differential volume formed by the cylindrical shell of thickness db and length dx,

$$\Pr(b)\,db\,dx = \rho\,N_A\left(\frac{Z}{A}\right)2\pi\,b\,db\,dx \tag{7.42}$$

where $\rho\,N_A(Z/A)$ is the electron number density of the medium. The product $b\,db$ is obtained by differentiating (7.41),

$$|b\,db| = m_e\left(\frac{z r_0}{\beta}\right)^2\frac{dQ}{Q^2} \tag{7.43}$$

From these two expressions, the probability of an energy transfer between Q and Q + dQ to an electron

occurring in a given differential pathlength dx of the traveling particle is,

$$\Pr(b) = \left(2\pi\, m_e\, N_A\, r_0^2\right)\left(\frac{Z}{A}\right)\left(\frac{z}{\beta}\right)^2 \frac{dQ}{Q^2}\rho\, dx \quad (7.44)$$

This expression is simplified by defining a constant which will appear frequently in this chapter,

$$\begin{aligned} C &= 2\pi\, m_e N_A r_0^2 \\ &= 0.154\,\text{MeV atom cm}^2/\text{mole} \end{aligned} \quad (7.45)$$

to give,

$$\Pr(b) = C\left(\frac{Z}{A}\right)\left(\frac{z}{\beta}\right)^2 \frac{dQ}{Q^2}\rho\, dx \quad (7.46)$$

This is Rutherford's formula for energy loss and demonstrates the major features of collision energy loss through electromagnetic interactions with atomic electrons:

- The probability of a collision with energy transfer Q is proportional to Q^{-2}, demonstrating that soft collisions (small Q) are more likely than hard collisions.
- The probability is proportional to β^{-2} or, crudely, is greater for short collision times (i.e., the probability of an energy transfer decreases if the electrons are allowed to react adiabatically).
- The probability is proportional to the electron density of the medium.
- The probability is independent of projectile mass
- The probability increases with the square of the incident particle charge, z^2.

7.3.3 Soft Collision Stopping Power

7.3.3.1 Introduction

The soft collision stopping power is the energy loss due to soft collisions per unit distance traveled by a projectile in a medium. In this subsection, the two most prominent theories as developed by Bohr and Bethe are derived. In Bohr's model, energy is transferred to the atomic electrons which are treated as charged harmonic oscillators. The energy loss is calculated using classical electrodynamics for a heavy projectile interacting with a single electron of a single atom. On the other hand, the Bethe theory is the quantum-mechanical description of the inelastic projectile-atom collision.

7.3.3.2 Bohr Theory

Introduction

The main assumptions of the Bohr theory of soft collisions are that, firstly, the nucleus has infinite mass and, secondly, the projectile transfers energy to harmonically-bound atomic electrons. The Bohr mass soft collision stopping power is derived in three steps:

- Deriving the role that the impact parameter plays in separating the regions of soft- and hard collisions.
- Deriving the energy transfer to a harmonically-bound electron using the assumption that only the projectile's electric field acts upon the electron and that the field is spatially uniform at the position of the electron.
- Using these results to derive the energy transferred per unit pathlength traveled.

The Bohr theory uses classical mechanics to calculate the energy transfer due to soft collisions with the atomic electron orbital frequencies dictating the energy transfer to the atomic electrons in the adiabatic limit.

Impact Parameter

The impact parameter, b, is fundamental to the Bohr theory. For b greater than some maximum value, b_{max}, the projectile will be unable to transfer sufficient energy to the atom in order to excite or ionize it. On the other hand, for b less than some minimum value, b_{min}, the particle will interact with an individual electron (i.e., undergo a hard collision). As a result, b_{min} and b_{max} set the boundaries for a soft collision during which the projectile interacts with the entire ensemble of atomic electrons.

One method of estimating b_{min} is to use the impulse approximation implicit to the Rutherford formula in which the target electron is assumed to be stationary

or, in effect, does not recoil a significant distance compared to the impact parameter. One calculates the recoil distance and, by fixing it to be much smaller than the impact parameter, obtain b_{min}. As the time domain over which an electron with speed $v = \beta c$ experiences the electrostatic force of the projectile is of the order of $b/\gamma v$, the recoil distance of the electron will be of the order of $qb/m_e\gamma v$, where q is the momentum transfer. The impulse approximation requires this to be much less than the impact parameter,

$$\frac{q}{m_e}\frac{b}{\gamma v} \ll b$$

to give

$$\frac{q}{m_e\gamma v} \ll 1. \tag{7.47}$$

Inserting the expression for the momentum transfer gives,

$$\frac{2z\,\alpha\hbar c}{bm_e\gamma v^2} \ll 1. \tag{7.48}$$

Rearrangement gives the inequality in terms of the ratio of the electrostatic potential and kinetic energies,

$$\frac{1}{\gamma}\frac{\left(\frac{z\,\alpha\hbar c}{b}\right)}{\left(\frac{1}{2}m_e v^2\right)} \ll 1 \tag{7.49}$$

or,

$$\left(\frac{1}{\gamma}\frac{2z}{\beta^2}\right)\frac{r_0}{b} \ll 1 \tag{7.50}$$

from which an expression for b_{min} can be defined,

$$b_{min} = 2\left(\frac{z}{\gamma\beta^2}\right)r_0 \tag{7.51}$$

As expected, b_{min} decreases with increasing projectile speed (or, equivalently, decreasing de Broglie wavelength).

Another approach to calculating b_{min} recognizes that only hard collisions will occur at impact parameters below this value. From Chap. 2, the maximum energy transferred to an electron as a result of a head-on collision with a massive projectile is $2m_e\gamma^2\beta^2$. Using (7.41),

$$2m_e\gamma^2\beta^2 = 2m_e\left(\frac{zr_0}{\beta b_{min}}\right)^2$$

and solving for b_{min} gives,

$$b_{min} = \left(\frac{z}{\gamma\beta^2}\right)r_0 \tag{7.52}$$

Two classical mechanical proposals for b_{min} have been derived, each differing by a factor of 2. As both show that b_{min} is associated with increasing particle momentum (and, hence, reduced de Broglie wavelength), the quantum-mechanical nature of the interaction cannot be ignored. Moreover, the impulse approximation assumes that the momentum transfer to the electron is negligible and that the projectile trajectory is unaffected. A negligible momentum transfer is clearly unrealistic and, from the Heisenberg uncertainty principle, the uncertainty of the impact parameter will be of the order of $\hbar c/m_e\gamma\beta$. One can thus specify a quantum-mechanical minimum of the impact parameter based upon the magnitude of this uncertainty,

$$b_{min}^{QM} = \frac{\hbar c}{m_e\gamma\beta} \tag{7.53}$$

Now review the three values of b_{min} that have been derived recognizing that, for any given situation, one must select the largest of the three values for b_{min}. Hence, that expression derived from two-body elastic scattering is excluded. This leaves the two expressions derived from the impulse approximation and from the uncertainty principle. The ratio of these two expressions can be used as the metric for determining which of the two to use,

$$\frac{b_{min}^{Q}}{b_{min}} = \left(\frac{\hbar c}{m_e\gamma\beta}\right)\left(\frac{\gamma\beta^2}{2zr_0}\right) = \frac{\beta}{2\alpha z}. \tag{7.54}$$

The appropriate minimum impact parameter expression is,

$$b_{min} = \frac{2z}{\gamma\beta^2}r_0 \quad \text{if } \beta < 2\,\alpha z \tag{7.55}$$

$$b_{min} = \frac{\hbar c}{m_e \gamma \beta} \quad \text{if } \beta > 2\alpha z \tag{7.56}$$

As an example, for the case of a proton projectile, the classically-derived impact parameter is used for $\beta < 2/137 = 0.0118$, equivalent to a kinetic energy of less than 100 keV.

An expression for the maximum impact parameter b_{max} which specifies the impact parameter beyond which the projectile cannot ionize or excite the atom is now derived. A simple approach would note that the energy transferred must exceed some (as yet-to-be specified) mean ionization energy, $\bar{I}$, in order for an electron to be elevated into the continuum. Equating this to the energy transfer gives,

$$\bar{I} = 2m_e \left(\frac{z r_0}{\beta b_{max}} \right)^2 \tag{7.57}$$

and solving for b_{max},

$$b_{max} = \frac{z r_0}{\beta} \sqrt{\frac{2m_e}{\bar{I}}} \tag{7.58}$$

A related approach to defining b_{max} was originally proposed by Bohr and sets the upper limit to the impact parameter such that the atomic electrons respond adiabatically. The duration of the interaction is of the order of $b/\gamma\beta c$ and, should it be sufficiently long, the natural motion of the electron can be ignored. The natural frequency of motion of a bound electron can be written as,

$$\omega_0 = \frac{E_B}{\hbar} \tag{7.59}$$

where E_B is an effective binding energy. An expression for b_{max} can be obtained by relating the duration of the interaction to the reciprocal of this frequency,

$$\frac{b_{max}}{\gamma \beta c} \approx \frac{1}{\omega_0} \tag{7.60}$$

to give,

$$\begin{aligned} b_{max} &= \frac{\gamma \beta c}{\omega_0} \\ &= \gamma \beta \frac{\hbar c}{E_B}. \end{aligned} \tag{7.61}$$

There are fundamental differences between these two expressions of b_{max}. Equation (7.58) predicts that the maximum impact parameter will be dependent upon the charge of the projectile and will decrease with increasing projectile speed. On the other hand, the result of (7.61) has no projectile charge dependence and predicts an increase in b_{max} with projectile speed.

Energy Transfer to a Harmonically-Bound Electron

The next steps of Bohr result of the soft collision energy loss are:

- Solve for the equation of motion for a harmonically-bound electron perturbed by the projectile's electric field.
- Use this result to relate the energy loss of the projectile to the electric field.
- Calculate the rate of energy loss with pathlength.

Equation of Motion of Target Electron

Consider a single atomic electron target harmonically bound to the atom with an oscillator natural frequency, ω_0. As the charged particle passes by, the electron is subject to a spatially- and time-dependent electric field, $\mathbf{E}(\mathbf{x},t)$ and the resulting equation of motion is,

$$m_e \frac{d^2\mathbf{x}}{dt^2} = -e\mathbf{E}(\mathbf{x},t) - m_e\omega_0^2\mathbf{x} - m_e\Gamma\frac{d\mathbf{x}}{dt}. \tag{7.62}$$

The second and third terms on the right-hand side are the restorative and damping forces upon the electron, respectively, where the latter is assumed small (i.e., $\omega_0 \gg \Gamma$) in order to simplify later derivations. As, by definition, soft collisions occur at large impact parameters, the spatial variation of the electric field at the position of the electron is neglected allowing the removal of the $\mathbf{x}$ dependence of the electric field. The electric field can thus be treated as being spatially uniform at the position of the electron making it possible to replace $\mathbf{E}(\mathbf{x},t)$ with $\mathbf{E}(t)$. This equation of motion is solved using the method of Fourier transform pairs,

$$\mathbf{E}(\omega') = \frac{1}{\sqrt{2\pi}} \int_{-\infty}^{\infty} dt\, e^{i\omega' t}\, \mathbf{E}(t) \tag{7.63}$$

and

$$\mathbf{E}(t) = \frac{1}{\sqrt{2\pi}} \int_{-\infty}^{\infty} d\omega' \, e^{-i\omega' t} \, \mathbf{E}(\omega'). \tag{7.64}$$

The differential equation of motion is first rearranged,

$$\frac{d^2\mathbf{x}}{dt^2} + \Gamma \frac{d\mathbf{x}}{dt} + \omega_0^2 \mathbf{x} = -\left(\frac{e}{m_e}\right)\mathbf{E} \tag{7.65}$$

where functional dependencies are omitted for clarity. Writing both sides of the equation of motion in terms of the inverse- transforms and differentiating with respect to time gives,

$$\begin{aligned} &\int_{-\infty}^{\infty} d\omega' \left(-\omega'^2 - i\omega'\Gamma + \omega_0^2\right) e^{-i\omega' t} \, \mathbf{x}(\omega') \\ &\quad = -\left(\frac{e}{m_e}\right) \int_{-\infty}^{\infty} d\omega' \, e^{-i\omega' t} \, \mathbf{E}(\omega'). \end{aligned} \tag{7.66}$$

Multiplying both sides by $e^{-i\omega t}$ and integrating over time,

$$\begin{aligned} &\int_{-\infty}^{\infty} dt \int_{-\infty}^{\infty} d\omega' \, e^{i(\omega-\omega')t} \left(-\omega'^2 - i\omega'\Gamma + \omega_0^2\right) \mathbf{x}(\omega') \\ &\quad = -\left(\frac{e}{m_e}\right) \int_{-\infty}^{\infty} dt \int_{-\infty}^{\infty} d\omega' \, e^{i(\omega-\omega')t} \, \mathbf{E}(\omega') \end{aligned}$$

results in the integral equation,

$$\begin{aligned} &\int_{-\infty}^{\infty} d\omega' \, \delta(\omega - \omega') \left(-\omega'^2 - i\omega'\Gamma + \omega_0^2\right) \mathbf{x}(\omega') \\ &\quad = -\left(\frac{e}{m_e}\right) \int_{-\infty}^{\infty} d\omega' \, \delta(\omega - \omega') \mathbf{E}(\omega') \end{aligned} \tag{7.67}$$

where the definition of the δ-function has been used. The integration over ω' is trivial and the resulting frequency-space solution to the equation of motion is,

$$\mathbf{x}(\omega) = -\left(\frac{e}{m_e}\right)\left(\frac{\mathbf{E}(\omega)}{\left(\omega_0^2 - \omega^2\right) - i\Gamma\omega}\right). \tag{7.68}$$

Energy Transfer as a Function of the Electric Field

The projectile energy loss is equal to the energy transferred to the electron,

$$Q = -e \int_{-\infty}^{\infty} dt \frac{d\mathbf{x}(t)}{dt} \mathbf{E}(t). \tag{7.69}$$

Writing the integrand in terms of the inverse Fourier transforms,

$$\begin{aligned} Q &= -e \int_{-\infty}^{\infty} dt \left(\frac{1}{\sqrt{2\pi}} \frac{d}{dt} \int_{-\infty}^{\infty} d\omega \, e^{-i\omega t} \mathbf{x}(\omega)\right) \\ &\quad \times \left(\frac{1}{\sqrt{2\pi}} \int_{-\infty}^{\infty} d\omega' \, e^{-i\omega' t} \, \mathbf{E}(\omega')\right) \\ &= i\left(\frac{e}{2\pi}\right) \int_{-\infty}^{\infty} d\omega' \int_{-\infty}^{\infty} d\omega \left(\int_{-\infty}^{\infty} dt \, e^{-i(\omega+\omega')t}\right) \\ &\quad \times \omega \mathbf{x}(\omega) \mathbf{E}(\omega') \\ &= ie \int_{-\infty}^{\infty} d\omega' \int_{-\infty}^{\infty} d\omega \, \delta(\omega + \omega') \omega \, \mathbf{x}(\omega) \mathbf{E}(\omega') \\ &= ie \int_{-\infty}^{\infty} d\omega \, \omega \, \mathbf{x}(\omega) \mathbf{E}(-\omega). \end{aligned} \tag{7.70}$$

The electric field is a real quantity (i.e., $\mathbf{E}(-\omega) = \mathbf{E}^*(\omega)$), so,

$$\begin{aligned} Q &= ie \int_{-\infty}^{\infty} d\omega \, \omega \, \mathbf{x}(\omega) \mathbf{E}^*(\omega) \\ &= 2e \, \mathrm{Re}\left(i \int_0^{\infty} d\omega \, \omega \, \mathbf{x}(\omega) \mathbf{E}^*(\omega)\right). \end{aligned} \tag{7.71}$$

The energy transfer as a function of the electric field can now be obtained by substituting the expression for $\mathbf{x}(\omega)$ into the integrand,

$$\begin{aligned}
Q&=\left(-\frac{2e^2}{m_e}\right)\mathrm{Re}\left(i\int_0^\infty d\omega\frac{\omega|\mathbf{E}(\omega)|^2}{\left(\omega_0^2-\omega^2\right)-i\Gamma\omega}\right)\\
&=\left(-\frac{2e^2}{m_e}\right)\mathrm{Re}\left(i\int_0^\infty d\omega\frac{\omega|\mathbf{E}(\omega)|^2\left(\left(\omega_0^2-\omega^2\right)+i\Gamma\omega\right)}{\left(\omega_0^2-\omega^2\right)^2+\Gamma^2\omega^2}\right)\\
&=\left(-\frac{2e^2}{m_e}\right)\mathrm{Re}\left(\int_0^\infty d\omega\frac{\omega|\mathbf{E}(\omega)|^2\left(-\Gamma\omega+i\left(\omega_0^2-\omega^2\right)\right)}{\left(\omega_0^2-\omega^2\right)^2+\Gamma^2\omega^2}\right)\\
&=\left(\frac{2e^2}{m_e}\right)\left(\int_0^\infty d\omega\frac{\Gamma\omega^2|\mathbf{E}(\omega)|^2}{\left(\omega_0^2-\omega^2\right)^2+\Gamma^2\omega^2}\right). \qquad (7.72)
\end{aligned}$$

Solving this integral is simplified as the damping of the electron motion is small (i.e., $\Gamma \ll \omega$). As a result of this, $\mathbf{E}(\omega_0) \approx \mathbf{E}(\omega)$ and $|\mathbf{E}(\omega)|^2$ is extracted from the integrand to give,

$$Q = \left(\frac{2e^2}{m_e}\right)|\mathbf{E}(\omega_0)|^2\int_0^\infty d\omega\frac{\Gamma\omega^2}{\left(\omega_0^2-\omega^2\right)^2+\Gamma^2\omega^2}. \qquad (7.73)$$

To complete the derivation, the integral is solved using the substitution of variable, $u = \omega/\Gamma$

$$\begin{aligned}
&\int_0^\infty d\omega\frac{\Gamma\omega^2}{\left(\omega_0^2-\omega^2\right)^2+\Gamma^2\omega^2}\\
&\quad=\int_0^\infty du\frac{u^2}{\left(k^2-u^2\right)^2+u^2} \qquad (7.74)
\end{aligned}$$

where $k = \omega_0/\Gamma$. The integrand is rearranged,

$$\begin{aligned}
\int_0^\infty du\frac{u^2}{\left(k^2-u^2\right)^2+u^2}&=\int_0^\infty\frac{du}{\left(\frac{(u-k)(u+k)}{u}\right)^2+1}\\
&=\int_{-k}^\infty\frac{dx}{\left(\frac{x(x+2k)}{x+k}\right)^2+1} \qquad (7.75)
\end{aligned}$$

where the substitution $x = u - k$ has been used. The small damping force requirement is equivalent to $x \ll k$ which enables the approximation,

$$\begin{aligned}
\int_{-k}^\infty\frac{dx}{\left(\frac{x(x+2k)}{x+k}\right)^2+1}&\approx\int_{-k}^\infty\frac{dx}{\left(\frac{1}{k^2}\right)(x^2+2kx)^2+1}\\
&\approx\int_{-k}^\infty\frac{dx}{1+4x^2} \qquad (7.76)
\end{aligned}$$

and to set the lower integration limit to $-\infty$. Hence,

$$\int_0^\infty d\omega\frac{\Gamma\omega^2}{\left(\omega_0^2-\omega^2\right)^2+\Gamma^2\omega^2}\approx\int_{-\infty}^\infty\frac{dx}{1+4x^2}. \qquad (7.77)$$

Residue theory is used to solve this integral, which is of the form $\int_{-\infty}^{\infty}\frac{dz}{\left(\frac{1}{4}\right)+z^2}$ where $z = x + iy$. The integrand has poles at $z = \pm i/2$ and is holomorphic everywhere else. Consider the semicircular contour of radius R in the upper half-plane as shown in Fig. 7.8. For $R > 1/2$, the singularity of the integrand lies within the interior of the contour bounded by the segment of $-R \le x \le R$ with $y = 0$ and the upper half C_R of the circle $|z| = R$. Integrating counter-clockwise over this contour,

$$\begin{aligned}
\int_{-R}^R\frac{dx}{\left(\frac{1}{4}\right)+x^2}+\int_{C_R}\frac{dz}{\left(\frac{1}{4}\right)+z^2}&=\int_{-\infty}^\infty\frac{dz}{\left(\frac{1}{4}\right)+z^2}\\
&=2\pi\,i\,B \qquad (7.78)
\end{aligned}$$

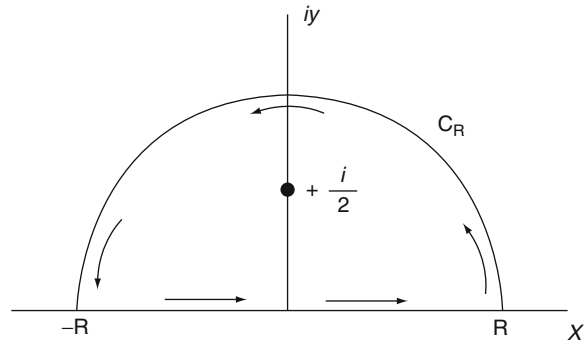

Fig. 7.8 Integration contour in the complex plane $z = x + iy$ for calculating the integral of (7.77)

where B is the residue of the integrand at the point $z = \pm\, \mathrm{i}/2$,

$$\mathrm{B} = \lim_{\mathrm{z} \to \frac{\mathrm{i}}{2}} \left(\mathrm{z} - \frac{\mathrm{i}}{2}\right)\left(\frac{1}{\left(\frac{1}{4}\right) + \mathrm{z}^2}\right) = -\mathrm{i}. \tag{7.79}$$

Hence,

$$\begin{aligned}\int_{-\infty}^{\infty} \frac{\mathrm{dx}}{\left(\frac{1}{4}\right) + \mathrm{x}^2} &= 2\pi - \int_{\mathrm{C_R}} \frac{\mathrm{dz}}{\left(\frac{1}{4}\right) + \mathrm{z}^2} \\ &= 2\pi\end{aligned} \tag{7.80}$$

which is valid for all $\mathrm{R} > 1/2$ as the integral along the contour on the right-hand side is equal to zero as can be shown by considering the point z on the contour $\mathrm{C_R}$ for which,

$$\int_{\mathrm{C_R}} \frac{\mathrm{dz}}{1/4 + \mathrm{z}^2} \leq \frac{\pi \mathrm{R}}{1/4 + \mathrm{R}^2} \tag{7.81}$$

where $\pi\mathrm{R}$ is the length of the contour. Thus, as $\frac{\pi \mathrm{R}}{1/4+\mathrm{R}^2} \to 0$ as $\mathrm{R} \to \infty$, then $\int_{\mathrm{C_R}} \frac{\mathrm{dz}}{1/4+\mathrm{z}^2} \to 0$ as $\mathrm{R} \to \infty$ and the energy transfer to the electron is,

$$\mathrm{Q} = \left(\pi \frac{\mathrm{e}^2}{\mathrm{m_e}}\right) |\mathbf{E}(\omega_0)|^2. \tag{7.82}$$

Calculation of the Electric Field

An expression for the squared modulus of the electric field at the position of the atomic electrons is found by first calculating the Fourier transforms of the two electric field components for impact parameter b, parallel and orthogonal to the particle trajectory, by rewriting (7.36) and (7.37),

$$\mathbf{E}_{\perp}(\mathrm{t}) = \left(\frac{\mathrm{z}\,\alpha\hbar\mathrm{c}}{\mathrm{eb}^2}\right) \frac{\gamma}{\left[1 + \left(\frac{\gamma \mathrm{vt}}{\mathrm{b}}\right)^2\right]^{\frac{3}{2}}} \hat{\mathbf{v}}_{\perp} \tag{7.83}$$

$$\mathbf{E}_{\parallel}(\mathrm{t}) = -\left(\frac{\mathrm{z}\,\alpha\hbar\mathrm{c}}{\mathrm{eb}^3}\right) \frac{\gamma \mathrm{vt}}{\left[1 + \left(\frac{\gamma \mathrm{vt}}{\mathrm{b}}\right)^2\right]^{\frac{3}{2}}} \hat{\mathbf{v}}_{\parallel}. \tag{7.84}$$

The Fourier transform of the perpendicular component of the electric field is,

$$\begin{aligned}\mathbf{E}_{\perp}(\omega) &= \frac{1}{\sqrt{2\pi}} \int_{-\infty}^{\infty} \mathrm{dt}\, \mathrm{e}^{\mathrm{i}\omega \mathrm{t}}\, \mathbf{E}_{\perp}(\mathrm{t}) \\ &= \frac{\gamma}{\sqrt{2\pi}} \left(\frac{\mathrm{z}\,\alpha\hbar\mathrm{c}}{\mathrm{eb}^2}\right) \int_{-\infty}^{\infty} \mathrm{dt} \frac{\mathrm{e}^{\mathrm{i}\omega \mathrm{t}}}{\left[1 + \left(\frac{\gamma \mathrm{vt}}{\mathrm{b}}\right)^2\right]^{\frac{3}{2}}} \hat{\mathbf{v}}_{\perp}.\end{aligned} \tag{7.85}$$

The integral is solved by using the substitution of variable, $\mathrm{x} = \gamma \mathrm{vt}/\mathrm{b}$,

$$\begin{aligned}\mathbf{E}_{\perp}(\omega) &= \frac{\mathrm{z}\,\alpha\hbar\mathrm{c}}{\sqrt{2\pi}\,\mathrm{ebv}} \int_{-\infty}^{\infty} \mathrm{dx} \frac{\mathrm{e}^{\mathrm{i}\left(\frac{\omega \mathrm{b}}{\gamma \mathrm{v}}\right)\mathrm{x}}}{\left[1 + \mathrm{x}^2\right]^{\frac{3}{2}}} \hat{\mathbf{v}}_{\perp} \\ &= \sqrt{\frac{2}{\pi}} \frac{\mathrm{z}\,\alpha\hbar\mathrm{c}}{\mathrm{ebv}} \int_{0}^{\infty} \mathrm{dx} \frac{\cos\left(\frac{\omega \mathrm{b}}{\gamma \mathrm{v}}\mathrm{x}\right)}{\left[1 + \mathrm{x}^2\right]^{\frac{3}{2}}} \hat{\mathbf{v}}_{\perp}\end{aligned} \tag{7.86}$$

with the last step following from $\cos\left(\frac{\omega \mathrm{b}}{\gamma \mathrm{v}}\mathrm{x}\right)$ and $\sin\left(\frac{\omega \mathrm{b}}{\gamma \mathrm{v}}\mathrm{x}\right)$ being even and odd functions, respectively. The integral is a form of the modified Bessel function of the second kind (Abramowitz and Stegun 1972),

$$\mathrm{K}_{\nu}(\mathrm{y}) = \frac{2^{\nu}\Gamma\left(\nu + \frac{1}{2}\right)}{\sqrt{\pi}\mathrm{y}^{\nu}} \int_{0}^{\infty} \mathrm{dx} \frac{\cos(\mathrm{xy})}{\left[1 + \mathrm{x}^2\right]^{\nu + \frac{1}{2}}} \tag{7.87}$$

where ν is 0 or an integer. Use of $\mathrm{K}_{\nu}(\mathrm{y})$ for $\nu = 0, 1$ will be required,

$$\mathrm{K}_0(\mathrm{y}) = \int_{0}^{\infty} \mathrm{dx} \frac{\cos(\mathrm{xy})}{\sqrt{1 + \mathrm{x}^2}} \tag{7.88}$$

$$\mathrm{K}_1(\mathrm{y}) = \frac{1}{\mathrm{y}} \int_{0}^{\infty} \mathrm{dx} \frac{\cos(\mathrm{xy})}{\left[1 + \mathrm{x}^2\right]^{\frac{3}{2}}}. \tag{7.89}$$

The expression of the electric field orthogonal to the projectile trajectory is now,

$$\begin{aligned}\mathbf{E}_{\perp}(\omega) &= \sqrt{\frac{2}{\pi}} \frac{\mathrm{z}\,\alpha\hbar\mathrm{c}}{\mathrm{ebv}} \int_{0}^{\infty} \mathrm{dx} \frac{\cos\left(\frac{\omega \mathrm{b}}{\gamma \mathrm{v}}\mathrm{x}\right)}{\left[1 + \mathrm{x}^2\right]^{\frac{3}{2}}} \hat{\mathbf{v}}_{\perp} \\ &= \sqrt{\frac{2}{\pi}} \frac{\mathrm{z}\,\alpha\hbar\mathrm{c}}{\mathrm{ebv}} \left(\frac{\omega \mathrm{b}}{\gamma \mathrm{v}}\right) \mathrm{K}_1\left(\frac{\omega \mathrm{b}}{\gamma \mathrm{v}}\right) \hat{\mathbf{v}}_{\perp} \\ &= \frac{\mathrm{e}}{(2\pi)^{3/2}\varepsilon_0} \left(\frac{\mathrm{z}\omega}{\gamma \mathrm{v}^2}\right) \mathrm{K}_1\left(\frac{\omega \mathrm{b}}{\gamma \mathrm{v}}\right) \hat{\mathbf{v}}_{\perp}\end{aligned} \tag{7.90}$$

and the Fourier transform of the electric field component parallel to the particle's trajectory is,

$$\mathbf{E}_{||}(\omega) = -\frac{\gamma v}{\sqrt{2\pi}} \frac{z\alpha\hbar c}{eb^3} \int_{-\infty}^{\infty} dt \frac{te^{i\omega t}}{\left[1+\left(\frac{\gamma v t}{b}\right)^2\right]^{\frac{3}{2}}} \hat{\mathbf{v}}_{||}. \quad (7.91)$$

Using, again, the substitution of variable, $x = \gamma v t/b$,

$$\mathbf{E}_{||}(\omega) = -\frac{z\alpha\hbar c}{\sqrt{2\pi}\, eb\gamma v} \int_{-\infty}^{\infty} dx \frac{xe^{i\left(\frac{\omega b}{\gamma v}\right)x}}{\left[1+x^2\right]^{\frac{3}{2}}} \hat{\mathbf{v}}_{||}. \quad (7.92)$$

This integral is solved by parts (for clarity, $y = \omega b/\gamma v$),

$$\begin{aligned} \int_{-\infty}^{\infty} dx \frac{xe^{ixy}}{\left[1+x^2\right]^{\frac{3}{2}}} &= \int_{-\infty}^{\infty} dr\, s \\ &= s\, r\Big|_{-\infty}^{\infty} - \int_{-\infty}^{\infty} ds\, r \end{aligned} \quad (7.93)$$

where

$$\begin{aligned} s &\equiv e^{ixy} & ds &= dx\, i\, y\, e^{ixy} \\ dr &\equiv dx \frac{x}{\left[1+x^2\right]^{\frac{3}{2}}} & r &= -\frac{1}{\sqrt{1+x^2}} \end{aligned}$$

to give,

$$\begin{aligned} \int_{-\infty}^{\infty} dx \frac{xe^{i\left(\frac{\omega b}{\gamma v}\right)x}}{\left[1+x^2\right]^{\frac{3}{2}}} &= 2i\left(\frac{\omega b}{\gamma v}\right) \int_{0}^{\infty} dx \frac{\cos\left(\frac{\omega b}{\gamma v}x\right)}{\sqrt{1+x^2}} \\ &= 2i\left(\frac{\omega\, b}{\gamma v}\right) K_0\left(\frac{\omega\, b}{\gamma v}\right). \end{aligned} \quad (7.94)$$

The Fourier transform of the electric field component parallel to the particle's trajectory is now had,

$$\mathbf{E}_{||}(\omega) = -\frac{i}{(2\pi)^{3/2}\varepsilon_0} \frac{ze\omega}{(\gamma v)^2} K_0\left(\frac{\omega b}{\gamma v}\right) \hat{\mathbf{v}}_{||}. \quad (7.95)$$

The squared modulus of the electric field in frequency space is,

$$\begin{aligned} |\mathbf{E}(\omega_0)|^2 &= |\mathbf{E}_{\perp}(\omega_0)|^2 + |\mathbf{E}_{||}(\omega_0)|^2 \\ &= \frac{1}{(2\pi)^3\varepsilon_0^2}\left(\frac{ze\omega_0}{v}\right)^2 \left[K_1^2\left(\frac{\omega_0 b}{\gamma v}\right) + \frac{K_0^2\left(\frac{\omega_0 b}{\gamma v}\right)}{\gamma^2}\right]. \end{aligned} \quad (7.96)$$

The frequency ω_0 is written in terms of the maximum impact parameter, b_{max}, beyond which no energy is transferred to the atom, as determined from the adiabatic response result, $\omega_0 = \gamma v/b_{max}$. Hence, the electric field can be written as a function of the impact parameter,

$$|\mathbf{E}(b)|^2 = \frac{1}{(2\pi)^3\varepsilon_0^2}\left(\frac{ze\gamma}{b_{max}}\right)^2 \left[K_1^2\left(\frac{b}{b_{max}}\right) + \frac{K_0^2\left(\frac{b}{b_{max}}\right)}{\gamma^2}\right]. \quad (7.97)$$

The energy transfer to a harmonically-bound electron is,

$$\begin{aligned} Q &= \left(\pi\frac{e^2}{m_e}\right)|\mathbf{E}(b)|^2 \\ &= 2m_e\left(\frac{r_0}{b_{max}}\right)^2\left(\frac{z}{\beta}\right)^2 \left[K_1^2\left(\frac{b}{b_{max}}\right) + \frac{K_0^2\left(\frac{b}{b_{max}}\right)}{\gamma^2}\right]. \end{aligned} \quad (7.98)$$

Consider the dependence of the energy transfer as a function of impact parameter. For small impact parameters, the low-argument limits of the modified Bessel functions are required,

$$yK_0(y) \to 0 \quad \text{as} \quad y \to 0 \quad (7.99)$$

$$yK_1(y) \to 1 \quad \text{as} \quad y \to 0. \quad (7.100)$$

In this case,

$$Q \to 2m_e\left(\frac{zr_0}{\beta\, b}\right)^2 \quad \text{as} \quad b \to 0. \quad (7.101)$$

Note that this is the same result of the energy transfer calculated from the impulse approximation. Invoking a minimum impact parameter, an expression for the maximum energy transfer in a soft collision corresponding to the minimum impact parameter can be written,

$$Q_{max} = 2m_e\left(\frac{zr_0}{\beta b_{min}}\right)^2. \quad (7.102)$$

For example, the magnitude of the energy transfer from a soft collision from an α particle with a kinetic energy of 5 MeV is $Q_{max} \approx 200$ eV. For large impact parameters, we can use the large-argument

approximations of the modified Bessel functions $K_{0,1}(y) \approx \sqrt{\frac{\pi}{2y}}e^{-y}$ for $y \gg 1$ to give,

$$Q \approx \pi m_e \left(\frac{r_0}{b_{max}}\right)^2 \left(\frac{z}{\beta}\right)\left[1+\frac{1}{\gamma^2}\right] \times \left(\frac{b_{max}}{b}\right)e^{-2b/b_{max}} \tag{7.103}$$

The exponential term in this expression introduces the desired rapid cut-off for very large impact parameters at which the energy transfer becomes inefficient beyond the adiabatically-limited impact parameter, b_{max}.

Bohr Soft Collision Mass Stopping Power

Using the Bohr soft energy transfer expression, the soft collision stopping power, which is the energy loss per unit pathlength due solely to soft collisions, is calculated. In a medium of electron density ρ_e, the number of electrons in a differential cylinder section of length dx with impact parameters between b and b + db is $2\pi\ \rho_e\ b\ dx\ db$ and the double-differential energy loss of a particle traversing this section is,

$$\begin{aligned} d^2E &= -2\pi\,\rho_e\,b\,Q\,db\,dx \\ &= -4\pi\,\rho_e\,m_e\left(\frac{r_0}{b_{max}}\right)^2\left(\frac{z}{\beta}\right)^2 \\ &\quad\times\left[K_1^2\left(\frac{b}{b_{max}}\right)+\frac{K_0^2\left(\frac{b}{b_{max}}\right)}{\gamma^2}\right]b\,db\,dx \\ &= -4\pi\,\rho_e\,m_e\left(\frac{zr_0}{\beta}\right)^2 y\left[K_1^2(y)+\frac{K_0^2(y)}{\gamma^2}\right]dy\,dx \end{aligned} \tag{7.104}$$

where the substitution of variable, $y = b/b_{max}$, has been used. Integrating over y, the linear soft collision stopping power[11] is

$$\begin{aligned} \left(\frac{dE}{dx}\right)_{Col,S} &= -4\pi\,\rho_e\,m_e\left(\frac{zr_0}{\beta}\right)^2 \\ &\quad\times\int_{\left(\frac{b_{min}}{b_{max}}\right)}^{\infty} dy\,y\left[K_1^2(y)+\frac{K_0^2(y)}{\gamma^2}\right] \\ &= -4\pi\,\rho_e\,m_e\left(\frac{zr_0}{\beta}\right)^2 \\ &\quad\times\int_{\left(\frac{b_{min}}{b_{max}}\right)}^{\infty} dy\,y\left[K_1^2(y)+K_0^2(y)-\beta^2K_0^2(y)\right]. \end{aligned} \tag{7.105}$$

The mass soft collision stopping power will be the linear collision stopping power normalized to the physical density of the medium the charged particle is moving through,

$$\begin{aligned} \left(\frac{dE}{\rho\,dx}\right)_{Col} &= -4\pi\,N_A\left(\frac{Z}{A}\right)m_e\left(\frac{zr_0}{\beta}\right)^2 \\ &\quad\int_{\left(\frac{b_{min}}{b_{max}}\right)}^{\infty} dy\,y\left[K_1^2(y)+K_0^2(y)-\beta^2K_0^2(y)\right] \\ &= -2C\left(\frac{Z}{A}\right)\left(\frac{z}{\beta}\right)^2 \\ &\quad\int_{\left(\frac{b_{min}}{b_{max}}\right)}^{\infty} dy\,y\left[K_1^2(y)+K_0^2(y)-\beta^2K_0^2(y)\right]. \end{aligned} \tag{7.106}$$

The integral is solved by simplifying the integrand using the properties of the derivatives of $K_0(y)$ and $K_1(y)$,

$$\frac{dK_0(y)}{dx} = -K_1(y) \tag{7.107}$$

and

$$\frac{dK_1(y)}{dy} = -K_0(y) - \frac{K_1(y)}{y}. \tag{7.108}$$

Then,

$$\begin{aligned} \frac{d}{dy}\left[y\,K_0(y)K_1(y)\right] &= K_0(y)K_1(y) \\ &\quad + y\frac{dK_0(y)}{dy}K_1(y) + yK_0(y)\frac{dK_1(y)}{dy} \\ &= -y\left(K_0^2(y)+K_1^2(y)\right) \end{aligned} \tag{7.109}$$

[11] Although the stopping power is also written as S and the mass collision stopping power as S/p, it will be written here as a differential.

and

$$\frac{d}{dy}\left[y^2\left(K_1^2(y)-K_0^2(y)\right)\right]=-2yK_0^2(y). \tag{7.110}$$

Incorporating these results into the integral of (7.106) gives,

$$\begin{aligned}
&\int_{\left(\frac{b_{min}}{b_{max}}\right)}^{\infty} dy\, y\left[K_1^2(y)+K_0^2(y)-\beta^2K_0^2(y)\right]\\
&=\int_{\left(\frac{b_{min}}{b_{max}}\right)}^{\infty} dy\left[y\left(K_1^2(y)+K_0^2(y)\right)-\beta^2yK_0^2(y)\right]\\
&=\int_{\left(\frac{b_{min}}{b_{max}}\right)}^{\infty} dy\left[-\frac{d}{dy}\left[yK_0(y)K_1(y)\right]+\frac{\beta^2}{2}\right.\\
&\left.\times\frac{d}{dy}\left[y^2(K_1^2(y)-K_0^2(y))\right]\right]
\end{aligned} \tag{7.111}$$

from which the Bohr mass soft collision stopping power is obtained,

$$\begin{aligned}
\left(\frac{dE}{\rho\,dx}\right)_{Col,S}=&-2C\left(\frac{Z}{A}\right)\left(\frac{z}{\beta}\right)^2\left[\frac{b_{min}}{b_{max}}K_0\left(\frac{b_{min}}{b_{max}}\right)K_1\left(\frac{b_{min}}{b_{max}}\right)\right.\\
&\left.-\frac{\beta^2}{2}\frac{b_{min}^2}{b_{max}^2}\left(K_1^2\left(\frac{b_{min}}{b_{max}}\right)-K_0^2\left(\frac{b_{min}}{b_{max}}\right)\right)\right]
\end{aligned} \tag{7.112}$$

The variable of interest is the ratio of the minimum to maximum impact parameters,

$$\left(\frac{b_{min}}{b_{max}}\right)=\frac{b_{min}}{\left(\frac{\gamma v}{\omega_0}\right)}=\frac{b_{min}\omega_0}{\gamma v}. \tag{7.113}$$

A form of the minimum impact parameter has not been explicitly provided as this will be dependent upon the projectile speed and electric charge. The magnitude of this ratio of impact parameters can be estimated by recognizing that the resonant frequency of a harmonically-bound electron is approximated by $\omega_0 = E_B/\hbar$ which leads to,

$$\begin{aligned}
\left(\frac{b_{min}}{b_{max}}\right)&=\frac{b_{min}E_B}{\hbar c\,\gamma\beta}\\
&=\frac{2zr_0E_B}{\hbar c\,\gamma^2\beta^3}\quad \beta<2\alpha Z
\end{aligned} \tag{7.114}$$

$$=\frac{E_B}{m_e(\gamma\beta)^2}\quad \beta>2\alpha Z. \tag{7.115}$$

As the binding energy can be written in approximate form, $E_B=-\hbar cR_\infty Z$, then $b_{min}/b_{max}\ll 1$and it is then possible to use the properties of the modified Bessel functions of the second kind for small arguments,

$$\begin{aligned}
K_0(y)&\approx-\ln\frac{y}{2}-\gamma_{EM}\\
&\approx\ln\left(\frac{2e^{-\gamma_{EM}}}{y}\right)\quad \text{for}\quad 0<y\ll 1
\end{aligned} \tag{7.116}$$

where $\gamma_{EM}\approx 0.5772\ldots$ is the Euler–Mascheroni constant, and

$$K_1(y)\approx\frac{1}{y}\quad \text{for}\quad 0<y\ll\sqrt{2}. \tag{7.117}$$

Using these expressions and recalling that $b_{min}/b_{max}\ll 1$,

$$\begin{aligned}
\left(\frac{dE}{\rho\,dx}\right)_{Col,S}&\approx-2C\left(\frac{Z}{A}\right)\left(\frac{z}{\beta}\right)^2\left[\ln\left(2e^{-\gamma_{EM}}\frac{b_{max}}{b_{min}}\right)-\frac{\beta^2}{2}\right]\\
&\approx-2C\left(\frac{Z}{A}\right)\left(\frac{z}{\beta}\right)^2\left[\ln\left(1.123\frac{b_{max}}{b_{min}}\right)-\frac{\beta^2}{2}\right].
\end{aligned} \tag{7.118}$$

Briefly return to the ratio of impact parameters,

$$\begin{aligned}
\left(\frac{b_{max}}{b_{min}}\right)&=\frac{(\gamma\beta c/\omega_0)}{\left(2zr_0/\gamma\beta^2\right)}\\
&=\frac{\gamma^2\beta^3c}{2zr_0\omega_0}
\end{aligned} \tag{7.119}$$

where a single harmonic oscillator with a resonance frequency, ω_0, which corresponds to a single atomic electron has been calculated for. For atoms other than

hydrogen, this should be replaced by the geometric average resonance frequency for the Z atomic electrons,

$$\ln \bar{\omega} = \frac{1}{Z} \sum_j f_j \ln \omega_j \tag{7.120}$$

where the Z electrons have been partitioned into groups each having the same resonance frequency, ω_j. Detailed discussion of the oscillator strengths is deferred until the derivation of the Bethe theory, but it will be noted here that the oscillator strengths must satisfy the requirement,

$$\sum_{j=1}^{Z} \omega_j \frac{df_j}{d\omega} = Z. \tag{7.121}$$

The final expression for the classical Bohr mass soft collision stopping power is now,

$$\left(\frac{dE}{\rho\, dx}\right)_{Col,S} = -2C\left(\frac{Z}{A}\right)\left(\frac{z}{\beta}\right)^2 \left[\ln\left(\frac{1.123\,\gamma^2\beta^3 c}{z r_0 \bar{\omega}}\right) - \frac{\beta^2}{2}\right] \tag{7.122}$$

7.3.3.3 Bethe Theory

Introduction

During the 1920s, various attempts were made to provide a quantum-mechanical description of the energy loss in inelastic charged-particle collisions with atoms. Bethe was the first to develop a successful quantum-mechanical theory[12] and which is based upon the first Born approximation.

This derivation of the Bethe soft collision stopping power will, for calculational ease, be limited to the nonrelativistic case.

[12]Reviews of the derivation of the Bethe theory can be found in Fano (1964), Inokuti (1971) and Ahlen (1980).

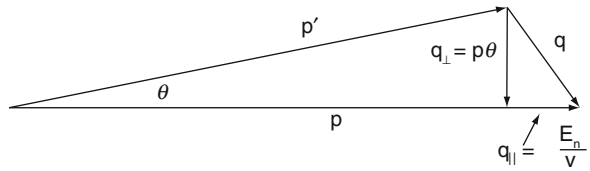

Fig. 7.9 Momentum transfer in the small-angle approximation

Collision Kinematics

It is necessary to first define the kinematics of the collision between the projectile and an atomic electron. A projectile with momentum **p** and kinetic energy T collides with an atomic electron and scatters through the angle θ with momentum **p** and kinetic energy T′. The momentum transfer is given through the derivation of (3.52) for elastic scatter but now allowing for energy loss, $p \neq p'$,

$$q = \sqrt{p^2 + p'^2 - 2pp' \cos\theta} \tag{7.123}$$

for the interaction kinematics of Fig. 7.9 for a small scattering angle. In this derivation, the target atomic electron is treated as being unbound and initially at rest, which is a reasonable assumption for high projectile incident kinetic energies. However, if the projectile speed is comparable to the orbital speeds of the atomic electrons, this assumption becomes untenable and corrections must be made as will be discussed later in this chapter. Following the collision, the kinetic energy of the recoil electron is,

$$Q = T - T' \tag{7.124}$$

which is related to its three-vector momentum through the relativistic relationship,

$$(Q + m_e)^2 = q^2 + m_e{}^2. \tag{7.125}$$

Upon rearrangement,

$$Q\left(1 + \frac{Q}{2m_e}\right) = \frac{q^2}{2m_e} \tag{7.126}$$

which, for the condition of $Q \ll 2m_e$, reduces to the familiar nonrelativistic form,

$$Q = \frac{q^2}{2m_e}. \tag{7.127}$$

Following the collision, the atom will be excited from its ground state 0 with energy eigenvalue E_0, which will be taken as being equal to zero, to a final state n with the energy eigenvalue, E_n. The energy transfer Q need not equal E_n as the recoil electron cannot be considered in isolation as a consequence of it being part of an ensemble of atomic electrons as energy transferred to it can be shared amongst others.

It is straightforward to calculate the component of the momentum transfer **q** that is parallel to the incident momentum **p** from the excitation energy,

$$\begin{aligned} E_n &\approx \frac{p^2}{2m} - \frac{|\mathbf{p}-\mathbf{q}|^2}{2m} \\ &\approx \frac{2\mathbf{p}\bullet\mathbf{q} - q^2}{2m} \\ &\approx \frac{\mathbf{q}\bullet\mathbf{p}}{m} \end{aligned} \tag{7.128}$$

where m is the projectile mass and, having assumed soft collisions, terms of the order of q^2 are neglected. This leads to,

$$q_{||} = \frac{E_n}{v} \equiv \frac{E_n}{\beta} \tag{7.129}$$

where both q and E_n are in units of energy. As this is a soft collision and q is small, the small-angle approximation can be used and the component of **q** perpendicular to **p** is,

$$q_{\perp} = p\theta. \tag{7.130}$$

In this small-angle approximation, the squared magnitude of the momentum transfer can be written as,

$$q^2 = q_{||}^2 + q_{\perp}^2 = \left(\frac{E_n}{\beta}\right)^2 + (p\theta)^2 \tag{7.131}$$

and the energy transfer to the electron is,

$$Q = \frac{q^2}{2m_e} = \frac{E_n^2}{2m_e\beta^2} + \frac{(p\theta)^2}{2m_e}. \tag{7.132}$$

Bethe Soft Collision Cross Section

The calculation of the Bethe mass soft collision stopping power follows that of the elastic atomic Coulomb scattering cross section, but using both of Fermi's Golden Rules as there is no direct coupling between the initial and final atomic states. Consider the projectile to have an electric charge ze and the atom to have atomic number Z and to be in its ground state, $|0\rangle$. The projectile is treated as a plane wave and the atom is excited to the state $|n\rangle$ as a result of the collision. Hence, the pre- and postcollision system states are,

$$\begin{aligned} \langle \mathbf{r}|\mathbf{p},0\rangle &= \frac{1}{\sqrt{L^3}} e^{i\frac{\mathbf{p}\bullet\mathbf{R}}{\hbar c}}|0\rangle \\ &= \frac{1}{\sqrt{L^3}} e^{i\frac{\mathbf{p}\bullet\mathbf{R}}{\hbar c}}\psi_0(\mathbf{r}_1,\mathbf{r}_2,\ldots\mathbf{r}_Z) \end{aligned} \tag{7.133}$$

and

$$\begin{aligned} \langle \mathbf{r}|\mathbf{p}',n\rangle &= \frac{1}{\sqrt{L^3}} e^{i\frac{\mathbf{p}'\bullet\mathbf{R}}{\hbar c}}|n\rangle \\ &= \frac{1}{\sqrt{L^3}} e^{i\frac{\mathbf{p}'\bullet\mathbf{R}}{\hbar c}}\psi_n(\mathbf{r}_1,\mathbf{r}_2,\ldots\mathbf{r}_Z). \end{aligned} \tag{7.133}$$

The system position vector, with the origin specified at the center of the atom, is given by $\mathbf{r} = (\mathbf{R}, \mathbf{r}_1 \ldots \mathbf{r}_Z)$ where **R** is the position vector of the projectile and the $\mathbf{r}_j$ is the position vector of the jth electron. The overall interaction between the projectile and the atomic electrons is handled in the Coulomb gauge in which there are two types of electromagnetic interactions. The first is the static unretarded potential between the projectile and electrons with a direct coupling between the initial and final states allowing the transition rate to be given by Fermi's Golden Rule No. 2. This is also referred to as the longitudinal excitation as it is directed parallel to the momentum transfer. The second type of interaction is through the emission and absorption of virtual photons between the projectile and atomic electrons which become significant at relativistic speeds. Because this is the result of the interaction between the particle currents with the quantized transverse vector potential, this is often referred to as transverse excitation. As there is no direct coupling between the initial $|0\rangle$ and final $|n\rangle$ states, the transition rate through

an intermediate state $|i\rangle$ will be given by Fermi's Golden Rule No. 1. Combining these two categories, the transition rate is,

$$\lambda_{fi} = \frac{2\pi}{\hbar}\left|\langle \mathbf{p}',\, n|U|\mathbf{p},\, 0\rangle + \sum_j \frac{\langle \mathbf{p}',\, n|U|\mathbf{k}\,, j\rangle\langle \mathbf{k},\, j|U|\mathbf{p},\, 0\rangle}{E_0 - E_j}\right|^2 \rho_f \tag{7.135}$$

where E_0 and E_j are the energy eigenvalues for states $|0\rangle$ and $|j\rangle$, respectively, and the summation is over all available intermediate states.

While the projectile will interact with both the ensemble of atomic electrons and the nucleus, it can be proven that the projectile-nucleus interaction does not lead to atomic excitation. The Coulomb potential between the projectile and the nucleus (both taken to be point-like charges) is $U(R) = -zZ\,\alpha\hbar c/R$ and the matrix element of the corresponding perturbation in position space is,

$$\begin{aligned}
&\langle \mathbf{p}', n|U|\mathbf{p}, 0\rangle \\
&\quad = \int d^3\mathbf{r}\, d^3\mathbf{r}' \langle \mathbf{p}', n|\mathbf{r}\rangle\langle \mathbf{r}|U|\mathbf{r}'\rangle\langle \mathbf{r}'|\mathbf{p}, 0\rangle \\
&\quad = \frac{1}{L^3}\int d^3\mathbf{R}\, e^{i\frac{\mathbf{q}\bullet\mathbf{R}}{\hbar c}} \prod_{j=1}^{Z} d^3\mathbf{r}_j\, \psi_n^*(\mathbf{r}_1, \ldots \mathbf{r}_Z) U(\mathbf{R}) \psi_0(\mathbf{r}_1, \ldots \mathbf{r}_Z) \\
&\quad = -zZ\frac{\alpha\hbar c}{L^3}\int d^3\mathbf{R}\frac{e^{i\frac{\mathbf{q}\bullet\mathbf{R}}{\hbar c}}}{R} \prod_{j=1}^{Z} d^3\mathbf{r}_j\, \psi_n^*(\mathbf{r}_1, \ldots \mathbf{r}_Z) \psi_0(\mathbf{r}_1, \ldots \mathbf{r}_Z) \\
&\quad = 0
\end{aligned} \tag{7.136}$$

due to the orthonormality of the two states.

The Coulomb potential between the projectile and the Z atomic electrons is given by,

$$U(\mathbf{r}) = -(z\,\alpha\hbar c)\sum_{j=1}^{Z}\frac{1}{|\mathbf{R} - \mathbf{r}_j|}. \tag{7.137}$$

The exchange process of transverse photons between the projectile and an electron has two intermediate states (assume that the electron can be treated as at rest). In the first, the projectile emits a photon of momentum $\mathbf{q} = \mathbf{p} - \mathbf{p}'$ which is absorbed by the electron to give it a momentum $\mathbf{q}$. In the second, the electron emits a photon with momentum $-\mathbf{q}$, to give it a momentum $\mathbf{q}$. The photon is absorbed by the projectile to give it a momentum $\mathbf{p}' = \mathbf{p} - \mathbf{q}$. From the derivation of the Klein–Nishina cross section in Chap. 6, the photon emission by the projectile is proportional to the matrix element of $z(\alpha\hbar c/e)(\boldsymbol{\alpha}\bullet\hat{\boldsymbol{\varepsilon}}_m)e^{-i\frac{\mathbf{q}\bullet\mathbf{r}}{\hbar c}}$ where $\boldsymbol{\alpha}$ is the Dirac velocity operator of the projectile and $\hat{\boldsymbol{\varepsilon}}_m$ is the photon's unit polarization vector and where m = 1,2 (see Sect. 24 of Heitler (1984) for a more detailed description). The absorption of this photon by the jth atomic electron is proportional to a matrix element of $\frac{z\,\alpha\hbar c}{e}\left(\boldsymbol{\alpha}_j\bullet\hat{\boldsymbol{\varepsilon}}_m\right)e^{i\frac{\mathbf{q}\bullet\mathbf{r}_j}{\hbar c}}$. For clarity, the Bethe collision stopping power due to the static Coulomb potential (longitudinal excitation) only will be derived and the final form, which includes the relativistic term, provided. Full derivations of the latter can be found in the review articles by Fano (1964) and Ahlen (1980).

The transition rate from the ground state $|0\rangle$, with an energy eigenvalue considered here to be zero, to the state $|n\rangle$, with energy eigenvalue E_n, through longitudinal excitation is given conveniently by Fermi's Golden Rule No. 2,

$$\lambda_{fi,long} = \frac{2\pi}{\hbar}\left|\langle \mathbf{p}', n|U|\mathbf{p}, 0\rangle\right|^2 \rho_f.$$

The phase–space term is common to both longitudinal and transverse excitations and is of the usual form $\rho_f\, dT' = \left(L/2\pi\hbar c\right)^3 d^3\mathbf{p}'$. This derivation of the phase–space term will parallel that of the elastic Coulomb scatter calculation except that the energy transfer rather than the momentum transfer will be used as the kinematic variable. The density of final sates is, as calculated before,

$$\rho_f = \frac{1}{4\pi^2\beta'}\left(\frac{L}{\hbar c}\right)^3 p'^2\, dp'\, d(\cos\theta). \tag{7.138}$$

From the inelastic momentum transfer, $d(\cos\theta) = (q/pp')$ and the momentum transfer is $q = \sqrt{Q(Q + 2m_e)}$ from which one obtains $q\,dq = m_e(1 + Q/m_e)dQ$. This gives the density of final states as,

$$\rho_f = \frac{m_e}{4\pi^2\beta'}\left(\frac{L}{\hbar c}\right)^3\left(\frac{p'}{p}\right)\left(1 + \frac{Q}{m_e}\right)dQ'. \tag{7.139}$$

For soft collisions, the energy transfer is much less than the projectile's kinetic energy (i.e., $Q \ll T$) and we can approximate $p'/p \approx \beta'/\beta \approx 1$ to give,

$$\rho_f \approx \frac{m_e}{4\pi^2\beta}\left(\frac{L}{\hbar c}\right)^3\left(1+\frac{Q}{m_e}\right)dQ. \tag{7.140}$$

The matrix element due to the unretarded Coulomb interactions between the projectile and the atomic electrons is calculated in the same fashion as in our calculation of the elastic scatter cross section,

$$\langle \mathbf{p}', n|U|\mathbf{p}, 0\rangle = \int d^3\mathbf{r}\, d^3\mathbf{r}' \langle \mathbf{p}', n|\mathbf{r}\rangle\langle \mathbf{r}|U|\mathbf{r}'\rangle\langle \mathbf{r}'|\mathbf{p}, 0\rangle. \tag{7.141}$$

The method of solving this matrix element is identical to that used in previous derivations in Chaps. 3 and 6,

$$\begin{aligned}\langle \mathbf{p}', n|U|\mathbf{p}, 0\rangle &= -4\pi\frac{z\,\alpha\hbar c}{L^3}\left(\frac{\hbar c}{q}\right)^2\left\langle n\left|\sum_{j=1}^{Z} e^{i\frac{\mathbf{q}\cdot\mathbf{r}_j}{\hbar c}}\right|0\right\rangle \\ &= -4\pi\frac{z\,\alpha\hbar c}{L^3}\left(\frac{\hbar c}{q}\right)^2 F_n(\mathbf{q}, Z).\end{aligned} \tag{7.142}$$

where $F_n(\mathbf{q}, Z)$ is the inelastic scattering form factor. The transition rate can be considered independent of azimuthal angle if the target atom is in the s-state (i.e., spherically symmetric) or if the target atoms in the medium are randomly oriented (as is the case in medical irradiation). This permits one to replace the vector momentum transfer $\mathbf{q}$ in the argument of the inelastic form factor with its scalar value, q, to give $F_n(q, Z)$. The squared amplitude of the matrix element is, in terms of the energy transfer,

$$\begin{aligned}|\langle \mathbf{p}', n|U|\mathbf{p}, 0\rangle|^2 &= 16\pi^2\frac{(z\,\alpha\hbar c)^2}{L^6}\left(\frac{\hbar c}{q}\right)^4|F_n(q, Z)|^2 \\ &= 4\pi^2\frac{(z\,\alpha\hbar c)^2}{L^6}\frac{(\hbar c)^4}{m_e^2Q^2\left(1+\frac{Q}{2m_e}\right)^2} \\ &\quad\times|F_n(q, Z)|^2.\end{aligned} \tag{7.143}$$

The inelastic Coulomb scatter transition rate for longitudinal excitation is,

$$\begin{aligned}\lambda_{fi,long} &= \frac{2\pi}{\hbar}|\langle \mathbf{p}', n|U|\mathbf{p}, 0\rangle|^2\rho_f \\ &= 2\pi\frac{(z\,\alpha\hbar c)^2\,c}{\beta\,L^3\,m_e}\frac{|F_n(q, Z)|^2}{Q^2\left(1+\frac{Q}{2m_e}\right)^2}\left(1+\frac{Q}{m_e}\right)dQ\end{aligned} \tag{7.144}$$

The differential cross section is the transition rate normalized to the incident particle flux, v/V, or,

$$\begin{aligned}d\sigma_{long} &= \frac{L^3}{\beta c}\lambda_{fi,long} \\ &= 2\pi\frac{z^2m_er_0^2}{\beta^2}\frac{|F_n(q, Z)|^2}{Q^2\left(1+\frac{Q}{2m_e}\right)^2}\left(1+\frac{Q}{m_e}\right)dQ.\end{aligned} \tag{7.145}$$

The inelastic form factor $F_n(q, Z)$ is related to the generalized (dipole) oscillator strength, GOS (which has already been seen in the derivation of the Bohr energy loss), which is a generalization of the optical oscillator strength (see, e.g., Fernández-Varea 1998) given, in the nomenclature used here, by,

$$f_n(q, Z) = \frac{E_n}{Q}|F_n(q, Z)|^2. \tag{7.146}$$

Analytical representations for the GOS are available for atomic hydrogen and the free electron gas for which the initial and final states are analytically calculable. In the more practical cases of heavier atoms and molecules, these wavefunctions are calculated numerically. This discussion will be limited to the simple details of the GOS required for obtaining an expression for the stopping power. The inelastic form factor can be related to the GOS per unit energy transfer,

$$\frac{df_n(q, Z)}{dE_n} = \frac{1}{Q}|F_n(q, Z)|^2. \tag{7.147}$$

The energy-weighted sum of the oscillator strengths equals the total number of electrons in the atom which, in integral form, is,

$$\int dE_n\frac{df_n(q, Z)}{dE_n} = Z. \tag{7.148}$$

The GOS can also be used to describe the mean ionization energy of the atomic system as the first energy moment of the oscillator strength distribution,

$$\begin{aligned}\ln \bar{I} &= \frac{\int dE \frac{df}{dE} \ln E}{\int dE \frac{df}{dE}} \\ &= \frac{1}{Z} \int dE \frac{df_n}{dE} \ln E.\end{aligned} \tag{7.149}$$

The GOS per unit energy transfer has a useful interpretation at low momentum transfers. Writing the GOS per unit excitation energy in bra-ket form,

$$\begin{aligned}\frac{df_n(q,Z)}{dE_n} &= \frac{1}{Q}|F_n(q,Z)|^2 \\ &= \frac{1}{Q}\left|\left\langle n\left|\sum_{j=1}^{Z} e^{i\frac{q r_j}{\hbar c}}\right|0\right\rangle\right|^2 \\ &= \frac{2m_e}{q^2}\left|\left\langle n\left|\sum_{j=1}^{Z} e^{i\frac{q r_j}{\hbar c}}\right|0\right\rangle\right|^2\end{aligned} \tag{7.150}$$

where, for low q, the nonrelativistic relationship between momentum and energy transfer has been used. Expanding the exponential to first order for small q,

$$\begin{aligned}\frac{df_n(q,Z)}{dE_n} &\approx \frac{2m_e}{q^2}\left|Z\langle n|0\rangle + \frac{i}{\hbar c}\left\langle n\left|\sum_{j=1}^{Z} q\, r_j\right|0\right\rangle\right|^2 \\ &\approx -\frac{2m_e}{(\hbar c)^2}\left|\left\langle n\left|\sum_{j=1}^{Z} r_j\right|0\right\rangle\right|^2 \quad \text{small q}\end{aligned} \tag{7.151}$$

where the orthogonality relationship $\langle n|0\rangle = 0$ has been used. $df_n(q,Z)/dE_n \to df_n(Z)/dE_n$ for small q, where $df_n(Z)/dE_n$ is the optical oscillator strength per unit excitation energy and which is proportional to the square of the dipole-matrix element.

Having introduced the GOS and its properties at low q, the expression of the differential cross section for longitudinal excitation is then simplified,

$$\begin{aligned}d\sigma_{long} &= 2\pi \frac{z^2 m_e r_0^2}{\beta^2} \frac{|F_n(q,Z)|^2}{Q^2\left(1+\frac{Q}{2m_e}\right)^2}\left(1+\frac{Q}{m_e}\right)dQ \\ &= 2\pi \frac{z^2 m_e r_0^2}{\beta^2} \frac{\left(1+\frac{Q}{m_e}\right)}{Q^2\left(1+\frac{Q}{2m_e}\right)^2}\frac{df_n(q,Z)}{dE_n}dQ \\ &= \frac{C}{N_A}\left(\frac{z}{\beta}\right)^2 \frac{\left(1+\frac{Q}{m_e}\right)}{Q^2\left(1+\frac{Q}{2m_e}\right)^2}\frac{df_n(q,Z)}{dE_n}dQ\end{aligned} \tag{7.152}$$

For $Q \ll m_e$, the cross section simplifies to,

$$d\sigma_{long} = \frac{C}{N_A}\left(\frac{z}{\beta}\right)^2 \frac{dQ}{Q}\frac{df_n(q,Z)}{dE_n}. \tag{7.153}$$

For calculational convenience, the kinetic variable is temporarily changed from the energy transfer to the momentum transfer,

$$d\sigma_{long} = \frac{2C}{N_A}\left(\frac{z}{\beta}\right)^2 \frac{dq}{q}\frac{df_n(q,Z)}{dE_n}. \tag{7.154}$$

Integrating over the momentum transfer yields the total cross section,

$$\sigma_{long} = \frac{2C}{N_A}\left(\frac{z}{\beta}\right)^2 \int_{q_{min}}^{q_{max}} dq \frac{1}{q}\frac{df_n(q,Z)}{dE_n}. \tag{7.155}$$

As q is small for soft collisions, $df_n(q,Z)/dE_n$ is replaced with the optical oscillator strength per unit excitation energy, $df_n(Z)/dE_n$. Then it is removed from the integrand to obtain the total cross section,

$$\begin{aligned}\sigma_{n,long} &= \frac{2C}{N_A}\left(\frac{z}{\beta}\right)^2 \frac{df_n(Z)}{dE_n}\int_{q_{min}}^{q_{max}} \frac{dq}{q} \\ &= \frac{2C}{N_A}\left(\frac{z}{\beta}\right)^2 \frac{df_n(Z)}{dE_n}\ln\left(\frac{q_{max}}{q_{min}}\right).\end{aligned} \tag{7.156}$$

This result highlights the fundamental difference between the Bohr and Bethe theories. Bohr's theory uses the impact parameter to distinguish between soft and hard collisions. This is clearly not possible in quantum theory in which the localization of a wave packet of a particle with well-defined momentum is limited by the uncertainty principle. Hence, one would expect the classical theory to break down for small impact parameters. In the Bethe theory, momentum (or energy) transfer is used to separate the soft and hard collision regimes. For later convenience when expressions for soft and hard collision stopping powers are merged to determine the complete collision stopping power, instead of using the momentum transfer, the use the energy transfer will be returned to as a means of defining soft and hard collisions. The collision is said to be "soft" if $Q < Q_C$ and to be "hard" if $Q > Q_C$. The exact specification of the transition energy transfer Q_C is insignificant as this quantity

will cancel out when the expressions for the soft and hard collision stopping powers are summed. Even so, limits should be applied to Q_C in order to ensure that the necessary approximations used in the derivations remain valid. Q_C must exceed atomic binding energies but it must also not be sufficiently great that the projectile's de Broglie wavelength becomes comparable to nuclear dimensions. A value of between 10 and 100 keV for Q_C would allow both conditions to be simultaneously met (Uehling 1954).

The limits of the momentum transfers which define a soft collision are now calculated. The lower limit, q_{min}, is given by $q_{||} = E_n/v$. Clearly, q_{max} will be set by the energy transfer separation between soft and hard collisions,

$$q_{max} = \sqrt{2m_e Q_C} \tag{7.157}$$

Applying these limits to the momentum transfer,

$$\begin{aligned}\sigma_{n,long} &= \frac{2C}{N_A}\left(\frac{z}{\beta}\right)^2 \frac{df_n}{dE_n} \ln\left(\frac{\sqrt{2m_e Q_C}}{E_n} v\right) \\ &= \frac{C}{N_A}\left(\frac{z}{\beta}\right)^2 \frac{df_n}{dE_n} \ln\left(\frac{2m_e Q_C}{E_n^2}\beta^2\right)\end{aligned} \tag{7.158}$$

Bethe Soft Collision Stopping Power

The mean energy transfer per unit fluence is,

$$\begin{aligned}\overline{\Delta E}_{long} &= \int dE_n \, \sigma_{n,long} \\ &= \frac{C}{N_A}\left(\frac{z}{\beta}\right)^2 \int dE_n \frac{df_n}{dE_n} \ln\left(\frac{2m_e Q_C}{E_n^2}\beta^2\right).\end{aligned} \tag{7.159}$$

The logarithm is split,

$$\ln\left(\frac{2m_e Q_C}{E_n^2}\beta^2\right) = -2\ln E_n + \ln\left(2m_e Q_C \beta^2\right) \tag{7.160}$$

where it is implicitly required for E_n, m_e, and Q_C to have the same units of energy. This enables the integral of (7.159) to be written as,

$$\begin{aligned}&\int dE_n \frac{df_n}{dE_n} \ln\left(\frac{2m_e Q_c}{E_n^2}\beta^2\right) \\ &\quad = -2\int dE_n \frac{df_n}{dE_n} \ln E_n \\ &\qquad + \ln\left(2m_e Q_c \beta^2\right) \int dE_n \frac{df_n}{dE_n} \\ &\quad = -2Z\ln\bar{I} + Z\ln\left(2m_e Q_c \beta^2\right) \\ &\quad = Z\ln\left(\frac{2m_e Q_c}{\bar{I}^2}\beta^2\right).\end{aligned} \tag{7.161}$$

Then, the mean energy loss per interaction as,

$$\overline{\Delta E}_{long} = C\left(\frac{Z}{N_A}\right)\left(\frac{z}{\beta}\right)^2 \ln\left(\frac{2m_e Q_C}{\bar{I}^2}\beta^2\right) \tag{7.162}$$

and the mass soft collision stopping power due to longitudinal excitations only is,

$$\left(\frac{dE}{\rho\, dx}\right)_{Col,S,long} = C\left(\frac{Z}{A}\right)\left(\frac{z}{\beta}\right)^2 \ln\left(\frac{2m_e Q_C}{\bar{I}^2}\beta^2\right) \tag{7.163}$$

This is the quantum-mechanical result of the energy transfer between a charged projectile and an atom due to an unretarded Coulomb potential and which is the nonrelativistic result of the Bethe theory. As shown by Fano (1964) and Ahlen (1980), the full form of the Bethe mass soft collision stopping power, accounting for both longitudinal and transverse excitations, is slightly modified from this result,

$$\begin{aligned}\left(\frac{dE}{\rho dx}\right)_{Col,S} &= C\left(\frac{Z}{A}\right)\left(\frac{z}{\beta}\right)^2 \left[\ln\left(\frac{2m_e Q_C}{\bar{I}^2}\gamma^2\beta^2\right) - \beta^2\right] \\ &= C\left(\frac{Z}{A}\right)\left(\frac{z}{\beta}\right)^2 \left[\ln\left(\frac{2m_e Q_C}{\bar{I}^2}\beta^2\right)\right. \\ &\quad \left. + \ln\left(\frac{1}{1-\beta^2}\right) - \beta^2\right]\end{aligned} \tag{7.164}$$

where the $\ln(1/1-\beta^2)$ and β^2 terms arise from retarded transverse photon interactions. It can be seen that, since these two terms go to zero as $\beta \to 0$, this relativistic form reduces to the nonrelativistic result.

7.3.3.4 Comparison of Bohr and Bethe Soft Collision Theories

The Bohr classical and Bethe quantum-mechanical results are compared by considering the mass soft

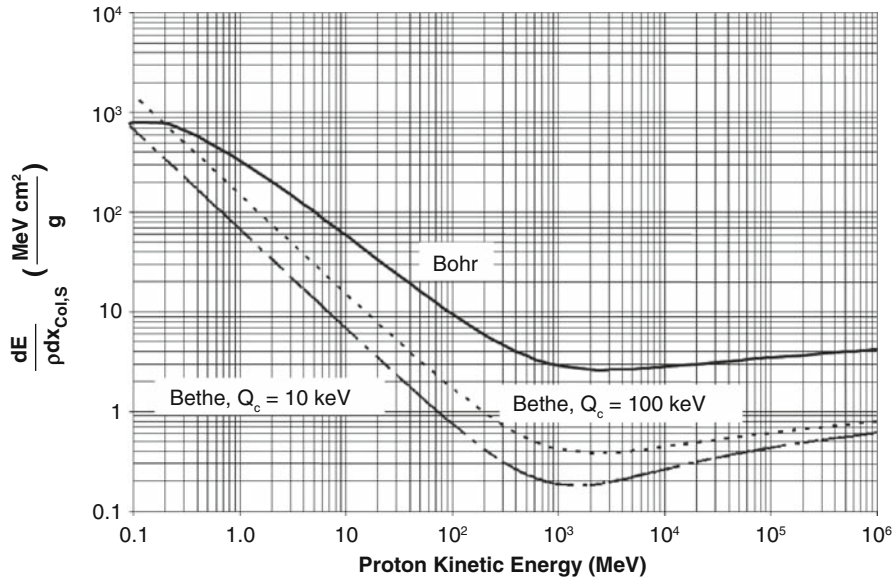

Fig. 7.10 Mass soft collision stopping powers calculated from the Bohr and Bethe theories for protons ranging in kinetic energy from 100 keV to 1 TeV in carbon. The Bethe results are shown for two values of Q_C which separates the energy transfers of soft and hard collisions

collision stopping powers for protons in carbon as given in Fig. 7.10. For the Bethe result, the mean ionization potential has been set to 6hcR, where the Rydberg energy is $hcR_\infty = 13.61$ eV, and stopping powers calculated for the extrema for Q_C equal to 10 and 100 keV. For the Bohr result, the mean oscillator frequency has been set to $\bar{\omega} = 6\,hcR_\infty/\hbar = 1.24 \times 10^{17}\ s^{-1}$. It should be recalled that the derivations of the Bohr and Bethe soft collision theories have been with single ground state atoms or electrons or, in other words, the medium through which the projectile travels has been treated as a cold and dilute monatomic gas rather than as a condensed medium. The results of Fig. 7.10 are those for "carbon" in so far as we have calculated for a homogeneous medium in which $Z = 6$ and $A = 12$. The Bohr result is explicitly truncated for kinetic energies less than 0.1 MeV: the calculated soft collision stopping power changes sign, corresponding to the unphysical condition of the gain of energy by the particle, due to the condition of $1.123\,\gamma^2\beta^3 c/(zr_0\bar{\omega}) \leq \beta^2/2$ at low energies.

Although the two theories do not agree quantitatively (except at low projectile kinetic energies), they exhibit similar behaviors by demonstrating a decreasing stopping power with increasing projectile energy proportional to β^{-2}. In both cases the mass collision stopping powers reach broad minima at proton kinetic energies of about 3 GeV and then exhibit a slow increase. The magnitude of the Bohr mass soft collision stopping power is greater than that obtained from the Bethe theory by roughly a factor of 5. The Bethe result shows a slight dependence upon the selection of Q_C with that calculated for $Q_C = 100$ keV being about a factor of 2 greater than that calculated for $Q_C = 10$ keV.

7.3.4 Hard Collision Stopping Power

7.3.4.1 Introduction

In a hard collision, the projectile interacts with a single atomic electron at a speed much greater than the orbital speed thus allowing the target electron to be assumed to be at rest. In this case, the collision can be treated as being elastic.

7.3.4.2 Differential Cross Sections in Energy Transfer

Massive Projectile Electron Scatter ($m \gg m_e$)

Spin-0

Consider a massive spin-zero projectile (e.g., an α particle) of charge ze with kinetic energy T. The differential cross section for the energy transfer

between Q and Q + dQ to an electron at rest is (Bhabha 1938),

$$\frac{d\sigma}{dQ} = 2\pi r_0^2 m_e \left(\frac{z}{\beta}\right)^2 \frac{1}{Q^2}\left(1 - \beta^2 \frac{Q}{Q_{max}}\right) \quad \text{Spin-0} \tag{7.165}$$

where Q_{max} is the maximum energy transfer to the electron

Spin-1/2

Consider the case of a massive spin-1/2 projectile (e.g., a proton) of mass m and charge ze with kinetic energy T. The differential cross section for the energy transfer between Q and Q + dQ to the electron at rest is (Bhabha 1938; Massey and Corben 1939),

$$\frac{d\sigma}{dQ} = 2\pi r_0^2 m_e \left(\frac{z}{\beta}\right)^2 \frac{1}{Q^2} \times \left[1 - \beta^2 \frac{Q}{Q_{max}} + \frac{1}{2}\left(\frac{Q}{T+m}\right)^2\right] \quad \text{Spin-}1/2. \tag{7.166}$$

Spin-1

Finally, for completeness, consider the case of a massive spin-1 particle with mass m, charge ze, and kinetic energy T. The differential cross section for the energy transfer between Q and Q + dQ to an electron at rest is (Massey and Corben 1939; Oppenheimer et al., 1940) is,

$$\frac{d\sigma}{dQ} = 2\pi r_0^2 m_e \left(\frac{z}{\beta}\right)^2 \frac{1}{Q^2}\left[\left(1 - \beta^2 \frac{Q}{Q_{max}}\right)\left(1 + \frac{1}{3}\frac{Q}{Q_0}\right) + \frac{1}{3}\left(\frac{Q}{T+m}\right)^2\left(1 + \frac{1}{2}\frac{Q}{Q_0}\right)\right] \quad \text{Spin-1} \tag{7.167}$$

where the energy Q_0 is defined as $Q_0 = m^2/m_e$.

It will be noted that, for low projectile energies and low-recoil kinetic energies, the above differential cross sections for spin-0, spin-1/2, and spin-1 massive projectiles reduce to the classical Rutherford result. Hence, spin contributions to the differential cross section become significant only at high projectile energies.

Electron–Electron (Møller) Scatter

Now consider the case of the projectile being an electron with kinetic energy, T. The Feynman diagrams of electron–electron (Møller) scatter are shown in Fig. 7.11. Two graphs necessarily arise as a result of the inability to distinguish between the two exiting electrons of which was the projectile or the target. From Chap. 2, the maximum energy transferred to the target electron is equal to the kinetic energy of the incident. Because of the indistinguishability between the projectile and target electrons, the exiting electron with the highest energy is assumed to be the primary. As the electron is a fermion, the wavefunction of an electron pair system must be antisymmetric in the interchange of the two electrons. Should the electron spins be parallel (i.e., the system is in the triplet state), the system will be symmetric under the exchange of spins thus requiring the spatial wavefunctions to be antisymmetric under the exchange of the electron's relative coordinates. Hence, the triplet state scattering amplitude is,

$$f_t(\theta) = f(\theta) - f(\pi - \theta) \tag{7.168}$$

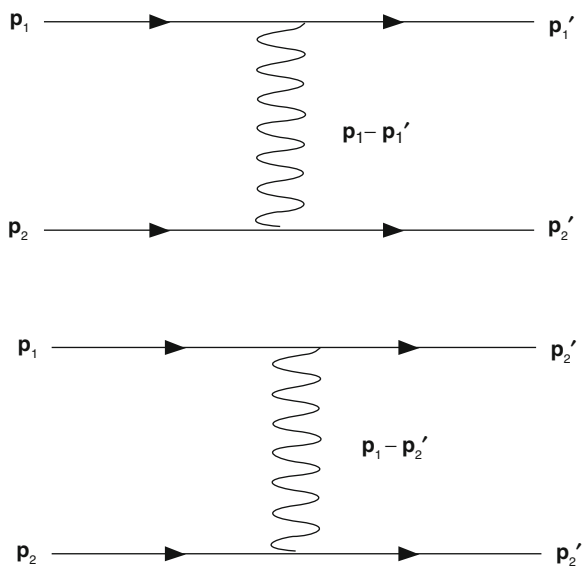

Fig. 7.11 Feynman diagrams for electron–electron Coulomb scatter. *Top*: direct interaction; *bottom*: exchange interaction

where f(θ) is the scattering amplitude of elastic Coulomb scatter. The transformation from θ to π − θ is the equivalent of the interchange of the two electrons. For antiparallel spins (i.e., the singlet state), the system is antisymmetric under the interchange of spins and, as a result, the spatial wavefunctions must be symmetric,

$$f_s(\theta) = f(\theta) + f(\pi - \theta). \tag{7.169}$$

In dosimetry calculations, the projectile and target electrons are considered to be unpolarized and $e^- e^-$ scatter has a random distribution of spins. Hence, singlet and triplet states will have a ratio of relative probabilities of 1:3 and the differential cross section is,

$$\begin{aligned}\frac{d\sigma}{d\Omega} &= \frac{1}{4}|f_s(\theta)|^2 + \frac{3}{4}|f_t(\theta)|^2 \\ &= \frac{1}{4}|f(\theta) + f(\pi-\theta)|^2 + \frac{3}{4}|f(\theta) - f(\pi-\theta)|^2 \\ &= |f(\theta)|^2 + |f(\pi-\theta)|^2 - |f(\theta)||f(\pi-\theta)| \\ &= \left(\frac{m_e\,\alpha\hbar c}{2p^2}\right)^2 \left(\frac{1}{\sin^4\frac{\theta}{2}} + \frac{1}{\cos^4\frac{\theta}{2}} - \frac{1}{\sin^2\frac{\theta}{2}\cos^2\frac{\theta}{2}}\right) \\ &= \left(\frac{\alpha\hbar c}{4T}\right)^2 \left(\frac{1}{\sin^4\frac{\theta}{2}} + \frac{1}{\cos^4\frac{\theta}{2}} - \frac{1}{\sin^2\frac{\theta}{2}\cos^2\frac{\theta}{2}}\right).\end{aligned} \tag{7.170}$$

The first term is that of the elastic Coulomb scatter cross section, whereas the second reflects the impossibility of distinguishing between the incident and scattered electrons. The third "cross" term is the exchange term. The full relativistic Møller differential cross section in energy transfer is, for an incident electron of kinetic energy T transferring an energy between Q and Q + dQ to another electron (Møller 1932; Rohrlich and Carlson 1954),

$$\begin{aligned}\frac{d\sigma}{dQ} = \frac{\pi}{T}\left(\frac{\alpha\hbar c}{T}\right)^2 \Bigg[&\left(\frac{T}{Q}\right)^2 + \left(\frac{Q}{T-Q}\right) + \left(\frac{\gamma-1}{\gamma}\right)^2 \\ &- \left(\frac{2\gamma-1}{\gamma^2}\right)\left(\frac{T}{Q}\right)\left(\frac{Q}{T-Q}\right)\Bigg]\end{aligned} \tag{7.171}$$

This describes the probability that, following Møller scatter, one electron has a kinetic energy of Q and the other has T − Q. Thus, all possible outcomes of the scatter are obtained for Q ranging in value from 0 to $T/2$. The nonrelativistic form of the differential cross section is had by setting $\gamma = 1$,

$$\frac{d\sigma}{dQ} = \frac{\pi}{T}\left(\frac{\alpha\hbar c}{T}\right)^2 \left[\left(\frac{T}{Q}\right)^2 + \left(\frac{Q}{T-Q}\right) - \left(\frac{T}{Q}\right)\left(\frac{Q}{T-Q}\right)\right] \tag{7.172}$$

Electron–Positron (Bhabha) Scatter

Now consider the case of a positron projectile with kinetic energy, T. The Feynman diagrams for positron–electron (Bhabha) scatter are given in Fig. 7.12. While the first graph is similar to that of Møller scatter, the fact that it is possible for the electron and positron to annihilate requires the provision of an additional graph accounting for the production of a virtual photon from which the exiting electron–positron pair is created. The differential cross section that an incident positron with kinetic energy T will suffer a kinetic energy loss between and Q and Q + dQ which is transferred to the target electron is (Bhabha 1936),

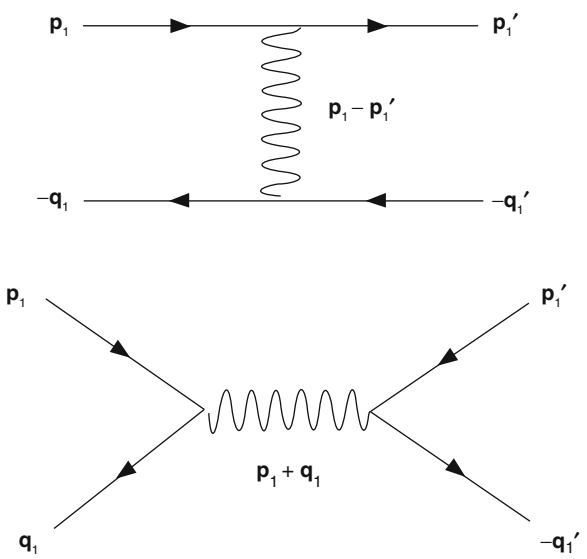

Fig. 7.12 Feynman diagrams for positron–electron Coulomb scatter. *Top*: direct interaction; *bottom*: annihilation intermediate-state interaction

$$\frac{d\sigma}{dQ}=\frac{2\pi r_0^2 m_e}{\beta^2 T^2}\left[\left(\frac{T}{Q}\right)^2-\left(\frac{\gamma^2-1}{\gamma^2}\right)\left(\frac{T}{Q}\right)+\frac{1}{2}\left(\frac{\gamma-1}{\gamma}\right)^2 -\left(\frac{\gamma-1}{\gamma+1}\right)\left\{\left(\frac{\gamma+2}{\gamma}\right)\left(\frac{T}{Q}\right)-2\left(\frac{\gamma^2-1}{\gamma^2}\right) +\left(\frac{\gamma-1}{\gamma}\right)^2\left(\frac{Q}{T}\right)\right\}+\left(\frac{\gamma-1}{\gamma+1}\right)^2 \times\left\{\frac{1}{2}+\frac{1}{\gamma}+\frac{3}{2\gamma^2}-\left(\frac{\gamma-1}{\gamma}\right)^2\left(\frac{Q}{T}\right)\left(1-\left(\frac{Q}{T}\right)\right)\right\}\right]. \tag{7.173}$$

7.3.4.3 Hard Collision Stopping Powers

Massive Projectiles ($m \gg m_e$)

As the differential cross sections in energy transfer for massive spin-1/2 and spin-1 projectiles reduce to that for a massive spin-0 projectile at low kinetic energies, the spin-0 case is considered first. The general expression for the mass hard collision stopping power is,

$$\left(\frac{dE}{\rho dx}\right)_{col,H}=N_A\left(\frac{Z}{A}\right)\int_{Q_C}^{Q_{max}} dQ\,Q\frac{d\sigma}{dQ} \tag{7.174}$$

where the integral limits are Q_C, which separates soft and hard collisions, and the maximum energy transferred to the target electron, Q_{max}, which is set by the relevant kinematics as shown in Chap. 2. The mass hard collision stopping power for a massive spin-0 particle is,

$$\begin{aligned}\left(\frac{dE}{\rho dx}\right)_{col,H}&=N_A\left(\frac{Z}{A}\right)\int_{Q_C}^{Q_{max}} dQ\,Q\frac{d\sigma}{dQ}\\&=C\left(\frac{Z}{A}\right)\left(\frac{z}{\beta}\right)^2\int_{Q_C}^{Q_{max}}\frac{dQ}{Q}\left[1-\beta^2\frac{Q}{Q_{max}}\right]\\&=C\left(\frac{Z}{A}\right)\left(\frac{z}{\beta}\right)^2\left[\ln\left(\frac{Q_{max}}{Q_C}\right)-\beta^2\left(\frac{Q_{max}-Q_C}{Q_{max}}\right)\right].\end{aligned} \tag{7.175}$$

In a hard collision, the energy transfer is assumed to be sufficiently high ($Q_{max} \gg Q_C$) to allow this to be simplified to the form,

$$\left(\frac{dE}{\rho dx}\right)_{Col,H}=C\left(\frac{Z}{A}\right)\left(\frac{z}{\beta}\right)^2\left[\ln\left(\frac{Q_{max}}{Q_C}\right)-\beta^2\right] \quad \text{Spin-0.} \tag{7.176}$$

Now consider the mass hard collision stopping power for a massive spin-1/2 projectile ,

$$\begin{aligned}\left(\frac{dE}{\rho dx}\right)_{col,H}&=C\left(\frac{Z}{A}\right)\left(\frac{z}{\beta}\right)^2\int_{Q_C}^{Q_{max}}\times\frac{dQ}{Q}\left[1-\beta^2\frac{Q}{Q_{max}}+\frac{1}{2}\left(\frac{Q}{T+m}\right)^2\right]\\&=C\left(\frac{Z}{A}\right)\left(\frac{z}{\beta}\right)^2\times\left[\ln\left(\frac{Q_{max}}{Q_C}\right)-\beta^2\left(\frac{Q_{max}-Q_C}{Q_{max}}\right)+\frac{1}{4}\frac{Q_{max}^2-Q_C^2}{(T+m)^2}\right]\\&=C\left(\frac{Z}{A}\right)\left(\frac{z}{\beta}\right)^2\left[\ln\left(\frac{Q_{max}}{Q_C}\right)-\beta^2+\left(\frac{Q_{max}}{2(T+m)}\right)^2\right]\quad \text{Spin-}1/2.\end{aligned} \tag{7.177}$$

where $Q_{max} > Q_C$. Note that, for a massive spin-1/2 projectile with a rest mass much greater than the maximum energy transfer, the last squared-term in the square brackets can be neglected and this result reduces to the simpler spin-0 expression.

Electron and Positron Projectiles

The restricted mass hard collision stopping power for an electron projectile is,

$$\left(\frac{dE}{\rho\,dx}\right)_{Col,H,\Delta}=N_A\left(\frac{Z}{A}\right)\int_{Q_C}^{\Delta} dQ\,Q\frac{d\sigma}{dQ} \tag{7.178}$$

where the Møller differential cross section is to be used in the integral. Unlike the derivations of the massive particle hard collision stopping powers, an

upper limit of integration $\Delta Q_{max} = T/2$ has been specified so as to ignore those energy transfers greater than Δ. Although the restricted mass collision stopping power can be defined for any projectile, the discussion here will be limited to the electron projectile for dosimetric interest.

The mass collision stopping power for the Møller cross section is,

$$\left(\frac{dE}{\rho\, dx}\right)_{Col,H,\Delta} = C\left(\frac{Z}{A}\right)\frac{1}{\beta^2 T^2}\int_{Q_C}^{\Delta} dQQ \times\left[\left(\frac{T}{Q}\right)^2+\left(\frac{Q}{T-Q}\right)+\left(\frac{\gamma-1}{\gamma}\right)^2 -\left(\frac{2\gamma-1}{\gamma^2}\right)\left(\frac{T}{Q}\right)\left(\frac{Q}{T-Q}\right)\right] = C\left(\frac{Z}{A}\right)\frac{1}{\beta^2}\left[\ln\frac{\Delta(T-\Delta)}{Q_C(T-Q)} +\left(\frac{T}{T-\Delta}-\frac{T}{T-Q}\right)+\left(\frac{\gamma-1}{\gamma}\right)^2 \times\left(\frac{\Delta^2-Q_C^2}{2T^2}\right)-\left(\frac{2\gamma-1}{\gamma^2}\right)\ln\left(\frac{T-Q_C}{T-\Delta}\right)\right]. \tag{7.179}$$

This expression can be simplified by defining the normalized kinematic variables,

$$\delta \equiv \frac{\Delta}{T} \tag{7.180}$$

$$\tau_C \equiv \frac{Q_C}{T} \tag{7.181}$$

to obtain,

$$\left(\frac{dE}{\rho\, dx}\right)_{Col,H,\Delta} = C\left(\frac{Z}{A}\right)\frac{1}{\beta^2}\left[\ln\frac{\delta(1-\delta)}{\tau_C(1-\tau_C)} +\left(\frac{1}{1-\delta}-\frac{1}{1-\tau_C}\right)+\left(\frac{\gamma-1}{\gamma}\right)^2 \times\left(\frac{\delta^2-\tau_C^2}{2}\right)-\left(\frac{2\gamma-1}{\gamma^2}\right)\ln\left(\frac{1-\tau_C}{1-\delta}\right)\right]. \tag{7.182}$$

As the selection of Q_C is somewhat arbitrary, its value should ensure that $\tau_C \ll 1$ which allows the ${\tau_C}^2$ term to be neglected and to reduce this expression for the electron restricted mass hard collision stopping power to,

$$\left(\frac{dE}{\rho\, dx}\right)_{Col,H,\Delta} = C\left(\frac{Z}{A}\right)\frac{1}{\beta^2}\left[\ln\frac{\delta(1-\delta)}{\tau_C} +\left(\frac{1}{1-\delta}-1\right)+\left(\frac{\gamma-1}{\gamma}\right)^2\left(\frac{\delta^2}{2}\right) +\left(\frac{2\gamma-1}{\gamma^2}\right)\ln(1-\delta)\right] - \text{Electron (restricted)}. \tag{7.183}$$

The unrestricted mass hard collision stopping power is simply that for the parameter $\delta = 1/2$, and,

$$\left(\frac{dE}{\rho\, dx}\right)_{Col,H,\Delta=T/2} = C\left(\frac{Z}{A}\right)\frac{1}{\beta^2} \times\left[\ln\frac{1}{4\tau_C}+1+\frac{1}{8}\left(\frac{\gamma-1}{\gamma}\right)^2 -\left(\frac{2\gamma-1}{\gamma^2}\right)\ln 2\right] - \text{Electron(unrestricted)}. \tag{7.184}$$

which corresponds to the result originally given by Rohrlich and Carlson (1954).

The unrestricted mass hard collision stopping power for a positron projectile is calculated as for an electron project but with the Bhabha differential cross section.

7.3.5 Combined Mass Hard and Soft Collision Stopping Powers

7.3.5.1 Introduction

Having now derived the soft and hard collision stopping powers, these can be combined to form the complete collision stopping power. The Bethe quantum-mechanical result will be used for the soft collision stopping power expression.

7.3.5.2 Massive Projectiles ($m \gg m_e$)

The Bethe mass collision stopping power, for when spin is neglected, is given by the sum of the Bethe

mass soft collision and the mass hard collision stopping power of a massive spin-0 projectile,

$$\left(\frac{dE}{\rho dx}\right)_{Col} = \left(\frac{dE}{\rho dx}\right)_{Col,S} + \left(\frac{dE}{\rho dx}\right)_{Col,H}$$
$$= C\left(\frac{Z}{A}\right)\left(\frac{z}{\beta}\right)^2\left[\ln\left(\frac{2m_e Q_C}{\bar{I}^2}\gamma^2\beta^2\right) - \beta^2 + \ln\left(\frac{Q_{max}}{Q_C}\right) - \beta^2\right]$$
$$= C\left(\frac{Z}{A}\right)\left(\frac{z}{\beta}\right)^2\left[\ln\left(\frac{2m_e Q_{max}}{\bar{I}^2}\gamma^2\beta^2\right) - 2\beta^2\right]. \quad (7.185)$$

From Chap. 2, the maximum energy transfer to an electron for the case of a heavy projectile is $Q_{max} = 2m_e\gamma^2\beta^2$. Inserting this gives the complete mass collision stopping power for a massive spin-0 projectile,

$$\left(\frac{dE}{\rho\, dx}\right)_{Col} = 2C\left(\frac{Z}{A}\right)\left(\frac{z}{\beta}\right)^2\left[\ln\left(\frac{2m_e\gamma^2\beta^2}{\bar{I}}\right) - \beta^2\right] \quad \text{Spin-0.} \quad (7.186)$$

For a massive spin-1/2 projectile (proton),

$$\left(\frac{dE}{\rho dx}\right)_{Col} = \left(\frac{dE}{\rho dx}\right)_{Col,S} + \left(\frac{dE}{\rho dx}\right)_{Col,H}$$
$$= C\left(\frac{Z}{A}\right)\left(\frac{z}{\beta}\right)^2\left[\ln\left(\frac{2m_e Q_C}{\bar{I}^2}\gamma^2\beta^2\right) - \beta^2 + \left(\frac{Q_{max}}{2(T+m)}\right)^2 + \ln\left(\frac{Q_{max}}{Q_C T_{e,C}}\right) - \beta^2\right]$$
$$= C\left(\frac{Z}{A}\right)\left(\frac{z}{\beta}\right)^2\left[\ln\left(\frac{2m_e Q_{max}}{\bar{I}^2}\gamma^2\beta^2\right) - 2\beta^2 + \left(\frac{Q_{max}}{2(T+m)}\right)^2\right] = 2C\left(\frac{Z}{A}\right)\left(\frac{z}{\beta}\right)^2 \times\left[\ln\left(\frac{2m_e\gamma^2\beta^2}{\bar{I}}\right) - \beta^2 + \left(\frac{1}{2}\frac{m_e}{(T+m)}\gamma^2\beta^2\right)^2\right] \quad \text{Spin-}1/2. \quad (7.187)$$

As $m \gg m_e$, it is clear that the mass collision stopping power for a massive spin-1/2 projectile reduces to that for a spin-0 projectile at low kinetic energies (i.e., $\gamma^2\beta^2 \to 0$). Figure 7.13 shows the mass collision stopping power calculated for a proton in carbon and lead. Here, the mean ionization potentials for carbon and lead are taken to be equal to 78 and 823 eV, respectively. Both curves of $(dE/\rho\, dx)_{Col}$ exhibit the same characteristic behavior of a decrease

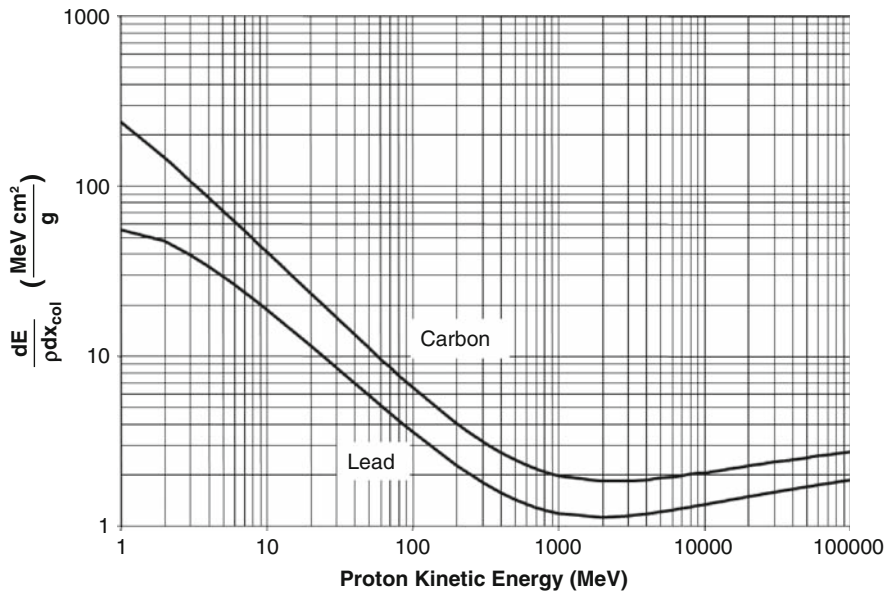

Fig. 7.13 Mass collision stopping powers for protons in carbon and lead

with increasing kinetic energy, due to the β^{-2} factor, to a broad minimum of about 1–2 MeV cm^2/g which occurs at a particle kinetic energy equal to about three times its rest mass. This is referred to as the minimally-ionizing region. With increasing kinetic energy, the mass collision stopping power increases logarithmically due to the $\ln(\gamma^2\beta^2) - \beta^2$ term. This increase is monotonic as the medium is still considered to be a dilute monatomic gas, but could be quenched in condensed media due to polarization of the medium. It should be noted that, for a given projectile kinetic energy, the mass collision stopping power for carbon ($Z = 6$) is greater than that for lead ($Z = 82$). This is a result of the energy loss being dominated by interactions with atomic electrons over those with the nucleus and the electron density being proportional to the ratio Z/A. As a result, the ratio of the carbon to lead mass collision stopping powers is (excluding the effect of the mean ionization potential which is limited due to its placement within the logarithm),

$$\frac{\left(\frac{Z}{A}\right)_C}{\left(\frac{Z}{A}\right)_{Pb}} = \frac{\left(\frac{6}{12}\right)}{\left(\frac{82}{208}\right)} = 1.268$$

In other words, the mass collision stopping power for carbon is greater than that for lead due to the greater number of electrons per unit mass.

7.3.5.3 Electron and Positron Projectiles

To obtain the unrestricted mass collision stopping power of an electron projectile, the Bethe mass soft collision stopping power and the Møller mass hard collision stopping power are summed,

$$\begin{aligned}\left(\frac{dE}{\rho dx}\right)_{Col} &= \left(\frac{dE}{\rho dx}\right)_{Col,S} + \left(\frac{dE}{\rho dx}\right)_{Col,H} \\ &= C\left(\frac{Z}{A}\right)\left(\frac{1}{\beta}\right)^2\left[\ln\left(\frac{2m_eQ_C}{\bar{I}^2}\gamma^2\beta^2\right)\right. \\ &\quad -\beta^2 + \ln\left(\frac{T}{4Q_C}\right) + 1 + \frac{1}{8}\left(\frac{\gamma-1}{\gamma}\right)^2 \\ &\quad \left.-\left(\frac{2\gamma-1}{\gamma^2}\right)\ln 2\right] = C\left(\frac{Z}{A}\right)\left(\frac{1}{\beta}\right)^2 \\ &\quad \times\left[\ln\left(\frac{m_eT}{2\bar{I}^2}\gamma^2\beta^2\right) + f^-(\gamma)\right]\end{aligned} \tag{7.188}$$

where T is the electron kinetic energy and

$$f^-(\gamma) = 1 - \beta^2 + \frac{1}{8}\left(\frac{\gamma-1}{\gamma}\right)^2 - \left(\frac{2\gamma-1}{\gamma^2}\right)\ln 2. \tag{7.189}$$

By using the relativistic relationship,

$$\begin{aligned} m_e\gamma^2\beta^2 &= m_e(\gamma^2 - 1) \\ &= T(\gamma + 1)\end{aligned}$$

the electron mass hard collision stopping power is simplified to,

$$\left(\frac{dE}{\rho dx}\right)_{Col} = C\left(\frac{Z}{A}\right)\left(\frac{1}{\beta}\right)^2\left[\ln\left(\frac{T^2(\gamma+1)}{2\langle I\rangle^2}\right) + f^-(\gamma)\right] - \text{Electron(unrestricted)}. \tag{7.190}$$

The electron restricted mass collision stopping power (i.e., that which excludes energy transfers to the medium greater than Δ) is,

$$\begin{aligned}\left(\frac{dE}{\rho dx}\right)_{Col,\Delta} &= \left(\frac{dE}{\rho dx}\right)_{Col,S} + \left(\frac{dE}{\rho dx}\right)_{Col,H,\Delta} \\ &= C\left(\frac{Z}{A}\right)\left(\frac{1}{\beta}\right)^2\left[\ln\left(\frac{2m_eQ_C}{\bar{I}^2}\gamma^2\beta^2\right)\right. \\ &\quad -\beta^2 + \ln\left(\frac{\Delta\left(1-\frac{\Delta}{T}\right)}{Q_C}\right) + \left(\frac{1}{1-\left(\frac{\Delta}{T}\right)} - 1\right) \\ &\quad \left.+\left(\frac{\gamma-1}{\gamma}\right)^2\frac{\Delta^2}{2T^2} + \left(\frac{2\gamma-1}{\gamma}\right)\ln\left(1-\frac{\Delta}{T}\right)\right] \\ &= C\left(\frac{Z}{A}\right)\left(\frac{1}{\beta}\right)^2\left(\ln\left(\frac{2\Delta(T-\Delta)}{\langle I\rangle^2}(\gamma+1)\right)\right. \\ &\quad \left.+ f^-(\gamma,\Delta)\right) \\ &\quad - \text{Electron (restricted)}.\end{aligned} \tag{7.191}$$

where,

$$f^{-}(\gamma,\Delta)=\left(\frac{\Delta}{T-\Delta}\right)-\beta^2+\left(\frac{2\gamma-1}{\gamma}\right)\times\ln\left(\frac{T-\Delta}{T}\right)+\left(\frac{\gamma-1}{\gamma}\right)^2\frac{\Delta^2}{2T^2}. \tag{7.192}$$

Similarly, to obtain the positron complete collision stopping power, the Bethe mass soft and the Bhabha mass hard collision stopping powers are summed,

$$\left(\frac{dE}{\rho dx}\right)_{Col}=C\left(\frac{Z}{A}\right)\frac{1}{\beta^2}\left[\ln\left(\frac{T^2(\gamma+1)}{2\bar{I}^2}\right)+f^{+}(\gamma)\right] \quad \text{Positron} \tag{7.193}$$

where

$$f^{+}(\gamma)=2\ln 2-\frac{\beta^2}{12}\times\left[23+\frac{14}{(\gamma+1)}+\frac{10}{(\gamma+1)^2}+\frac{4}{(\gamma+1)^3}\right] \tag{7.194}$$

A comparison of the (unrestricted) electron and positron mass collision stopping powers shows that the difference between the electron and positron mass collisions stopping powers resides within the difference between $f^{-}(\gamma)$ and $f^{+}(\gamma)$. These two terms are plotted in Fig. 7.14 as functions of the kinetic energy of the incident electron/positron (only the unrestricted version of $\Delta = T/2$ is used for the electron term). At low energies, $f^{+}(\gamma)$ exceeds $f^{-}(\gamma)$ by about a factor of 3 and decreases with positron kinetic energy to equal $f^{-}(\gamma)$ at about 0.32 MeV. Note that both $f^{-}(\gamma)$ and $f^{+}(\gamma)$ become negative with increasing kinetic energy. However, when the electron and positron unrestricted mass collision stopping powers for carbon and lead are compared, as shown in Fig. 7.15, it is sees that there is little difference between the two stopping powers which reflects the dominance of the logarithmic term in the collision stopping power expression over the magnitudes of $f^{-}(\gamma)$ and $f^{+}(\gamma)$. The mass collision stopping power curves exhibit the same characteristics as those derived earlier for the proton. A clear comparison of the curves shows that while the mass collision stopping power of protons, electrons, and positrons are roughly equal in the minimally-ionizing region, the kinetic energy at which this region occurs is equal to roughly equal to 3 times the particle rest mass (3 GeV for protons and

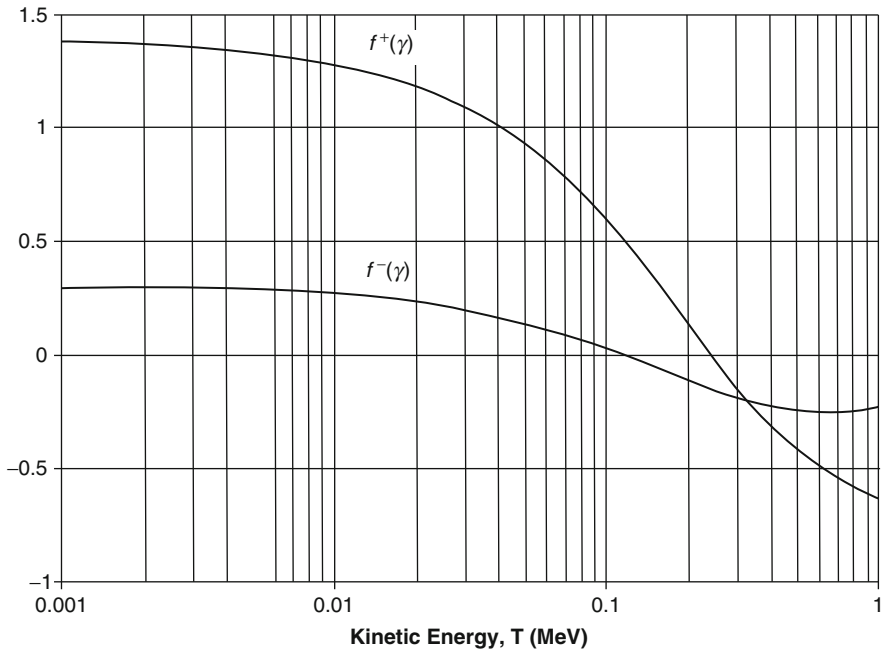

Fig. 7.14 The functions $f^{-}(\gamma)$ and $f^{+}(\gamma)$ of the mass collision stopping powers of electrons and positrons, respectively, as a function of the kinetic energy of the electron or positron

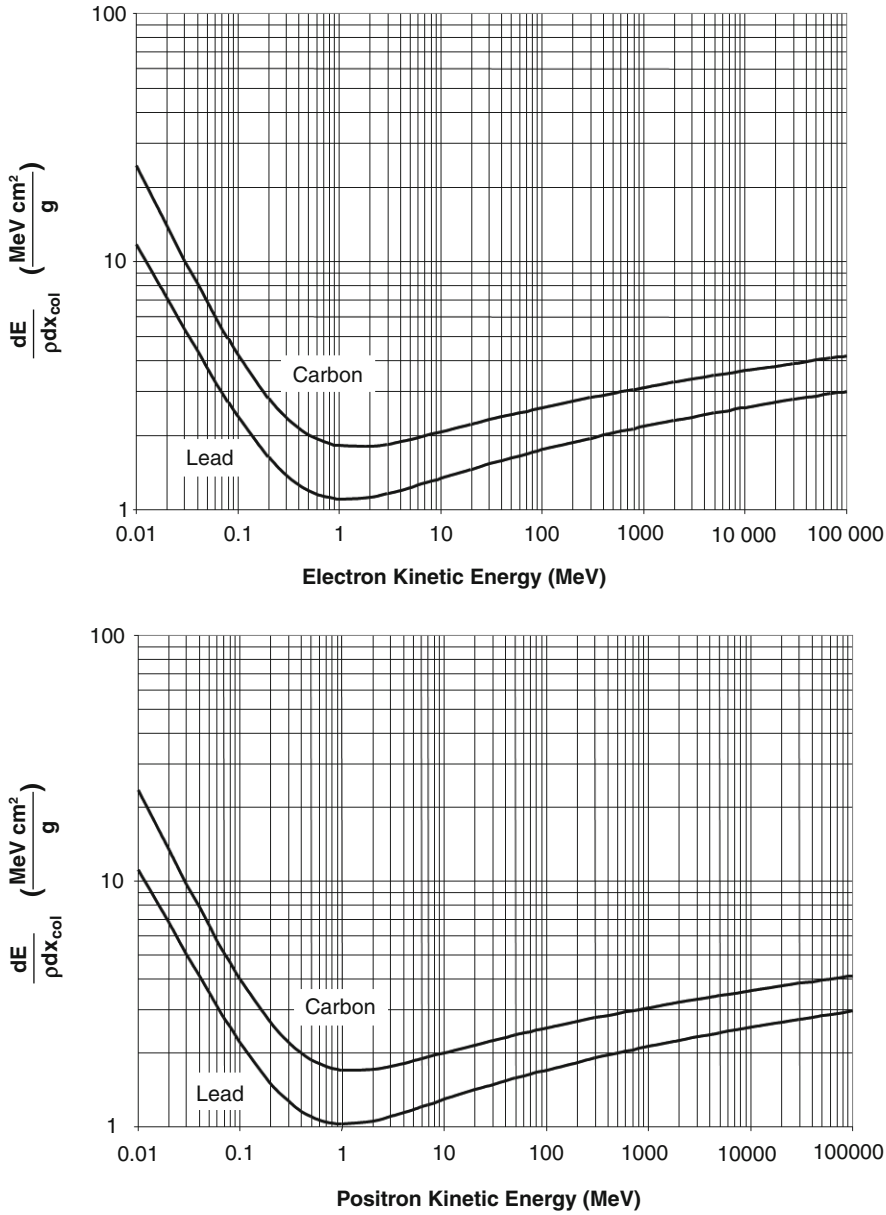

Fig. 7.15 Mass collision stopping powers of electrons and positrons in carbon and lead. Note that no density effect corrections have been applied

1.5 MeV for electrons and positrons) or for a particle speed of the order of $\beta \approx 0.8$.

7.3.6 Mean Excitation Energy

Except for the atomic number and atomic mass number, the only other explicit property of the medium which appears in the expression for the mass collision stopping power is the mean excitation energy (or ionization potential) $\bar{I}$, which is contained within the logarithmic term. The logarithm of the mean ionization potential can be obtained by ab initio calculations for a gas of free atoms or using measured optical oscillator distribution data (Nobel et al. 2005). In a closely related fashion, it is also possible to calculate it from measured dielectric properties of the medium and, as explicitly shown later, to extract it from measured stopping power data. The placement of $\bar{I}$ within the

logarithm ensures that variations in the calculated collision stopping power are relatively insensitive to the uncertainty in the value of $\bar{I}$. Hence, for practical dosimetry evaluations, a theoretical discussion of $\bar{I}$ can be provided in reduced detail. Expansive discussions of the mean ionization potential can be found in those reviews by Uehling (1954) and Fano (1964) and in ICRU Reports 37 (1984) and 49 (1993).

Recall that, as a consequence of the derivation of the Bethe mass soft collision stopping power, the mean excitation energy was shown to be described by the first energy moment of the optical oscillator distribution,

$$\ln \bar{I} = \frac{1}{Z} \int dE_n \frac{df_n(Z)}{dE_n} \ln E_n$$

with the normalization,

$$\int dE_n \frac{df_n(Z)}{dE_n} = Z.$$

While it is possible to calculate $\ln \bar{I}$ for a gas of free atoms using calculated oscillator strength distributions, another approach is to use the moments of this distribution as defined by (Dalgarno 1960),

$$M(m) = \int dE_n \frac{df_n(Z)}{dE_n} E_n^m \tag{7.195}$$

where, from the normalization requirement, the zeroth moment is,

$$M(0) = Z.$$

The logarithm of the mean ionization potential can be written by using $dE_n^m/dm = E_n^m \ln E_n$,

$$\ln \bar{I} = \frac{\left.\frac{dM(m)}{dm}\right|_{m=0}}{M(0)}. \tag{7.196}$$

ICRU Report 37 (1993) notes that the moments for m equal to -1, 1, and 2 can be determined theoretically and that for m equal to -2 can be extracted from measured data. An analytical fit to these four moments and can be made, from which the ratio in (7.196) can be determined.

Another method was proposed by Lindhard and Scharff (1953) using a free electron gas model,

$$\ln \bar{I} = \frac{1}{Z} \int d^3\mathbf{r}\, \rho_e(r) \ln\left(\sqrt{2}\hbar\omega_p(r)\right) \tag{7.197}$$

where ω_p is the electron plasma frequency for the electron density $\rho_e(r)$[13] and $\ln \bar{I}$ and $\hbar\omega_p(r)$ must have the same units of energy.

The approaches above are limited to gaseous media within which the positions of the electrons considered uncorrelated. For condensed media, $\ln \bar{I}$ can be calculated from an expression originally derived by Fano (1956),

$$\ln \bar{I} = \frac{2}{\pi\omega_p^2} \int_0^\infty d\omega\ \mathrm{Im}\left[-\frac{1}{\varepsilon_R(\omega)}\right] \omega \ln \hbar\omega \tag{7.198}$$

where $\varepsilon_R(\omega)$ is the complex relative dielectric permittivity and the imaginary component describes the absorption of electromagnetic energy.

Parametric expressions of $\bar{I}$ are useful for dosimetry calculations. Because $\bar{I}$ is found within the logarithmic term of the collision stopping power, any effects upon the stopping power due to uncertainties in $\bar{I}$ will be correspondingly limited. Some authors have approximated the mean excitation potential as a linear function of the medium's atomic number,

$$\bar{I} = Z\ hcR_\infty \tag{7.199}$$

where hcR is the Rydberg energy, 13.6 eV. A number of semi-empirical representations of $\bar{I}$ as a function of the medium's atomic number have been provided in the literature. One particularly useful one is presented by Segrè (1977),

$$\bar{I} = 9.1\left(1 + \frac{1.9}{Z^{2/3}}\right) \text{eV} \quad \text{for} \quad Z \geq 4 \tag{7.200}$$

[13] The plasma frequency describes the oscillatory motion of free electrons in a plasma displaced from a uniform background of ions. The equation of motion for an electron in the simplest case is given by $m_e d^2x/dt^2 = -eE - (\rho_e e^2/\varepsilon_0)x$ where we have taken the restoring electric field to be equal to $-\mathbf{P}/\varepsilon_0$ where $\mathbf{P}$ is the polarization. Solving this equation yields the plasma frequency, $\omega_p = \sqrt{\rho_e e^2/\varepsilon_0 m_e}$.

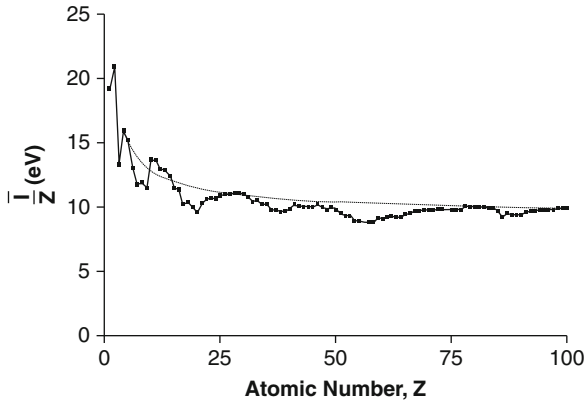

Fig. 7.16 Mean ionization potential normalized to atomic number as a function of atomic number. The curve is the parameterization of Segrè and the data points with connecting lines are from tabulated data provided by ICRU Report 37 (1984)

Segrè's parameterization of $\bar{I}$, normalized to the atomic number of the medium, is shown in Fig. 7.16. Also shown are values from ICRU Report 37 for condensed media. While $\bar{I}/Z$ rapidly decreases with atomic number to an approximately constant value of about 10 eV, it can be seen that there are irregularities attributable to atomic shell structure.

7.3.7 Stopping Number

7.3.7.1 Introduction

The mass collision stopping powers derived to this point are what can be crudely considered to be "zeroth"-order results is that they were obtained on the basis of three simplifying assumptions:

- The projectile speed is much higher than the atomic electron orbital speed allowing the collision kinematics to be derived with the electron assumed to be at rest.
- For a single atom, the atomic electron "cloud" is not displaced by the electric field of the moving charged particle.
- The medium is treated as a cold dilute gas which is not polarized by the projectile's electric field.

In order to extend the expressions of the mass collision stopping powers to enable calculations for more realistic cases, "higher order" correction terms are applied in order to compensate for these simplifying assumptions. A transparent way of doing so is by writing the mass collision stopping power as a series in order to isolate these individual corrections,

$$\left(\frac{dE}{\rho\, dx}\right)_{Col} = 2C\left(\frac{Z}{A}\right)\left(\frac{z}{\beta}\right)^2 L(\beta) \tag{7.201}$$

where $L(\beta)$ is defined as the stopping number given in terms of a summation weighted by powers of the projectile electric charge (normalized to the unit charge, e),

$$L(\beta) = \sum_{j=0}^{2} z^j L_j(\beta). \tag{7.202}$$

For convenience, the zeroth-order term of this expansion is written as a series itself,

$$L_0(\beta) = \sum_{k=0}^{2} L_{0k}(\beta) \tag{7.203}$$

to give,

$$L(\beta) = \sum_{k=0}^{2} L_{0k}(\beta) + \sum_{j=1}^{2} z^j L_j(\beta). \tag{7.204}$$

Note that the stopping number and its terms are explicit functions of the projectile speed through momentum or kinetic energy. From the expression of the mass collision stopping power for a spin-less massive projectile, the zeroth-order term in the $L_0(\beta)$ summation is,

$$L_{00}(\beta) = \ln\left(\frac{2m_e\gamma^2\beta^2}{\bar{I}}\right) - \beta^2 \tag{7.205}$$

The $L_{01}(\beta)$ term accounts for the reduction in stopping power as a result of the projectile slowing down to speeds comparable to those of the target atomic electrons,

$$L_{01}(\beta) = -\frac{C_e(\beta)}{Z} \tag{7.206}$$

and is known as the shell correction term. As it is to be independent of the atomic number of the medium, it

contains that quantity in the denominator in order to cancel the corresponding factor in the leading multiplicative term of (7.201). In a dense medium, the projectile polarizes the atoms and reduces the penetration of the electric field into the medium thus diminishing the stopping power. The $L_{02}(\beta)$ term accounts for this reduction in stopping power,

$$L_{02}(\beta) = \delta/2. \tag{7.207}$$

This can be an important effect for fast electrons in soft tissue. The first-order term of the stopping number, $zL_1(\beta)$ is actually proportional to the cube of the projectile's atomic number due to the z^2 in the leading multiplicative term. Hence, this term accounts for the minute difference in stopping powers between a particle and its antiparticle as a result of the differential displacement of the atomic electron cloud by each: a positively-charged projectile will attract the atomic electrons to bring them closer to its trajectory to yield a slightly greater stopping power than its negatively-charged antiparticle which repels the electrons. Finally, the second-order term, $z^2L_2(\beta)$, arises from the reconciliation by Bloch of the Bohr and Bethe theories.

The $L_{01}(\beta)$, $zL_1(\beta)$, and $z^2L_2(\beta)$ terms are now discussed; the polarization effect accounted for by $L_{02}(\beta)$ is discussed separately.

7.3.7.2 Atomic Electron Shell Correction

Up to this point, in the calculation of the collision stopping power the orbital speeds of the atomic electrons have been assumed to be much less than the projectile speed or, equivalently, the electrons are considered to be initially at rest. Clearly, this simplified the kinematics of the hard stopping power calculation. However, for low-energy projectiles with a speed comparable to the orbital speeds, this simplification no longer holds. Moreover, if the slow projectile is an ion (e.g., an α particle), it can capture these electrons, reducing its effective charge and even further diminishing the stopping power.

The first electrons to be affected are those in the K-shell which are the most tightly bound and have the greatest speeds, followed by the L-shell electrons, etc. Thus, as the particle speed decreases, the contributions to the stopping power decrease sequentially. The term accounting for this effect is $L_{01}(\beta)$ given by where the $C_e(\beta)$ term is averaged over the contributions of all atomic electrons. Should the density effect described by $L_{02}(\beta)$ be negligible, $L_{01}(\beta)$ can be taken from the definition of the stopping number,

$$\begin{aligned} L_{01}(\beta) &= \frac{1}{2C}\left(\frac{A}{Z}\right)\left(\frac{\beta}{z}\right)^2\left(\frac{dE}{\rho\, dx}\right)_{Col} - L_{00}(\beta) \\ &= \frac{1}{2C}\left(\frac{A}{Z}\right)\left(\frac{\beta}{z}\right)^2\left(\frac{dE}{\rho\, dx}\right)_{Col} \\ &\quad - \ln\left(\frac{2m_e\gamma^2\beta^2}{\bar{I}}\right) + \beta^2. \end{aligned} \tag{7.208}$$

Thus,

$$\begin{aligned} C_e(\beta) &= -Z\,L_{01}(\beta) \\ &= \frac{1}{2C}A\left(\frac{\beta}{z}\right)^2\left(\frac{dE}{\rho\, dx}\right)_{Col} \\ &\quad + Z\left(\ln\left(\frac{2m_e\gamma^2\beta^2}{\bar{I}}\right) - \beta^2\right) \end{aligned} \tag{7.209}$$

Details of how $C_e(\beta)$ can be derived are provided by Ziegler (1999) and ICRU Report 37 (1984). A semi-empirical parameterization of $C_e(\beta)$, useful for calculational purposes, was provided by Barkas (1962),

$$\begin{aligned} C_e = \bar{I}^2\Bigg\{&\left(\frac{0.42237}{(\gamma\beta)^2} + \frac{0.0304}{(\gamma\beta)^4} - \frac{0.00038}{(\gamma\beta)^6}\right) \times 10^{-6} \\ &+ \bar{I}\left(\frac{3.858}{(\gamma\beta)^2} - \frac{0.1668}{(\gamma\beta)^4} + \frac{0.00158}{(\gamma\beta)^6}\right) \times 10^{-9}\Bigg\} \end{aligned} \tag{7.210}$$

where $\bar{I}$ is in units of electron volt. The validity of this expression for C_e is limited to $\gamma\beta > 0.13$. Figure 7.17

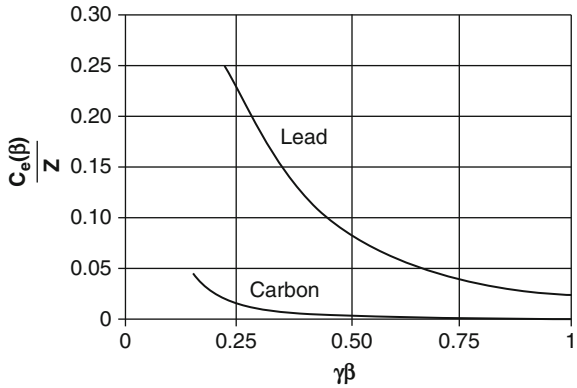

Fig. 7.17 Shell correction terms for carbon and lead as a function of $\gamma\beta$

shows the shell correction term $C_e(\beta)/Z$ for carbon and lead as functions of proton kinetic energy. The $C_e(\beta)/Z$ values decrease with increasing kinetic energy (i.e., increasing particle speed beyond the atomic electron speeds) with $C_e(\beta)/Z$ greater for lead than for carbon due to the higher atomic electron speeds.

7.3.7.3 Barkas Correction Term

As noted earlier, the first-order term of the stopping number is proportional to z^3 due to the z^2 weighting applied to the series. As a result, it will be sensitive to the sign of that charge. The fact that this should be so (even though the Bethe result predicts no such dependence due to the z^2 term) was first apparent in measurements by Barkas et al. (1956) of the kaon decay to three pions which showed that the range of the product π^+ was slightly less (of the order of 0.4%) than that of the π^- for the same initial speed. This indicated that the stopping power for the positively-charged particle was greater than its negatively-charged antiparticle, an effect due to the respective repulsion and attraction of the atomic electrons with a corresponding decrease and increase in energy transfer. Additional measurements (Barkas et al. 1963) of the $K^- + p \rightarrow \Sigma^{\pm} + \pi^{\mp}$ reaction repeated this observation. Precise work by Andersen et al. (1969) showed that the α particle stopping power was greater than the factor-of-four multiple over those of protons and deuterons as predicted by the z^2-dependence. Ashley et al. (1972, 1973) provided a thorough theoretical evaluation of the Barkas effect and Lindhard (1976) gave an explicit representation of this effect. The $zL_1(\beta)$ term in the stopping number expansion reduces the stopping power for a negatively-charged projectile relative to its positively-charged antiparticle. From the work by Ashley et al., the Barkas correction term can be written in the form,

$$zL_1(\beta) = \left(\frac{\alpha}{\beta}\right)^3 zZ\,F\left(\frac{\alpha}{\beta} b\sqrt{Z}\right) \tag{7.211}$$

where F(x) is a numerically-evaluated function and b is related to the minimum impact parameter. Values for this correction term are provided in ICRU Report 49 (1993). For high atomic media, Bichsel (1990) extracted the Barkas correction term from measured stopping power data and found that it could be accurately described by a power-law dependence upon the particle speed,

$$L_1(\beta) = k_1\,\beta^{-k_2} \tag{7.212}$$

where, for the example of a gold absorber,

$$k_1 = 0.002833$$

$$k_2 = 1.2$$

Figure 7.18 shows $L_1(\beta)$ for protons and antiprotons in gold as a function of proton kinetic energy. Clearly, the Barkas term becomes significant at low projectile speeds only. The only particle–antiparticle pair of interest to nuclear medicine is that of the electron and positron. As the target particle is also an electron, the Barkas effect would be swamped by the differences between the Møller and Bhabha cross sections.

7.3.7.4 Bloch Correction Term

In the early 1930s, Bloch reconciled the Bohr classical and Bethe quantum-mechanical calculations of the soft collision stopping power by demonstrating that the Bohr result was valid quantum-mechanically if the Bohr energy loss were to be interpreted as a mean value over all possible atomic electron transitions (Ahlen 1980). Bloch then looked at close collisions without the assumption that the target electron being considered as a plane wave in the center-of-mass reference frame and allowed them to be perturbed by the projectile's Coulomb field. This Bloch refinement produced a correction term that was overall proportional to z^4 or, in terms of the stopping number expansion,

$$z^2L_2(\beta) = \psi(1) - \mathrm{Re}\psi\left(1 + i\alpha\frac{z}{\beta}\right) \tag{7.213}$$

where $\psi(z)$ is the logarithmic derivative of the gamma function,[14]

$$\psi(z) = \frac{d\ln\Gamma(z)}{dz} = \frac{1}{\Gamma(z)}\frac{d\Gamma(z)}{dz}. \tag{7.214}$$

[14] This is also referred to as the digamma function.

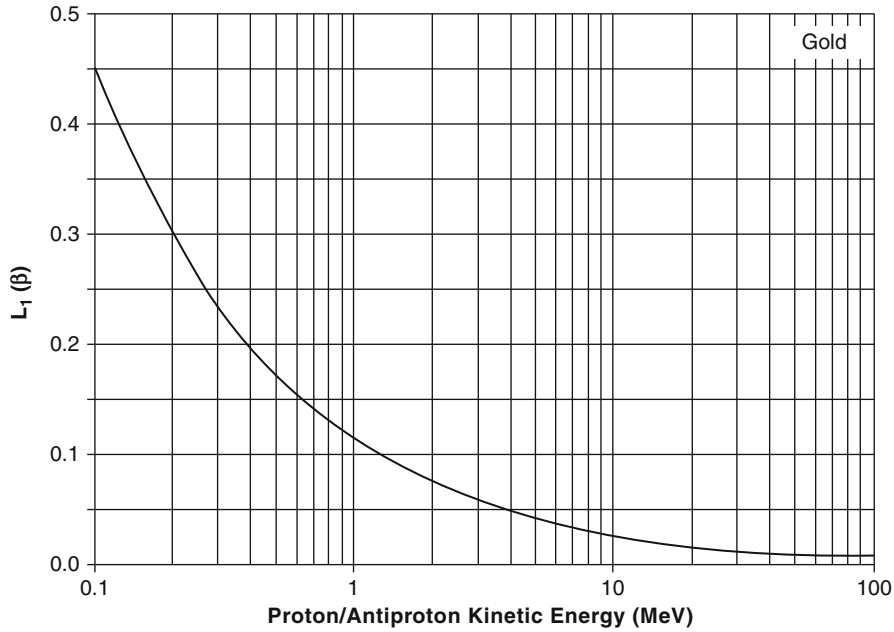

Fig. 7.18 Barkas correction factor in gold for protons and antiprotons calculated from Bichsel's (1990) parameterization

It is possible to rewrite the Bloch correction term as a series by using the identity,

$$\psi(1) = \gamma_{EM}$$

and the series expansion,

$$\mathrm{Re}\psi(1+iy) = -0.5772\cdots + y^2\sum_{n=1}^{\infty}\frac{1}{n(n^2+y^2)},$$

to give,

$$z^2L_2(\beta) = -\left(\alpha\frac{z}{\beta}\right)^2\sum_{n=1}^{\infty}\frac{1}{n\left(n^2+\left(\alpha\frac{z}{\beta}\right)^2\right)}. \quad (7.215)$$

Now consider the asymptotic behaviors of the Bloch correction term due to the projectile charge and speed. To do so, use the asymptotic formula,

$$\mathrm{Re}\psi(1+iy) = \ln y + \frac{1}{12y^2} + \frac{1}{120y^4} + \frac{1}{252y^6} + \cdots \quad \text{for } y \to \infty.$$

Thus, for a slow heavy charged particle (i.e., $\alpha z/\beta \gg 1$), the Bloch correction term is,

$$z^2L_2(\beta) \approx -\gamma_{EM} - \ln\left(\alpha\frac{z}{\beta}\right) \quad (7.216)$$

In this limit, the Bloch correction leads to the Bohr classical form of the collision stopping power. On the other hand, one does not achieve the Bethe result in the relativistic case of $\alpha z/\beta \to 0$ due to an error in the original derivation and which is discussed by Ahlen (1980). This has a negligible calculational consequence, however, as the Bloch term becomes insignificant in such a case.

7.3.7.5 Complete Stopping Number (excluding density effect)

If the zeroth-, first-, and second-order terms of the stopping number of the past three sections are summed, one obtains the complete stopping power, excluding the $L_{02}(\beta)$ term,

$$L(\beta) = \ln\left(\frac{2m_e}{\bar{I}}\gamma^2\beta^2\right) - \beta^2 - \frac{C_e(\beta)}{Z} - \frac{\delta}{2} + \left(\frac{\alpha}{\beta}\right)^3 zZF\left(\frac{\alpha}{\beta}b\sqrt{Z}\right) - \left(\alpha\frac{z}{\beta}\right)^2 \times\sum_{n=1}^{\infty}\frac{1}{n\left(n^2+\left(\alpha\frac{z}{\beta}\right)^2\right)}. \quad (7.217)$$

7.3.7.6 Effect of Medium Polarization Upon the Stopping Power

Introduction

So far, the projectile's electric field has been implicitly assumed to be in vacuo and, using this approximation, the medium has been assumed to be a cold and dilute monatomic gas. Such simplifications ignore any response of a realistic medium to this moving electric field. Should the particle be traveling in a dense dielectric medium (such as tissue), atoms will be polarized, creating an array of electric dipoles which generate a secondary electric field limiting the particle's electric field at a distance and reducing the stopping power. This effect is expected to be significant at high particle speeds, as shown by Fig. 7.2, where, as $\beta \to 1$, the electric field parallel to the trajectory flattens and the orthogonal component extends such that the dielectric response of the medium limits the relativistic rise in stopping power. Because the magnitude of this dielectric response will be directly related to the number of secondary electric dipoles, it will clearly depend upon the medium's physical density.[15] This reduction in stopping power is referred to as the polarization or density effect and is characterized by a correction term, δ, which is treated as a higher order correction term to the zeroth-order term of the Born series description of the stopping power.

The density effect leads to a reduction in the stopping power of fast electrons in tissue and its consequences are to be investigated in detail. The semiclassical work of Fermi (1940) will guide this derivation.

Electronic Polarization

In order to characterize the properties of a dielectric medium in a time-varying electric field, begin with those of an individual atom. The simplest model of the medium is that of an isotropic monatomic gas with

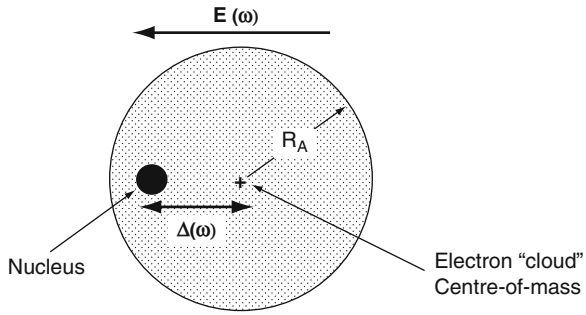

Fig. 7.19 Electronic polarization due to an external electric field

interatomic distances sufficiently large that an atom can be treated in isolation. The atom is taken to be a negatively-charged and mobile spherical electron cloud of charge $-Ze$ and mass Zm_e which, in its unperturbed state, is centered on a fixed nucleus of charge Ze. The electric field of the passing charged particle will perturb the position of this electron cloud and polarize the atom, as shown in Fig. 7.19. At high particle speeds, the shortness of the time duration of the electric field "pulse" experienced by the atom, as shown in Fig. 7.2, will be dominated by high-frequency components and, in frequency space, one can consider the atom as being exposed to a high-frequency electric field. The displacement, Δ, will be limited due to the short duration of the pulse and one can effectively ignore the spatial variation of the field over the atom as a result. The electron cloud will experience a restorative force due to the mutual attraction between it and the nucleus and thus go into oscillatory motion. The attractive force can be calculated by modeling the electron cloud as a uniformly charged sphere of radius R_A with an electric charge density, $(3/4\pi)Ze/R_A^3$. The radial electric field due to this charge at a distance Δ from the center of the atom is found by applying Gauss' law to the sphere of radius Δ,

$$\varepsilon_0\left(4\pi\Delta^2\right)E = \frac{4\pi}{3}\Delta^3\left(\frac{3}{4\pi}\frac{Ze}{R_A^3}\right)$$

from which one obtains an expression for the electric field in terms of the displacement of the atomic electron cloud,

$$E = \frac{Ze}{4\pi\varepsilon_0}\frac{\Delta}{R_A^3} \tag{7.218}$$

[15] Because the interatomic spacings in a gas are greater than those in a solid or liquid, the wider dispersion of atoms in the gaseous phase will limit the dielectric response such that the mass collision stopping power for a given medium will be greater for the condensed phases than for the vapor phase and, hence, this interest in this phenomenon in tissue.

The restoring force is F = ZeE, or

$$F = \frac{(Ze)^2}{4\pi\,\varepsilon_0 R_A^3}\Delta = \eta\Delta. \tag{7.219}$$

This gives,

$$ZeE = \frac{(Ze)^2}{4\pi\,\varepsilon_0}\,\frac{\Delta}{R_A^3}$$

from which the magnitude of the product of the charge and its displacement, electric dipole moment, is obtained,

$$p = Ze\,\Delta = 4\pi\,\varepsilon_0\,R_A^3\,E \tag{7.220}$$

or, in terms of vector quantities,

$$\mathbf{p} = 4\pi\,\varepsilon_0\,R_A^3\,\mathbf{E} \equiv \alpha_e\,\mathbf{E} \tag{7.221}$$

where α_e is defined as the electronic polarizability. It will be noted that the magnitude of the ratio, $\alpha_e/\varepsilon_0 = 4\pi R_A^3$, is the atomic volume.

The resulting equation of motion of the displaced electron cloud is,

$$Zm_e\frac{d^2\Delta(t)}{dt^2} = ZeE(t) - \eta\Delta(t) - \Gamma Zm_e\frac{d\Delta(t)}{dt} \tag{7.222}$$

where a damping force $\Gamma Zm_e\ d\Delta(t)/dt$ with a positive damping constant Γ has been allowed for. This differential equation is readily solvable, as demonstrated earlier in the derivation of the Bohr soft collision stopping power through the Fourier transform. The result in frequency space is,

$$\Delta(\omega) = \frac{\left(\frac{e}{m_e}\right)\mathbf{E}(\omega)}{\left(\omega_0^2 - \omega^2\right) + i\Gamma\omega} \tag{7.223}$$

with a resonant frequency given by,

$$\omega_0 = c\sqrt{Z\frac{r_0}{R_A^3}}. \tag{7.224}$$

As the atomic radius R_A of the order of 10^{-10} m, the resonant frequency will consequently be of the order of 10^{16}–10^{17}/s with a corresponding wavelength in the ultraviolet range of the electromagnetic spectrum. The electric dipole moment in frequency-space is,

$$\begin{aligned}\mathbf{p}(\omega) &= Z\,e\,\Delta(\omega)\\ &= Z\frac{\left(\frac{e^2}{m_e}\right)\mathbf{E}(\omega)}{\left(\omega_0^2 - \omega^2\right) + i\Gamma\omega}.\end{aligned} \tag{7.225}$$

Next, the scale is expanded from that of the individual atom to the macroscopic medium which is taken to be linear and isotropic.[16] The polarization is the number of electric dipoles per unit volume, or,

$$\mathbf{P}(\omega) = \rho_e\frac{\left(\frac{e^2}{m_e}\right)\mathbf{E}(\omega)}{\left(\omega_0^2 - \omega^2\right) + i\Gamma\omega}. \tag{7.226}$$

The electric-flux density vector is related to the electric field and the polarization in frequency space by,

$$\begin{aligned}\mathbf{D}(\omega) &= \varepsilon_0\mathbf{E}(\omega) + \mathbf{P}(\omega)\\ &\equiv \varepsilon_0\mathbf{E}(\omega) + \chi_e(\omega)\varepsilon_0\mathbf{E}(\omega)\\ &= \varepsilon_0(1 + \chi_e(\omega))\mathbf{E}(\omega)\\ &= \varepsilon_0\,\varepsilon_R(\omega)\mathbf{E}(\omega)\end{aligned} \tag{7.227}$$

where $\chi_e(\omega)$ is the electric susceptibility and $\varepsilon_R(\omega) = 1 + \chi_e(\omega)$ is the relative dielectric constant. This result is algebraically manipulated to relate the polarization to the electric field by,

$$\mathbf{P}(\omega) = \varepsilon_0(\varepsilon_R(\omega) - 1)\mathbf{E}(\omega). \tag{7.228}$$

By equating these two expressions for the polarization, the relative dielectric constant can be written as,

$$\begin{aligned}\varepsilon_R(\omega) &= 1 + \frac{\left(\frac{\rho_e}{\varepsilon_0}\,\frac{e^2}{m_e}\right)}{\left(\omega_0^2 - \omega^2\right) + i\Gamma\omega}\\ &= 1 + \frac{\omega_P^2}{\left(\omega_0^2 - \omega^2\right) + i\Gamma\omega}.\end{aligned} \tag{7.229}$$

[16] Should this not be the case, the electric susceptibility and dielectric permittivity scalars would be replaced by tensors.

Separate $\varepsilon_R(\omega)$ into real and imaginary components in order to form the set of dielectric dispersion formulae,

$$\begin{aligned}\varepsilon_R(\omega) &= \left(1+\omega_P^2\left(\frac{\omega_0^2-\omega^2}{\left(\omega_0^2-\omega^2\right)^2+\Gamma^2\omega^2}\right)\right)\\ &\quad -i\,\omega_P^2\left(\frac{\Gamma\omega}{\left(\omega_0^2-\omega^2\right)^2+\Gamma^2\omega^2}\right)\\ &\equiv \varepsilon_R{}'(\omega)-i\varepsilon_R{}''(\omega)\end{aligned} \tag{7.230}$$

As the imaginary component of the relative dielectric permittivity is proportional to Γ, it is also proportional to the power loss within the dielectric.

Electromagnetic Fields in a Dielectric Medium

The next step to calculating the response of a dielectric medium to a moving charged particle requires the calculation of the electromagnetic fields of the projectile within the medium. To do this, Maxwell's equations are solved in Fourier space,

$$\nabla \bullet \mathbf{D} = \rho \tag{7.231}$$

$$\nabla \bullet \mathbf{B} = 0 \tag{7.232}$$

$$\nabla \times \mathbf{E} = -\frac{\partial \mathbf{B}}{\partial t} \tag{7.233}$$

$$\nabla \times \mathbf{H} = \mathbf{J} + \frac{\partial \mathbf{D}}{\partial t} \tag{7.234}$$

where

$$\mathbf{D} = \varepsilon_R\,\varepsilon_0\,\mathbf{E} \tag{7.235}$$

and where it is assumed that the magnetic polarizability of the medium is negligible,

$$\mathbf{B} = \mu_0\,\mathbf{H}. \tag{7.236}$$

The electric field and the magnetic flux density are also defined through scalar and vector potentials,

$$\mathbf{E} = -\nabla\Phi - \frac{\partial \mathbf{A}}{\partial t} \tag{7.237}$$

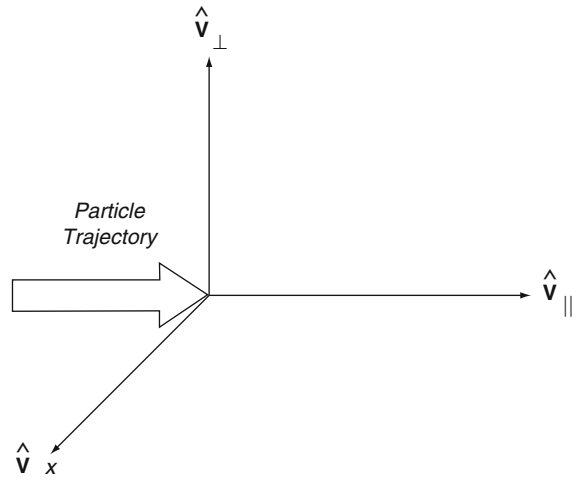

Fig. 7.20 Coordinate system used in the calculation of the electromagnetic fields of a moving charged particle in a dielectric medium

$$\mathbf{B} = \nabla \times \mathbf{A}. \tag{7.238}$$

It is possible to determine these potentials using the four-dimensional Fourier transform,

$$F(\mathbf{k},\omega) = \frac{1}{4\pi^2}\int_{-\infty}^{\infty} d^3\mathbf{x}\int_{-\infty}^{\infty} dt\, F(\mathbf{x},t)e^{-i(\mathbf{k}\bullet\mathbf{x}-\omega t)} \tag{7.239}$$

where k is the wavenumber and ω is the frequency. The coordinate system of Fig. 7.20 where the unit vector $\hat{\mathbf{v}}_{||}$ lies along the particle's trajectory is used. The Fourier transforms of the divergence of **D** and the curl of **B** are,

$$i\mathbf{k}\bullet\mathbf{E}(\mathbf{k},\omega) = \frac{\rho(\mathbf{k},\omega)}{\varepsilon_R(\omega)\varepsilon_0} \tag{7.240}$$

$$-i\,\mathbf{k}\times\mathbf{H}(\mathbf{k},\omega) = \mathbf{J}(\mathbf{k},\omega) + i\omega\varepsilon_R(\omega)\varepsilon_0\mathbf{E}(\mathbf{k},\omega). \tag{7.241}$$

The Fourier transforms of the fields as defined by the potentials are,

$$\mathbf{E}(\mathbf{k},\omega) = -i\mathbf{k}\Phi(\mathbf{k},\omega) + i\omega\mathbf{A}(\mathbf{k},\omega) \tag{7.242}$$

$$\mathbf{H}(\mathbf{k},\omega) = -\frac{\mathrm{i}}{\mu_0}\mathbf{k}\times\mathbf{A}(\mathbf{k},\omega). \tag{7.243}$$

Expressions for $\mathbf{E}(\mathbf{k},\omega)$ and $\mathbf{H}(\mathbf{k},\omega)$ are derived by first determining the scalar and vector potentials. Substituting (7.242) into (7.240),

$$-\mathrm{i}\mathbf{k}\bullet(\mathrm{i}\mathbf{k}\Phi(\mathbf{k},\omega)-\mathrm{i}\omega\mathbf{A}(\mathbf{k},\omega)) = \frac{\rho(\mathbf{k},\omega)}{\varepsilon_R(\omega)\varepsilon_0}$$

which leads to,

$$\mathrm{k}^2\Phi(\mathbf{k},\omega)-\omega\,\mathbf{k}\bullet\mathbf{A}(\mathbf{k},\omega) = \frac{\rho(\mathbf{k},\omega)}{\varepsilon_R(\omega)\varepsilon_0}. \tag{7.244}$$

As both the scalar and vector potentials appear in this equation, we can decouple them by applying the Lorentz gauge condition. This sets the divergence of the vector potential to being proportional to the time derivative of the scalar potential,

$$\begin{aligned}\nabla\bullet\mathbf{A}(\mathbf{x},\mathrm{t}) &= -\mu_0\varepsilon_R\varepsilon_0\frac{\partial\Phi(\mathbf{x},\mathrm{t})}{\partial\mathrm{t}}\\ &= -\frac{\varepsilon_R}{\mathrm{c}^2}\frac{\partial\Phi(\mathbf{x},\mathrm{t})}{\partial\mathrm{t}}\end{aligned} \tag{7.245}$$

where $1/\sqrt{\mu_0\varepsilon_0} = \mathrm{c}$ has been used. By transforming this Lorentz gauge condition into wavenumber- and frequency-space,

$$\mathbf{k}\bullet\mathbf{A}(\mathbf{k},\omega) = \frac{\omega\,\varepsilon_R(\omega)}{\mathrm{c}^2}\Phi(\mathbf{k},\omega). \tag{7.246}$$

Applying this to (7.244) results in the wave equation for the scalar potential,

$$\left(\mathrm{k}^2-\frac{\omega^2\,\varepsilon_R(\omega)}{\mathrm{c}^2}\right)\Phi(\mathbf{k},\omega) = \frac{\rho(\mathbf{k},\omega)}{\varepsilon_R(\omega)\varepsilon_0}. \tag{7.247}$$

The corresponding wave equation in the vector potential is next derived by substituting the Fourier transforms of the electromagnetic fields into the Fourier transform of $\nabla\times\mathbf{B}$,

$$\begin{aligned}\frac{1}{\mu_0}\mathbf{k}\times(\mathbf{k}\times\mathbf{A}(\mathbf{k},\omega)) = \mathbf{J}(\mathbf{k},\omega) &+ \mathrm{i}\omega\varepsilon_R(\omega)\varepsilon_0\\ &\times(\mathrm{i}\mathbf{k}\Phi(\mathbf{k},\omega)-\mathrm{i}\omega\mathbf{A}(\mathbf{k},\omega)).\end{aligned}$$

Expanding the vector triple cross-product gives,

$$\begin{aligned}\frac{1}{\mu_0}\left(\mathbf{k}(\mathbf{k}\bullet\mathbf{A}(\mathbf{k},\omega))-\mathrm{k}^2\mathbf{A}(\mathbf{k},\omega)\right)&\\ = \mathbf{J}(\mathbf{k},\omega)-\omega\varepsilon_R(\omega)\varepsilon_0\mathbf{k}\Phi(\mathbf{k},\omega)&\\ +\omega^2\varepsilon_R(\omega)\varepsilon_0\mathbf{A}(\mathbf{k},\omega).&\end{aligned}$$

Applying the Lorentz gauge condition to this result gives,

$$\left(\mathrm{k}^2-\frac{\omega^2\,\varepsilon_R(\omega)}{\mathrm{c}^2}\right)\mathbf{A}(\mathbf{k},\omega) = \mu_0\mathbf{J}(\mathbf{k},\omega). \tag{7.248}$$

These wave equations provide the first steps in determining the potentials $\Phi(\mathbf{k},\omega)$ and $\mathbf{A}(\mathbf{k},\omega)$. These are obtained by first calculating the Fourier transforms of the charge and current densities, $\rho(\mathbf{k},\omega)$ and $\mathbf{J}(\mathbf{k},\omega)$. The net charge distribution is that of the projectile,

$$\rho(\mathbf{x},\mathrm{t}) = \mathrm{ze}\,\delta\left(\mathbf{x}-\beta\mathrm{ct}\ \ \hat{\mathbf{v}}_{||}\right) \tag{7.249}$$

with the Fourier transform,

$$\begin{aligned}\rho(\mathbf{k},\omega) &= \frac{1}{4\pi^2}\int_{-\infty}^{\infty}\mathrm{d}^3\mathbf{x}\int_{-\infty}^{\infty}\mathrm{dt}\,\rho(\mathbf{x},\mathrm{t})\mathrm{e}^{-\mathrm{i}(\mathbf{k}\bullet\mathbf{x}-\omega\mathrm{t})}\\ &= \frac{\mathrm{ze}}{4\pi^2}\int_{-\infty}^{\infty}\mathrm{d}^3\mathbf{x}\int_{-\infty}^{\infty}\mathrm{dt}\,\mathrm{e}^{-\mathrm{i}\left(\beta\,\mathrm{c}\,\mathbf{k}\bullet\hat{\mathbf{v}}_{||}-\omega\right)\mathrm{t}}\\ &= \frac{\mathrm{ze}}{2\pi}\delta\left(\omega-\beta\mathrm{ck}_{||}\right).\end{aligned} \tag{7.250}$$

The current density is,

$$\mathbf{J}(\mathbf{x},\mathrm{t}) = \beta\mathrm{c}\,\rho(\mathbf{x},\mathrm{t})\hat{\mathbf{v}}_{||}$$

and its Fourier transform is,

$$\begin{aligned}\mathbf{J}(\mathbf{k},\omega) &= \beta\mathrm{c}\,\rho(\mathbf{k},\omega)\hat{\mathbf{v}}_{||}\\ &= \frac{\mathrm{ze}\,\beta\mathrm{c}}{2\pi}\delta\left(\omega-\beta\mathrm{ck}_{||}\right)\hat{\mathbf{v}}_{||}.\end{aligned} \tag{7.251}$$

Having obtained these, it is possible to write the Fourier transforms of the scalar and vector potentials as,

$$\begin{aligned}\Phi(\mathbf{k},\omega) &= \frac{\rho(\mathbf{k},\omega)}{\varepsilon_R(\omega)\varepsilon_0\left(\mathrm{k}^2-\frac{\omega^2\,\varepsilon_R(\omega)}{\mathrm{c}^2}\right)}\\ &= \frac{\mathrm{ze}}{2\pi\,\varepsilon_R(\omega)\varepsilon_0\left(\mathrm{k}^2-\frac{\omega^2\,\varepsilon_R(\omega)}{\mathrm{c}^2}\right)}\\ &\quad\times\delta\left(\omega-\beta\mathrm{ck}_{||}\right)\end{aligned} \tag{7.252}$$

and

$$\mathbf{A}(\mathbf{k},\omega) = \frac{\mu_0 \mathbf{J}(\mathbf{k},\omega)}{\left(k^2 - \frac{\omega^2 \varepsilon_R(\omega)}{c^2}\right)} = \frac{ze\,\mu_0 \beta c}{2\pi\left(k^2 - \frac{\omega^2 \varepsilon_R(\omega)}{c^2}\right)} \delta\left(\omega - \beta c k_{||}\right) \hat{\mathbf{v}}_{||} \tag{7.253}$$

and the fields in wavenumber- and frequency-space,

$$\begin{aligned}\mathbf{E}(\mathbf{k},\omega) = i\Bigg(& \omega \frac{ze\,\mu_0 \beta c}{2\pi\left(k^2 - \frac{\omega^2 \varepsilon_R(\omega)}{c^2}\right)} \delta\left(\omega - \beta c k_{||}\right) \hat{\mathbf{v}}_{||} \\ & - \mathbf{k} \frac{ze}{2\pi \varepsilon_R(\omega) \varepsilon_0 \left(k^2 - \frac{\omega^2 \varepsilon_R(\omega)}{c^2}\right)} \delta\left(\omega - \beta c k_{||}\right) \Bigg) \\ = i & \frac{ze \delta\left(\omega - \beta c k_{||}\right)}{2\pi \varepsilon_0 \varepsilon_R(\omega)\left(k^2 - \frac{\omega^2 \varepsilon_R(\omega)}{c^2}\right)} \\ & \times \left(\omega \varepsilon_R(\omega) \frac{\beta}{c} \hat{\mathbf{v}}_{||} - \mathbf{k}\right)\end{aligned} \tag{7.254}$$

and

$$\mathbf{H}(\mathbf{k},\omega) = i \frac{ze\,\beta c}{2\pi\left(k^2 - \frac{\omega^2 \varepsilon_R(\omega)}{c^2}\right)} \delta\left(\omega - \beta c k_{||}\right) \mathbf{k} \times \hat{\mathbf{v}}_{||}. \tag{7.255}$$

Energy Loss in a Dielectric Medium

Now that the electromagnetic fields $\mathbf{E}(\mathbf{k},\omega)$ and $\mathbf{H}(\mathbf{k},\omega)$ arising from a moving charged particle in a dielectric medium have been evaluated, the energy loss to a single electron at the position associated with the impact parameter, b, is calculated at the vectorial position,

$$\mathbf{x} = b\,\hat{\mathbf{v}}_{\perp}. \tag{7.256}$$

This energy loss is equal to the electromagnetic energy flow which is described by the magnitude of the Poynting vector. In order to calculate this vector, begin by taking the inverse Fourier transform of the previously-derived electric field into the spatial domain,

$$\begin{aligned}\mathbf{E}(b\hat{\mathbf{v}}_{\perp},\omega) &= \frac{1}{(2\pi)^{3/2}} \int_{-\infty}^{\infty} d^3\mathbf{k}\, \mathbf{E}(\mathbf{k},\omega) e^{ib\mathbf{k}\bullet\hat{\mathbf{v}}_{\perp}} \\ &= i \frac{ze}{(2\pi)^{5/2} \varepsilon_0 \varepsilon_R(\omega)} \\ &\quad \times \int_{-\infty}^{\infty} d^3\mathbf{k} \frac{\left(\omega \varepsilon_R(\omega) \frac{\beta}{c} \hat{\mathbf{v}}_{||} - \mathbf{k}\right)}{\left(k^2 - \frac{\omega^2 \varepsilon_R(\omega)}{c^2}\right)} \\ &\quad \times e^{ib\mathbf{k}\bullet\hat{\mathbf{v}}_{\perp}} \delta\left(\omega - \beta\, c k_{||}\right) \\ \mathbf{E}(b\hat{\mathbf{v}}_{\perp},\omega) &= i \frac{ze}{(2\pi)^{5/2} \varepsilon_0 \varepsilon_R(\omega)} \int_{-\infty}^{\infty} d^3\mathbf{k} \\ &\quad \times \frac{\left(-k_x \hat{\mathbf{v}}_x + \left(\omega \varepsilon_R(\omega) \frac{\beta}{c} - k_{||}\right) \hat{\mathbf{v}}_{||} - k_{\perp} \hat{\mathbf{v}}_{\perp}\right)}{\left(k_x^2 + k_{||}^2 + + k_{\perp}^2 - \frac{\omega^2 \varepsilon_R(\omega)}{c^2}\right)} \\ &\quad \times e^{ibk_{\perp}} \delta\left(\omega - \beta c k_{||}\right)\end{aligned} \tag{7.257}$$

In order to evaluate the integral, first use the substitution of variable $\xi = \beta c k_{||}$ to take it to the form,

$$\begin{aligned}\mathbf{E}(b\hat{\mathbf{v}}_{\perp},\omega) = i & \frac{ze}{(2\pi)^{5/2} \varepsilon_0 \varepsilon_R(\omega) \beta c} \int_{-\infty}^{\infty} dk_x \int_{-\infty}^{\infty} d\xi \int_{-\infty}^{\infty} dk_{\perp} \\ & \times \frac{-k_x \hat{\mathbf{v}}_x + \left(\omega \varepsilon_R(\omega) \frac{\beta}{c} - \frac{\xi}{\beta c}\right) \hat{\mathbf{v}}_{||} - k_{\perp} \hat{\mathbf{v}}_{\perp}}{\left(k_x^2 + \left(\frac{\xi}{\beta c}\right)^2 + + k_{\perp}^2 - \frac{\omega^2 \varepsilon_R(\omega)}{c^2}\right)} \\ & \times e^{ibk_{\perp}} \delta(\omega - \xi)\end{aligned} \tag{7.258}$$

The integration over ξ is trivial due to the δ-function and results in,

$$\begin{aligned}\mathbf{E}(b\hat{\mathbf{v}}_{\perp},\omega) = & \; i \frac{ze}{(2\pi)^{5/2} \varepsilon_0 \varepsilon_R(\omega) \beta c} \int_{-\infty}^{\infty} dk_x \int_{-\infty}^{\infty} dk_{\perp} \\ & \times \frac{-k_x \hat{\mathbf{v}}_x + \frac{\omega}{\beta c}\left(\varepsilon_R(\omega) \beta^2 - 1\right) \hat{\mathbf{v}}_{||} - k_{\perp} \hat{\mathbf{v}}_{\perp}}{\left(k_x^2 + k_{\perp}^2 + \lambda(\omega)^2\right)} e^{ibk_{\perp}}\end{aligned} \tag{7.259}$$

where the quantity,

$$\lambda^2(\omega) = \left(\frac{\omega}{\beta c}\right)^2 \left(1 - \beta^2 \varepsilon_R(\omega)\right) \tag{7.260}$$

has been defined. In a convenient approach to solving this integral, it is split it up into the integral expression for the Fourier transform of the electric field of three integrals along each orthogonal direction and each are solved separately,

$$\mathbf{E}(b\hat{\mathbf{v}}_\perp, \omega) = i \frac{ze}{(2\pi)^{5/2} \varepsilon_0 \varepsilon_R(\omega) \beta c} \times \left(I_x \hat{\mathbf{v}}_x + I_{||} \hat{\mathbf{v}}_{||} + I_\perp \hat{\mathbf{v}}_\perp\right). \tag{7.261}$$

The integrals are,

$$\begin{aligned} I_x &= -\int_{-\infty}^{\infty} dk_\perp e^{ibk_\perp} \int_{-\infty}^{\infty} dk_x \frac{k_x}{\left(k_x^2 + k_\perp^2 + \lambda(\omega)^2\right)} \\ &= 0 \end{aligned} \tag{7.262}$$

and

$$\begin{aligned} I_{||} &= \frac{\omega}{\beta c}\left(\varepsilon_R(\omega)\beta^2 - 1\right) \int_{-\infty}^{\infty} dk_\perp e^{ibk_\perp} \\ &\quad \times \int_{-\infty}^{\infty} \frac{dk_x}{\left(k_x^2 + k_\perp^2 + \lambda(\omega)^2\right)} \\ &= \frac{\pi\omega}{\beta c}\left(\varepsilon_R(\omega)\beta^2 - 1\right) \int_{-\infty}^{\infty} dk_\perp \frac{e^{ibk_\perp}}{\sqrt{k_\perp^2 + \lambda(\omega)^2}} \\ &= \frac{2\pi\omega}{\beta c}\left(\varepsilon_R(\omega)\beta^2 - 1\right) \int_{-\infty}^{\infty} dk_\perp \frac{\cos bk_\perp}{\sqrt{k_\perp^2 + \lambda(\omega)^2}} \\ &= \frac{2\pi\omega}{\beta c}\left(\varepsilon_R(\omega)\beta^2 - 1\right) \int_0^{\infty} \frac{dk_\perp}{\lambda(\omega)} \frac{\cos\left(\lambda(\omega) b \left(\frac{k_\perp}{\lambda(\omega)}\right)\right)}{\sqrt{1 + \left(\frac{k_\perp}{\lambda(\omega)}\right)^2}} \\ &= \frac{2\pi\omega}{\beta c}\left(\varepsilon_R(\omega)\beta^2 - 1\right) K_0(\lambda(\omega) b) \end{aligned} \tag{7.263}$$

and

$$\begin{aligned} I_\perp &= -\int_{-\infty}^{\infty} dk_\perp k_\perp e^{ibk_\perp} \int_{-\infty}^{\infty} \frac{dk_x}{\left(k_x^2 + k_\perp^2 + \lambda(\omega)^2\right)} \\ &= -\pi \int_{-\infty}^{\infty} dk_\perp \frac{k_\perp e^{ibk_\perp}}{\sqrt{k_\perp^2 + \lambda(\omega)^2}} \\ &= -i\pi \frac{d}{db} \int_{-\infty}^{\infty} dk_\perp \frac{e^{ibk_\perp}}{\sqrt{k_\perp^2 + \lambda(\omega)^2}} \\ &= -i\, 2\pi \frac{d}{db} \int_{-\infty}^{\infty} dk_\perp \frac{\cos bk_\perp}{\sqrt{k_\perp^2 + \lambda(\omega)^2}} \\ &= -i\, 2\pi \frac{d}{db} K_0(\lambda(\omega) b) \\ &= i\, 2\pi\, \lambda(\omega) K_1(\lambda(\omega) b). \end{aligned} \tag{7.264}$$

The electric field at the position of the electron $b\hat{\mathbf{v}}_\perp$ is, then,

$$\begin{aligned} \mathbf{E}(b\hat{\mathbf{v}}_\perp, \omega) = &\frac{ze}{(2\pi)^{3/2} \varepsilon_0 \varepsilon_R(\omega) \beta c} \\ &\times \left(\lambda(\omega) K_1(\lambda(\omega) b) \hat{\mathbf{v}}_\perp - i \frac{\omega}{\beta c}\right. \\ &\left. \times \left(1 - \varepsilon_R(\omega)\beta^2\right) K_0(\lambda(\omega) b) \hat{\mathbf{v}}_{||}\right). \end{aligned} \tag{7.265}$$

One can see from the definition of λ^2 that, for a real relative dielectric constant,

$$\lambda^2 > 0 \quad \text{for} \quad \beta < \frac{1}{\sqrt{\varepsilon_R(\omega)}} \tag{7.266}$$

$$\lambda^2 < 0 \quad \text{for} \quad \beta > \frac{1}{\sqrt{\varepsilon_R(\omega)}}. \tag{7.267}$$

In other words, λ can only be real if the particle speed is less than the phase velocity of the medium. It should be noted that, if polarization is neglected, i.e.,

$\varepsilon_R(\omega) = 1$, then $\lambda^2(\omega) = (\omega/\gamma\beta c)^2$ and the expression for the electric field reduces to,

$$\begin{aligned}\mathbf{E}(b\hat{\mathbf{v}}_\perp,\omega) =& \frac{ze}{(2\pi)^{3/2}\varepsilon_0\beta c}\left(\frac{\omega}{\gamma\beta c}K_1\left(\frac{\omega}{\gamma\beta c}b\right)\hat{\mathbf{v}}_\perp\right.\\ &\left.- i\frac{\omega}{\gamma^2\beta c}K_0\left(\frac{\omega}{\gamma\beta c}b\right)\hat{\mathbf{v}}_{||}\right)\\ =& \frac{ze}{(2\pi)^{3/2}\varepsilon_0}\frac{\omega}{\gamma(\beta c)^2}\\ &\times\left(K_1\left(\frac{\omega}{\gamma\beta c}b\right)\hat{\mathbf{v}}_\perp - i\frac{1}{\gamma}K_0\left(\frac{\omega}{\gamma\beta c}b\right)\hat{\mathbf{v}}_{||}\right)\\ &\text{for}\quad \varepsilon_R(\omega) = 1 \end{aligned} \tag{7.268}$$

which is the result which was derived previously for a heavy charged particle interacting with an harmonically-bound electron.

In a fashion similar to the above calculation for the electric field, one can next calculate the magnetic field strength at the position of the target electron,

$$\begin{aligned}\mathbf{H}(b\hat{\mathbf{v}},\omega) =& -i\frac{ze\beta c}{(2\pi)^{5/2}}\int_{-\infty}^{\infty} d^3\mathbf{k}\frac{\mathbf{k}\times\hat{\mathbf{v}}_{||}}{\left(k^2 - \frac{\omega^2\varepsilon_R(\omega)}{c^2}\right)}\\ &\times e^{ib\mathbf{k}\bullet\hat{\mathbf{v}}_\perp}\delta\left(\omega - \beta c k_{||}\right)\\ =& -i\frac{ze\beta c}{(2\pi)^{5/2}}\int_{-\infty}^{\infty} dk_x\int_{-\infty}^{\infty} dk_{||}\int_{-\infty}^{\infty} dk_\perp\\ &\times\frac{k_x\hat{\mathbf{v}}_\perp - k_\perp\hat{\mathbf{v}}_x}{\left(k_x^2 + k_{||}^2 + k_\perp^2 - \frac{\omega^2\varepsilon_R(\omega)}{c^2}\right)}\\ &\times e^{ibk_\perp}\delta\left(\omega - \beta c k_{||}\right)\\ =& -i\frac{ze}{(2\pi)^{5/2}}\int_{-\infty}^{\infty} dk_\perp e^{ibk_\perp}\int_{-\infty}^{\infty} dk_x\\ &\times\frac{k_x\hat{\mathbf{v}}_\perp - k_\perp\hat{\mathbf{v}}_x}{\left(k_x^2 + k_\perp^2 + \lambda^2(\omega)\right)}\\ =& -i\frac{ze}{(2\pi)^{5/2}}(I_x\hat{\mathbf{v}}_x + I_\perp\hat{\mathbf{v}}_\perp). \end{aligned} \tag{7.269}$$

where

$$\begin{aligned}I_x =& -\int_{-\infty}^{\infty} dk_\perp\, k_\perp\, e^{ibk_\perp}\\ &\times\int_{-\infty}^{\infty}\frac{dk_x}{\left(k_x^2 + k_\perp^2 + \lambda^2(\omega)\right)}\\ =& \, i\,2\pi\,\lambda(\omega)K_1(\lambda(\omega)b) \end{aligned} \tag{7.270}$$

and

$$\begin{aligned}I_\perp =& \int_{-\infty}^{\infty} dk_\perp\, e^{ibk_\perp}\int_{-\infty}^{\infty} dk_x\frac{k_x}{\left(k_x^2 + k_\perp^2 + \lambda^2(\omega)\right)}\\ =& \, 0 \end{aligned} \tag{7.271}$$

to give,

$$\mathbf{H}(b\hat{\mathbf{v}},\omega) = \frac{ze}{(2\pi)^{3/2}}\lambda(\omega)K_1(\lambda(\omega)b)\hat{\mathbf{v}}_x. \tag{7.272}$$

Now that the electric and magnetic fields have been derived in Fourier space at the position of the electron at $b\,\hat{\mathbf{v}}_\perp$, the energy loss due to collisions at an impact parameter of $b \geq b_{min}$ can be readily calculated from the energy flow through a cylinder of radius b_{min} centered on the particle's trajectory through the inverse Fourier transform. The energy flow through this cylinder is equal to the power loss of the particle,

$$\left(\frac{dE}{dx}\right)_{b\geq b_{min}} = \frac{1}{\beta c}\frac{dE}{dt}. \tag{7.273}$$

The power flow is given by the outgoing component of the Poynting vector, $\mathbf{P} = \mathbf{E}\times\mathbf{H}$,

$$\begin{aligned}\mathbf{P} =& \left(E_{||}\hat{\mathbf{v}}_{||} + E_\perp\hat{\mathbf{v}}_\perp\right)\times H_x\hat{\mathbf{v}}_x\\ =& \, E_\perp H_x\hat{\mathbf{v}}_{||} - E_{||}H_x\hat{\mathbf{v}}_\perp. \end{aligned} \tag{7.274}$$

The outgoing component of the vector is $-E_{||}H_x$ and,

$$\begin{aligned}\left(\frac{dE}{dx}\right)_{b>b_{min}} &= -\frac{2\pi\, b_{min}}{\beta c}\int_{-\infty}^{\infty} dx\, E_{||}H_x \\ &= -2\pi\, b_{min}\int_{-\infty}^{\infty} dt\, E_{||}H_x \\ &= -2\pi\, b_{min}\left(\frac{1}{2\pi}\int_{-\infty}^{\infty} dt\int_{-\infty}^{\infty} d\omega\int_{-\infty}^{\infty} d\omega' \right. \\ &\quad \left. \times E_{||}(\omega)H_x(\omega)e^{-i(\omega+\omega')t}\right) \\ &= -2\pi\, b_{min}\int_{-\infty}^{\infty} d\omega\, E_{||}(\omega)\, H_x^*(\omega) \\ &= -4\pi\, b_{min}\,\mathrm{Re}\left(\int_0^{\infty} d\omega\, E_{||}(\omega)\, H_x^*(\omega)\right) \\ &= \frac{(ze)^2\, b_{min}}{2\pi^2\varepsilon_0(\beta c)^2}\mathrm{Re}\left(\int_0^{\infty} d\omega(i\omega\lambda^*(\omega)) \right. \\ &\quad \times\left(\frac{1}{\varepsilon_R(\omega)}-\beta^2\right)K_0(\lambda(\omega)b_{min}) \\ &\quad \left.\times K_1\left(\lambda^*(\omega)b_{min}\right)\right) \end{aligned} \tag{7.275}$$

Although the i can be removed from the integrand through the use of $\mathrm{Re}\, iz = -\mathrm{Im}\, z$, it is retained in anticipation of a future complex integration. In order to have the result of a non-zero stopping power, this integral must have a real component which requires that either λ or $\varepsilon_R(\omega)$ be complex. Even if the relative dielectric permittivity were to be real, it is possible for the stopping power to be non-zero when λ is complex which is a result of the particle speed exceeding the phase velocity of the medium. This energy loss is manifested as the Čerenkov radiation discussed below. On the other hand, if the particle speed were to be less than the phase velocity, λ would be complex only if $\varepsilon_R(\omega)$ was. Because of the $\beta^2\varepsilon_R(\omega)$ term in the expression for λ^2, this effect becomes significant at high projectile speeds. One can simplify the expression for the stopping power in a dielectric medium by taking advantage of this and limiting the derivation to the extreme relativistic case of $\beta \approx 1$ for which,

$$\lambda^2 \approx \left(\frac{\omega}{c}\right)^2(1-\varepsilon_R(\omega)) \quad \text{for} \quad \beta \approx 1. \tag{7.276}$$

From the earlier discussion of electronic polarization, the integral will be significant for ω in the ultraviolet region (10^{16}–10^{17}/s). As b_{min} is of the order of the atomic radius, R_A, the argument of the modified Bessel function will thus be of the order of,

$$|\lambda\, b| < \left(\frac{\omega_0\, R_A}{c}\right) \approx 0.003.$$

As a result, one can use the small-argument limits,

$$K_0(y) \approx \ln\frac{1.123}{y} \text{ and } K_1(y) \approx \frac{1}{y}.$$

Substituting these limits into the stopping power expression gives,

$$\begin{aligned}\frac{dE}{dx} &= \frac{(ze)^2}{2\pi^2\,\varepsilon_0(\beta c)^2}\mathrm{Re}\left(\int_0^{\infty} d\omega(i\omega)\left(\frac{1}{\varepsilon_R(\omega)}-\beta^2\right)\right. \\ &\quad \left.\times\ln\frac{1.123}{\lambda(\omega)b_{min}}\right) \\ &= \frac{(ze)^2}{2\pi^2\varepsilon_0(\beta c)^2}\mathrm{Re}\left(\int_0^{\infty} d\omega(i\omega)\left(\frac{1}{\varepsilon_R(\omega)}-\beta^2\right)\right. \\ &\quad \left.\times\ln\frac{1.123}{\left(\frac{\omega b_{min}}{\beta c}\right)\sqrt{1-\beta^2\varepsilon_R(\omega)}}\right) \\ &= \frac{(ze)^2}{2\pi^2\,\varepsilon_0(\beta c)^2}\mathrm{Re}\left(\int_0^{\infty} d\omega(i\omega)\left(\frac{1}{\varepsilon_R(\omega)}-\beta^2\right)\right. \\ &\quad \left.\times\left(\ln\left(\frac{1.123\,\beta c}{\omega b_{min}}\right)-\frac{1}{2}\ln\left(1-\beta^2\varepsilon_R(\omega)\right)\right)\right) \end{aligned} \tag{7.277}$$

(Note that, in the limit of $\varepsilon_R(\omega) \to 1$, $-\frac{1}{2}\ln\left(1-\beta^2\varepsilon_R(\omega)\right) \to \ln\gamma$). In making the extreme relativistic case even more explicit, set $\beta = 1$,

$$\begin{aligned}\frac{dE}{dx} &= \frac{(ze)^2}{2\pi^2\,\varepsilon_0\,c^2}\mathrm{Re}\left(\int_0^{\infty} d\omega\,(i\omega)\left(\frac{1}{\varepsilon_R(\omega)}-1\right)\right. \\ &\quad \left.\times\left(\ln\left(\frac{1.123\,c}{\omega b_{min}}\right)-\frac{1}{2}\ln(1-\varepsilon_R(\omega))\right)\right) \end{aligned} \tag{7.278}$$

For a small damping constant Γ, the imaginary part of the relative dielectric permittivity can be neglected and the expression for the stopping power becomes,

$$\frac{dE}{dx} = \frac{(ze)^2}{2\pi^2\varepsilon_0 c^2}\mathrm{Re}\left(\int_0^\infty d\omega\,(i\omega)\left(\frac{-\frac{\omega_P^2}{(\omega_0^2-\omega^2)+i\Gamma\omega}}{1+\frac{\omega_P^2}{(\omega_0^2-\omega^2)+i\Gamma\omega}}\right)\right.$$
$$\left.\times\left(\ln\left(\frac{1.123\,c}{\omega b_{min}}\right)-\frac{1}{2}\ln\left(-\frac{\omega_P^2}{(\omega_0^2-\omega^2)+i\Gamma\omega}\right)\right)\right)$$
$$=-\frac{(ze)^2}{2\pi^2\varepsilon_0 c^2}\mathrm{Re}\left(i\int_0^\infty d\omega\,\omega\left(\frac{\omega_P^2}{(\omega_0^2-\omega^2+\omega_P^2)+i\Gamma\omega}\right)\right.$$
$$\left.\times\left(\ln\left(\frac{1.123\,c}{\omega b_{min}}\right)+\frac{1}{2}\ln\left(\frac{(\omega^2-\omega_0^2)+i\Gamma\omega}{\omega_P^2}\right)\right)\right) \tag{7.279}$$

The integral of (7.279),

$$i\int_0^\infty d\omega\,\omega\left(\frac{\omega_P^2}{(\omega_0^2-\omega^2+\omega_P^2)+i\Gamma\omega}\right)$$
$$\times\left(\ln\left(\frac{1.123\,c}{\omega b_{min}}\right)+\frac{1}{2}\ln\left(\frac{(\omega^2-\omega_0^2)+i\Gamma\omega}{\omega_P^2}\right)\right)$$
$$=i\int_0^\infty d\omega\,\omega\left(\frac{\omega_P^2}{(\omega_0^2-\omega^2+\omega_P^2)+i\Gamma\omega}\right)$$
$$\times\left(\ln\left(\frac{1.123\,c}{\omega_P b_{min}}\right)+\frac{1}{2}\ln\left(\frac{(\omega^2-\omega_0^2)+i\Gamma\omega}{\omega^2}\right)\right) \tag{7.280}$$

is determined using the Cauchy–Goursat theorem by changing the integration over positive real ω (i.e., $0 \le \omega \le \infty$) to that over positive imaginary ω minus the integration over the quarter-circle to infinity, as shown in Fig. 7.21, with the intent of isolating the integration I_X. It can be seen from the integrand that poles occur for,

$$(\omega_0^2-\omega^2+\omega_P^2)+i\Gamma\omega=0$$

and

$$\frac{(\omega^2-\omega_0^2)+i\Gamma\omega}{\omega^2}=0.$$

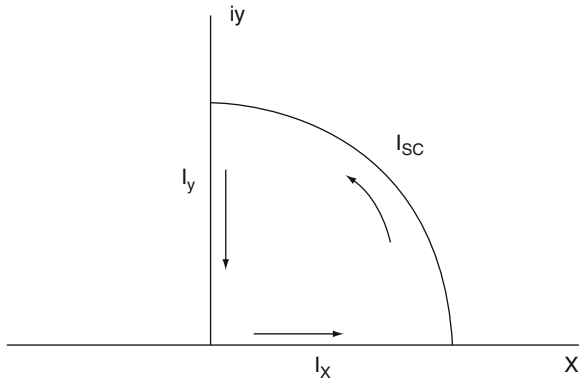

Fig. 7.21 Integration contour in the complex plane z = x + iy used to evaluate the integral of (7.280)

In both cases, ω would be imaginary and the poles of the integrand exist in the lower half-plane. As there are no poles within the quarter-circle of the contour, the total integral is equal to zero, or,

$$\mathrm{Re}(I_X+I_Y+I_{SC})=0$$

The integral down the imaginary axis is evaluated first using $\omega = i\Omega$,

$$I_Y=-i\int_0^\infty d\Omega\,\Omega\left(\frac{\omega_P^2}{(\omega_0^2+\Omega^2+\omega_P^2)-i\Gamma\Omega}\right)$$
$$\times\left(\ln\left(\frac{1.123\,c}{\omega_P b_{min}}\right)+\frac{1}{2}\ln\left(\frac{-(\Omega^2+\omega_0^2+\Gamma\Omega)}{(i\Omega)}\right)\right) \tag{7.281}$$

It is clear that, as this integral is pure imaginary (i.e., Re $I_Y = 0$), its contribution to the stopping power will be zero. As a result,

$$\mathrm{Re}\,I_X=-\mathrm{Re}\,I_{SC}. \tag{7.282}$$

In order to calculate the integral over the quarter-circle, I_{SC}, write ω in terms of complex polar coordinates, or,

$$\omega=re^{i\theta} \tag{7.283}$$

where r is a constant. Thus,

$$\begin{aligned}\mathrm{Re}\, I_X &= -\mathrm{Re}\, I_{SC} \\ &= -\mathrm{Re} \int_0^{\pi/2} d\theta\, r^2 e^{i2\theta} \left(\frac{\omega_P^2}{\left(\omega_0^2 - r^2 e^{i2\theta} + \omega_P^2\right) + i\Gamma r e^{i\theta}} \right) \\ &\quad \times \left(\ln\left(\frac{1.123\, c}{\omega_P b_{min}} \right) \right. \\ &\quad \left. + \frac{1}{2} \ln\left(\frac{\left(r^2 e^{i2\theta} - \omega_0^2\right) + i\Gamma r e^{i\theta}}{r^2} e^{-i2\theta} \right) \right). \end{aligned} \tag{7.284}$$

Maintaining the assumption that the damping Γ is small and constant,

$$\begin{aligned}&-\mathrm{Re} \int_0^{\pi/2} d\theta\, r^2 e^{i2\theta} \left(\frac{\omega_P^2}{\left(\omega_0^2 - r^2 e^{i2\theta} + \omega_P^2\right) + i\Gamma r e^{i\theta}} \right) \\ &\times \left(\ln\left(\frac{1.123\, c}{\omega_P b_{min}} \right) + \frac{1}{2} \ln\left(\frac{\left(r^2 e^{i2\theta} - \omega_0^2\right) + i\Gamma r e^{i\theta}}{r^2} e^{-i2\theta} \right) \right) \\ &= \mathrm{Re}\, I_1 + \mathrm{Re}\, I_2 \end{aligned}$$

where, by rearranging the variables within the integrand,

$$\begin{aligned} I_1 &= \omega_P^2 \ln\left(\frac{1.123\, c}{\omega_P b_{min}} \right) \int_0^{\pi/2} d\theta \frac{e^{i2\theta}}{\left(\frac{\omega_0^2 + \omega_P^2}{r^2} \right) - e^{i2\theta} + i\left(\frac{\Gamma}{r}\right) e^{i\theta}} \\ &\approx -\frac{\pi \omega_P^2}{2} \ln \frac{1.123}{b \omega_P}. \end{aligned} \tag{7.285}$$

The facts that the ratio $\Gamma/|\omega|$ is negligible and that $\omega^2 \gg \left|\omega_0^2 + \omega_P^2\right|$ have been used. The second integral is,

$$\begin{aligned} I_2 &= \frac{1}{2} \int_0^{\pi/2} d\theta\, r^2 e^{i2\theta} \left(\frac{\omega_P^2}{\left(\omega_0^2 - r^2 e^{i2\theta} + \omega_P^2\right) + i\Gamma r e^{i\theta}} \right) \\ &\quad \times \left(\ln\left(\frac{\left(r^2 e^{i2\theta} - \omega_0^2\right) + i\Gamma r e^{i\theta}}{r^2} e^{-i2\theta} \right) \right) \\ &= \frac{1}{2} \int_0^{\pi/2} d\theta \frac{e^{i2\theta}}{\left(\frac{\omega_0^2 + \omega_P^2}{r^2} \right) - e^{i2\theta} + i\left(\frac{\Gamma}{r}\right) e^{i\theta}} \\ &\quad \times \left(\ln\left(\frac{\left(r^2 e^{i2\theta} - \omega_0^2\right) + i\Gamma r e^{i\theta}}{r^2} e^{-i2\theta} \right) \right) \\ &\approx -\frac{1}{2} \int_0^{\pi/2} d\theta \left(\ln\left(\frac{\left(r^2 e^{i2\theta} - \omega_0^2\right) + i\Gamma r e^{i\theta}}{r^2} e^{-i2\theta} \right) \right) \\ &\approx -\frac{1}{2} \int_0^{\pi/2} d\theta\, \ln\left(\left(e^{i2\theta} - \left(\frac{\omega_0}{r}\right)^2 + i\frac{\Gamma}{r} e^{i\theta r} \right) e^{-i2\theta} \right) \\ &\approx -\frac{1}{2} \int_0^{\pi/2} d\theta\, \ln\left(1 - \left(\frac{\omega_0}{r}\right)^2 e^{-i2\theta} + i\frac{\Gamma}{r} e^{-i\theta r} \right) \\ &\approx 0. \end{aligned}$$

Thus,

$$\begin{aligned} &\mathrm{Re}\left(i \int_0^{\infty} d\omega\, \omega \left(\frac{\omega_P^2}{\left(\omega_0^2 - \omega^2 + \omega_P^2\right) + i\Gamma\omega} \right) \right. \\ &\quad \left. \times \left(\ln\left(\frac{1.123\, c}{\omega_P\ b_{min}} \right) + \frac{1}{2} \ln\left(\frac{\left(\omega^2 - \omega_0^2\right) + i\Gamma\omega}{\omega^2} \right) \right) \right) \\ &\approx \frac{\pi \omega_P^2}{2} \ln \frac{1.123}{b \omega_P}. \end{aligned} \tag{7.286}$$

One now writes the linear stopping power in a dielectric medium in the extreme relativistic limit as,

$$\left(\frac{dE}{dx} \right)_{b > b_{min}} = \frac{(ze)^2 \omega_P^2}{4\pi\varepsilon_0 c^2} \ln \frac{1.123\, c}{b_{min}\ \omega_P}. \tag{7.287}$$

One can recast this as the mass collision stopping power

$$\left(\frac{dE}{\rho\, dx} \right)_{Col} = 2C \left(\frac{Z}{A} \right) z^2 \ln \frac{1.123\, c}{b_{min}\ \omega_P} \tag{7.288}$$

where the identifier of $b > b_{min}$ has been removed and the identifier "Col" added to indicate that this is a stopping power due to collisions (i.e., nonradiative interactions). A significant difference between this

expression, which accounts for the medium's dielectric response to the charged particle, and the relativistic forms of those that do not is that the former is no longer a function of the medium's atomic structure, which appears in the form of $\bar{I}$ or $\bar{\omega}$ within the logarithmic term, but rather of the medium's electron density which appears through the electron plasma frequency. That is, in the extreme relativistic regime, the mass collision stopping powers of two media are equal provided that the electron densities and the Z/A ratios are the same.

In the absence of any polarization effect, the corresponding relativistic mass collision stopping power is, where for clarity the Bohr result is used,

$$\left(\frac{dE}{\rho\, dx}\right)_{b>b_{min}} = 2C\left(\frac{Z}{A}\right)z^2 \ln\frac{1.123\,\gamma\, c}{b_{min}\ \bar{\omega}}. \qquad (7.289)$$

An analytical form of the density correction term given by the difference between these two mass collision stopping powers is,

$$\delta = 2C\left(\frac{Z}{A}\right)z^2 \ln\frac{\gamma\omega_P}{\bar{\omega}} \qquad (7.290)$$

Sternheimer–Peierls Parameterization of the Density/Polarization Effect

While the above provides a theoretical expression for the polarization/density effect, for practical purposes, a parameterization of the effect is frequently required in dosimetry calculations. A frequently-used parameterization which can accelerate the calculation of δ is that of Sternheimer and Peierls (1971) who presented an expression for δ applicable to both condensed media and gases

$$\delta = (2\ln 10)x + \Phi \qquad x \geq x_1 \qquad (7.291)$$

$$\delta = (2\ln 10)x + \Phi + a(x_1 - x)^n \qquad x_0 \leq x \leq x_1 \qquad (7.292)$$

$$\delta = 0 \qquad x < x_0 \qquad (7.293)$$

where the kinematic variable is, for a particle of mass m and momentum p,

$$x = \log_{10}\left(\frac{p}{m}\right) \qquad (7.294)$$

and where x_0 and x_1 are defined below. This reproduces the logarithmic increase in the density effect with $p/m \approx E/m \approx \gamma$ at high energies. The remaining quantities are,

$$\Phi = -2\ln\left(\frac{\bar{I}}{\hbar\omega_P}\right) - 1 \qquad (7.295)$$

$$a = \frac{-\Phi - (2\ln 10)x_0}{(x_1 - x_0)^n} \qquad (7.296)$$

The values of x_0 and x_1 also depend upon the values of the mean ionization potential, $\bar{I}$, and the phase of the medium. For liquid and solid media, these are:

$$\begin{aligned} x_0 &= 0.2 && \text{if } \bar{I} < 100\,\text{eV} \text{ and } -\Phi \leq 3.681 \\ &= -0.326\Phi - 1.0 && \text{if } \bar{I} < 100\,\text{eV} \text{ and } -\Phi > 3.681 \\ &= 0.2 && \text{if } \bar{I} \geq 100\,\text{eV} \text{ and } -\Phi \leq 5.215 \\ &= -0.326\Phi - 1.5 && \text{if } \bar{I} \geq 100\,\text{eV} \text{ and } -\Phi > 5.215 \end{aligned} \qquad (7.297)$$

$$\begin{aligned} x_1 &= 2.0 && \text{if } \bar{I} < 100\,\text{eV} \\ &= 3.0 && \text{if } \bar{I} \geq 100\,\text{eV} \end{aligned} \qquad (7.298)$$

In all cases, $n = 3$. The relative magnitude of δ and its growth with particle speed are shown in Fig. 7.22 which plots fitted values for δ for carbon and lead as a function of p/m; for example, the value of δ for carbon reaches 2 for $p/m = 9.8$, corresponding to a kinetic energy of about 5 MeV for electrons. In the context of examples of radionuclides used in nuclear medicine, the maximum β-particle energy of ^{131}I is 606 keV, for which the value of δ in carbon is equal to 0.124. The maximum recoil electron energy for the 140.5 keV γ ray from ^{99m}Tc is 49.6 keV, for which δ is essentially negligible.

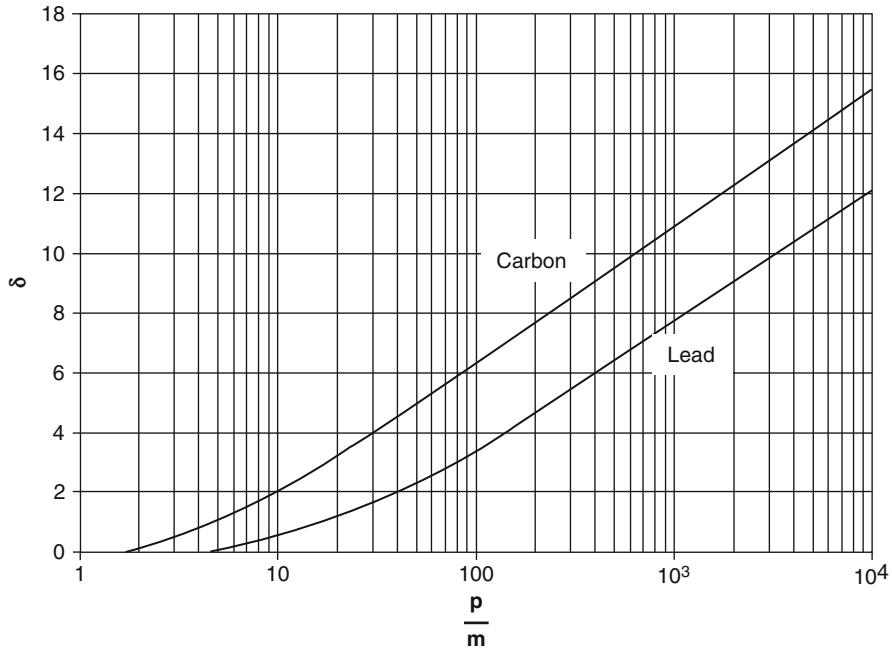

Fig. 7.22 Polarization/density correction terms for carbon and lead as functions of the ratio of the particle momentum normalized to particle mass

Čerenkov Radiation

Čerenkov (1934) reported his observations of the eponymous radiation following the irradiation of various liquids to γ rays. Tamm and Frank (1937) published their interpretation of this observation shortly afterwards. As will be demonstrated, the magnitude of the energy loss associated with Čerenkov radiation is negligible for dosimetry considerations and, as a result, its interest to medical physics applications will be limited. However, as it is straightforward to extend the above derivation of the density effect to explain this phenomenon, Čerenkov radiation is derived here.

Equation (7.287) gives the energy loss per unit distance traveled to regions within the medium with impact parameters greater than a value, b_{min}. It was assumed that b_{min} is of the order of atomic dimensions and that $|\lambda b_{min}| \ll 1$, so that the small-argument limits of the modified Bessel functions could be used. Consequently, the final result represents the rate of local energy deposition with distance. On the other hand, by permitting $|\lambda b_{min}| \ll 1$, one obtains the rate of energy deposited at great distances per distance traveled from the projectile's trajectory. Recalling the large-argument expression for the modified Bessel function,

$$\left(\frac{dE}{dx}\right)_{b>b_{min}} = \frac{(ze)^2}{4\pi\varepsilon_0(\beta c)^2} \times \mathrm{Re}\left(\int_0^\infty d\omega \left(i\omega\sqrt{\frac{\lambda^*(\omega)}{\lambda(\omega)}}\right)\left(\frac{1}{\varepsilon_R(\omega)} - \beta^2\right) \times e^{-(\lambda(\omega)+\lambda^*(\omega))b_{min}}\right). \quad (7.299)$$

Consider,

$$\lambda(\omega) = \left(\frac{\omega}{\beta c}\right)\sqrt{1 - \beta^2\varepsilon_R(\omega)}. \quad (7.300)$$

In general, Re $\lambda(\omega) > 0$ and the exponential term in the integrand will, as a consequence, rapidly attenuate the energy loss with distance from the trajectory as expected. However, $\lambda(\omega)$ will be purely imaginary if the damping constant Γ is negligible, which allows $\varepsilon_R(\omega)$ to be purely real resulting in $\beta\varepsilon_R{}^2(\omega) > 1$. For purely imaginary $\lambda(\omega)$,

$$\sqrt{\frac{\lambda^*(\omega)}{\lambda(\omega)}} = i$$

and

$$e^{-(\lambda(\omega)+\lambda^*(\omega))b_{min}} = 1.$$

Thus, for the conditions of purely real $\varepsilon_R(\omega)$ and $\beta^2\varepsilon_R(\omega) > 1$, the stopping power expression simplifies to,

$$\left(\frac{dE}{dx}\right) = z^2\hbar \int_{\omega_1}^{\infty} d\omega\, \omega \left(1 - \frac{1}{\beta^2\varepsilon_R(\omega)}\right) \qquad (7.301)$$

where the lower frequency limit is specified by the requirement of

$$\varepsilon_R(\omega > \omega_1) > \frac{1}{\beta^2} \qquad (7.302)$$

and there is no longer a dependence of the energy transfer upon b_{min}. This result describes the rate per distance traveled by the projectile at which energy is radiated. The projectile's speed must exceed the phase velocity of the medium for the given frequency, ω, for Čerenkov radiation to occur.

In Fig. 7.23 the real component of $\varepsilon_R(\omega)$ is plotted as a function of ω for negligible Γ (i.e., negligible energy absorption). There is a discontinuity at $\omega = \omega_0$ and the "Čerenkov band" is shown for which $\varepsilon_R(\omega) > 1/\beta^2$ and which identifies the lower frequency integration limit.

Before investigating the spectrum of Čerenkov radiation, the frequently-used geometrical description

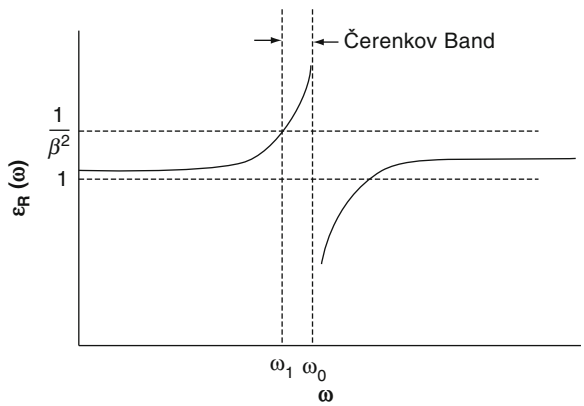

Fig. 7.23 The relative dielectric permittivity (assumed to be purely real) of a medium as a function of frequency. The Čerenkov band, within which Cerenkov radiation can occur, is shown

of a charged particle moving through a dielectric medium at a speed βc exceeding the phase velocity is investigated. The index of refraction of the medium is $n(\omega) = \sqrt{\varepsilon_R(\omega)}$; however, for conciseness, the frequency dependence is ignored. The electric field will thus propagate with speed c/n and, for the condition of $\beta c > c/n$, Huygens' constructions are used for the electromagnetic waves emitted by the particle as shown in Fig. 7.24. Let the particle be at point A at time $t = 0$. In the time that it takes the particle to travel the distance AB, which is equal to,

$$T = \frac{AB}{\beta c} \qquad (7.303)$$

(for temporary convenience units where $c \neq 1$ are used) a wavefront emitted at $t = 0$ (i.e., at point A) will have reached point C, where

$$AC = T\frac{c}{n}. \qquad (7.304)$$

Thus,

$$\theta = \cos^{-1}\frac{AC}{AB} = \cos^{-1}\frac{1}{\beta n}. \qquad (7.305)$$

Note that Fig. 7.24 shows a single plane and that, due to axial symmetry about AB, the Čerenkov wavefronts form a cone. As Čerenkov radiation can only occur if the particle speed $\beta > 1/n$, this effect will be limited to high energies in most media of dosimetric interest (e.g., as $n = 1.5$ for Perspex, the threshold value for β is 0.67). The threshold energy for which

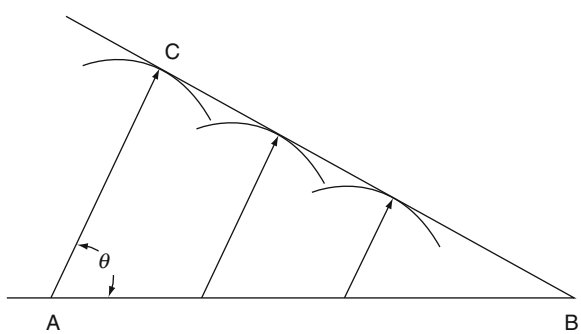

Fig. 7.24 Huygens' reconstruction of the coherent wavefront of Čerenkov radiation

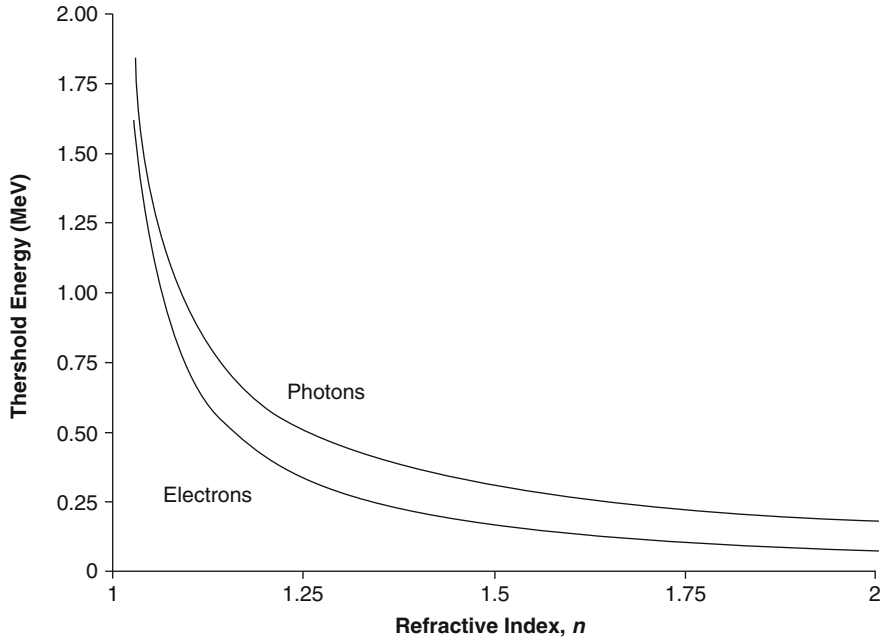

Fig. 7.25 Čerenkov radiation energy threshold for electrons and for Compton-scattered electrons set in motion by backscattered photons (labeled as "photons") as functions of the refractive index

Čerenkov radiation will occur follows as $\beta_{Thr} = 1/n$ where

$$\beta_{Thr} = \sqrt{1 - \left(\frac{m}{T_{Thr} + m}\right)^2} \tag{7.306}$$

where T_{Thr} is the threshold kinetic energy of the charged particle and m is its mass.

Figure 7.25 shows the variation of the threshold energy as a function of refractive index for electrons and for those electrons set in motion by backscattered photons following incoherent scatter. It can be seen that, within the energy range of 0.1–0.3 MeV, Čerenkov radiation presents a means of detecting γ rays in low-Z media where the probability of a photoelectric absorption is much less than that of incoherent scatter.

The differential spectrum in frequency of Čerenkov radiation is provided by the integrand of (7.301). The number of photons emitted per centimeter of projectile path length with a frequency between ω and ω + dω is,

$$dN = \frac{\alpha}{c}\left(1 - \frac{1}{(\beta n)^2}\right)d\omega. \tag{7.307}$$

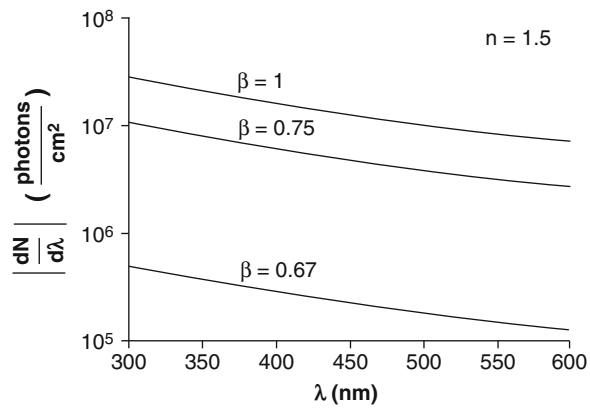

Fig. 7.26 Number of Čerenkov photons emitted per unit path-length per unit wavelength in Perspex (n = 1.5) for three values of β

As $d\omega = -2\pi c\, d\lambda/\lambda^2$, we can rewrite this more conveniently in terms of the photon wavelength,

$$\frac{dN}{d\lambda} = -\frac{2\pi\alpha}{\lambda^2}\left(\beta^2 n^2 - 1\right). \tag{7.308}$$

This spectrum is plotted as a function of photon wavelength for Perspex (n = 1.5) for values of β of 0.67 (threshold), 0.75 and 1 in Fig. 7.26. For protons,

this threshold value corresponds to a kinetic energy of about 375 MeV. The λ^{-2} dependence shows that the Čerenkov spectrum is dominated by short wavelength photons. Integrating the Čerenkov spectrum yields the number of Čerenkov photons emitted per centimeter between the spectrum limits of λ_{min} and λ_{max},

$$N = 2\pi\alpha\left(1 - \frac{1}{(\beta n)^2}\right)\left(\frac{1}{\lambda_{min}} - \frac{1}{\lambda_{max}}\right). \quad (7.309)$$

Using $\cos\theta = 1/\beta n$, one can also write the spectrum as,

$$\frac{dN}{d\lambda} = 2\pi\,\alpha\sin^2\theta\left(\frac{1}{\lambda_{max}} - \frac{1}{\lambda_{min}}\right). \quad (7.310)$$

Within the spectrum limits of 300 and 600 nm, a total of 764 $\sin^2\theta$ Čerenkov photons are emitted per centimeter of particle path length, which clearly demonstrates the low level of light output. As for minimally-ionizing particles in a low-Z medium this corresponds to a conversion efficiency of about 0.2%, the contribution of Čerenkov radiation to the overall energy loss of a charged particle traversing a medium is small and can be neglected for dosimetry purposes.

7.3.7.7 Empirical Determination of Mean Excitation Energy and Shell Correction Factor

It has been noted earlier that, instead of calculating $\bar{I}$ and $C_e(\beta)/Z$ for a given medium, it is possible to empirically evaluate their combined effect upon the collision stopping power from detailed experimental measurements of the energy loss of a charged particle (typically a proton) traversing a thin foil of the medium in question (Ammi et al. 2005). At sufficiently low projectile energies, the diminishment of the stopping power due to polarization of the medium (described by $L_{02}(\beta)$) is negligible and the Barkas $L_2(\beta)$ term may also be neglected. Radiative energy transfer is also negligible and the energy loss will be due solely to collisions between the projectile and the atomic electrons. Under these conditions, the mass collision stopping power reduces to,

$$\left(\frac{dE}{\rho\,dx}\right)_{Col} = 2C\left(\frac{Z}{A}\right)\left(\frac{z}{\beta}\right)^2 L_0(\beta). \quad (7.311)$$

Consider a proton ($z = 1$) with speed βc traversing a thin foil of medium with an areal thickness $\rho\,\Delta x$ sufficiently small that the proton's measured energy loss is,[17]

$$\begin{aligned}\Delta E &= (\rho\,\Delta x)\left(\frac{dE}{\rho\,dx}\right)_{Col} \\ &= 2C\left(\frac{Z}{A}\right)\frac{1}{\beta^2}L_0(\beta).\end{aligned} \quad (7.312)$$

Inverting this to obtain the zeroth-order stopping power number,

$$L_0(\beta) = -\left(\frac{A}{Z}\right)\left(\frac{\beta^2}{2C}\right)\frac{1}{\rho\,\Delta x}\Delta E_{meas} \quad (7.313)$$

where ΔE_{meas} is the measured energy loss of the proton. For the measurement conditions specified,

$$\begin{aligned}L_0(\beta) &= L_{00}(\beta) + L_{01}(\beta) \\ &= \ln\left(\frac{2m_e}{\bar{I}}\gamma^2\beta^2\right) - \beta^2 - \frac{C_e(\beta)}{Z} \\ &= -\left(\ln\bar{I} + \frac{C_e(\beta)}{Z}\right) + \ln\left(2m_e\gamma^2\beta^2\right) - \beta^2\end{aligned} \quad (7.314)$$

where $\bar{I}$ and m_e implicitly have the same units of energy. Equating these two expressions for $L_0(\beta)$ and solving for $(\ln\bar{I} + C_e(\beta)/Z)$ gives,

$$\begin{aligned}\left(\ln\bar{I} + \frac{C_e(\beta)}{Z}\right) = \left(\frac{A}{Z}\right)\left(\frac{\beta^2}{2C}\right)\frac{1}{\rho\,\Delta x}\Delta E_{meas} \\ + \ln\left(2m_e\gamma^2\beta^2\right) - \beta^2.\end{aligned} \quad (7.315)$$

It is clear that the mean excitation potential and the shell correction effect are not separated (although at sufficiently high projectile energies, we can neglect the latter). However, since both quantities appear in this combination in the collision stopping power expression, this is not problematic for calculating the collision stopping power.

[17] ICRU Report 49 (1993) provides a comprehensive historical summary of the various experimental techniques used to measure the stopping power.

7.3.8 Mean Energy Required to Create an Ion Pair

The immediate consequence of ionization in a liquid or gaseous medium is the creation of an electron-ion pair. In some solids, ionization can elevate electrons into the conduction band, thus forming an electron-hole pair (following the convention used by ICRU Report No 31 (1979), the term "ion pair" will be used to describe both electron-ion and electron-hole pairs). Of fundamental interest to experimental radiation dosimetry is the mean energy expended to create an ion pair, W, by electrons. Knowledge of W coupled with the collision stopping power is required in order to estimate the number of ion pairs produced per unit pathlength. Measurement of this number (in, e.g., an ionization chamber) can be used to infer the stopping power or, equivalently, the energy absorption in the medium.

It was seen in the derivation of the collision stopping power that the electromagnetic interaction between an incident charged particle and an atom can lead to both atomic excitation and the elevation of an atomic electron into the continuum. Hence, the competing effects of nonionization energy channels leads to the fact that the value of W will exceed the first ionization potential of the atom. Consider a charged particle with kinetic energy T that has been completely stopped in a gaseous medium. The equation of energy balance is,

$$T = N_{Ion}(\bar{E}_{Ion} + \bar{\varepsilon}) + N_{Exc}\bar{E}_{Exc} \tag{7.316}$$

where N_{Ion} is the total number of electrons generated through ionization and N_{Exc} is the total number of excited atomic states. $\bar{E}_{Ion}$ is the mean energy required to produce an ion, $\bar{\varepsilon}$ is the mean energy of the secondary electrons (δ rays) which are not energetic enough to cause further ionizations and $\bar{E}_{Exc}$ is the mean energy of the discrete excited atomic states. By definition, the mean energy expended to produce an ion pair is given by,

$$\begin{aligned} W &= \frac{T}{N_{Ion}} \\ &= (\bar{E}_{Ion} + \bar{\varepsilon}) + \left(\frac{N_{Exc}}{N_{Ion}}\right)\bar{E}_{Exc} \end{aligned} \tag{7.317}$$

and the ratio of W to the ionization energy I is,

$$\frac{W}{I} = \frac{\bar{E}_{Ion}}{I} + \frac{\bar{\varepsilon}}{I} + \left(\frac{N_{Exc}}{N_{Ion}}\right)\frac{\bar{E}_{Exc}}{I}. \tag{7.318}$$

It is possible to describe qualitatively the magnitude of the three terms on the right-hand side of (7.318) from first principles. First, one would expect,

$$\frac{\bar{E}_{Ion}}{I} > 1 \tag{7.319}$$

due to the fact that excitation and other nonionization channels exist, especially for molecules where there are rotational and vibrational modes available. Similarly, one would also expect that,

$$\frac{\bar{E}_{Exc}}{I} > 1 \tag{7.320}$$

although this ratio is not that much different from unity as the energy levels of most discrete excited states are relatively near I. The ratio $\bar{\varepsilon}/I$ will be small with values typically about 0.3 for noble gases and smaller for molecular gases. Finally, the ratio of the number of discrete excited states to the number of ionizations, N_{Exc}/N_{Ion} is estimated in ICRU Report Number 31 (1979) to be about 0.3 for closed-shell atoms and close to 1 for closed-shell molecules. Overall, the magnitude of W/I is greater than unity with values ranging from about 1.7 for noble gases to up to 3.2 for alkaline earths.

The total number of electrons produced is also expected to be a function of the particle's kinetic energy. Consider a medium in which the atoms have a single ionization energy, I, through which a single electron with kinetic energy T slows down and stops. The number of electrons produced as a result is (Fowler 1923),

$$\begin{aligned} N_e(T) = {} & \frac{\sigma_{Ion}(T)}{\sigma_{Inel}(T)} + \frac{1}{\sigma_{Inel}(T)}\sum_n \sigma_n(T)\, N(T - \Delta E_n) \\ & + \frac{1}{\sigma_{Inel}(T)} \int_I^{\frac{1}{2}(T+I)} d(\Delta E_n)\frac{d\sigma_{Ion}(T, \Delta E_n)}{d(\Delta E)_n} \\ & \times (N_{Ion}(T - \Delta E_n) + N_{Ion}(\Delta E_n - I)) \end{aligned} \tag{7.321}$$

where $\sigma_{Inel}(T)$ is the total inelastic cross section, $\sigma_{Ion}(T)$ is the total ionization cross section and

$\sigma_n(T)$ is the total cross section for excitation to the nth atomic state. Obviously, the total inelastic cross section is the sum of the ionization and excitation cross sections,

$$\sigma_{Inel}(T) = \sigma_{Ion}(T) + \sigma_n(T). \tag{7.322}$$

The first term on the right-hand side of (7.321) describes the number of secondary electrons produced as a consequence of the first inelastic collision. If this collision leads to the excitation of the atom to an energy level ΔE_n, the incident electron is scattered with a kinetic energy $T - \Delta E_n$ and the mean of the total number of ion pairs produced by the scattered electron is given by $(\sigma_N(T)/\sigma_{Inel}(T))\, N(T - \Delta E_n)$. The sum of this contribution over all excited states is the second term on the right-hand side of the equation. Finally, one must account for the fact that the first inelastic collision is itself ionizing and results in an electron-ion pair: the scattered electron with kinetic energy $T - \Delta E_n$ and an ejected electron (δ ray) with kinetic energy $\Delta E_n - I$. This event contributes both to the first and third terms on the right-hand side.

Obviously, knowledge of the energy dependence of the inelastic, ionization, and excitation cross sections is required in order to evaluate (7.322). Another approach to calculating for $N_e(T)$ was proposed by Spencer and Fano (1954) and uses the concept of the degradation spectrum. Imagine a monoenergetic beam of electrons with kinetic energy T incident to a gas. Within this medium, these electrons will, through deceleration and the production of secondary electrons, yield a net flux of electrons with an energy spectrum. The pathlength of all electrons with kinetic energies between T' and $T' + dT'$ is $y(T, T')dT'$, which is also a descriptor of the electron spectrum. This spectrum will not be derived here; one can note that in the extreme case of the CSDA for $T \gg 1$ in which the projectile loses only a small amount of energy, the number of produced electrons is,

$$N_e(T) = \rho_{Molec} \int_I^T dT'\, \sigma_{Ion}(T')y(T, T') \tag{7.323}$$

where ρ_{Molec} is the number of molecules per unit volume in the medium (i.e., the molecular number density). A scaling property of $y(T, T')dT'$ was found by Douthat (1975) who showed that the quantity $\rho_{Molec}(T'/T)\ln(T/I)\sigma_{Ion}(T')y(T, T')$ plotted as a function of the variable,

$$\xi = \frac{\ln\left(\frac{T'}{I}\right)}{\ln\left(\frac{T}{I}\right)},$$

was virtually independent of the projectile electron's kinetic energy, Fano and Spencer (1975) subsequently defined the quantity

$$z(\xi) = \rho_{Molec}\, \sigma_{St}(T') \left(\frac{\ln\left(\frac{T'}{I}\right)}{\xi}\right) \left(\frac{T'}{T}\right) y(T', T) \tag{7.324}$$

where $\sigma_{St}(\xi)$ is the stopping cross section. Using this, the expression for $N_e(T)$ can now be rewritten as,

$$N_e(T) = T \int_0^1 d\xi\, z(\xi) \frac{\sigma_{Ion}(\xi)}{\sigma_{St}(\xi)} \tag{7.325}$$

which leads to an expression of the mean energy required to produce an ion pair,

$$W(T) = \frac{1}{\int_0^1 d\xi\, z(\xi) \frac{\sigma_{Ion}(\xi)}{\sigma_{St}(\xi)}}. \tag{7.326}$$

It should be noted that $\Delta T' \frac{\sigma_{Ion}(\xi)}{\sigma_{St}(\xi)}$ is the number of ion pairs produced directly by the projectile electron within the energy interval $T' - \Delta T'$ to T'.

W has a limited sensitivity to the charge, mass and kinetic energy of the projectile, although the dependence upon projectile kinetic energy increases when the projectile speed becomes comparable to those of the valence electrons. This general insensitivity to projectile kinetic energy at high energies is a consequence of the fact that the ratio of the ionization cross section to the sum of excitation cross sections has a limited energy dependence. For dry air as a medium,

$$W_{Dry\,Air} = 33.8_5 \pm 0.15\,eV$$

Thus a 5 MeV α particle completely stopped in dry air will create about 1.25×10^5 electron-ion pairs.

Values of W for solids will be much less than for gases as a result of the difference between the ~1 eV gap between the valence and electron bands of a solid and the ~10 eV ionization energy of gases. For example, W for electrons in solid silicon is

$$W_{Si} = 3.68 \pm 0.02\,eV$$

7.3.9 Restricted Mass Collision Stopping Power for Electrons

Here, the discussion of the restricted mass collision stopping power for electrons is returned to,

$$\left(\frac{dE}{\rho dx}\right)_{Col,\Delta} = -C\left(\frac{Z}{A}\right)\left(\frac{1}{\beta}\right)^2 \times \left(\ln\left(\frac{2\Delta(T-\Delta)}{\bar{I}^2}(\gamma+1)\right) + f^-(\gamma,\Delta)\right)$$

where,

$$f^-(\gamma,\Delta) = \left(\frac{\Delta}{T-\Delta}\right) - \beta^2 + \left(\frac{2\gamma-1}{\gamma}\right)\ln\left(\frac{T-\Delta}{T}\right) + \left(\frac{\gamma-1}{\gamma}\right)^2\frac{\Delta^2}{2T^2}$$

and where Δ is the kinetic energy of the knock-on electron, $\Delta < T/2$. The restricted collision stopping power focuses our attention on the local energy deposition along the electron's track. A given value for Δ will denote the extent of the region around the projectile electron's trajectory that we are interested in knowing the energy transferred to or absorbed within the medium. In particular, if one is interested in the energy deposited in a small volume that the electron is passing through, then the use of the unrestricted collision stopping power will overestimate the deposited energy (unless the condition of charged particle equilibrium exists, in which the energy removed from the volume by the δ rays is compensated for by energy brought into the volume by δ rays generated from outside the volume). This will have important consequences in microdosimetry which we will be considering in following chapters. Tables of restricted and unrestricted collision stopping powers for electrons can be found in ICRU Report 37 (1984).

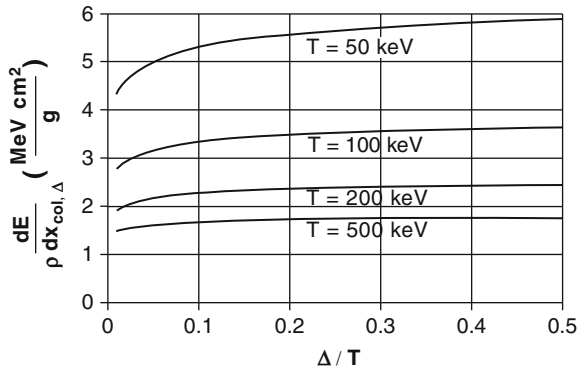

Fig. 7.27 Restricted mass collision stopping power for electrons in carbon as a function of the secondary electron kinetic energy normalized to the incident kinetic energy

Figure 7.27 shows $(dE/\rho dx)_{Col,\Delta}$ calculated as a function of $\Delta/T \leq 1/2$ for 50, 100, 200, and 500 keV electrons in carbon (excluding shell and polarization correction effects in order to show the effect of secondary electron energy restriction more clearly). The unrestricted mass collision stopping power is that for $\Delta = T/2$.[18] One sees that the restricted collision stopping power is always less than the unrestricted and that this difference decreases with increasing T, as to be expected. The increase in $(dE/\rho dx)_{Col,\Delta}$ with increasing Δ/T is the result of including more collisions which result in the transfer of energy to the medium. On the other hand, the decreasing difference between the unrestricted and restricted collision stopping powers with increasing T as shown in the figure is due to the approaching region of minimal ionization.

7.3.10 Summary of the Mass Collision Stopping Power

As the Barkas polarization term is negligible for practical dosimetry purposes, it is neglected in this summary of the collision stopping power. Including the shell-, density-, and Bloch correction factors, the mean

[18] A closely related quantity is the linear energy transfer, or LET, which is simply the restricted linear collision stopping power.

collision stopping power for a massive spin-0 projectile with charge ze is,

$$\left(\frac{dE}{\rho dx}\right)_{Col} = -2C\left(\frac{Z}{A}\right)\left(\frac{z}{\beta}\right)^2\left[\ln\left(\frac{2m_e}{\bar{I}}\gamma\beta^2\right) - \beta^2 - \frac{C_e}{Z} - \frac{\delta}{2} - \gamma_{EM} - \ln\left(\alpha\frac{z}{\beta}\right)\right]. \tag{7.327}$$

The mean collision stopping power for electrons and positrons is,

$$\left(\frac{dE}{\rho dx}\right)_{Col\pm} = -C\left(\frac{Z}{A}\right)\left(\frac{1}{\beta}\right)^2\left[\ln\left(\frac{T^2(\gamma+1)}{2\bar{I}^2}\right) + f_{\pm}(\gamma) - \frac{C_e}{Z} - \frac{\delta}{2} - \gamma_{EM} - \ln\left(\alpha\frac{z}{\beta}\right)\right] \tag{7.328}$$

The functional dependencies of the mass collision stopping power are:

- At low projectile energies, the mass collision stopping power decreases with increasing kinetic energy as β^{-2} until reaching the minimally-ionizing region which corresponds to $\beta \approx 0.8$. At very low energies where the projectile speed is comparable to those of the atomic electrons, $(dE/\rho dx)_{Col}$ decreases with decreasing projectile energy due to the shell correction factor.
- This general β^{-2} dependence competes with the relativistic increase in the collision stopping power leading to a minimum of about 1.5 Mev • cm^2/g at a kinetic energy equal to about 3 times the projectile mass.
- The relativistic increase in $(dE/\rho dx)_{Col}$ due to the $\ln(\gamma^2\beta^2)$ and $\ln(\gamma+1)$ terms are quenched by the density correction $\delta/2$ term leading to what is also known as the "Fermi Plateau."

Neglecting the small effect of the Barkas correction, further generalizations can be made:

Projectile rest mass, m: There is no dependence of the mass collision stopping power upon the particle's mass. Thus, for example, the mass collision stopping powers of a proton and a single-ionized helium ion (i.e., equal charges) at the same speed are the same.

Projectile charge, z: The mass collision stopping power increases with the square of the particle charge. Extending the previous example to a proton and an α particle at the same speed, the $(dE/\rho dx)_{Col}$ for the α particle will be four times greater than that of the proton.

Medium atomic number Z and atomic mass number A: For low atomic media $Z/A \approx 1/2$ decreasing with increasing Z (e.g., Z/A = 0.5 and approaches 0.4 for carbon and lead, respectively). As a result the mass collision stopping power at a given kinetic energy is greater for a low-Z medium than for one with high-Z. There is an additional dependence upon the atomic number contained within the $\approx -\ln\bar{I}$ term. The mean ionization potential $\bar{I}$ increases with Z thus further contributing to the decrease in $(dE/\rho dx)_{col}$ with Z.

Finally, it is of interest to consider the energy loss resulting from the Coulomb interaction between the heavy charged particle and the nucleus rather than an atomic electron. There will be an immediate increase of a factor of Z^2. However, there is a reciprocal dependence upon the target mass, thus the net change in the collision stopping power will be by a factor of Z^2m_e/M where M is the nuclear mass. As $Z^2m_e/M = 1.6 \times 10^3$ for carbon and 1.7×10^2 for lead, it can be seen that the contribution of the nucleus to the collision stopping power can be neglected.

7.4 Stochastic Collision Energy Loss: Energy Straggling

7.4.1 Introduction

It has been assumed in the prior derivations that energy loss is a continuous function or, for a particle traversing a distance t through a medium,

$$\Delta E = \int_0^t dx \left(\frac{dE}{dx}\right)_{Col}(x) \tag{7.329}$$

However, the energy is lost by the particle through discrete interactions with atomic electrons and, as a result, the energy loss process is not continuous but stochastic. In the simplest approximation, for a beam of monoenergetic particles incident to the medium, (7.329) provides the mean energy lost by the ensemble of particles and the actual energy loss will described by a probability distribution function with the exiting

particle beam having an energy spectrum reflecting this pdf. This phenomenon is commonly referred to as energy straggling and the energy loss pdfs describing this phenomenon are the subject of this section.

Practical applications of these pdfs in nuclear medicine dosimetry reside primarily in Monte Carlo codes used to simulate radiation transport and calculate energy deposition in a medium. Such Monte Carlo codes have been categorized in terms of how they calculate for the energy straggling of moving charged particles in a medium (Chibani 2002). Some codes, such as MCNP (Briesmeister 2000) and ETRAN (Seltzer 1991), use a pdf to sample the energy loss corresponding to a given pathlength. Other codes simulate the inelastic collision between the projectile and the secondary electron as a distinct event should the energy transfer Q exceed the energy level Q_c (i.e., the collision is consider hard). A mean energy loss due to soft collisions is calculated through the use of the restricted collision stopping power. An example of such a code widely used in medical physics is EGSnrc (Kawrakow and Rogers 2003).[19] The GEANT code can be considered to straddle both categories as pdfs are sampled to evaluate hard-energy losses, but the user can also treat hard collisions as independent events (GEANT Team 2001).[20]

The pdfs describing these energy losses are derived in this section.

7.4.2 One-Dimensional Continuity Equation

Figure 7.28 shows a slab of material with physical density ρ to which is incident a monoenergetic beam of charged particles with kinetic energy T_0. The model is one-dimensional and multiple scatter is neglected, i.e., the particles travel in straight lines. Let N(x,ΔE) be the number of particles that have penetrated a depth x with a net energy loss ΔE. Now consider the number

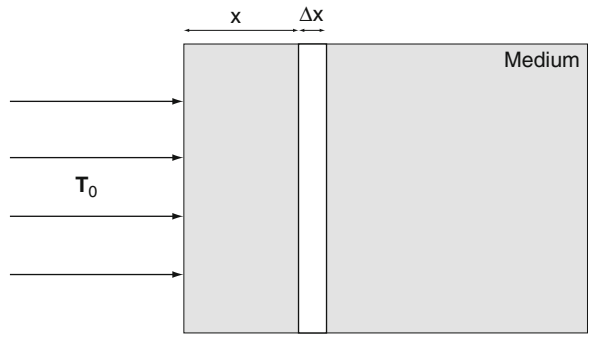

Fig. 7.28 Geometry for derivation of one-dimensional continuity equation. A monoenergetic beam of charged particles with kinetic energy T_0 is incident from the left to a medium with physical density ρ

of particles which, traversing an additional distance Δx, will also have a net energy loss ΔE (the thickness Δx is sufficiently small that a particle can only lose energy within it as the result of a single collision). This number will be the original number of particles with energy loss ΔE at x and which did not lose energy crossing Δx minus the number of particles with energy loss ΔE at x which suffered any additional energy loss as a result of traversing Δx, and plus the number of particles with energy loss $\Delta E' < \Delta E$ at x and which undergo an additional energy loss $\Delta E - \Delta E'$ (where $\Delta E' - \Delta E \leq Q_{max}$) traversing Δx so that they have a net energy loss ΔE at a depth x+Δx.

Define $\Pr(\Delta x, \Delta E \rightarrow \Delta E')$ to be the probability that a particle with an energy loss ΔE in penetrating to x will experience an additional energy loss $\Delta E' - \Delta E$ through crossing x to have a total energy loss $\Delta E'$ at a depth of x + Δx. Hence, the number of particles with energy loss ΔE at the depth x + Δx is,

$$\begin{aligned} N(x+\Delta x, \Delta E) &= N(x, \Delta E) \\ &- \int_{\Delta E}^{\infty} d(\Delta E') \Pr(\Delta x, \Delta E \rightarrow \Delta E') N(x, \Delta E) \\ &+ \int_{0}^{\Delta E} d(\Delta E') \Pr(\Delta x, \Delta E' \rightarrow \Delta E) N(x, \Delta E'). \end{aligned} \tag{7.330}$$

The first integral describes the reduction in particle number with energy loss ΔE at the depth x + Δx due to particles with energy loss ΔE at x experiencing an energy loss while passing through Δx. The second integral yields the increase in the number of particles

[19] Both classes represent conceptual difficulties: a Class I code does not link the sampling of the energy loss pdf with secondary recoil electrons and the Class II code neglects any energy straggling associated with soft collisions.

[20] Further discussion of the practical matters of the Monte Carlo simulation of the transport of charged particles can be found in the articles by Salvat et al. (1999) and Chibani (2002).

with energy loss ΔE at the depth $x + \Delta x$ due to particles with energy loss $\Delta E' < \Delta E$ undergoing that energy loss within the thickness Δx to bring the net energy loss at $x + \Delta x$ to ΔE. The differential change with distance in particle number with energy loss ΔE at depth x is,

$$\begin{aligned}\frac{\partial N(x,\Delta E)}{\partial x} &\equiv \lim_{\Delta x \to 0} \frac{N(x+\Delta x,\Delta E) - N(x,\Delta E)}{\Delta x} \\ &= \lim_{\Delta x \to 0} \left[-\int_{\Delta E}^{\infty} d(\Delta E') \right. \\ &\quad \times \frac{\Pr(\Delta x, \Delta E \to \Delta E')}{\Delta x} N(x,\Delta E) \\ &\quad \left. + \int_{0}^{\Delta E} d(\Delta E') \frac{\Pr(\Delta x, \Delta E' \to \Delta E)}{\Delta x} N(x,\Delta E') \right] \\ &= -\int_{\Delta E}^{\infty} d(\Delta E') \omega(\Delta E' - \Delta E) N(x,\Delta E) \\ &\quad + \int_{0}^{\Delta E} d(\Delta E') \omega(\Delta E' - \Delta E) N(x,\Delta E')\end{aligned} \tag{7.331}$$

where $\omega(\delta E)$ is the probability per unit pathlength of the particle losing energy δE. One can use the change of variables to rewrite this integrodifferential equation, noting that $\omega(\delta E) = 0$ for $\delta E > Q_{max}$, to obtain

$$\begin{aligned}\frac{\partial N(x,\Delta E)}{\partial x} &= -\int_{0}^{Q_{max}} dQ\, \omega(Q) N(x,\Delta E) \\ &\quad + \int_{0}^{\min(Q_{max},\Delta E)} dQ\, \omega(Q) N(x,\Delta E - Q).\end{aligned} \tag{7.332}$$

As the probability distribution function describing the collision energy loss is,

$$f(x,\Delta E) = \frac{N(x,\Delta E)}{\int_{0}^{T_0} d(\Delta E') N(x,\Delta E')} \tag{7.333}$$

it is possible to write the continuity equation for the pdf in the integrodifferential form,

$$\begin{aligned}\frac{\partial f(x,\Delta E)}{\partial x} &= -f(x,\Delta E) \int_{0}^{Q_{max}} dQ\, \omega(Q) \\ &\quad + \int_{0}^{\min(Q_{max},\Delta E)} dQ\, \omega(Q) f(x,\Delta E - Q).\end{aligned} \tag{7.334}$$

7.4.3 Gaussian Probability Distribution Function for ΔE

The first solution to the integrodifferential continuity equation is provided by following an approach first described by Rossi (1952) and expanded upon by Kase and Nelson (1978) (Segrè (1977) provides a simpler and perhaps more intuitive method based on the central-limit theorem and which is traceable to early work by Bohr). A complete derivation of the Gaussian pdf as a solution to the continuity equation is provided here. By the use of a number of simplifying assumptions, the integrodifferential continuity equation is converted into a differential equation which can be solved via Fourier transform pairs. The assumptions for this solution method are:

- The mean energy lost by the particle penetrating to depth x is small, $\overline{\Delta E} << T_0$.
- The collision stopping power can be approximated as a constant over the distance traveled x so that the mean energy loss at the depth of penetration x is given by

$$\overline{\Delta E} = x \left(\frac{dE}{dx} \right)_{Col} \tag{7.335}$$

- The probability distribution function $f(x,\Delta E)$ varies slightly with energy loss enabling $f(x,\Delta E - Q)$ to be expanded into a second-order Taylor's series

$$\begin{aligned}f(x,\Delta E - Q) \cong f(x,\Delta E) &- \frac{\partial f(x,\Delta E)}{\partial(\Delta E)} Q \\ &+ \frac{1}{2} \frac{\partial^2 f(x,\Delta E)}{\partial(\Delta E)^2} Q^2.\end{aligned} \tag{7.336}$$

By noting that $\omega(Q) = 0$ for $Q > Q_{max}$, the continuity equation can be rewritten using the Taylor series expansion to form a differential equation in $f(x, \Delta E)$,

$$\begin{aligned}\frac{\partial f(x,\Delta E)}{\partial x} &= -\int_0^\infty dQ\,\omega(Q) f(x,\Delta E) \\ &\quad + \int_0^\infty dQ\,\omega(Q) f(x,\Delta E - Q) \\ &= \int_0^\infty dQ\,\omega(Q)(f(x,\Delta E - Q) - f(x,\Delta E)) \\ &= \int_0^\infty dQ\,\omega(Q)\left(-\frac{\partial f(x,\Delta E)}{\partial(\Delta E)}Q\right. \\ &\quad \left. + \frac{1}{2}\frac{\partial^2 f(x,\Delta E)}{\partial(\Delta E)^2}Q^2\right) \\ &= -\frac{\partial f(x,\Delta E)}{\partial(\Delta E)}\int_0^\infty dQ\,\omega(Q)Q \\ &\quad + \frac{1}{2}\frac{\partial^2 f(x,\Delta E)}{\partial(\Delta E)^2}\int_0^\infty dQ\,\omega(Q)\,Q^2 \\ &= -k_1\frac{\partial f(x,\Delta E)}{\partial(\Delta E)} + \frac{k_2^2}{2}\frac{\partial^2 f(x,\Delta E)}{\partial(\Delta E)^2}\end{aligned} \tag{7.337}$$

where,

$$\begin{aligned}k_1 &= \int_0^\infty dQ\,\omega(Q)Q \\ &= \frac{\overline{\Delta E}}{x}\end{aligned} \tag{7.338}$$

and

$$k_2^2 = \int_0^\infty dQ\,\omega(Q)Q^2. \tag{7.339}$$

As the expression for k_1 contains the factor Q whereas that for k_2^2 contains Q^2, the role of soft collisions will be less significant in the evaluation of k_2^2 than for k_1, so one consequently calculates k_1 using the total collision stopping power and uses only the hard collision stopping power in the determination of k_2^2. In other words, the width of the pdf is a function of the hard collision energy transfer alone. This observation becomes important when considering asymmetric pdfs for ΔE.

In order to solve this differential equation, one again uses the Fourier transform method,

$$\xi(x,\tau) = \frac{1}{\sqrt{2\pi}}\int_{-\infty}^\infty d(\Delta E)e^{-i\tau\Delta E} f(x,\Delta E) \tag{7.340}$$

$$f(x,\Delta E) = \frac{1}{\sqrt{2\pi}}\int_{-\infty}^\infty d\tau\, e^{i\tau\Delta E}\,\xi(x,\tau). \tag{7.341}$$

The Fourier transform of (7.337) is,

$$\frac{\partial\xi(x,\tau)}{\partial x} = -\left(ik_1\tau + \frac{k_2^2\tau^2}{2}\right)\xi(x,\tau) \tag{7.342}$$

which is straightforward to solve,

$$\xi(x,\tau) = \xi(0,\tau)e^{-\left(ik_1\tau + \frac{k_2^2\tau^2}{2}\right)x}. \tag{7.343}$$

The initial condition is determined by noting that

$$f(0,\Delta E) = \delta(\Delta E). \tag{7.344}$$

The Fourier transform of this initial condition is,

$$\xi(0,\tau) = \frac{1}{\sqrt{2\pi}} \tag{7.345}$$

Inserting this and the definition of k_1 into (7.343) gives the Fourier transform of the probability distribution function,

$$\xi(x,\tau) = \frac{1}{\sqrt{2\pi}}e^{-\left(i\tau\overline{\Delta E} + \frac{k_2^2\tau^2}{2}\right)x}. \tag{7.346}$$

The pdf is recovered through the inverse Fourier transform,

$$\begin{aligned}f(x,\Delta E) &= \frac{1}{\sqrt{2\pi}}\int_{-\infty}^\infty d\tau\, e^{i\tau\Delta E}\,\xi(x,\tau) \\ &= \frac{1}{2\pi}\int_{-\infty}^\infty d\tau\, e^{-i\tau\left(\overline{\Delta E} - \Delta E\right) - \frac{k_2^2\tau^2}{2}x}.\end{aligned} \tag{7.347}$$

This integral is solved by first algebraically rearranging the exponent,

$$i\tau\left(\overline{\Delta E}-\Delta E\right)+\frac{k_2^2\tau^2}{2}x=\left(k_2\tau\sqrt{\frac{x}{2}}+i\frac{\overline{\Delta E}-\Delta E}{k_2\sqrt{2x}}\right)^2+\frac{\left(\overline{\Delta E}-\Delta E\right)^2}{2k_2^2x} \tag{7.348}$$

which allows the pdf to be rewritten as,

$$f(x,\Delta E)=\frac{1}{2\pi}e^{-\frac{\left(\overline{\Delta E}-\Delta E\right)^2}{2k_2^2x}}\int_{-\infty}^{\infty}d\tau\, e^{-\left(k_2\tau\sqrt{\frac{x}{2}}+i\frac{\overline{\Delta E}-\Delta E}{k_2\sqrt{2x}}\right)^2}. \tag{7.349}$$

Changing variables,

$$z=k_2\tau\sqrt{\frac{x}{2}}+i\frac{\overline{\Delta E}-\Delta E}{k_2\sqrt{2x}} \tag{7.350}$$

$$d\tau=\sqrt{\frac{2}{x}}\frac{dz}{k_2} \tag{7.351}$$

the integral can be simplified to,

$$\int_{-\infty}^{\infty}d\tau\, e^{-\left(k_2\tau\sqrt{\frac{x}{2}}+i\frac{\overline{\Delta E}-\Delta E}{k_2\sqrt{2x}}\right)^2}=\frac{1}{k_2}\sqrt{\frac{2}{x}}\int_{-\infty+iy_0}^{\infty+iy_0}dz\, e^{-z^2} \tag{7.352}$$

where

$$y_0=\frac{\overline{\Delta E}-\Delta E}{k_2\sqrt{2x}} \tag{7.353}$$

The integral is solved by writing it in the complex form $\int_{-K+iy_0}^{K+iy_0}dz\, e^{-z^2}$ where K is a real constant to be later allowed to go to ∞. As e^{-z^2} is holomorphic on and within the contour and there are no singularities within the contour, the Cauchy–Goursat theorem states that,

$$\int_C dz\, e^{-z^2}=0. \tag{7.354}$$

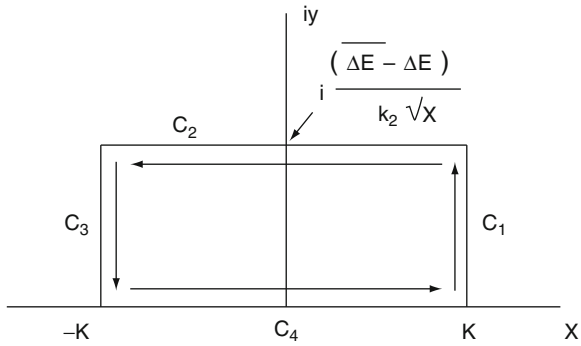

Fig. 7.29 Rectangular contour in the complex z = x + iy plane for solving the integral of (7.352)

The closed contour in the complex plane is shown in Fig. 7.29 and is made up of four individual contours,

$$C=C_1\cup C_2\cup C_3\cup C_4. \tag{7.355}$$

Thus,

$$\int_{C_1}dz\, e^{-z^2}+\int_{C_2}dz\, e^{-z^2}+\int_{C_3}dz\, e^{-z^2}+\int_{C_4}dz\, e^{-z^2}=0. \tag{7.356}$$

This then leads to,

$$\int_{-K+iy_0}^{K+iy_0}dz\, e^{-z^2}=-\int_{C_2}dz\, e^{-z^2}=\int_{C_1}dz\, e^{-z^2}+\int_{C_3}dz\, e^{-z^2}+\int_{C_4}dz\, e^{-z^2}. \tag{7.357}$$

This type of integral is solved in the Appendices,

$$\int_{-\infty+iy_0}^{\infty+iy_0}dz\, e^{-z^2}=\sqrt{\pi} \tag{7.358}$$

leading to,

$$\int_{-\infty}^{\infty}d\tau\, e^{-\left(k_2\tau\sqrt{\frac{x}{2}}+i\frac{\overline{\Delta E}-\Delta E}{k_2\sqrt{2x}}\right)^2}=\frac{1}{k_2}\sqrt{\frac{2\pi}{x}}. \tag{7.359}$$

The above result provides the Gaussian probability distribution function for energy loss ΔE at a depth x,

$$f(x,\Delta E)=\frac{1}{\sqrt{2\pi\,k_2^2 x}}e^{-\frac{\left(\overline{\Delta E}-\Delta E\right)^2}{2k_2^2 x}}. \tag{7.360}$$

In order to verify that this result is a pdf, it is necessary to require the normalization,

$$\int_0^\infty d(\Delta E)\,f(x,\Delta E)=1$$

or, since the maximum energy loss cannot exceed the incident kinetic energy,

$$\int_0^{T_0} d(\Delta E)\,f(x,\Delta E)=1.$$

Inserting the expression for the pdf into this integral,

$$\frac{1}{\sqrt{2\pi\,k_2^2 x}}e^{-\frac{\left(\overline{\Delta E}-\Delta E\right)^2}{2k_2^2 x}}=\frac{1}{\sqrt{\pi}}\int_{y_1}^{y_2}dy\,e^{-y^2} \tag{7.361}$$

where the change of variables,

$$y=\frac{\overline{\Delta E}-\Delta E}{\sqrt{2k_2^2 x}} \tag{7.362}$$

has been used. The limits of integration are,

$$y_1=\frac{\overline{\Delta E}-T_0}{\sqrt{2k_2^2 x}} \tag{7.363}$$

and

$$y_2=\frac{\overline{\Delta E}}{\sqrt{2k_2^2 x}}. \tag{7.364}$$

If $T_0-\overline{\Delta E}\gg\sqrt{2k_2^2 x}$ and $\overline{\Delta E}\gg\sqrt{2k_2^2 x}$, then the result of (7.361) can be written as,

$$\frac{1}{\sqrt{\pi}}\int_{-\infty}^{\infty}dy\,e^{-y^2}=1$$

thus demonstrating that $f(x,\Delta E)$ is the pdf sought and is a Gaussian distribution with mean and most probable energy loss,

$$\overline{\Delta E}=x\left(\frac{dE}{dx}\right)_{Col} \tag{7.365}$$

and variance,

$$\sigma^2=k_2^2 x. \tag{7.366}$$

The width of this Gaussian (2σ) must be greater than the maximum energy transferred in a single collision (i.e., $2k_2\sqrt{x}\gg Q_{max}$, which follows from the central-limit theorem) but smaller than the incident kinetic energy ($2k_2\sqrt{x}\ll T_0$) and the mean energy loss, or $2k_2\sqrt{x}\ll\overline{\Delta E}$. As an example, calculate the variance for the limiting case for a massive spin-0 projectile,

$$\begin{aligned}\frac{d\sigma}{dQ}&=2\pi r_0^2 m_e\left(\frac{z}{\beta}\right)^2\frac{1}{Q^2}\left(1-\beta^2\frac{Q}{Q_{max}}\right) && Q\le Q_{max}\\ &=0 && Q>Q_{max}\end{aligned}$$

and the probability of energy loss per unit distance traveled is,

$$\begin{aligned}\omega(Q)&=N_A\rho\left(\frac{Z}{A}\right)\frac{d\sigma}{dQ}\\ &=C\rho\left(\frac{Z}{A}\right)\left(\frac{z}{\beta}\right)^2\frac{1}{Q^2}\left(1-\beta^2\frac{Q}{Q_{max}}\right)\\ &\equiv\frac{\zeta}{Q^2}\left(1-\beta^2\frac{Q}{Q_{max}}\right)\end{aligned} \tag{7.367}$$

where C is the constant pervading this chapter and the factor,

$$\zeta\equiv C\rho\left(\frac{Z}{A}\right)\left(\frac{z}{\beta}\right)^2 \tag{7.368}$$

has been defined. This constant has units of MeV per centimeter. Hence, the variance of the energy loss pdf is,

$$\begin{aligned}\sigma^2&=x\int_0^\infty dQ\,\omega(Q)Q^2\\ &=x\zeta\int_0^{Q_{max}}dQ\left(1-\beta^2\frac{Q}{Q_{max}}\right)\\ &=x\zeta\,Q_{max}\left(1-\frac{\beta^2}{2}\right)\end{aligned} \tag{7.369}$$

The energy inequalities resulting from above are,

$$\frac{Q_{max}}{2} \ll k_2\sqrt{x} \ll \frac{T_0}{2} \tag{7.370}$$

and

$$k_2\sqrt{x} \ll \frac{\bar{E}}{2}. \tag{7.371}$$

These can be grouped into the requirement that the ratio

$$\kappa = \frac{x\zeta}{Q_{max}} \tag{7.372}$$

must be large in order for the probability distribution function for energy loss to be approximated by a Gaussian.

7.4.4 Asymmetric Probability Distribution Functions for ΔE

7.4.4.1 Introduction

Having demonstrated that a symmetric Gaussian pdf for the energy loss is the consequence of a large value of κ which corresponds to a thick pathlength x and, from the definition of ζ, to nonrelativistic particles ($\beta \ll 1$). For small κ, which corresponds to a thin absorber and/or increasingly relativistic charged particles, the mean energy loss will also decrease. However, because the probability of a hard collision remains constant, its relative contribution to the statistical distribution of energy losses will increase as κ decreases, leading to increasing asymmetry in the pdf for ΔE. In this case, the integrodifferential form of the continuity equation cannot be reduced to a simple differential equation and must, instead, be solved directly.

7.4.4.2 Vavilov Probability Distribution Function

Historically, it was Landau (1944) who first derived a solution to the general integrodifferential continuity equation leading to an asymmetric pdf through the use of Laplace transforms. Landau's result, however, was derived for the Rutherford differential cross section (which is equivalent to neglecting the $\beta^2 Q/Q_{max}$ term in the Bhabha cross section) and was dependent upon a variety of approximations. A more general and exact solution to the one-dimensional continuity equation was provided by Vavilov (1957) which reaches the Gaussian pdf as a limit for $\kappa \to \infty$ and the Landau result for $\kappa \to 0$. Hence, the Landau probability distribution function for energy loss will be treated as a special limiting case of the Vavilov. This derivation follows Vavilov's approach and solves the integrodifferential continuity equation for f(x,ΔE) by using Laplace transform pairs,

$$\xi(x,\tau) = \int_0^\infty d(\Delta E)\, e^{-\tau \Delta E} f(x,\Delta E) \tag{7.373}$$

$$f(x,\Delta E) = \frac{1}{2\pi i}\int_{K-i\infty}^{K+i\infty} d\tau\, e^{\tau \Delta E}\xi(x,\tau) \tag{7.374}$$

$$\Omega(\tau) = \int_0^\infty dQ\, e^{-\tau Q}\, \omega(Q) \tag{7.375}$$

$$\omega(Q) = \frac{1}{2\pi i}\int_{K-i\infty}^{K+i\infty} d\tau\, e^{\tau Q}\, \Omega(\tau) \tag{7.376}$$

where K is an arbitrary real constant. For a thin absorber, the energy loss will be small and it is reasonable to assume that the pdf will vary slowly with energy over this range thus allowing us to make the approximation $f(x,\Delta E) \approx f(x,\Delta E - Q)$. Applying the convolution theorem, then,

$$\frac{\partial \xi(x,\tau)}{\partial x} = \Omega(\tau)\xi(x,\tau) - \xi(x,\tau) \times \int_0^{Q_{max}} dQ\, \omega(Q) \tag{7.377}$$

which has the solution,

$$\xi(x,\tau) = \xi(0,\tau)\exp\left(\left(\Omega(\tau) - \int_0^{Q_{max}} dQ\, \omega(Q)\right)x\right). \tag{7.378}$$

From the obvious result,

$$\xi(0,\tau) = \int_0^\infty d(\Delta E) e^{-\tau \Delta E}\, \delta(\Delta E) = 1 \tag{7.379}$$

the Laplace transform of the pdf is obtained,

$$\begin{aligned}\xi(x,\tau) &= \exp\left(\left(\Omega(\tau) - \int_0^{Q_{max}} dQ\,\omega(Q)\right)x\right)\\ &= \exp\left(\left(\int_0^{\infty} dQ e^{-\tau Q}\omega(Q) - \int_0^{Q_{max}} dQ\,\omega(Q)\right)x\right)\\ &= \exp\left(x\int_0^{\infty} dQ\omega(Q)\left(e^{-\tau Q}-1\right)\right)\end{aligned} \tag{7.380}$$

as $\omega(Q) = 0$ for $Q > Q_{max}$. The pdf is recovered from this result by calculating its inverse Laplace transform,

$$\begin{aligned}f(x,\Delta E) &= \frac{1}{2\pi i}\int_{K-i\infty}^{K+i\infty} d\tau\, e^{\tau\Delta E}\,\xi(x,\tau)\\ &= \frac{1}{2\pi i}\int_{K-i\infty}^{K+i\infty} d\tau \exp\\ &\quad\times\left(\tau\Delta E + x\int_0^{\infty} dQ\omega(Q)\left(e^{-\tau Q}-1\right)\right)\end{aligned} \tag{7.381}$$

To solve for this, the exponent is first evaluated,

$$\begin{aligned}&\tau\Delta E + x\int_0^{\infty} dQ\omega(Q)\left(e^{-\tau Q}-1\right)\\ &\quad= \tau\Delta E + x\int_0^{\infty} dQ\omega(Q)e^{-\tau Q} - x\int_0^{\infty} dQ\omega(Q)\\ &\quad= \tau\left(\Delta E - \overline{\Delta E}\right) - x\int_0^{Q_{max}} dQ\,\omega(Q)\\ &\qquad\times\left(1 - e^{-\tau Q} - \tau Q\right)\end{aligned} \tag{7.382}$$

where $\overline{\Delta E}$ is the mean energy loss over the distance traversed, x. For the Bhabha cross section of a massive spin-0 projectile, this exponent becomes,

$$\begin{aligned}&\tau\left(\Delta E - \overline{\Delta E}\right) - x\int_0^{Q_{max}} dQ\,\omega(Q)\left(1 - e^{-\tau Q} - \tau Q\right)\\ &\quad= \tau\left(\Delta E - \overline{\Delta E}\right) - x\zeta\int_0^{Q_{max}} \frac{dQ}{Q^2}\left(1 - \beta^2\frac{Q}{Q_{max}}\right)\\ &\qquad\times\left(1 - e^{-\tau Q} - \tau Q\right) = \tau\left(\Delta E - \overline{\Delta E}\right)\\ &\qquad- x\zeta\int_0^{Q_{max}} dQ\frac{1-e^{-\tau Q}}{Q^2} + \kappa\beta^2\int_0^{Q_{max}} dQ\frac{1-e^{-\tau Q}}{Q}\\ &\qquad+ \tau x\zeta\int_0^{Q_{max}}\frac{dQ}{Q} - \tau\beta^2 x\zeta.\end{aligned} \tag{7.383}$$

Three separate integrals must now be solved. The first integral is, following a change of variables,

$$\int_0^{Q_{max}} dQ\frac{1-e^{-\tau Q}}{Q^2} = \tau\int_0^{\tau Q_{max}} du\frac{1-e^{-u}}{u^2} \tag{7.384}$$

which is readily solved by parts,

$$\begin{aligned} f(u) &= -\frac{1}{u} & \frac{df}{du} &= \frac{1}{u^2}\\ \frac{dg}{du} &= e^{-u} & g(u) &= 1 - e^{-u}\end{aligned} \tag{7.385}$$

to give,

$$\tau\int_0^{\tau Q_{max}} du\frac{1-e^{-u}}{u^2} = \tau\left(-\left(\frac{1-e^{-u}}{u}\right)\Big|_0^{\tau Q_{max}} + \int_0^{\tau Q_{max}} du\frac{e^{-u}}{u}\right). \tag{7.386}$$

From l'Hôpital's rule,

$$\lim_{u\to 0}\frac{1-e^{-u}}{u} = 1 \tag{7.387}$$

then,

$$\int_0^{Q_{max}} dQ\frac{1-e^{-\tau Q}}{Q^2} = \tau - \frac{1-e^{-\tau Q_{max}}}{Q_{max}} + \tau\int_0^{\tau Q_{max}} du\frac{e^{-u}}{u}. \tag{7.388}$$

The second integral of (7.383) can be found from tables (Abramowitz and Stegun 1972),

$$\int_0^{Q_{max}} dQ \frac{1-e^{-\tau Q}}{Q} = -Ei(-\tau Q_{max}) + \ln \tau Q_{max} + \gamma_{EM} \tag{7.389}$$

where Ei(x) is the exponential integral, $Ei(x) = \int_{-x}^{\infty} dt \frac{e^{-t}}{t}$.

The third integral is rewritten as,

$$\int_0^{Q_{max}} \frac{dQ}{Q} = \int_0^{\tau Q_{max}} \frac{du}{u}. \tag{7.390}$$

Using these results, the following form of the exponential term in the inverse Laplace transform of the pdf is given,

$$\begin{aligned} &\tau\left(\Delta E - \overline{\Delta E}\right) - x\zeta \int_0^{Q_{max}} dQ \frac{1-e^{-\tau Q}}{Q^2} + \kappa\beta^2 \\ &\times \int_0^{Q_{max}} dQ \frac{1-e^{-\tau Q}}{Q} + \tau x\zeta \int_0^{Q_{max}} \frac{dQ}{Q} - \tau\beta^2 x\zeta \\ &= \tau\left(\Delta E - \overline{\Delta E}\right) - \tau x\zeta\left(1+\beta^2\right) + \kappa(1-e^{-z}) \\ &+ \left(\kappa\beta^2 + \tau x\zeta\right)(-Ei(-z) + \ln z + \gamma_{EM}) \end{aligned} \tag{7.391}$$

where $z = \tau Q_{max}$. Inserting this expression for the exponent into the inverse Laplace transform for the energy loss pdf yields the form attributable to Vavilov,

$$\begin{aligned} f(x,\Delta E) = \frac{1}{2\pi i Q_{max}} e^{\kappa\left(1+\beta^2\gamma_{EM}\right)} \int_{K-i\infty}^{K+i\infty} dz \\ \times \exp\left[z\lambda_V + \kappa\left((z+\beta^2)\right.\right. \\ \left.\left.\times\left(-Ei(-z) + \ln z\right) - e^{-z}\right)\right] \end{aligned} \tag{7.392}$$

where the dimensionless Vavilov parameter is,

$$\lambda_V = \frac{\Delta E - \overline{\Delta E}}{Q_{max}} - \kappa\left(1 + \beta^2 - \gamma_{EM}\right). \tag{7.393}$$

The solutions of this expression of the Vavilov pdf will be considered in a variety of ways. First, integrate this expression over the imaginary axis (i.e., set K = 0 and z = iy),

$$\begin{aligned} f(x,\Delta E) = \frac{1}{2\pi Q_{max}} e^{\kappa\left(1+\beta^2\gamma_{EM}\right)} \int_{-\infty}^{\infty} dy \\ \times \exp\left[iy\lambda_V + \kappa((iy+\beta^2)\right. \\ \left.\times\left(-Ei\left(-iy\right) + \ln iy\right) - e^{-iy}\right)\right] \end{aligned} \tag{7.394}$$

From complex variable theory (Churchill et al. 1974),

$$\begin{aligned} \ln iy &= i\frac{\pi}{2} + \ln|y| \qquad y > 0 \\ &= -i\frac{\pi}{2} + \ln|y| \quad y < 0 \end{aligned} \tag{7.395}$$

and

$$\begin{aligned} Ei(-iy) &= Ci(|y|) - iSi(y) + i\frac{\pi}{2} \quad y > 0 \\ &= Ci(|y|) - iSi(y) - i\frac{\pi}{2} \quad y < 0 \end{aligned} \tag{7.396}$$

where Ci(x) and Si(x) are the cosine and sine integrals, respectively,

$$Ci(x) = \gamma_{EM} + \ln x + \int_0^x dt \frac{\cos t - 1}{t}$$

$$Si(x) = \int_0^x dt \frac{\sin t}{t}.$$

By inserting these into (7.396) and defining the two functions,

$$g_1(y) = \beta^2(\ln|y| - Ci(y)) - \cos y - ySi(y) \tag{7.397}$$

$$g_2(y) = y\ (\ln|y| - Ci(y)) + \sin y + \beta^2 Si(y), \tag{7.398}$$

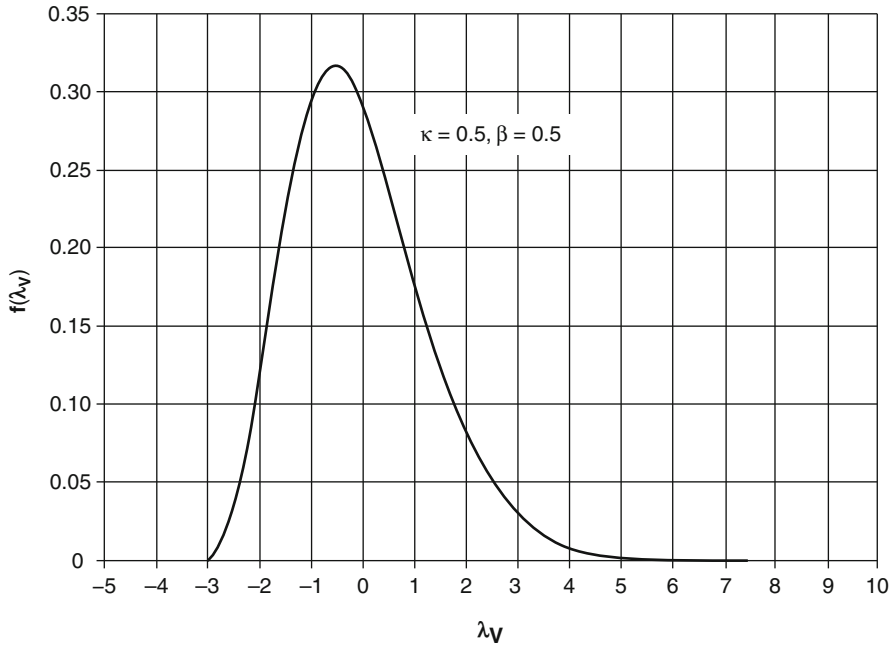

Fig. 7.30 Vavilov energy loss pdf for $\kappa = 0.5$, $\beta = 0.5$ calculated using the Edgeworth polynomial expansion described in Sect. 7.4.4.5

a simpler integral form of the Vavilov pdf is obtained,

$$f(x,\Delta E) = \left(\frac{\kappa}{\pi x \zeta}\right) e^{\kappa\left(1+\beta^2\gamma_{EM}\right)} \int_0^\infty dy\, e^{\kappa g_1(y)} \times \cos\left(\lambda_V y + \kappa\, g_2(y)\right) \tag{7.399}$$

This result can be solved numerically and through the use of approximations for the cosine and sine integrals. A variety of other approximations also exist and these will be discussed shortly. Figure 7.30 shows the Vavilov pdf (calculated using an Edgeworth expansion method) for $\kappa = 0.5$ and $\beta = 0.5$ as a function of the Vavilov parameter λ_V.

7.4.4.3 Gaussian Limit to the Vavilov Probability Distribution Function

It can now be shown that the Vavilov pdf approaches the Gaussian limit for $\kappa \to \infty$. Begin with another approach to solving the pdf given by the inverse Laplace transform by expanding the exponential. Because of the asymmetry of the Vavilov pdf, the expansion is made to third order in τ Q,

$$\begin{aligned} f(x,\Delta E) &= \frac{1}{2\pi i}\int_{K-i\infty}^{K+i\infty} d\tau\, \exp \\ &\quad \times \left(\tau\,\Delta E - x\int_0^\infty dQ\omega(Q)\left(1-e^{-\tau Q}\right)\right) \\ &= \frac{1}{2\pi i}\int_{K-i\infty}^{K+i\infty} d\tau\, \exp\left(\tau\,\Delta E - x\int_0^\infty dQ\omega(Q)\right. \\ &\quad \left.\times\left(\tau Q - \frac{(\tau Q)^2}{2} + \frac{(\tau Q)^3}{6}\right)\right) \\ &\approx \frac{1}{2\pi i}\int_{K-i\infty}^{K+i\infty} d\tau\, \exp\left(\tau\left(\Delta E - \overline{\Delta E}\right)\right. \\ &\quad \left. + \tau^2\frac{x}{2}\vartheta - \tau^3\frac{x}{6}\varphi\right) \end{aligned} \tag{7.400}$$

where,

$$\vartheta = \int_0^{Q_{max}} dQ\omega(Q)Q^2 \tag{7.401}$$

and

$$\varphi = \int_0^{Q_{max}} dQ\omega(Q)Q^3 \tag{7.402}$$

Note that ϑ corresponds to $k_2{}^2$ in the derivation of the Gaussian pdf from the pure differential form of the continuity equation. As a Gaussian result for the pdf will be obtained if the integral is evaluated only up to ϑ, the $\exp(-\tau^3 x/6\varphi)$ term provides the asymmetry of the pdf which, as it is proportional to e^{-x}, must decrease with increasing absorber thickness so that the pdf approaches the Gaussian form. This can be shown explicitly for the Bhabha cross section for a massive spin-0 projectile,

$$\vartheta = \zeta Q_{max}\left(1 - \frac{\beta^2}{2}\right) \tag{7.403}$$

and,

$$\varphi = \zeta Q_{max}^2\left(\frac{1}{2} - \frac{\beta^2}{3}\right) \tag{7.404}$$

The pdf is solved for by the substitution of variables. First, define,

$$u = \left(\frac{x\varphi}{2}\right)^{1/3}\left(\tau - \frac{\vartheta}{\varphi}\right) \tag{7.405}$$

from which,

$$d\tau = \left(\frac{2}{x\varphi}\right)^{1/3} du \tag{7.406}$$

For simplicity, define,

$$\eta = \left(\frac{x\varphi}{2}\right)^{1/3} \tag{7.407}$$

which leads to a simplified expression of the Vavilov pdf,

$$f(x, \Delta E) = \frac{e^{at-\frac{a^3}{3}}}{2\pi i\,\eta}\int_{K-i\infty}^{K+i\infty} du\, e^{ut-\frac{u^3}{3}} \tag{7.408}$$

where

$$\begin{aligned} a &= \eta\frac{\vartheta}{\varphi} \\ &= \left(1 - \frac{\beta^2}{2}\right)\left(\frac{2\kappa}{\left(1 - \frac{2}{3}\beta^2\right)^2}\right)^{\frac{1}{3}} \end{aligned} \tag{7.409}$$

and

$$t = \frac{\Delta E - \overline{\Delta E}}{\eta} + a^2. \tag{7.410}$$

The integral of (7.408) is integrated over the imaginary axis,

$$\begin{aligned} \frac{1}{2\pi i}\int_{K-i\infty}^{K+i\infty} du\, e^{ut-\frac{u^3}{3}} &= \frac{1}{2\pi}\int_{-\infty}^{\infty} dy\, e^{\frac{y^3}{3}+iyt} \\ &= \frac{1}{\pi}\int_0^{\infty} dy\cos\left(yt + \frac{y^3}{3}\right) \end{aligned} \tag{7.411}$$

which will be recognized as being the Airy function, Ai(t). The pdf is now written as,

$$f(x, \Delta E) = \frac{e^{at-\frac{a^3}{3}}}{\eta}\mathrm{Ai}(t). \tag{7.412}$$

Consider the function for large values of κ. Equation (7.409) shows that $a \to (2\kappa)^{1/3}$ for $\kappa \to \infty$ and (7.410) shows that $t \to \infty$ for $a \to \infty$. Thus, for $\kappa \to \infty$, one can use the limiting form of the Airy function,

$$\mathrm{Ai}(t) \to \frac{e^{-\frac{2}{3}t^{3/2}}}{2\sqrt{\pi}\,t^{1/4}} \quad \text{as } t \to \infty \tag{7.413}$$

so that the pdf will be,

$$f(x, \Delta E) = \frac{e^{\left(at-\frac{a^3}{3}-\frac{2}{3}t^{3/2}\right)}}{2\eta\sqrt{\pi}^{\,1/4}} \quad \text{as } t \to \infty \tag{7.414}$$

This result is further manipulated by noting that,

$$t^{\frac{1}{4}} \to \sqrt{a} \quad \text{as } \kappa \to \infty \tag{7.415}$$

and that

$$at - \frac{2}{3}t^{\frac{3}{2}} \to \frac{a^2}{3} - \frac{z^2}{4a} \quad \text{as } \kappa \to \infty \tag{7.416}$$

where

$$z = \frac{\Delta E - \overline{\Delta E}}{\eta} \ll a \tag{7.417}$$

to give,

$$f(x, \Delta E) = \frac{e^{-\frac{z^2}{4a}}}{2\eta\sqrt{\pi a}}. \tag{7.418}$$

The final result for $\kappa \to \infty$ is,

$$f(x, \Delta E) \approx \frac{1}{\sqrt{2\pi\vartheta x}} e^{-\left(\frac{(\Delta E - \overline{\Delta E})^2}{2\vartheta x}\right)} \tag{7.419}$$

Thus, the Vavilov expression reduces to the Gaussian pdf for large κ.

7.4.4.4 Landau Limit to the Vavilov Probability Distribution Function

Having established that the Vavilov pdf approaches the Gaussian pdf for large κ, now look at the opposite limit of the pdf for $\kappa \to 0$. Recall the original Vavilov pdf,

$$\begin{aligned} f(x, \Delta E) = & \frac{1}{2\pi i Q_{max}} e^{\kappa\left(1+\beta^2\gamma_{EM}\right)} \\ & \times \int_{K-i\infty}^{K+i\infty} dz \exp\left[z\lambda_V + \kappa\left((z+\beta^2)\right.\right. \\ & \left.\left. \times \left(-Ei(-z) + \ln z\right) - e^{-z}\right)\right]. \end{aligned}$$

By changing variables, $p = \kappa z$, the pdf is,

$$\begin{aligned} f(x, \Delta E) = & \frac{1}{2\pi i x\zeta} e^{\kappa\left(1+\beta^2\gamma_{EM}\right)} \times \int_{K-i\infty}^{K+i\infty} dp \\ & \times \exp\left[p\frac{\lambda_V}{\kappa} + \kappa\left(\left(\frac{p}{\kappa}+\beta^2\right)\left(-Ei\left(-\frac{p}{\kappa}\right)\right.\right.\right. \\ & \left.\left.\left. + \ln p - \ln\kappa\right) - e^{-\frac{p}{\kappa}}\right)\right] \\ = & \frac{1}{2\pi i x\zeta} e^{\kappa\left(1+\beta^2\gamma_{EM}\right)} \int_{K-i\infty}^{K+i\infty} dp \\ & \times \exp\left[p\left(\frac{\lambda_V}{\kappa} - \ln\kappa\right) + p\left(-Ei\left(-\frac{p}{\kappa}\right) + \ln p\right)\right. \\ & \left. + \kappa\beta^2\left(-Ei\left(-\frac{p}{\kappa}\right) + \ln p - \ln\kappa\right) - \kappa e^{-p/\kappa}\right]. \end{aligned} \tag{7.420}$$

For $\kappa \to 0$, this reduces to the Landau pdf,

$$f(x, \Delta E) = \frac{1}{2\pi i x\zeta} \int_{K-i\infty}^{K+i\infty} dp\, e^{p(\lambda_L + \ln p)} \tag{7.421}$$

where the Landau and Vavilov parameters are related to each other by,

$$\begin{aligned} \lambda_L &= \frac{\lambda_V}{\kappa} - \ln\kappa \\ &= \frac{\Delta E - \langle\Delta E\rangle}{x\zeta} - \left(1+\beta^2\right) + \gamma_{EM} - \ln\kappa. \end{aligned} \tag{7.422}$$

By changing variables,

$$p = iy \tag{7.423}$$

the Landau pdf can be written in a form readily amenable to numerical integration,

$$f(\lambda_L) = \frac{1}{\pi x\zeta} \int_0^\infty dy\, e^{-\left(\frac{\pi}{2}\right)y} \cos(y\ln y + \lambda_L y) \tag{7.424}$$

Figure 7.31 shows the product $xf(\lambda_L)$ as a function of the Landau parameter λ_L. The maximum of $f(\lambda_L)$ occurs at $\lambda_{L,Max} = -0.22278$ (Kölbig and Schorr 1984) from which the most probable energy loss can be calculated by noting that the Landau parameter can be written as,

$$\lambda_L = \frac{\Delta E - (\Delta E)_{MP}}{x\zeta} + \lambda_{L,Max} \tag{7.425}$$

where $(\Delta E)_{MP}$ is the most probable energy loss which can be solved for, using (7.422) and (7.425),

$$(\Delta E)_{MP} = x\left[\left(\frac{dE}{dx}\right)_{Col} + \zeta(\lambda_{L.Max} + 1 + \beta^2 + \ln\kappa - \gamma_{EM})\right]. \tag{7.426}$$

A closed analytic form of a pdf has been presented by Moyal (1955) as a representation of the Landau pdf,

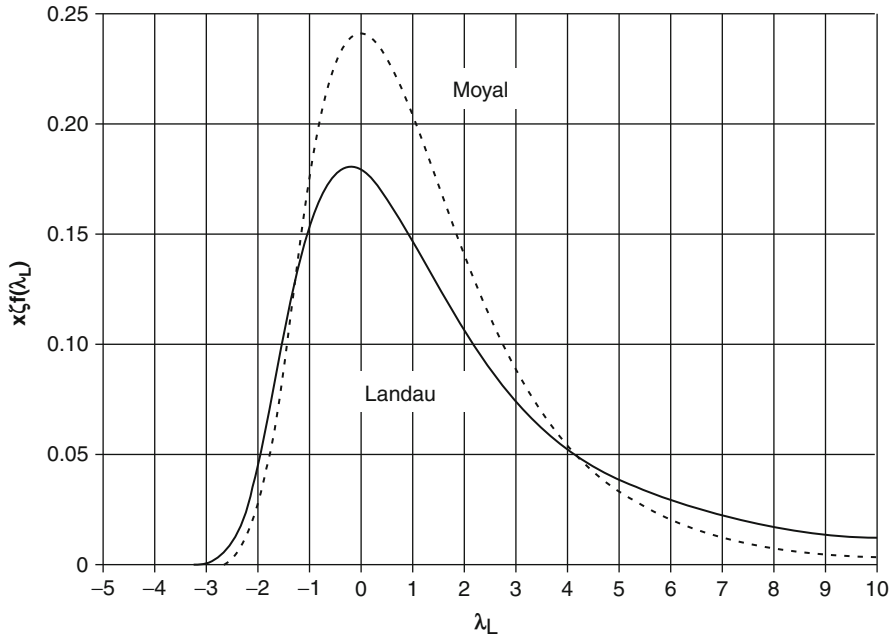

Fig. 7.31 Weighted Landau and Moyal probability distribution functions as functions of the Landau parameter

$$f(\lambda) = \frac{1}{x\zeta\sqrt{2\pi}} e^{-\frac{1}{2}(\lambda + \exp(-\lambda))} \tag{7.427}$$

where

$$\lambda = \frac{\Delta E - (\Delta E)_{MP}}{x\zeta}. \tag{7.428}$$

The Moyal result $x\zeta f(\lambda)$ is also plotted in Fig. 7.31. As can be seen, it is not an entirely accurate reproduction of the Landau result due to both the differing positions of the most probable energy loss (the Moyal curve peaks at $\lambda_L = 0$) and the different magnitudes of the maximum values of the two pdfs. Importantly, the Moyal approximation underestimates the high-energy loss tail. Even so, the Moyal approximation clearly has calculational advantages over the Landau integral result and is used as its approximation.[21] Rotondi and Montagna (1990) have proposed an improvement upon the Moyal approximation,

$$f_{\kappa,\beta}(\lambda) = \left(\frac{a_1}{x\zeta}\right) \exp\left[-a_2(\lambda + a_5\lambda^2) - a_3 \exp(-a_4(\lambda + a_6\lambda^2))\right] \tag{7.429}$$

where the six parameters, a_i, are functions of and β and were determined by fitting (7.427) to the numerical solution for the Vavilov pdf for $\kappa \leq 3$. They are provided as the weighted sum of the products of two Tchebyshev polynomials and the reader is referred to that publication for further details.

7.4.4.5 Practical Methods of Calculating the Vavilov pdf

Introduction

The form of the pdf to be used to describe the energy loss is dictated by the value of κ where, by convention, the appropriate pdf to use for a given range of values of κ is,

$$\begin{aligned} \kappa &\leq 0.01 \quad \text{Landau} \\ 0.01 \leq \kappa &\leq 10 \quad \text{Vavilov} \\ 10 \leq \kappa &\quad \text{Gaussian} \end{aligned}$$

Direct analytical solutions of the Vavilov integral are difficult and one typically resorts to approximations, numerical methods, or parameterizations to solve them. This is especially true in Monte Carlo

[21] See, for example, Sauli's description of multiwire proportional chambers (1977).

applications where calculation speed is critical. Three methods of calculating the Vavilov pdf are summarized here; no derivations will be provided, but the interested reader can refer to the original publications.

Edgeworth Series

For values of κ that are not too small, the Vavilov distribution is Gaussian-like where the perturbation from the Gaussian described in terms of an Edgeworth series (Symon 1948; Rotondi and Montagna 1990; Van Ginneken 2000). In the nomenclature of Rotondi and Montagna, the Vavilov pdf is approximated by,

$$\begin{aligned} f(x,\Delta E) = \frac{e^{-\frac{\Delta E^2}{2\sigma^2}}}{\sqrt{2\pi}\sigma}\Bigg[1 + \frac{1}{3!}\frac{\mu_3}{\sigma^3}H_3\left(\frac{\Delta E}{\sigma}\right) + \frac{1}{4!}\left(\frac{\mu_4}{\sigma^4} - 3\right) \\ \times H_4\left(\frac{\Delta E}{\sigma}\right) + \frac{1}{5!}\left(\frac{\mu_5}{\sigma^5} - 10\frac{\mu_3}{\sigma^3}\right)H_5\left(\frac{\Delta E}{\sigma}\right) \\ + \frac{10}{6!}\left(\frac{\mu_3}{\sigma^3}\right)^2 H_6\left(\frac{\Delta E}{\sigma}\right) + \frac{35}{7!}\frac{\mu_3}{\sigma^3}\left(\frac{\mu_4}{\sigma^4} - 3\right) \\ \times H_7\left(\frac{\Delta E}{\sigma}\right) + \frac{280}{9!}\left(\frac{\mu_3}{\sigma^3}\right)^3 H_9\left(\frac{\Delta E}{\sigma}\right)\Bigg] \end{aligned} \tag{7.430}$$

where the H_i are the Hermite polynomials and the μ_i and σ are related to the moments of the Vavilov distribution,

$$\mu_n = x\int_0^{Q_{max}} dQ\,\omega(Q)Q^n \quad n = 2,3 \tag{7.431}$$

$$\mu_4 = 3\mu_2^2 + \left(x\int_0^{Q_{max}} dQ\,\omega(Q)Q^4\right)^2 \tag{7.432}$$

$$\mu_5 = 10\mu_2\mu_3 + x\int_0^{Q_{max}} dQ\,Q^5\,\omega(Q) \tag{7.433}$$

$$\sigma^2 = \mu_2 \tag{7.434}$$

This expansion is reported to be valid for $0.29 \le \kappa$ and for $\lambda_L \le \lambda \le \lambda_H$ where the limits λ_L and λ_H define the limits of 0 and 1 in the cumulative distribution function and are determined from empirical fits.

Fourier Series Solution

Schorr (1974, 1975) developed an algorithm for calculating both the Landau and Vavilov pdfs using a Fourier series methodology. The approximation to the Vavilov pdf, written in the form,

$$f(\lambda_V) = \frac{1}{2\pi i}\int_{K-i\infty}^{K+i\infty} ds\,\phi(s)e^{\lambda_V s} \tag{7.435}$$

with

$$\phi(s) = e^{\kappa\left(1+\beta^2\gamma_G\right)}e^{\psi(s)}$$

and

$$\begin{aligned} \psi(s) = s\ln\kappa + \left(s + \beta^2\kappa\right) \\ \times\left[\int_0^{Q_{max}} ds\frac{1 - e^{-s/\kappa}}{s} - \gamma_{EM}\right] - \kappa e^{-s/\kappa} \end{aligned}$$

is

$$g(\lambda_L) = \frac{\omega}{\pi}\left(\frac{1}{2} + \sum_{k=1}^{\infty}\left[A_k\cos(k\omega\lambda_V) + B_k\sin(k\omega\lambda_V)\right]\right) \tag{7.436}$$

where

$$\omega = \frac{2\pi}{T_+ - T_-} \tag{7.437}$$

$$A_k = Re\phi(ik\omega) \tag{7.438}$$

$$B_k = -Im\phi(ik\omega) \tag{7.439}$$

Schorr provides the methodology for calculating T_- and T_+ so as to minimize the difference $g(\lambda_L) - f(\lambda_L)$. As this method requires a point-by-point calculation of the pdfs, it is not suitable as a sampling method for Monte Carlo simulations.

Distorted Log-Normal Distribution

Chibani (1998, 2002) has described two algorithms for calculating the Vavilov pdf in the interval $\kappa \in [0.01,1.0]$. The first algorithm is valid for $\kappa \in [0.01,0.3]$ and describes the Vavilov pdf as the convolution of log-normal and Poisson distributions. The second method, for $\kappa \in [0.3,1.0]$, takes advantage of the similarity of the shape of the log-normal distribution to that of the Vavilov pdf. The reader is referred to these two papers for further details.

7.4.4.6 Vavilov pdf for Electron Projectiles

Monte Carlo simulations of practical dosimetric interest will concern those cases of electron and positron projectiles. In such cases, energy straggling is accounted for by modifying the Landau or Vavilov distributions. In particular, the Vavilov pdf is calculated using the Møller cross section for electron–electron collisions. Chibani simplifies this calculation by approximating the Møller cross section by a fourth-order polynomial in order to allow the Vavilov pdf to be calculated analytically (this is also done for positron projectiles by doing the same for the Bhabha positron–electron collision cross section).

7.4.4.7 Atomic Electron Binding Effects

In the case of a high-Z thin absorber, energy losses through resonant transfers to atomic electrons become important. Such effects can be managed by convolving the Landau distribution with a Gaussian function. In this application, because it is easy to convolve two Gaussian functions, the Landau *pdf* is represented by a weighted sum of four Gaussian pdfs (Blunck and Leisegang, 1951). Even though there are difficulties with this approach that require addressing (Findlay and Dusautoy 1980), they have relatively little immediate application to nuclear medicine dosimetry.

7.5 Multiple Elastic Scattering

7.5.1 Introduction

In addition to being able to calculate for the transfer of energy to the medium from a moving charged particle, it is necessary to know both the number and phase space of the particles. Transport is dominated by the elastic Coulomb scatter in which, for electrons and positrons, negligible amounts of energy are transferred in these scatters and can be neglected. The three most important results obtained from the derivation of the differential cross sections for a single elastic Coulomb scatter are that:

- The θ^{-4} dependence showing that forward-directed elastic scatter will dominate.
- The mean free pathlength between elastic scatters is small due to the large total cross section.
- The differential cross section has a $(p\beta)^{-2}$ dependence.

The combination of the first two results leads to the dominance of forward-directed multiple scatter. The last result shows that, at energies typical of nuclear medicine, electrons and positrons are more subject to multiple scatter than are heavier α particles. Hence, the interest in this section will be on e^-/e^+ multiple scatter.

By using the small-angle approximation, recalling the θ^{-4} dependence and noting that $d\Omega \cong 2\pi\,\theta\,d\theta$ (which implicitly assumes azimuthal symmetry), one can write the mean-square angle of a single elastic Coulomb scatter (assuming that screening at small scattering angles invokes a cut-off in angle),

$$\begin{aligned}\overline{\theta^2} &= \frac{\int d\Omega\,\theta^2 \frac{d\sigma_{Ruth}}{d\Omega}}{\int d\Omega \frac{d\sigma_{Ruth}}{d\Omega}} \\ &\approx \frac{\int_{\chi_0}^{\theta_{max}} \frac{d\theta}{\theta}}{\int_{\chi_0}^{\theta_{max}} \frac{d\theta}{\theta^3}} \\ &= \frac{\ln\left(\theta_{max}/\chi_0\right)}{\left(1/\chi_0^2\right) - \left(1/\theta_{max}^2\right)}.\end{aligned} \tag{7.440}$$

The minimum scattering angle is the screening angle χ_0 of (7.6) for the Thomas–Fermi model. As $\chi_0 \ll 1$ and $\chi_0 \ll \theta_{max}$ (recall Fig. 7.3), the root-mean square (RMS) scattering angle is approximately,

$$\sqrt{\overline{\theta^2}} = -\chi_0 \ln \chi_0 \tag{7.441}$$

Hence, $\sqrt{\overline{\theta^2}}$ will be a relatively small multiple of χ_0 and the net deflection of the electron will be small

(e.g., from Fig. 7.3 $\chi_0 \approx 25$ mrad for a 100 keV electron in carbon which leads to $\sqrt{\overline{\theta^2}} = 3.7\,\chi_0$ or about 93 mrad). Because the number of elastic Coulomb scatters in a pathlength of practical interest will be high, the central-limit theorem indicates that the probability distribution function describing the scattering angle will be Gaussian with a small variance, $\overline{\theta^2}$. This Gaussian approximation is not entirely accurate as it neglects the small, but not negligible, probability of large-angle Coulomb scatter that increases the "tail" of the pdf. But the Gaussian assumption will provide the basis upon which to explore the three main multiple scattering theories in common use in modern-day calculations of charged-particle transport.

7.5.2 Multiple Elastic Scattering Theory

7.5.2.1 Introduction

Since the 1940s, a number of theories describing the multiple scatter of charged particles have been developed. Two theories (Goudsmit and Saunderson 1940, Molière 1947, 1948) are predominant in the Monte Carlo codes currently used to model charged-particle transport in medical applications. Prior to deriving these theories, the simpler Fermi–Eyges theory (Eyges 1948) is derived (which, while not used in transport calculations for nuclear medicine applications, has been widely employed in software developed for external electron beam treatment planning software in radiation oncology (Hogstrom et al. 1981; McParland et al. 1988). Importantly, the Fermi–Eyges theory justifies the expectation of a Gaussian pdf for the spatial deflection and angular distribution of multiply-scattered charged particles which appears as the "zeroth-order" case in the Goudsmit–Saunderson and Molière multiple scatter theories.

7.5.2.2 Fermi–Eyges Theory

The genesis of this theory was the derivation by Fermi of the diffusion equation for a calculation of the transport of cosmic rays in the atmosphere (given in the review by Rossi and Greisen (1941)). Because of the high kinetic energies of the cosmic rays, ionizational energy losses were neglected in Fermi's derivation and Eyges (1948) extended Fermi's result by allowing for the energy losses suffered particles through ionization. The derivation below of the Fermi diffusion equation will follow that of Jette (1988) which is itself a slightly more general version of the original. Having obtained the diffusion equation, Eyges' approach of allowing for an energy dependence will be used to solve the diffusion equation using the methods developed earlier in this chapter.

Before deriving Fermi's diffusion equation, some preparatory work is required. Consider Fig. 7.32 in which a beam of monoenergetic charged particles with zero lateral width is incident along the $+z$-axis to a semi-infinite scattering medium with the entrance plane defined by the $x - y$ plane. The particle is scattered through the polar θ and azimuthal ϕ angles as shown. Due to the central Coulomb potentials associated with the scattering centers within the medium, azimuthal symmetry exists and ϕ will be uniformly distributed between 0 and 2π. The angles θ_x and θ_y are the projections of the polar scattering angle onto the xz- and yz-planes, respectively, as shown, where,

$$\theta_x = \tan^{-1}(\tan\theta\,\cos\phi) \tag{7.442}$$

$$\theta_y = \tan^{-1}(\tan\theta\,\sin\phi) \tag{7.443}$$

and the mean-square values of these projected scattering angles are,

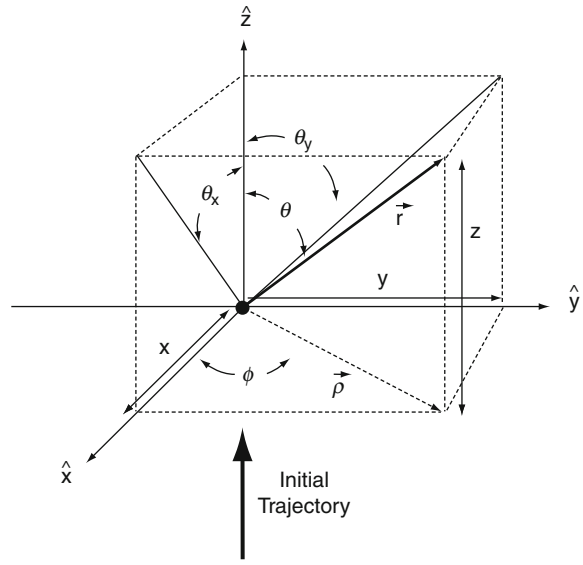

Fig. 7.32 Scattering of a particle with an initial trajectory along the z-axis through (θ,ϕ). θ_x and θ_y are the projections of the polar scattering angle onto the x – z and y – z planes, respectively

$$\begin{aligned}\overline{\theta_x^2} &= \frac{\int d\Omega\, \theta_x^2(\theta,\phi)\, \frac{d\sigma_{Ruth}}{d\Omega}}{\int d\Omega\, \frac{d\sigma_{Ruth}}{d\Omega}} \\ &\approx \frac{\int d\Omega\, \theta^2 \cos^2\phi\, \frac{d\sigma_{Ruth}}{d\Omega}}{\int d\Omega\, \frac{d\sigma_{Ruth}}{d\Omega}} \\ &= \left(\frac{1}{2\pi}\int_0^{2\pi} d\phi \cos^2\phi\right)\overline{\theta^2} \\ &= \frac{\overline{\theta^2}}{2}\end{aligned} \tag{7.444}$$

and, similarly,

$$\overline{\theta_y^2} = \frac{\overline{\theta^2}}{2}. \tag{7.445}$$

Hence, in the small-angle approximation, the mean-square scatter angle is,

$$\overline{\theta^2} = \overline{\theta_x^2} + \overline{\theta_y^2}. \tag{7.446}$$

Recalling the earlier invocation of the central-limit theorem, one conjectures that the scattering pdf of the two projected scattering angles are Gaussian. For example,

$$f(\theta_x) = \frac{1}{\sqrt{2\pi\overline{\theta_x^2}}} \exp\left(-\frac{1}{2}\frac{\theta_x^2}{\overline{\theta_x^2}}\right) \tag{7.447}$$

with zero mean and variance $\overline{\theta_x^2}$. At this point, the linear scattering power is defined as the derivative of the mean-square scattering angle with respect to the pathlength traveled,

$$\Im = \frac{d\overline{\theta_s^2}}{ds}. \tag{7.448}$$

Of course, this can only be an approximation in that it assumes that the change in the mean-square scattering angle with distance is continuous whereas the processes are stochastic. For calculational purposes, this will be approximated by a continuous derivative with the ratio of the mean-square scattering angle over a pathlength Δs,

$$\Im = \frac{\overline{\theta^2}}{\Delta s} \tag{7.449}$$

where,

$$\begin{aligned}\Delta s &= \frac{\Delta z}{\cos\theta} \\ &\approx \Delta z\end{aligned} \tag{7.450}$$

for forward-directed scatter. The Gaussian pdf for θ_x can now be written as,

$$f(\theta_x) = \frac{1}{\sqrt{\pi\,\Im\,\Delta z}} \exp\left(-\frac{\theta_x^2}{\Im\,\Delta z}\right). \tag{7.451}$$

It is reasonable to presume, for future use, that the pdf for a change in scattering angle from the mean, $\Delta\theta_x = \theta_x - \overline{\theta_x}$, over Δz is also Gaussian,

$$g(\Delta\theta_x;\Delta z) = \frac{1}{\sqrt{\pi\,\Im\,\Delta z}} \exp\left(-\frac{(\Delta\theta_x)^2}{\Im\,\Delta z}\right). \tag{7.452}$$

In the derivation of the Gaussian pdf, use will be needed of the first three moments of $g(\Delta\theta_x;\Delta z)$,

$$\begin{aligned}&\int_{-\infty}^{\infty} d(\Delta\theta_x) g(\Delta\theta_x;\Delta z) \\ &\quad= \frac{1}{\sqrt{\pi\,\Im\,\Delta z}} \int_{-\infty}^{\infty} d(\Delta\theta_x) \exp\left(-\frac{(\Delta\theta_x)^2}{\Im\,\Delta z}\right) \\ &\quad= 1\end{aligned} \tag{7.453}$$

$$\begin{aligned}&\int_{-\infty}^{\infty} d(\Delta\theta_x)\, \Delta\theta_x\, g(\Delta\theta_x;\Delta z) \\ &\quad= \frac{1}{\sqrt{\pi\,\Im\,\Delta z}} \int_{-\infty}^{\infty} d(\Delta\theta_x)\Delta\theta_x \exp\left(-\frac{(\Delta\theta_x)^2}{\Im\,\Delta z}\right) \\ &\quad= 0\end{aligned} \tag{7.454}$$

$$\begin{aligned}&\int_{-\infty}^{\infty} d(\Delta\theta_x)(\Delta\theta_x)^2\, g(\Delta\theta_x;\Delta z) \\ &= \frac{1}{\sqrt{\pi\,\Im\,\Delta z}} \int_{-\infty}^{\infty} d(\Delta\theta_x)(\Delta\theta_x)^2 \exp\left(-\frac{(\Delta\theta_x)^2}{\Im\,\Delta z}\right) = \frac{\Im\,\Delta z}{2}.\end{aligned} \tag{7.455}$$

The limits of integration of $\Delta\theta_x$ can be extended to $\pm\infty$ as $g(\Delta\theta_x;\Delta z)$ is sharply peaked around $\Delta\theta_x = 0$.

The Fermi diffusion equation is next derived. Assume that the initial condition for the particle is $\delta(x)\delta(y)\delta(z)\delta(\theta)$ and define $f(x,\theta_x;y,\theta_y;z)\Delta x\,\Delta\theta_x\,\Delta y\,\Delta\theta_y$ as the probability at a depth z that the particle will be between x and $x+\Delta x$ and between y and $y+\Delta y$ and have projected scattering angles between θ_x and $\theta_x+\Delta\theta_x$ and between θ_y and $\theta_y+\Delta\theta_y$. In order

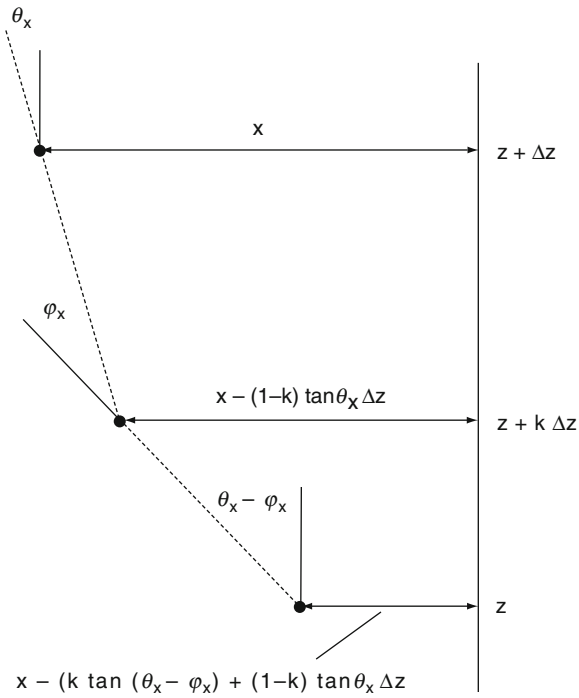

Fig. 7.33 Trajectory of a charged particle twice scattered between depths of z and z + Δz

to simplify the derivation, the calculation is initially restricted to the two-dimensional case and then extended to three dimensions. The intent is to find the variation in $f(x, \theta_x; z)$ with increasing penetration into the medium, z. To do so, consider the trajectory of a particle in two-dimensions as shown in Fig. 7.33. The particle's end-point is at a depth $z + \Delta z$ with projected lateral displacement x and projected polar direction θ_x following an intermediate scatter occurring at a depth $z + k\Delta z$, where $0 < k < 1$. This position is projected back to the particle's original position at a depth z. At the intermediate scattering point, the particle was at a projected lateral displacement,

$$x - (1 - k)\tan\theta_x \Delta z \approx x - (1 - k)\theta_x \Delta z \quad (7.456)$$

(using the small-angle approximation for θ_x) and was scattered through an angle φ_x. If one further back projects the trajectory to the depth z, the particle had been scattered through an angle $\theta_x - \varphi_x$ and was at a projected lateral displacement,

$$\begin{aligned} &x - (\tan\theta_x + k(\tan(\theta_x - \varphi_x) - \tan\theta_x))\Delta z \\ &\quad \approx x - (\theta_x - k\varphi_x)\Delta z. \end{aligned} \quad (7.457)$$

For any value of k in the range (0,1), one obtains the pdf $f(x,\theta_x;z+\Delta z)$ by convolving over all φ_x,

$$\begin{aligned} f(x, \theta_x; z + \Delta z) = &\int_{-\infty}^{\infty} d\varphi_x \, f(x - (\theta_x - k\varphi_x) \\ &\times \Delta z, \theta_x - \varphi_x; z) g(\varphi_x; \Delta z) \end{aligned} \quad (7.458)$$

where $g(\varphi_x; \Delta z)$ is given by (7.452).

This integral is solved by first expanding $f(x - (\theta_x - k\varphi_x)\Delta z, \theta_x - \varphi_x; z)g(\varphi_x; \Delta z)$ to second order in θ_x, φ_x and Δz,

$$\begin{aligned} &f(x - (\theta_x - k\varphi_x)\Delta z, \theta_x - \varphi_x; z)g(\varphi_x; \Delta z) \\ &\quad \cong f(x, \theta_x; z) - \frac{\partial f(x, \theta_x; z)}{\partial x}(\theta_x - k\varphi_x) \\ &\qquad \times \Delta z - \frac{\partial f(x, \theta_x; z)}{\partial \theta_x}\varphi_x + \frac{1}{2}\frac{\partial^2 f(x, \theta_x; z)}{\partial \theta_x^2}\varphi_x^2. \end{aligned} \quad (7.459)$$

Substituting this into the integrand of (7.458) gives,

$$\begin{aligned} &f(x, \theta_x; z + \Delta z) \\ &= \int_{-\infty}^{\infty} d\varphi_x \, f(x, \theta_x; z) g(\varphi_x; \Delta z) \\ &\quad - \int_{-\infty}^{\infty} d\varphi_x \frac{\partial f(x, \theta_x; z)}{\partial x}(\theta_x - k\varphi_x)\Delta z \, g(\varphi_x; x) \\ &\quad - \int_{-\infty}^{\infty} d\varphi_x \frac{\partial f(x, \theta_x; z)}{\partial \theta_x}\varphi_x \, g(\varphi_x; x) \\ &\quad + \frac{1}{2}\int_{-\infty}^{\infty} d\varphi_x \frac{\partial^2 f(x, \theta_x; z)}{\partial \theta_x^2}\varphi_x^2(\varphi_x; x) \\ &= f(x, \theta_x; z) \int_{-\infty}^{\infty} d\varphi_x \, g(\varphi_x; \Delta z) \\ &\quad - \frac{\partial f(x, \theta_x; z)}{\partial x} \int_{-\infty}^{\infty} d\varphi_x (\theta_x - k\varphi_x)\Delta z \, g(\varphi_x; x) \\ &\quad - \frac{\partial f(x, \theta_x; z)}{\partial \theta_x} \int_{-\infty}^{\infty} d\varphi_x \varphi_x \, g(\varphi_x; x) \\ &\quad + \frac{1}{2}\frac{\partial^2 f(x, \theta_x; z)}{\partial \theta_x^2} \int_{-\infty}^{\infty} d\varphi_x \varphi_x^2 \, g(\varphi_x; x). \end{aligned} \quad (7.460)$$

This expression is markedly simplified by using the moments of $g(\varphi_x;\Delta z)$ calculated previously,

$$f(x,\theta_x;z+\Delta z) = f(x,\theta_x;z) - \theta_x \frac{\partial f(x,\theta_x;z)}{\partial x}\Delta z + \frac{\Im}{4}\frac{\partial^2 f(x,\theta_x;z)}{\partial \theta_x^2}\Delta z. \tag{7.461}$$

Note that in this final expression for the pdf there is no dependence upon k and, as a result, the selection of the intermediate scatter position is purely arbitrary. From this result, one obtains the differential change in the pdf with penetration,

$$\frac{\partial f(x,\theta_x;z)}{\partial z} = \lim_{\Delta z \to 0} \frac{f(x,\theta_x;z+\Delta z) - f(x,\theta_x;z)}{\Delta z} \tag{7.462}$$

and the Fermi diffusion equation in two-dimensions follows,

$$\frac{\partial f(x,\theta_x;z)}{\partial z} = -\theta_x \frac{\partial f(x,\theta_x;z)}{\partial x} + \frac{\Im}{4} \times \frac{\partial^2 f(x,\theta_x;z)}{\partial \theta_x^2}. \tag{7.463}$$

The extension of the Fermi diffusion equation to 3 dimensions is straight forward,

$$\frac{\partial f}{\partial z} = -\theta_x \frac{\partial f}{\partial x} - \theta_y \frac{\partial f}{\partial y} + \frac{\Im}{4}\left(\frac{\partial^2 f}{\partial \theta_x^2} + \frac{\partial^2 f}{\partial \theta_y^2}\right) \tag{7.464}$$

where, for clarity, the functional dependencies of the pdf have been omitted.

Note that this derivation of the Fermi diffusion equation has ignored the fact that, as a particle penetrates within the medium, it loses energy. As the elastic single scatter cross section has a $(p\beta)^{-2}$ dependence, the scattering power will vary with the projectile kinetic energy and, hence, become a function of the depth of penetration. For the two-dimensional form of the Fermi diffusion equation,

$$\frac{\partial f(x,\theta_x;z)}{\partial z} = -\theta_x \frac{\partial f(x,\theta_x;z)}{\partial x} + \frac{\Im(z)}{4}\frac{\partial^2 f(x,\theta_x;z)}{\partial \theta_x^2} \tag{7.465}$$

where the explicit functional dependency of the scattering power upon z is noted.[22] This expression neglects the fact that once the particle has reached a depth z it will have actually traveled a distance greater than z due to multiple scattering events.

The two-dimensional Fourier pair will be used to solve for the pdf,

$$f(x,\theta_x;z) = \frac{1}{2\pi}\int_{-\infty}^{\infty}\int_{-\infty}^{\infty} d\xi\, d\Lambda\, \omega(\xi,\Lambda;z) e^{i(x\xi+\theta_x\Lambda)} \tag{7.466}$$

$$\omega(\xi,\Lambda;z) = \frac{1}{2\pi}\int_{-\infty}^{\infty}\int_{-\infty}^{\infty} dx\, d\theta_x\, f(x,\theta_x;z)\, e^{-i(x\xi+\theta_x\Lambda)}. \tag{7.467}$$

Applying these to the two-dimensional Fermi diffusion equation gives a differential equation in the Fourier transform of the pdf,

$$\frac{\partial \omega}{\partial z} = \xi\frac{\partial \omega}{\partial \Lambda} - \frac{\Lambda^2 \Im(z)}{4}\omega \tag{7.468}$$

which can be simplified by defining the variables,

$$\kappa = z + \frac{\Lambda}{\xi} \tag{7.469}$$

$$z' = z \tag{7.470}$$

to yield,

$$\frac{\partial \omega}{\partial z'} = -\frac{\xi^2(\kappa - z)^2 \Im(z)}{4}\omega. \tag{7.471}$$

The solution is,

$$\omega = k(\kappa)\exp\left(-\xi^2\int_{\lambda}^{z'} d\eta \frac{(\kappa-\eta)^2\Im(\eta)}{4}\right). \tag{7.472}$$

[22] In an inhomogeneous medium (such as the body), the scattering power would also be a function of x and y. That level of complexity is not required for this discussion.

The lower limit of the integral has been set to some arbitrary valuer, λ, and $k(\kappa)$ is specified from the initial condition of the problem. Assuming a single incident particle, this is, as before,

$$f(x, \theta_x; z = 0) = \delta(x)\delta(\theta_x) \tag{7.473}$$

with the usual Fourier transform,

$$\omega(\xi, \Lambda; z = 0) = \frac{1}{2\pi}. \tag{7.474}$$

Writing out the solution for $\omega(\xi, \Lambda; z)$ in the original variables gives,

$$\omega(\xi, \Lambda; z) = k\left(z + \frac{\Lambda}{\xi}\right) \times \exp\left(-\xi^2 \int_{\lambda}^{z} d\eta \frac{\left(z + \frac{\Lambda}{\xi} - \eta\right)^2 \Im(\eta)}{4}\right). \tag{7.475}$$

From the initial conditions,

$$k\left(\frac{\Lambda}{\xi}\right) \exp\left(-\xi^2 \int_{\lambda}^{0} d\eta \frac{\left(\frac{\Lambda}{\xi} - \eta\right)^2 \Im(\eta)}{4}\right) = \frac{1}{2\pi} \tag{7.476}$$

which enables the Fourier transform of the pdf to be written as,

$$\omega(\xi, \Lambda; z) = \frac{1}{2\pi} \exp\left(-\xi^2 \int_{\lambda}^{z} d\eta \frac{\left(z + \frac{\Lambda}{\xi} - \eta\right)^2 \Im(\eta)}{4}\right). \tag{7.477}$$

Prior to taking the inverse Fourier transform in order to recover the pdf, this expression is simplified by defining the functions,

$$A_0(z) = \int_0^z d\eta \frac{\Im(\eta)}{4} \tag{7.478}$$

$$A_1(z) = \int_0^z d\eta (z - \eta) \frac{\Im(\eta)}{4} \tag{7.479}$$

$$A_2(z) = \int_0^z d\eta (z - \eta)^2 \frac{\Im(\eta)}{4} \tag{7.480}$$

so as to write a simpler form of the Fourier transform of the pdf,

$$\omega(\xi, \Lambda; z) = \frac{1}{2\pi} \exp\left(-A_0\Lambda^2 + 2A_1\Lambda\xi + A_2\xi^2\right) \tag{7.481}$$

where the z-dependencies of the A_i have been omitted for clarity. Taking the inverse Fourier transform of the result will result in the multiple scattering pdf,

$$f(x, \theta_x; z) = \frac{1}{2\pi\sqrt{A_0A_2 - A_1^2}} \times \exp\left(-\frac{\theta_x^2 A_2 - 2A_1 x\theta_x + x^2 A_0}{4A_0\left(A_0A_2 - A_1^2\right)}\right) \tag{7.482}$$

which is the Fermi–Eyges result for two dimensions. The three-dimensional result is given by the product of the two-dimensional pdfs in (x,θ_x) and (y,θ_y).

Equation (7.482) provides a Gaussian pdf; as the result of the small-angle approximation, in terms of the functions $A_0(z)$, $A_1(z)$, and $A_2(z)$. The depth of penetration, z, is now explicitly included in the pdf through these functions. As the linear scattering power will have an energy dependence (i.e., a less-energetic particle will be more readily scattered than an energetic one), a direct functional dependence upon particle energy is implicit.

7.5.2.3 Scattering Power

Introduction

The linear scattering power is the change in mean-square scattering angle per unit distance traveled by the particle. In analogy to the linear and mass stopping powers, one removes the dependence of the scattering power upon the physical density of the medium by defining the mass scattering power, $\Im/\rho$, which is the change in mean-square scattering angle per unit mass thickness traveled,

$$\frac{\Im}{\rho} = \frac{d\overline{\theta^2}}{\rho\, ds} \tag{7.483}$$

Or,

$$\frac{\Im}{\rho} = 2\pi \frac{N_A}{A} \int_{\chi_0}^{1} d\theta\, \theta^2 \frac{d\sigma}{d\Omega} \tag{7.484}$$

where, since the differential cross is in units of square centimeter·radian square per atom, the N_A/A factor is required for the mass collision stopping power to have units of square centimeter·radian square per gram of medium. χ_0 is the screening angle of (7.6).

Spin-0 Projectile Scattering

The mass scattering powers for the unscreened and screened Rutherford cross sections for an electron projectile (i.e., $z = 1$), but where spin is neglected, are derived. Beginning with the unscreened cross section the corresponding mass scattering power is,

$$\frac{\Im}{\rho} = 8\pi \left(\frac{N_A Z^2}{A}\right) \left(\frac{\alpha\hbar c}{p\beta}\right)^2 \ln\frac{1}{\chi_0} \tag{7.485}$$

Unscreened cross section.

By incorporating the definition of the screening angle χ_0,

$$\begin{aligned} \chi_0 &\approx 1.130 \left(\frac{\hbar c}{p r_B}\right) Z^{1/3} \\ &\approx \left(\frac{4.22 \times 10^{-3}}{p}\right) Z^{1/3} \end{aligned} \tag{7.486}$$

where p is in units of MeV. One can rewrite the electron mass scattering power in the form,

$$\frac{\Im}{\rho} = 8\pi \left(\frac{N_A Z^2}{A}\right) \left(\frac{\alpha\hbar c}{p\beta}\right)^2 \ln\left(237\, p\, Z^{-1/3}\right). \tag{7.487}$$

The screened cross section leads to an expression of the mass scattering power of the form,

$$\begin{aligned} \frac{\Im}{\rho} &= 4\pi \left(\frac{N_A Z^2}{A}\right) \left(\frac{\alpha\hbar c}{p\beta}\right)^2 \\ &\quad \times \left[\ln\left(1 + \frac{1}{\chi_0^2}\right) - \frac{1}{2}\left(\frac{1-\chi_0^2}{1+\chi_0^2}\right) - \ln 2\right] \end{aligned} \tag{7.488}$$

Screened Rutherford cross section.

This expression can be simplified for electrons typical of that encountered in nuclear medicine in low-Z media (i.e., $p \ll 1.6\,\text{MeV}$) for which $(1 + 1/\chi_0^2) \approx 1/\chi_0^2$ and $(1 - \chi_0^2)/(1 + \chi_0^2) \approx 1$ to give,

$$\begin{aligned} \frac{\Im}{\rho} &\approx 4\pi \left(\frac{N_A Z^2}{A}\right) \left(\frac{\alpha\hbar c}{p\beta}\right)^2 \\ &\quad \times \left[\ln\left(5.6 \times 10^4\, p^2\, Z^{-2/3}\right) - 1.193\right] \end{aligned} \tag{7.489}$$

where p is in units of MeV.

The mass scattering powers of electrons in carbon evaluated from the screened and unscreened cross sections above are shown in Fig. 7.34 as functions of electron kinetic energy.

Mott Cross Section

To include the effect of the electron's intrinsic spin, the Mott elastic scatter cross section is used,

$$\frac{d\sigma_{Mott}}{d\Omega} = \left(\frac{Z\,\alpha\hbar c}{2\,p\beta}\right)^2 \frac{F(\theta, Z)}{\sin^4\left(\frac{\theta}{2}\right)}$$

where the multiplicative factor

$$F(\theta, Z) = 1 - \beta^2 \sin^2\left(\frac{\theta}{2}\right)$$

is a consequence of the electron's intrinsic spin. McKinley and Feshbach (1948) have expanded Mott's original result to include a corrective term to F(θ,Z) in order to correct for the Born approximation used in the original derivation,

$$F(\theta, Z) = 1 - \beta^2 \sin^2\left(\frac{\theta}{2}\right) + \pi\alpha\beta Z\left(1 - \sin\frac{\theta}{2}\right) \sin\frac{\theta}{2} \tag{7.490}$$

This expression is valid for $\beta \approx 1$ and $\alpha Z < 0.2$ (i.e., $Z < 27$) which are conditions suitable for most instances of nuclear medicine dosimetry. McParland (1989) derived an analytical expression for the electron mass scattering power using this expanded Mott

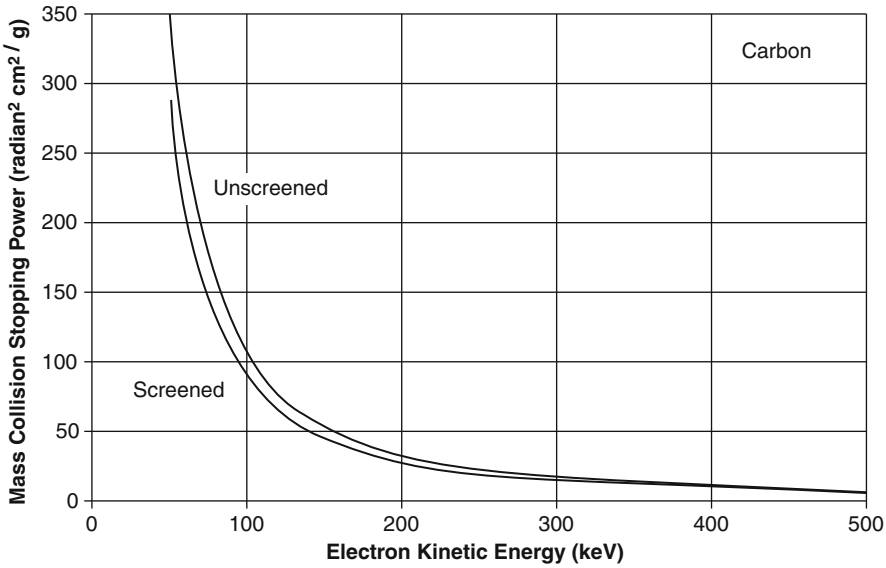

Fig. 7.34 Mass scattering power for electrons in carbon as a function of electron kinetic energy calculated using unscreened and screened potentials and neglecting spin

cross section and excluding any small-angle approximations,

$$\frac{\Im}{\rho} = 8\pi\left(\frac{N_A Z^2}{A}\right)\left(\frac{r_0}{\gamma\beta}\right)^2 (I_1 + \pi\alpha\beta Z I_2 - \beta(\beta + \pi\alpha Z) I_3) \tag{7.491}$$

where

$$I_1 = \ln\left(\frac{\sin(1/2)}{\sin(\chi_0/2)}\right) + \frac{1}{8}\left(\frac{\chi_0^2}{\sin^2(\chi_0/2)} - \frac{1}{\sin^2(1/2)}\right) + \frac{1}{2}\left(\chi_0 \cot\frac{\chi_0}{2} - \cot\frac{1}{2}\right) \tag{7.492}$$

$$I_2 = \chi_0\left(\frac{(\chi_0/2)}{\sin(\chi_0/2)} - 1 + 2\sum_{k=1}^{\infty}(-1)^k c_{2k}\left(\frac{\chi_0}{2}\right)^{2k}\right) - \left(\frac{1}{2\sin(\chi_0/2)} - 1 + 2\sum_{k=1}^{\infty}(-1)^k c_{2k}\left(\frac{1}{2}\right)^{2k}\right) \tag{7.493}$$

$$I_3 = \left(1 + \sum_{k=1}^{\infty}(-1)^k d_{2k}\left(\frac{1}{2}\right)^{2k}\right) - \chi_0^2\left(1 + \sum_{k=1}^{\infty}(-1)^k d_{2k}\left(\frac{\chi_0}{2}\right)^{2k}\right). \tag{7.494}$$

Table 7.1 Values of the coefficients c_{2k} and d_{2k}

k	c_{2k}	d_{2k}
1	2.78×10^{-2}	8.30×10^{-2}
2	-1.94×10^{-3}	-3.71×10^{-3}
3	1.46×10^{-4}	2.65×10^{-4}
4	-1.17×10^{-5}	-2.12×10^{-5}
5	9.70×10^{-7}	1.78×10^{-6}
6	-8.32×10^{-8}	-1.55×10^{-7}
7	7.31×10^{-9}	1.37×10^{-8}

The coefficients in these expressions are,

$$c_{2k} = \left(\frac{2^{2k-1} - 1}{(2k+1)!}\right) B_{2k} \tag{7.495}$$

$$d_{2k} = \left(\frac{2^{2k}}{(2+2k)(2k)!}\right) B_{2k} \tag{7.496}$$

B_{2k} is the 2kth Bernoulli number ($B_2 = 1/6$, $B_4 = -1/30$, $B_6 = 1/42$, etc.) The coefficients c_{2k} and d_{2k} rapidly diminish with k, as shown in Table 7.1, and, for practical calculation purposes, the summations for integrals I_2 and I_3 can be truncated at $k = 4$.

Contributions to the Scattering Power from Atomic Electrons

In the previous derivation of electron mass scattering powers for which a term of the form Z^2 appears, the

scattering has been calculated from an infinitely-massive point scattering center with charge Ze. This is a reasonable approximation, in most cases, from the nucleus. However, for an atomic scattering center made up from a nucleus with charge Ze and Z electrons, an accounting of the contributions of the atomic electrons to the mass scattering power is required. This inclusion of the Møller scatter is most frequently performed by assuming that it is coherent with the nuclear Rutherford/Mott results derived previously. This assumptions leads to the approximation in which the Z^2 term is replaced by $Z(Z+1)$, resulting in an increase in our previously-calculated mass scattering powers for carbon and lead by 16.7 and 1.2%, respectively.

7.5.2.4 Specific Electron Multiple Scattering Theories

Introduction

Although a considerable number of multiple scattering theories of varying complexity and utility have been developed, in this subsection, the review of such theories are limited to two – those of Goudsmit and Saunderson (1940) and Molière (1947, 1948), which are two of the more popular theories employed in Monte Carlo simulations of charged particle transport.

Goudsmit–Saunderson Theory

Goudsmit and Saunderson (1940) derived a multiple scatter pdf using multiple independent Coulomb single scatters and the addition theorem of spherical harmonics. The scattering angle is assumed to be small so that the electron's pathlength is equal to the thickness of the scatterer (in other words, the result is strictly valid only for thin foils or short discrete steps in a Monte Carlo simulation) and collisions resulting in energy loss are neglected. The theory does have the advantage in that any underlying single scattering differential cross section can be used. The derivation begins by defining the normalized single scatter angular distribution,

$$f_1(\theta) = \frac{\frac{d\sigma}{d\Omega}(\theta)}{\int d\Omega \frac{d\sigma}{d\Omega}(\theta)}. \tag{7.497}$$

The subscript "1" refers to a single Coulomb scatter and axial symmetry is assumed, which is valid for spherically symmetric atomic scattering centers or randomly-oriented molecules. In order to calculate the distribution for $n > 1$ scatters the distribution is first expanded as a weighted series of Legendre polynomials,

$$f_1(\theta) = \frac{1}{4\pi} \sum_{l=0}^{\infty} (2l+1) F_l P_l(\cos\theta). \tag{7.498}$$

The coefficients are given by,

$$\begin{aligned} F_l &= \int d\Omega\, f_1(\theta) P_l(\cos\theta) \\ &= \overline{P_l(\cos\theta)}. \end{aligned} \tag{7.499}$$

The single scatter angular distribution can now be written in the form,

$$f_1(\theta) = \frac{1}{4\pi} \sum_{l=0}^{\infty} (2l+1) \left[\overline{P_l(\cos\theta)}\right] P_l(\cos\theta). \tag{7.500}$$

In order to evaluate the coefficients of the expansion for $n > 1$ scatters, the addition property of spherical harmonics when written in terms of associated Legendre polynomials is used. Let the electron be first scattered through an angle of deflection θ_1 with a corresponding azimuthal angle ϕ_1. It then undergoes a second scatter through the corresponding angles (θ_2,ϕ_2). The total scattering angle is thus $\theta_1 + \theta_2$ and the addition property of spherical harmonics gives,

$$\begin{aligned} P_l(\cos(\theta_1+\theta_2)) = P_l(\cos\theta_1) P_l(\cos\theta_2) \\ + \sum_{m=-l}^{l} P_l^m(\cos\theta_1) \\ \times P_l^m(\cos\theta_2) \sin(m(\phi_2-\phi_1)). \end{aligned} \tag{7.501}$$

Averaging both sides leads to,

$$\overline{P_l(\cos(\theta_1+\theta_2))} = \overline{P_l(\cos\theta_1) P_l(\cos\theta_2)}. \tag{7.502}$$

The generalization of this result for n scatters is,

$$\overline{P_l(\cos(n\theta))} = \left[\overline{P_l(\cos\theta_1)}\right]^n. \tag{7.503}$$

Applying this to (7.500), one obtains the angular distribution following n scatters,

$$f_n(\theta) = \frac{1}{4\pi}\sum_{l=0}^{\infty}(2l+1)\left[\overline{P_l(\cos\theta)}\right]^n P_l(\cos\theta). \quad (7.504)$$

Consider the combination of a pathlength t and a mean free path between elastic collisions λ. The mean number of collisions is given by (t/λ) and the probability that an electron will undergo n collisions while traversing t is Poisson distributed,

$$p(n;t) = \frac{e^{-(t/\lambda)}\left(\frac{t}{\lambda}\right)^n}{n!}. \quad (7.505)$$

The probabilities of electron elastic scatter for n = 0, 1, and 2 scatters are provided in Fig. 7.35 as functions of the ratio of the pathlength to the elastic scatter mean free path. In order to calculate the angular distribution of the electrons exiting the foil, one must sum over the probabilities of all possible collisions,

$$\begin{aligned} f_{GS}(\theta;t) &= \sum_{n=0}^{\infty} p(n;t) f_n(\theta) \\ &= \frac{1}{4\pi}\sum_{n=0}^{\infty} e^{-(t/\lambda)}\frac{(t/\lambda)^n}{n!} \\ &\quad \times \sum_{l=0}^{\infty}(2l+1)\left[\overline{P_l(\cos\theta)}\right]^n P_l(\cos\theta) \\ &= \frac{1}{4\pi}\sum_{l=0}^{\infty}(2l+1)P_l(\cos\theta)e^{-(t/\lambda)} \\ &\quad \times \sum_{n=0}^{\infty}\frac{(t/\lambda)^n}{n!}\left[\overline{P_l(\cos\theta)}\right]^n \\ &= \frac{1}{4\pi}\sum_{l=0}^{\infty}(2l+1)e^{-(t/\lambda)}\, e^{-(t/\lambda)\overline{P_l(\cos\theta)}}P_l(\cos\theta) \\ &\equiv \frac{1}{4\pi}\sum_{l=0}^{\infty}(2l+1)e^{-tG_l}P_l(\cos\theta) \end{aligned} \quad (7.506)$$

where the series expansion of e^x has been used and the coefficient,

$$G_l = \frac{1-\overline{P_l(\cos\theta)}}{\lambda} \quad (7.507)$$

has been defined. This is referred to as the l th-order transport coefficient, as will be made evident shortly.

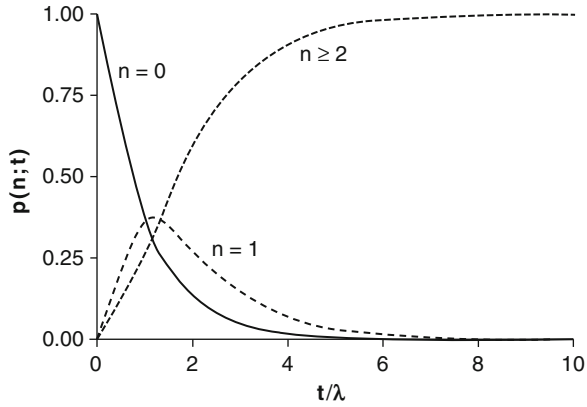

Fig. 7.35 The probability of electron elastic scatter for n = 0,1 and 2 scatters as a function of the ratio of the pathlength t to the elastic scatter mean free path

As $\overline{P_0(\cos\theta)} = 1$ then $e^{-tG_0} = 1$ and the zeroth-order term of the expansion $f_{GS}(\theta;t)$ is $1/4\pi$. As $P_l(\cos\theta)$ decreases with increasing l due to the growing oscillatory nature of the Legendre polynomial, the e^{-tG_l} term will tend to $e^{-(t/\lambda)}$ for increasing l. $f_{GS}(\theta;t)$ is forward peaked for small foil thickness t values but, as $t \to \infty$ only the $l = 0$ term contributes to the pdf and $f_{GS}(\theta;t) \to 1/4\pi$. Hence, as expected and because energy loss is ignored, the angular distribution becomes isotropic.

Now look at the first-order transport coefficient,

$$\begin{aligned} G_1 &= \frac{1}{\lambda}\left(1-\overline{P_1(\cos\theta)}\right) \\ &= \frac{1}{\lambda}\int d\Omega\, f_1(\theta)(1-\cos\theta). \end{aligned} \quad (7.508)$$

Recalling the definition of the mean free path between collisions given by (7.7), this result is rewritten as,

$$G_1 = \frac{\rho N_A}{A}\int d\Omega \frac{d\sigma}{d\Omega}(\theta)(1-\cos\theta). \quad (7.509)$$

Invoking the small-angle approximation, $1-\cos\theta = 2\sin^2(\theta/2) \approx \theta^2/2$ (which is justifiable in this application as the differential cross section is highly forward-peaked),

$$\begin{aligned} G_1 &= \frac{\rho N_A}{2A}\int d\Omega \frac{d\sigma}{d\Omega}(\theta)\theta^2 \\ &= \frac{\Im}{2} \end{aligned} \quad (7.510)$$

which, of course, is proportional to the linear scattering power.

It will be noted that the Goudsmit–Saunderson pdf is exact in that the single scatter differential cross section appears within the transport coefficient. Hence, these coefficients need only be calculated. Goudsmit and Saunderson provide examples of such calculations for analytical forms of the single scatter differential cross section and a series approximation of the Legendre polynomials. The number of terms required in the summation over l to achieve convergence in the calculation of $f_{GS}(\theta;t)$ will increase as the pathlength t decreases due to the e^{-tG_l} term. It is possible to improve the convergence of the calculation for small pathlengths by isolating the contributions from unscattered electrons.

Molière Theory

The Goudsmit–Saunderson result provides the electron multiple scatter pdf as the weighted summation of Legendre polynomials where the underlying single scatter theory is incorporated through the mean free pathlength between elastic collisions and the averaged Legendre polynomial. The Molière multiple scattering theory (Molière 1947, 1948) evolved from consideration of consecutive scatters which, in practice, is the solution of the transport equation. Like the previous theory, the result of Molière's theory is both independent of an individual form of the single scatter cross section and neglects energy loss. On the other hand, the single scatter cross section is input to the Molière theory through only a single parameter, the Molière screening angle, χ_a'. The shape of the multiple scatter pdf is dependent upon a single parameter, b, which is primarily a function of the areal thickness of the medium the particle is traversing and is largely dependent upon the medium's atomic number for most media of dosimetric interest.

Molière's result is derived here using Bethe's (1953) approach, which is mathematically more transparent than the original, and incorporating further improvements suggested by Andreo et al. (1993).[23]

Again, because of the θ^{-4} dependence of the scattering cross section and its consequently being forward peaked, the derivation is simplified using the small-angle approximation. Consider a monodirectional beam of electrons incident to a medium of physical density ρ, atomic number[24] Z, and atomic mass A. The number of scattering centers per unit volume is given by $\rho N_A/A$. χ is the scattering angle after a single scatter and θ is the cumulative scattering angle after multiple scatters an electron undergoes traversing a finite thickness of medium. $f_M(\theta;t)\theta d\theta$ is the number of scattered electrons in the angular interval dθ following traveling a distance t of the medium. By equating the multiple scattering problem to the diffusion of electrons in the scattering plane, the electron transport equation is, for the scattering pdf,

$$\frac{\partial f(\theta;s)}{\partial s} = \rho\left(\frac{N_A}{A}\right)\left(\int d\chi\, f\left(\hat{\boldsymbol{\theta}}';s\right)\frac{d\sigma(\chi)}{d\chi} - f(\theta;s)\int dX\,\chi\frac{d\sigma(\chi)}{d\chi}\right) \tag{7.511}$$

where $\hat{\boldsymbol{\theta}}' = \hat{\boldsymbol{\theta}} - \hat{\mathbf{X}}$ is the direction vector of the electron prior to the last scatter at t and $dX = \chi\, d\chi\, d\phi/2\pi$ where φ is the azimuthal angle of χ in the prescattering plane of the electron. Defining the transforms,

$$f_M(\theta;t) = \int_0^\infty d\eta\,\eta\,J_0(\eta\theta)g(\eta;t) \tag{7.512}$$

and

$$g(\eta;t) = \int_0^\infty d\theta\,\theta\,J_0(\eta\theta)f(\theta;t) \tag{7.513}$$

and applying them to the transport equation gives,

$$\frac{\partial g(\eta;t)}{\partial t} = -g(\eta;t)\left(\rho\frac{N_A}{A}\right) \times \int_0^\infty d\chi\,\chi(1 - J_0(\eta\chi))\frac{d\sigma}{d\chi}. \tag{7.514}$$

[23] Fernández-Varea et al. (1993) have provided an additional and shorter derivation of the theory beginning with the Goudsmit–Saunderson result.

[24] Unlike Molière, Bethe included the contributions of the atomic electrons and assumed these to be coherent so that Z is replaced by Z(Z + 1). This is repeated here.

The solution to this equation is,

$$g(\eta;t) = e^{(\Omega(\eta;t)-\Omega_0)} \tag{7.515}$$

where

$$\Omega(\eta;t) = \left(\rho\frac{N_A}{A}\right)t\int_0^\infty d\chi\,\chi\frac{d\sigma}{d\chi}J_0(\eta\chi). \tag{7.516}$$

Note that, as $J_0(0) = 1$, the parameter

$$\begin{aligned}\Omega_0 &= \Omega(0;t)\\ &= \left(\rho\frac{N_A}{A}\right)t\int_0^\infty d\chi\,\chi\frac{d\sigma}{d\chi}\end{aligned} \tag{7.517}$$

is equal to the total number of collisions occurring along the pathlength t. One then obtains an expression for the Molière multiple scattering pdf,

$$\begin{aligned}f_M(\theta;t) = &\int_0^\infty d\eta\,\eta\,J_0(\eta\theta)\\ &\times\exp\left[-\rho\left(\frac{N_A}{A}\right)t\int_0^\infty d\chi\,\chi\frac{d\sigma}{d\chi}(1-J_0(\eta\chi))\right].\end{aligned} \tag{7.518}$$

Because of the explicit inclusion of the scattering differential cross section in this expression, it is apparent that, as with the Goudsmit–Saunderson theory, the multiple scattering pdf will not be restricted to a particular single Coulomb scatter theory.

A simpler form of the Molière pdf can be obtained by taking advantage of the fact that the elastic single scatter differential cross section is proportional to θ^{-4}, becoming complicated only (as shown in Fig. 7.2) when the scattering angle is of the order of, or less than, the screening angle. Using Bethe as a guide, $f_M(\theta;t)$ is calculated using the unscreened Rutherford cross section beginning with evaluating the ratio of the actual to Rutherford cross section,

$$q(\chi) = \frac{(d\sigma_{Act}/d\chi)}{\left(d\sigma_{Ruth}/d\chi\right)} \tag{7.519}$$

where the axial symmetry of the Coulomb interaction is noted. The subscript Act identifies the actual cross section. For the unscreened Rutherford cross section,

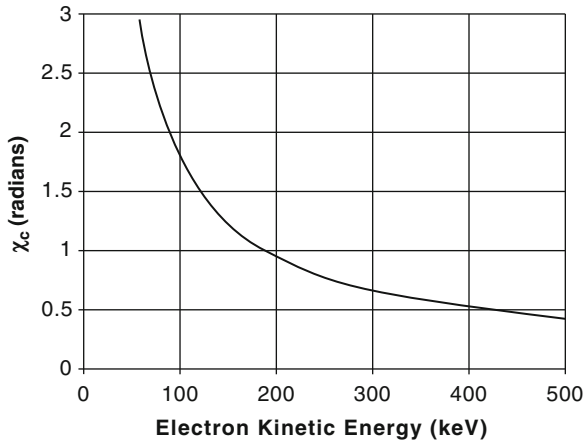

Fig. 7.36 Molière angle χ_c for carbon (Z = 6, A = 12, ρ = 2 g/cm^3, t = 0.1 cm) as a function of electron kinetic energy

$$q(\chi) = \left(\rho\frac{N_A}{A}\right)t\left(\frac{\chi^4}{2\chi_c^2(t)}\right)\frac{d\sigma_{Act}}{d\chi} \tag{7.520}$$

where the unit-probability angle χ_c is defined by,

$$\chi_c^2(t) = \left(\rho\frac{N_A}{A}\right)t\left(\frac{\alpha\hbar c}{p\beta}\right)^2 Z(Z+1). \tag{7.521}$$

The Molière angle χ_c has the physical interpretation of being the angle beyond which the probability of a single elastic scatter occurring is equal to unity; it is plotted as a function of electron kinetic energy in 1 mm carbon in Fig. 7.36.

$q(\chi)$ has properties that will prove useful in the derivation. Clearly, $q(\chi) \to 0$ as $\chi \to 0$ due to the χ^{-4} dependence of the unscreened cross section. By extension, as the screened and unscreened cross sections converge for large scattering angles, $q(\chi) \to 1$ as $\chi \to \infty$ (again, for calculational purposes, the maximum scattering angle is set to infinity and advantage is taken of the sharp forward-angle peak of the single scatter cross section). As suggested by Figs. 7.2 and 7.3, the most rapid change in $q(\chi)$ occurs for $\chi \approx 0$. The next step of the derivation is to return to (7.512) and, by taking logarithms of (7.515) and using (7.516), obtain,

$$\begin{aligned}-\ln g(\eta;t) &= \Omega_0 - \Omega(\eta)\\ &= \rho\left(\frac{N_A}{A}\right)t\int_0^\infty d\chi\,\chi(1-J_0(\eta\chi))\frac{d\sigma_{Act}}{d\Omega}\\ &= 2\chi_c^2(t)\int_0^\infty d\chi\,\chi\frac{(1-J_0(\eta\chi))}{\chi^3}q(\chi)\end{aligned} \tag{7.522}$$

As $q(\chi) < 1$ for $\chi \approx \chi_0$ where $\chi \ll \chi_c$, the integral can be split by defining an intermediate angle $\chi_0 \ll \chi_S \ll \chi_c$, for which $q(\chi)$ can be set equal to unity for scattering angles greater than χ_S,

$$\begin{aligned}
&\int_0^\infty d\chi\,\chi\frac{(1-J_0(\eta\chi))}{\chi^3}q(\chi)\\
&=\int_0^{\chi_s} d\chi\,\chi\frac{(1-J_0(\eta\chi))}{\chi^3}q(\chi)+\int_{\chi_s}^\infty d\chi\,\chi\frac{(1-J_0(\eta\chi))}{\chi^3}q(\chi)\\
&\cong\int_0^{\chi_s} d\chi\,\chi\frac{(1-J_0(\eta\chi))}{\chi^3}q(\chi)+\int_{\chi_s}^\infty d\chi\,\chi\frac{(1-J_0(\eta\chi))}{\chi^3}\\
&\equiv I_1(\eta;\chi_s)+I_2(\eta;\chi_s). \qquad (7.523)
\end{aligned}$$

The first integral is solved by the change of variable $x = \eta\chi_s$ and using the small-argument approximation of the Bessel function (as $\eta\chi_s$ is small), $J_0(x) \approx 1 - (x/2)^2$,

$$I_1(\eta;\chi_s) = \frac{\eta^2}{4}\int_0^{\chi_s} d\chi\frac{q(\chi)}{\chi}. \qquad (7.524)$$

The second integral is,

$$\begin{aligned}
I_2(\eta;\chi_s) &= \int_{\chi_s}^\infty d\chi\frac{(1-J_0(\eta\chi))}{\chi^3}\\
&= \int_{\chi_s}^\infty \frac{d\chi}{\chi^3} - \int_{\chi_s}^\infty d\chi\frac{J_0(\eta\chi)}{\chi^3} \qquad (7.525)\\
&= \frac{1}{2\chi_s^2} - I_3(\eta;\chi_s).
\end{aligned}$$

The indefinite form of the integral $I_3(\eta;\chi_s)$ can be expressed in terms of the Meijer G function, but here Bethe's approach of straightforward, but tedious, sequential integrations by parts and ignoring terms of order $(\eta\chi_s)^2$ is followed. Beginning with the change of variable, $x = \eta\chi_s$, the integral is rewritten as,

$$I_3(\eta;\chi_S) = \eta^2\int_{\eta\chi_S}^\infty dx\frac{J_0(x)}{x^3} \qquad (7.526)$$

where the integral is,

$$\begin{aligned}
\int_{\eta\chi_s}^\infty dx\frac{J_0(x)}{x^3} &= \int_{\eta\chi_s}^\infty dr\,s\\
&= s\,r\Big|_{\eta\chi_s}^\infty - \int_{\eta\chi_s}^\infty ds\,r
\end{aligned} \qquad (7.527)$$

where

$$s \equiv J_0(x) \quad ds = -dx\,J_1(x)$$

$$dr \equiv \frac{dx}{x^3} \qquad r \equiv -\frac{1}{2x^2}$$

to give

$$\begin{aligned}
\int_{\eta\chi_s}^\infty dx\frac{J_0(x)}{x^3} &= \frac{J_0(\eta\chi_s)}{2(\eta\chi_s)^2} - \frac{1}{2}\int_{\eta\chi_s}^\infty dx\frac{J_1(x)}{x^2}\\
&= \frac{J_0(\eta\chi_s)}{2(\eta\chi_s)^2} - \frac{1}{2}I_4(\eta;t).
\end{aligned} \qquad (7.528)$$

This new integral is also solved by parts,

$$\begin{aligned}
I_4(\eta;t) &= \int_{\eta\chi_s}^\infty dx\frac{J_1(x)}{x^2}\\
&= s\,r\Big|_{\eta\chi_s}^\infty - \int_{\eta\chi_s}^\infty ds\,r
\end{aligned} \qquad (7.529)$$

where

$$s \equiv J_1(x) \quad ds = dx\left(J_0(x) - \frac{J_1(x)}{x}\right)$$

$$dr \equiv \frac{dx}{x^2} \qquad r \equiv -\frac{1}{x}.$$

Then,

$$\begin{aligned}
I_4(\eta;t) &= \frac{J_1(\eta\chi_s)}{\eta\chi_s} + \int_{\eta\chi_s}^\infty dx\frac{J_0(x)}{x} - I_4(\eta;t)\\
&= \frac{1}{2}\left(\frac{J_1(\eta\chi_s)}{\eta\chi_s} + \int_{\eta\theta\chi}^\infty dx\frac{J_0(x)}{x}\right).
\end{aligned} \qquad (7.530)$$

This result is simplified by using the small-argument approximation, $J_1(x) \cong x/2$, and the solution to the definite integral $\int_t^\infty dx \frac{J_0(x)}{x} = \int_0^t dx \frac{1-J_0(x)}{x} - \gamma_{EM} - \ln\frac{t}{2}$,

$$I_4(\eta;t) = \frac{1}{2}\left(\frac{1}{2} - \gamma_{EM} - \ln\frac{\eta\chi_s}{2}\right) + \mathbf{O}\left((\eta\chi_s)^2\right). \tag{7.531}$$

Terms of order $(\eta\chi_s)^2$ are neglected. Working backwards,

$$I_3(\eta;\chi_S) = \frac{\eta^2}{2}\frac{J_0(\eta\chi_s)}{(\eta\chi_s)^2} - \frac{\eta^2}{4}\left(\frac{1}{2} - \gamma_{EM} - \ln\frac{\eta\chi_s}{2}\right). \tag{7.532}$$

Using the small-argument form of $J_0(\eta\chi_s)$, one then arrives at,

$$\begin{aligned} I_2(\eta;\chi_S) &= \frac{1}{2\chi_s^2} - I_3(\eta;\chi_s) \\ &= \frac{\eta^2}{4}\left(1 - \gamma_{EM} - \ln\frac{\eta\chi_s}{2}\right) \end{aligned} \tag{7.533}$$

One can now return to the original integral to give,

$$\begin{aligned} &\int_0^\infty d\chi\,\chi\frac{(1-J_0(\eta\chi))}{\chi^3}q(\chi) \\ &= \frac{\eta^2}{4}\left(\int_0^{\chi_s} d\chi\frac{q(\chi)}{\chi} + 1 - \gamma_{EM} - \ln\eta - \ln\chi_s + \ln 2\right). \end{aligned} \tag{7.534}$$

Molière next defined a characteristic screening angle,

$$-\ln\chi_a = \lim_{\chi_s\to\infty}\left(\int_0^{\chi_s} d\chi\frac{q(\chi)}{\chi} + \frac{1}{2} - \ln\chi_s\right)$$

allowing (7.534) to be written in the much simpler form,

$$\begin{aligned} &\int_0^\infty d\chi\,\chi\frac{(1-J_0(\eta\chi))}{\chi^3}q(\chi) \\ &= \frac{\eta^2}{4}\left(\frac{1}{2} - \gamma_{EM} - \ln\eta\chi_a + \ln 2\right) \end{aligned} \tag{7.535}$$

Then, the exponent of (7.515) can be written as,

$$\Omega_0 - \Omega(\eta) = \frac{(\eta\chi_c)^2}{2}\left(\frac{1}{2} - \gamma_{EM} - \ln\eta\chi_a + \ln 2\right). \tag{7.536}$$

In order to simplify the integral $f_M(\theta;t) = \int_0^\infty d\eta\,\eta\,J_0(\eta)e^{-(\Omega_0-\Omega(\eta;t))}$, Molière further defined the quantity,

$$\begin{aligned} b &= \ln\left(\frac{\chi_c}{\chi_a}\right)^2 + 1 - 2\gamma_{EM} \\ &\equiv \ln\left(\frac{\chi_c}{\chi_a'}\right)^2 \end{aligned} \tag{7.537}$$

where the modified characteristic scattering angle is,

$$\begin{aligned} \chi_a' &= \chi_a\, e^{\gamma_{EM}-1/2} \\ &\approx 1.08\,\chi_a \end{aligned} \tag{7.538}$$

leading to a simpler expression,

$$b = \ln\left(\frac{\chi_c^2}{1.167\,\chi_a^2}\right). \tag{7.539}$$

Using the change of variable $y = \eta\chi_c$, (7.536) is recast as,[25]

$$\Omega_0 - \Omega(\eta;t) = \frac{y^2}{4}\left(b - 2\ln\frac{y}{2}\right). \tag{7.540}$$

Finally, by writing $\lambda = \theta/\chi_c$, one at last obtains the transformed form of Molière's pdf,

$$\begin{aligned} f_M(\theta)\theta\,d\theta = \lambda\,d\lambda \int_0^\infty dy\,y\,J_0(\lambda y) \\ \times \exp\left(\left(\frac{y}{2}\right)^2\left(2\ln\left(\frac{y}{2}\right) - b\right)\right). \end{aligned} \tag{7.541}$$

It is necessary to modify the upper limit of this integration as the exponent goes to infinity for $y \to \infty$, as shown in Fig. 7.37 for $b = 3$. The exponent

[25] Molière achieved this result using an expansion of Hankel functions.

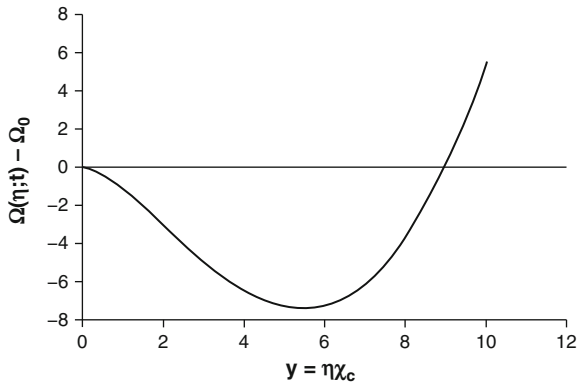

Fig. 7.37 Exponent in the transformed expression of the Molière pdf for b = 3

has a minimum at $y = 2e^{(b-1)/2}$, which is a consequence of the specified inequality $\chi_0 \ll \chi_s \ll \chi_c$. The upper limit of the integral is set to this minimum and the transformed Molière pdf is written as,

$$f_M(\theta)\theta\, d\theta = \lambda\, d\lambda \int_0^{2e^{(b-1)/2}} dy\, y\, J_0(\lambda y) \times \exp\left(\left(\frac{y}{2}\right)^2\left(2\ln\left(\frac{y}{2}\right) - b\right)\right). \tag{7.542}$$

This truncation of the integration limit will have a negligible effect as $e^b \approx (\chi_c/\chi_a)^2$ which is of the order of the total number of collisions in the pathlength considered. As the mean free pathlength between elastic collisions is small, this truncation of the integration is allowed.

Molière solved for the angular pdf by first defining a variable B through the transcendental equation,

$$B - \ln B = b. \tag{7.543}$$

Approximations to B have since been given by Scott (1963),

$$B = 1.153 + 2.583 \log_{10}\left(\frac{\chi_c}{\chi_a}\right)^2 \tag{7.544}$$

and Tabata and Ito (1976),

$$B = 2.6 + 2.3863 \log_{10}\left(\frac{\chi_c}{\chi_a}\right)^2 - \frac{3.234}{\log_{10}\left(\frac{\chi_c}{\chi_a}\right)^2 + 0.994} \tag{7.545}$$

(the value of B typically ranges from between 5 and 20). To complete the derivation, Molière defined the reduced angle,

$$\vartheta = \frac{\lambda}{B} = \frac{\theta}{\chi_c\sqrt{B}}. \tag{7.546}$$

The integration variable of the multiple scatter pdf is then changed to,

$$u = y\sqrt{B} \tag{7.547}$$

and the pdf then expanded in a power series in B^{-1},

$$f_M(\theta)\theta\, d\theta = \vartheta\, d\vartheta \sum_{n=0}^{\infty} f_M^{(n)}(\vartheta) B^{-n} \tag{7.548}$$

where the coefficients of the expansion are,

$$f_M^{(n)}(\vartheta) = \frac{1}{n!}\int_0^{2e^{(b-1)/2}} du\, u\, J_0(u)\left(\frac{u^2}{4}\ln\frac{u^2}{4}\right)^n \exp\left(-\frac{u^2}{4}\right). \tag{7.549}$$

The zeroth-order coefficient can be calculated from the following property of integer-order Bessel functions,

$$\int_0^{\infty} dt\, t^{\nu+1} e^{-a^2t^2} J_\nu(bt) = \frac{b^\nu}{(2a^2)^{\nu+1}} e^{-b^2/4a^2}; \quad \text{Re } a^2 > 0 \tag{7.550}$$

to give,

$$f_M^{(0)}(\vartheta) = \int_0^{\infty} du\, u\, J_0(u) \exp\left(-\frac{u^2}{4}\right) = 2e^{-\vartheta^2} \tag{7.551}$$

where the upper limit of the integral has been allowed to go to infinity due to the $e^{-u^2/4}$ term in the integrand. Clearly, this first term corresponds to a Gaussian multiple scattering pdf. Whereas Molière provided an analytical representation of $f^{(1)}(\vartheta)$ which was proportional to ϑ^{-4} for large ϑ, Bethe reported that he was only able to find numerical solutions to $f^{(n)}(\vartheta)$ for

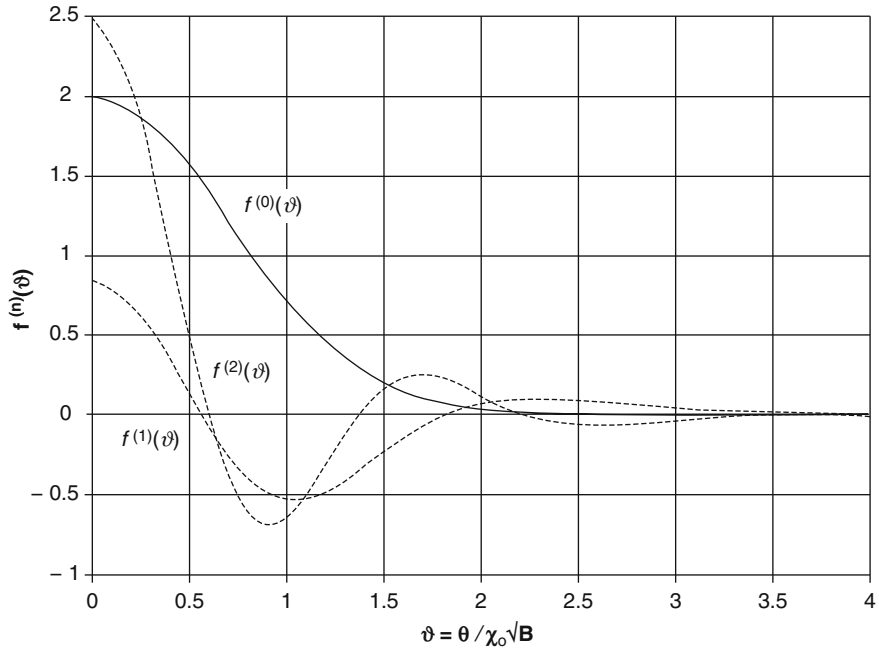

Fig. 7.38 The coefficients $f^{(0)}(\vartheta)$, $f^{(1)}(\vartheta)$, and $f^{(2)}(\vartheta)$ of the Molière expansion of the multiple scattering probability distribution function as functions of the reduced scattering angle ϑ

$n \geq 2$. Values of $f^{(0)}(\vartheta)$, $f^{(1)}(\vartheta)$, and $f^{(2)}(\vartheta)$ are plotted as functions of ϑ in Fig. 7.38. For, $\vartheta < 2$ $f^{(0)}(\vartheta)$ dominates and the multiple scattering pdf is Gaussian for small scattering angles. The $f^{(0)}(\vartheta)$ term decreases exponentially such that at larger values of ϑ, the $f^{(1)}(\vartheta)$ term dominates and, as it is proportional to ϑ^{-4} for large ϑ, it goes over into the Rutherford single scatter angular distribution.

One would expect from the expansion of (7.548) that the accuracy of the pdf would increase with the inclusion of an increasing number of terms. This is not the case due mainly to the omission of electron intrinsic spin and relativity, the effects of which grow at large single scattering angles. Andreo et al. (1993) have exhaustively studied the limitations to the Molière theory.

Now return to the transformed Molière result. In the Molière theory, the scatter is described by the characteristic screening angle and that the final angular distribution is a function of the ratio of this screening angle to the unit-probability scattering angle. The single scatter differential cross section enters the theory through the ratio of differential cross sections, $q(\chi)$. Molière provided a result for the Thomas–Fermi atom and Fernández-Varea et al. (1993) did so for the Yukawa-type screening. Molière's form is,

$$\chi_a^2 = 1.13 + 3.76\left(Z\frac{\alpha}{\beta}\right)^2. \tag{7.552}$$

The second term in the series accounts for deviation from the Born approximation. From the definition of b, for an electron of speed βc in a medium with atomic number Z and atomic mass number A and physical density ρ,

$$\begin{aligned} e^b &= \frac{\chi_c^2}{\chi_a'^2} \\ &= \frac{6680}{\beta^2}\rho t\frac{Z^{1/3}(Z+1)}{A\left(1+3.34\left(Z\frac{\alpha}{\beta}\right)^2\right)} \end{aligned} \tag{7.553}$$

where ρt is the pathlength given in units of cm^2/g. Bethe showed that the Z-dependence does not deviate from unity by more than about $\pm 30\%$ for Z ranging from 1 (for deuterium) to 92 (uranium), an observation that indicates that the number of collisions per square centimeter/gram is reasonably constant for all elements.

7.6 Bremsstrahlung

7.6.1 Introduction

Throughout this chapter, only the elastic scatter and the collision energy losses of a charged particle moving through a medium have been considered. Attention is now turned to radiative energy losses through which a charged particle is deflected by the nuclear Coulomb field and emits a photon as a result (*bremsstrahlung*).

In this section, discussions will be limited to those of the radiative energy losses of electron and positron projectiles with kinetic energies of the order of a few MeV or less in low-Z media representative of tissue[26] and omit a derivation of electron–electron *bremsstrahlung* as it is not a significant phenomenon at the energies of interest here.[27] Hence, only the *bremsstrahlung* resulting from electron-atom interactions is considered (i.e., the atom is treated as a nuclear Coulomb field screened by the atomic electrons).

Detailed elucidations of *bremsstrahlung* may be found in Koch and Motz (1959), Heitler (1984), Pratt et al. (1977), and Haug and Nakel (2004). Numerical data are also available from ICRU Publication 37 (1984) and Berger and Seltzer (1983).

[26]This limitation is reasonable for nuclear medicine purposes as the maximum electron energy resulting from the Compton scatter of a 511 keV photon is 340 keV for a backscattered photon and the maximum β^- kinetic energies of isotopes typical of clinical nuclear medicine interest are below a couple of MeV.

[27]There are two classical arguments that will allow electron-electron *bremsstrahlung* to be neglected. On the simplest level, in the dipole approximation, the energy radiated away by an accelerated charged particle is proportional to the dipole moment. As the dipole moment is also proportional to the center-of-mass (which is stationary of particles of identical mass), our first approximation is that electron-electron *bremsstrahlung* will be zero. One can also think of the accelerations of an electron projectile and electron target resulting in electromagnetic radiations of equal magnitude but opposite phase resulting in cancellation.

7.6.2 Classical Electron-Atom Bremsstrahlung Theory

7.6.2.1 Introduction

While the exact understanding of electron-atom *bremsstrahlung* requires a quantum-mechanical treatment, classical theory proves useful despite some fundamental differences. For example, classical theory demonstrates that a charged particle will radiate electromagnetic energy only when accelerated, but also states that this emission will occur at *any* time the particle is accelerated. On the other hand, the quantum-mechanical result shows that there can only be a finite probability that radiation occurs. Classical *bremsstrahlung* theory also fails to reproduce the cutoff of radiation at high frequency (corresponding to the full stopping of the moving charged particle and the complete transfer of its kinetic energy to radiation, neglecting nuclear recoil). In other words, in the classical theory the Fourier transforms of the time-dependent field strengths extend to infinite frequency. Nevertheless, a review of the classical *bremsstrahlung* theory is a useful foundation to the full quantum-mechanical development of the phenomenon.

7.6.2.2 Liénhard–Wiechert Retarded Potentials

In order to demonstrate that electromagnetic energy is radiated by an electron only when accelerated, one begins with the derivation of the Liénhard–Wiechert retarded potentials. Consider an electron moving *in vacuo* along the trajectory $\mathbf{r}(t)$ parametric in time t as shown in Fig. 7.39. It is desired to determine the electromagnetic field at point P (with position vector $\mathbf{x}$) associated with the electron at time t. At this time t, the electron will be at point A with position vector $\mathbf{r}(t)$. However, due to the finite propagation time of the radiation, the field at P at time t will be that due to the radiation emitted at the earlier time t' when the electron was at point A' with position vector $\mathbf{r}(t')$. The time taken for the radiation to travel from point A to point P is equal to $|\mathbf{x} - \mathbf{r}(t')|/c$ and the retarded time is the difference between this time and that when the radiation is observed at point P,

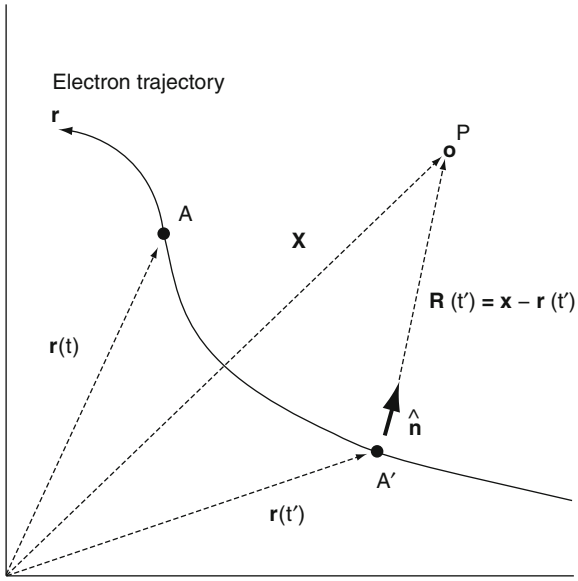

Fig. 7.39 Trajectory of a moving electron for calculation of the Liénhard–Wiechert retarded potentials

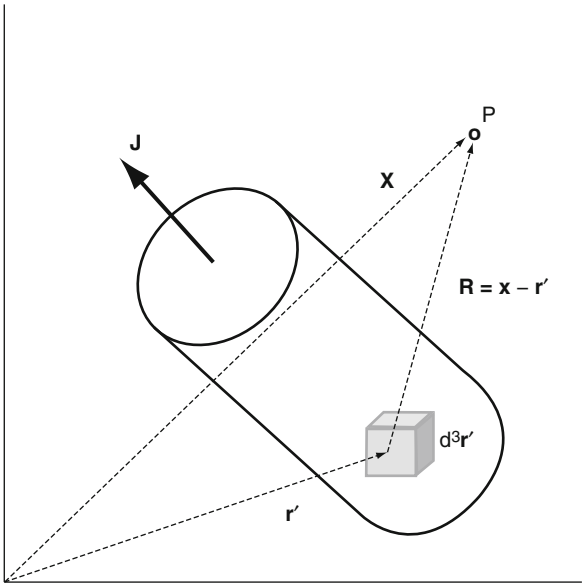

Fig. 7.40 Replacement of the single moving electron with an electric current density

$$\begin{aligned} t' &= t - \frac{|\mathbf{x} - \mathbf{r}(t')|}{c} \\ &\equiv t - \frac{|\mathbf{R}(t')|}{c} \\ &= t - \frac{R(t')}{c} \end{aligned} \tag{7.554}$$

where the vector $\mathbf{R}(t')$ has been defined. The unit vector directed along $\mathbf{R}(t')$ is

$$\hat{\mathbf{n}}(t') = \frac{\mathbf{R}(t')}{R(t')}. \tag{7.555}$$

To enable the calculation of the electromagnetic field at P, return to first principles, neglect retardation and replace the single moving electron with a uniformly moving current density as shown in Fig. 7.40. The resulting vector and scalar potentials at P will be,

$$\mathbf{A}(\mathbf{x}) = \frac{\mu_0}{4\pi} \int d^3\mathbf{r}' \, \frac{\mathbf{J}(\mathbf{r}')}{R} \tag{7.556}$$

and

$$\Phi(\mathbf{r}) = \frac{1}{4\pi\varepsilon_0} \int d^3\mathbf{r}' \, \frac{\rho(\mathbf{r}')}{R} \tag{7.557}$$

where $\mathbf{J}(\mathbf{r}')$ and $\boldsymbol{\rho}(\mathbf{r}')$ are the current and charge densities, respectively, and the integration is over a small volume element as shown. If the current and charge are allowed to vary with time and a finite propagation time is accounted for, these potentials can be rewritten in the forms,

$$\mathbf{A}(\mathbf{x}, t) = \frac{\mu_0}{4\pi} \int d^3\mathbf{r} \, \frac{\mathbf{J}\left(\mathbf{r}, t - \frac{R}{c}\right)}{R} \tag{7.558}$$

$$\Phi(\mathbf{x}, t) = \frac{1}{4\pi\varepsilon_0} \int d^3\mathbf{r} \, \frac{\rho\left(\mathbf{r}, t - \frac{R}{c}\right)}{R} \tag{7.559}$$

Having derived these potentials, return now to the example of a moving electron for which the potentials are evaluated following the approach of Feynman et al. (1963). First, the charge distribution is replaced with a cube of side dimension L moving towards the point P (i.e., $\hat{\mathbf{n}} = \boldsymbol{\beta}$) and it assumed that $L \ll R$. The integral of (7.559) is replaced by the finite summation,

$$\int d^3\mathbf{r}_0 \, \frac{\rho\left(\mathbf{r}_0, t - \frac{R}{c}\right)}{R} \cong \rho L^2 \Delta L \sum_{i=1}^{N} \frac{1}{r_i} \tag{7.560}$$

where the cube has been divided into N elements of thickness ΔL and r_i is the distance from the ith element to R. This summation is,

$$\begin{aligned} \rho L^2 \Delta L \sum_{i=1}^{N} \frac{1}{r_i} &= \rho L^2 \Delta L \sum_{i=1}^{N} \frac{1}{r_{eff}} \\ &= \frac{\rho L^3}{r_{eff}} \frac{N \Delta L}{L} \\ &= \frac{\rho L^3}{r_{eff}} \frac{L_{eff}}{L} \end{aligned} \tag{7.561}$$

where r_{eff} is the effective distance from the volume elements to P and L_{eff} is the length of the volume traversed by the moving cube over a time Δt, or,

$$L_{eff} = \frac{L}{1-\beta}. \tag{7.562}$$

As ρL^3 is the total charge (taken to be equal to e for an electron),

$$\frac{1}{4\pi\varepsilon_0}\int d^3\mathbf{r}_0 \frac{\rho\left(\mathbf{r}_0, t - R/c\right)}{R} = \frac{e}{4\pi\varepsilon_0}\frac{1}{R(t')(1-\beta(t'))}. \tag{7.563}$$

Hence, the potentials can be written as,

$$\Phi(\mathbf{x}, t) = \frac{e}{4\pi\varepsilon_0}\left\{\frac{1}{R\left(1-\hat{\mathbf{n}}\bullet\hat{\boldsymbol{\beta}}\right)}\right\}_{t'} \tag{7.564}$$

and

$$\mathbf{A}(\mathbf{x}, t) = \frac{e}{4\pi\varepsilon_0 c}\left\{\frac{\hat{\boldsymbol{\beta}}}{R\left(1-\hat{\mathbf{n}}\bullet\hat{\boldsymbol{\beta}}\right)}\right\}_{t'}. \tag{7.565}$$

Note that the $\mathbf{x}$ and t dependencies implicitly arise through the definition of the retarded time and that the use of brackets with the subscript t has been introduced in order to signify that the quantities within the brackets are to be evaluated at the retarded time, t'. $\hat{\boldsymbol{\beta}}$ is the electron velocity normalized to the speed of light (as $\beta \leq 1$, the normalized velocity is written as a unit vector for convenience) and the scalar product $\hat{\mathbf{n}}\bullet\hat{\boldsymbol{\beta}}$ is that component of the normalized electron velocity directed towards the detection point, P. Equations (7.564) and (7.565) are the Liénhard–Wiechert retarded potentials which are used to evaluate the radiation field at point P. However, before doing so, that derivation is anticipated by highlighting two features of the results provided of the vector and scalar potentials:

- As both potentials decrease as $1/R$, the resulting fields otherwise fall as $1/R^2$ leading to a net zero electromagnetic energy flow flux for $R \to \infty$. However, recalling that the retarded time has an explicit R-dependence, this leads to a net $1/R$ dependence upon differentiation. Hence, retardation is necessary in order to allow for the radiation of electromagnetic energy at a distance.
- The $\left(1-\hat{\mathbf{n}}\bullet\hat{\boldsymbol{\beta}}\right)$ term in the denominators of the expressions of the potentials predicts "geometric beaming" as $\beta \to 1$ with the field reaching a maximum along the direction of travel at high electron speeds.

7.6.2.3 Radiation Emission

Electromagnetic Fields at a Distance

The electric field strength is calculated from the potentials through $\mathbf{E} = -\nabla\Phi - \partial\mathbf{A}/\partial t$ (Jackson 1999). The differential with respect to the time t is found by differentiating the expression for $R(t')$,

$$\begin{aligned} R(t') &= \sqrt{(\mathbf{x}-\mathbf{r}(t'))\bullet(\mathbf{x}-\mathbf{r}(t'))} \\ &= c(t-t') \end{aligned} \tag{7.566}$$

to give,

$$\frac{\partial R(t')}{\partial t} = c\left(1-\frac{\partial t'}{\partial t}\right). \tag{7.567}$$

Applying the chain rule,

$$\begin{aligned} \frac{\partial R(t')}{\partial t} &= \frac{\partial R(t')}{\partial t'}\frac{\partial t'}{\partial t} \\ &= -\frac{\partial r(t')}{\partial t'}\frac{\partial t'}{\partial t} \\ &= -c\left\{\hat{\mathbf{n}}\bullet\hat{\boldsymbol{\beta}}\right\}_{t'}\frac{\partial t'}{\partial t}. \end{aligned} \tag{7.568}$$

Equating these two results gives,

$$c\left(1-\frac{\partial t'}{\partial t}\right) = -c\left\{\hat{\mathbf{n}}\bullet\hat{\boldsymbol{\beta}}\right\}_{t'}\frac{\partial t'}{\partial t}$$

leading to,

$$\frac{\partial t'}{\partial t} = \left\{\frac{1}{1-\hat{\mathbf{n}}\bullet\hat{\boldsymbol{\beta}}}\right\}_{t'} \tag{7.569}$$

which is then used to write the differential with respect to t,

$$\begin{aligned} \frac{\partial}{\partial t} &= \frac{\partial t'}{\partial t}\frac{\partial}{\partial t'} \\ &= \left\{\frac{1}{1-\hat{\mathbf{n}}\bullet\hat{\boldsymbol{\beta}}}\right\}_{t'}\frac{\partial}{\partial t'}. \end{aligned} \tag{7.570}$$

The gradient operator ∇ is evaluated by first separating it into spatial and time components,

$$\nabla = \nabla_x + \nabla_{t'} \tag{7.571}$$

where the first component refers to differentiation with respect to the observation point position vector (disregarding any retardation effects) and the second term accounts for retardation. This latter term is $\nabla_{t'} = \nabla t' \frac{\partial}{\partial t'}$ where,

$$\begin{aligned}\nabla t' &= -\frac{1}{c}\nabla R(t') \\ &= -\frac{1}{c}\left(\hat{\mathbf{n}} + \frac{\partial R(t')}{\partial t'}\nabla t'\right) \\ &= -\frac{1}{c}\left(\hat{\mathbf{n}} - \left(\hat{\mathbf{n}} \bullet \hat{\boldsymbol{\beta}} c\right)\nabla t'\right).\end{aligned} \tag{7.572}$$

Solving for $\nabla t'$ gives,

$$\nabla t' = -\frac{1}{c}\left\{\frac{1}{1 - \hat{\mathbf{n}} \bullet \hat{\boldsymbol{\beta}}}\right\}_{t'} \tag{7.573}$$

which leads to the expression for the gradient operator,

$$\nabla = \nabla_x - \frac{1}{c}\left\{\frac{\hat{\mathbf{n}}}{1 - \hat{\mathbf{n}} \bullet \hat{\boldsymbol{\beta}}}\right\}_{t'} \frac{\partial}{\partial t'}. \tag{7.574}$$

Having established these operators, one can now evaluate the electric and magnetic fields,

$$\begin{aligned}\mathbf{E}(\mathbf{x}, t) &= -\nabla\Phi - \partial\mathbf{A}/\partial t \\ &= -\left(\nabla_x - \frac{1}{c}\left\{\frac{\hat{\mathbf{n}}}{1 - \hat{\mathbf{n}} \bullet \hat{\boldsymbol{\beta}}}\right\}_{t'} \frac{\partial}{\partial t'}\right)\Phi(\mathbf{x}, t) \\ &\quad - \left\{\frac{1}{1 - \hat{\mathbf{n}} \bullet \hat{\boldsymbol{\beta}}}\right\}_{t'} \frac{\partial \mathbf{A}(\mathbf{x}, t)}{\partial t'} \\ &= -\nabla_x\Phi(\mathbf{x}, t) + \frac{1}{c}\left\{\frac{\hat{\mathbf{n}}}{1 - \hat{\mathbf{n}} \bullet \hat{\boldsymbol{\beta}}}\right\}_{t'} \frac{\partial \Phi(\mathbf{x}, t)}{\partial t'} \\ &\quad - \left\{\frac{1}{1 - \hat{\mathbf{n}} \bullet \hat{\boldsymbol{\beta}}}\right\}_{t'} \frac{\partial \mathbf{A}(\mathbf{x}, t)}{\partial t'} \\ &= \frac{e}{4\pi\varepsilon_0}\left(-\nabla_x\left\{\frac{1}{R}\frac{1}{\left(1 - \hat{\mathbf{n}} \bullet \hat{\boldsymbol{\beta}}\right)}\right\}_{t'}\right. \\ &\quad + \frac{1}{c}\left\{\frac{\hat{\mathbf{n}}}{1 - \hat{\mathbf{n}} \bullet \hat{\boldsymbol{\beta}}}\right\}_{t'} \frac{\partial}{\partial t'}\left\{\frac{1}{R}\frac{1}{\left(1 - \hat{\mathbf{n}} \bullet \hat{\boldsymbol{\beta}}\right)}\right\}_{t'} \\ &\quad \left. - \frac{1}{c}\left\{\frac{1}{1 - \hat{\mathbf{n}} \bullet \hat{\boldsymbol{\beta}}}\right\}_{t'} \frac{\partial}{\partial t'}\left\{\frac{1}{R}\frac{\hat{\boldsymbol{\beta}}}{\left(1 - \hat{\mathbf{n}} \bullet \hat{\boldsymbol{\beta}}\right)}\right\}_{t'}\right) \\ &= \frac{e}{4\pi\varepsilon_0}\left\{\frac{\left(1 - \beta^2\right)\left(\hat{\mathbf{n}} - \hat{\boldsymbol{\beta}}\right)}{\left(1 - \hat{\mathbf{n}} \bullet \hat{\boldsymbol{\beta}}\right)^3 R^2}\right. \\ &\quad \left. + \frac{1}{c}\frac{\hat{\mathbf{n}} \times \left(\left(\hat{\mathbf{n}} - \hat{\boldsymbol{\beta}}\right) \times \dot{\hat{\boldsymbol{\beta}}}\right)}{\left(1 - \hat{\mathbf{n}} \bullet \hat{\boldsymbol{\beta}}\right)^3 R}\right\}_{t'}\end{aligned} \tag{7.575}$$

where, in order to simplify the expression, an overlying dot is used to indicate differentiation with time. The magnetic field strength follows from $\mathbf{B} = \nabla \times \mathbf{A}$.

Consider the above expression for the electric field strength. The first term on the right-hand side is proportional to $1/R^2$ and the particle's velocity and is the Coulomb field for a uniformly moving electric charge. As the resulting radiated power is proportional to $|\mathbf{E}|^2$, the power will drop off as $1/R$ and can be neglected as the energy flow per unit area will simply go to zero at infinity as a result. On the other hand, the second term is proportional to $1/R$ and the particle's acceleration. Because of the latter feature, the energy flow per unit area will thus remain finite as $R \to \infty$. This second term is the radiation field of an accelerating electric charge (which only arises because of retardation). Having recognized this, isolate the electric and magnetic radiation fields accordingly,

$$\mathbf{E}_{rad}(\mathbf{x}, t) = \frac{e}{4\pi\varepsilon_0 c}\left\{\frac{\hat{\mathbf{n}} \times \left(\left(\hat{\mathbf{n}} - \hat{\boldsymbol{\beta}}\right) \times \dot{\hat{\boldsymbol{\beta}}}\right)}{\left(1 - \hat{\mathbf{n}} \bullet \hat{\boldsymbol{\beta}}\right)^3 R}\right\}_{t'} \tag{7.576}$$

$$\mathbf{B}_{rad}(\mathbf{x}, t) = \frac{\hat{\mathbf{n}} \times \mathbf{E}_{rad}(\mathbf{x}, t)}{c} \tag{7.577}$$

Radiated Power: Larmor Formula

The radiated power is calculated using the Poynting vector in the nonrelativistic case (i.e., $\beta \ll 1$) in which

$(\hat{\mathbf{n}} - \hat{\boldsymbol{\beta}}) \to \hat{\mathbf{n}}$ and $\left(1 - \hat{\mathbf{n}} \bullet \hat{\boldsymbol{\beta}}\right)^3 \to 1$. The radiative electric field reduces to the simpler form,

$$\mathbf{E}_{\text{rad}}(\mathbf{x}, t) = \frac{e}{4\pi\varepsilon_0 c}\left\{\frac{\hat{\mathbf{n}} \times \left(\hat{\mathbf{n}} \times \dot{\hat{\boldsymbol{\beta}}}\right)}{R}\right\}_{t'}; \quad \beta \ll 1. \tag{7.578}$$

The Poynting vector is,[28]

$$\begin{aligned}\mathbf{P}_{\text{rad}} &= \mathbf{E}_{\text{rad}} \times \mathbf{H}^*_{\text{rad}} \\ &= \frac{1}{\mu_0}\mathbf{E}_{\text{rad}} \times \mathbf{B}^*_{\text{rad}}\end{aligned} \tag{7.579}$$

From (7.576) and (7.577),

$$|\mathbf{E}_{\text{rad}}(\mathbf{x}, t)| = \frac{e}{4\pi\varepsilon_0 c}\left\{\frac{\dot{\beta}}{R}\sin\theta\right\}_{t'} \tag{7.580}$$

and

$$|\mathbf{B}_{\text{rad}}(\mathbf{x}, t)| = \frac{e}{4\pi\varepsilon_0 c^2}\left\{\frac{\dot{\beta}}{R}\sin\theta\right\}_{t'} \tag{7.581}$$

where θ is the angle between the unit vectors $\hat{\mathbf{n}}$ and $\dot{\hat{\boldsymbol{\beta}}}$. Inserting these results into the expression of the Poynting vector provides the magnitude of the radiated power,

$$\begin{aligned}P_{\text{rad}} &= \frac{e^2}{16\pi^2\varepsilon_0^2\mu_0 c^3}\left\{\frac{\dot{\beta}^2}{R^2}\sin^2\theta\right\}_{t'} \\ &= \frac{\alpha\hbar}{4\pi}\left\{\frac{\dot{\beta}^2}{R^2}\sin^2\theta\right\}_{t'}\end{aligned} \tag{7.582}$$

where $1/\varepsilon_0\mu_0 = c^2$ has been used. This angular distribution of (7.582) is clearly that of dipole radiation. Energy is radiated with a maximum orthogonal to the direction of travel and with none directed along the acceleration vector. This pattern will, however, alter in the laboratory frame-of-reference due to the Lorentz transformation as the electron becomes relativistic. As the magnitude of the Poynting vector is the electromagnetic energy radiated per unit time and per unit area,

$$|\mathbf{P}_{\text{rad}}| = \frac{d^2E}{R^2 dt\, d\Omega} \tag{7.583}$$

one can calculate the total instantaneous radiated power from the accelerated charge,

$$\begin{aligned}\frac{dE}{dt} &= \int d\Omega\, R^2 |\mathbf{P}_{\text{rad}}| \\ &= \frac{\alpha\hbar}{2}\left\{\dot{\beta}^2\right\}_{t'}\int_0^\pi d\theta \sin^3\theta \\ &= \frac{2}{3}\alpha\hbar\left\{\dot{\beta}^2\right\}_{t'}.\end{aligned} \tag{7.584}$$

This result is the Larmor formula for a nonelativistic accelerated electron (with explicit recognition that the acceleration is that of the electron at the time of emission). Note that the radiated power is proportional to the square of the particle's acceleration at the time of emission.

Classical Radiative Stopping Power

A classical expression of the radiative stopping power (i.e., the energy loss due to *bremsstrahlung* per unit length traveled) can now be derived. Assume that the acceleration is due to a deflection of the electron at an impact parameter b by a nucleus with charge Ze and that the duration of this deflection, τ_{Defl}, is short. The acceleration will be given by the ratio of the Coulomb force experienced by the electron and its mass,

$$\dot{\beta} = \left(\frac{\alpha\hbar c}{m_e}\right)\frac{Zc}{b^2}. \tag{7.585}$$

Inserting this expression for the normalized acceleration into the Larmor formula gives the radiated power,

$$\begin{aligned}\frac{dE}{dt} &= \frac{2}{3}\alpha\hbar\left\{\dot{\beta}^2\right\}_{t'} \\ &= \frac{2}{3}\alpha\hbar\left(\frac{\alpha\hbar c}{m_e}\right)^2\frac{(Zc)^2}{b^4} \\ &= \frac{2}{3}(\alpha\hbar c)^3\frac{Z^2 c}{m_e^2 b^4}.\end{aligned} \tag{7.586}$$

[28] As only the instantaneous power flow is being considered, the 1/2 multiplicative factor is excluded.

As the duration of the interaction is approximately

$$\tau_{Coll} \approx \frac{b}{\beta c} \tag{7.587}$$

then the total radiated energy as a result of the deflection is,

$$\begin{aligned} \Delta E &\approx \frac{dE}{dt}\tau_{Coll} \\ &\approx \frac{2}{3}(\alpha\hbar c)^3 \frac{Z^2}{\beta m_e^2 b^3}. \end{aligned} \tag{7.588}$$

This is the energy loss for a single interaction with a nucleus. To calculate the radiative stopping power, it is necessary to account for all of the nuclei that the electron may interact with,

$$\begin{aligned} \frac{dE}{\rho\, dx} &= \frac{2\pi}{3}(\alpha\hbar c)^3 \frac{N_A Z^2}{A\,\beta\, m_e^2} \int_{b_{min}}^{b_{max}} \frac{db}{b^2} \\ &= \frac{4\pi}{3}(\alpha\hbar c)^3 \frac{N_A Z^2}{A\,\beta\, m_e^2}\left(\frac{1}{b_{max}} - \frac{1}{b_{min}}\right). \end{aligned} \tag{7.589}$$

Using the expressions for the minimum impact parameter and the constant C of derived previously,

$$\frac{dE}{\rho\, dx} = \frac{2\alpha C}{3}\frac{Z^2}{A\sqrt{1-\beta^2}} \tag{7.590}$$

This predicts that the mass radiative stopping power increases to infinity with increasing electron speed and increases with atomic number.

Angular Distribution of Radiation Emission

In evaluating the angular distribution and the frequency spectrum of the radiation emission, the approach described by Jackson (1999) will be approximately followed, but with the use of SI units retained. Recall that the derivations of the nonrelativistic Larmor formula and subsequent radiative mass stopping power were nonrelativistic and, hence, based upon the assumption that $\beta \ll 1$. As a result, only the acceleration $\dot{\beta}$ appeared in the final expression of the radiated power and the angular distribution was that of a dipole, $\sin^2\theta$. As the electron's speed increases, it can no longer be ignored (in particular that of the effect of "beaming" caused by the $\left(1 - \hat{\mathbf{n}} \bullet \hat{\boldsymbol{\beta}}\right)^3$ term in the denominator). To evaluate the angular distribution, recalculate the magnitude of the radial component of the Poynting vector (i.e., along the direction of $\hat{\mathbf{n}}$) without using the previous nonrelativistic approximation,

$$\begin{aligned} \mathbf{P}_{rad} \bullet \hat{\mathbf{n}} &= \frac{1}{\mu_0}\left(\mathbf{E}_{rad} \times \mathbf{B}^*_{rad}\right) \bullet \hat{\mathbf{n}} \\ &= \frac{1}{\mu_0}\left(\mathbf{E}_{rad} \times \left(\hat{\mathbf{n}} \times \mathbf{E}^*_{rad}\right)\right) \bullet \hat{\mathbf{n}} \\ &= \frac{e^2}{16\pi^2\varepsilon_0 c}\left\{\frac{1}{R^2}\left|\frac{\hat{\mathbf{n}} \times \left(\left(\hat{\mathbf{n}} - \hat{\boldsymbol{\beta}}\right) \times \dot{\hat{\boldsymbol{\beta}}}\right)}{\left(1 - \hat{\mathbf{n}} \bullet \hat{\boldsymbol{\beta}}\right)^3}\right|^2\right\}_{t'}. \end{aligned} \tag{7.591}$$

This scalar product is the detected power per unit area at a distant point at time t of radiation that had been emitted by the electron at the earlier time t'. Assume that the acceleration of the electron at time t' resulting in the emission of radiation was due to an interaction with a nucleus of atomic number Z over a short finite time interval, τ_{Coll}, and further approximate $\hat{\boldsymbol{\beta}}$ and $\dot{\hat{\boldsymbol{\beta}}}$ as both being constant in magnitude and direction. The energy radiated during a finite time interval from $t' = 0$ to $t' = \tau_{Coll}$ will be,

$$\begin{aligned} E &= \int_{(R(t=0)/c)}^{\tau_{Coll}+(R(\tau_{Coll})/c)} dt\, \mathbf{P}_{rad} \bullet \hat{\mathbf{n}} \\ &= \int_0^{\tau_{Coll}} dt' \frac{dt}{dt'} \mathbf{P}_{rad} \bullet \hat{\mathbf{n}} \end{aligned} \tag{7.592}$$

The quantity $\frac{dt}{dt'}\left(\mathbf{P}_{rad} \bullet \hat{\mathbf{n}}\right)$ is the radiated power per unit area in terms of the electron's time. This can be used to give the power radiated per unit solid angle as,

$$\begin{aligned} \frac{dE}{dt'\, d\Omega} &= R^2\left(\mathbf{P}_{rad} \bullet \hat{\mathbf{n}}\right)\frac{dt}{dt'} \\ &= R^2\left(\mathbf{P}_{rad} \bullet \hat{\mathbf{n}}\right)\left\{1 - \hat{\mathbf{n}} \bullet \hat{\boldsymbol{\beta}}\right\}_{t'}. \end{aligned} \tag{7.593}$$

Substituting the expression for $\mathbf{P}_{\text{rad}} \bullet \hat{\mathbf{n}}$,

$$\frac{dE}{dt' d\Omega} = \frac{e^2}{16\pi^2 \varepsilon_0 c} \left\{ \frac{\left| \hat{\mathbf{n}} \times \left(\left(\hat{\mathbf{n}} - \hat{\boldsymbol{\beta}} \right) \times \dot{\hat{\boldsymbol{\beta}}} \right) \right|^2}{\left(1 - \hat{\mathbf{n}} \bullet \hat{\boldsymbol{\beta}} \right)^3} \left(1 - \hat{\mathbf{n}} \bullet \hat{\boldsymbol{\beta}} \right) \right\}_{t'}$$
$$= \frac{e^2}{16\pi^2 \varepsilon_0 c} \left\{ \frac{\left| \hat{\mathbf{n}} \times \left(\left(\hat{\mathbf{n}} - \hat{\boldsymbol{\beta}} \right) \times \dot{\hat{\boldsymbol{\beta}}} \right) \right|^2}{\left(1 - \hat{\mathbf{n}} \bullet \hat{\boldsymbol{\beta}} \right)^5} \right\}_{t'}. \tag{7.594}$$

This provides the angular distribution of the radiation emission provided that $\hat{\mathbf{n}}$ and R are reasonably constant (a requirement equivalent to the measurement point being at a sufficiently large distance from the electron). Considering the case of $\hat{\boldsymbol{\beta}}$ and $\dot{\hat{\boldsymbol{\beta}}}$ being collinear and defining θ as the angle between the direction of $\hat{\boldsymbol{\beta}}$ and $\dot{\hat{\boldsymbol{\beta}}}$ and the direction of emission, then (7.594) reduces to,

$$\frac{dE}{dt' d\Omega} = \frac{\alpha \hbar c}{4\pi} \dot{\beta}^2 \frac{\sin^2 \theta}{(1 - \beta \cos \theta)^5} \tag{7.595}$$

For $\beta \ll 1$, this result returns the $\sin^2\theta$ dependence of the nonrelativistic Larmor formula but, because of the $(1-\beta\cos\theta)^5$ term, the angular distribution becomes highly forward peaked at high electron speeds. The angle at which the radiation is at a maximum, $\theta_{\max}$ is,

$$\theta_{\max} = \cos^{-1} \frac{\sqrt{1 + 15\beta^2} - 1}{3\beta} \tag{7.596}$$

This maximum emission angle is shown as a function of the electron β in Fig. 7.41. At low electron energies, the maximum emission angle is near to 90° (reflecting the dipole radiation pattern in the laboratory reference frame) but the radiation becomes focused into a cone of decreasing angle with increasing β.

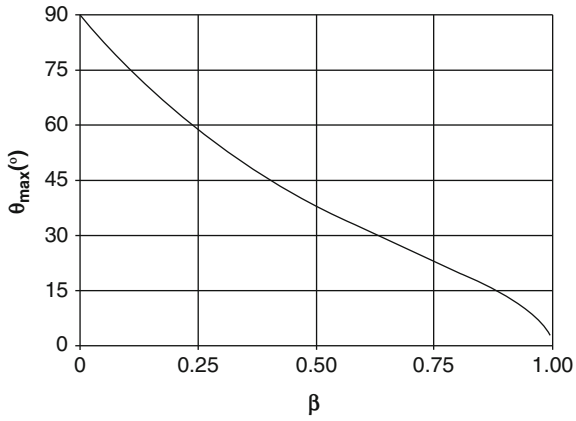

Fig. 7.41 Angle of maximum *bremsstrahlung* for an electron as a function of β

Spectrum of Radiation Emission

Nonrelativistic Case

The frequency (energy) spectrum of the radiated energy of classical *bremsstrahlung* is now calculated in the case of a nonrelativistic incident electron. Here, the shape of the energy spectrum is taken to reflect the shape of the impulse of the electron deflection. If one assumes that the impulse has a duration given by, $\tau_{\text{Coll}} = b/\beta c$, then the corresponding frequency spectrum can be approximated as being uniform up to an angular frequency of,

$$\omega \approx \frac{1}{\tau_{\text{Coll}}} \approx \frac{\beta c}{b}. \tag{7.597}$$

From this,

$$\frac{dE}{d\omega} \approx \Delta E \, \tau_{\text{Coll}} \approx \frac{2}{3c} (\alpha \hbar c)^3 \frac{Z^2}{\beta^2 m_e^2 b^2}. \tag{7.598}$$

The energy radiated per unit frequency and unit areal density is obtained in the usual manner,

$$\left(\frac{d^2 E}{\rho \, dx \, d\omega} \right)_{\text{Rad}} = \frac{2}{3c} \left(\frac{N_A}{A} \right) (\alpha \hbar c)^3 \frac{Z^2}{m_e^2 \beta^2} \left| \int_{b_{\min}}^{b_{\max}} db \, 2\pi b \frac{1}{b^2} \right|$$
$$= \frac{4\pi}{3c} \left(\frac{N_A}{A} \right) (\alpha \hbar c)^3 \frac{Z^2}{m_e^2 \beta^2} \left| \int_{b_{\min}}^{b_{\max}} \frac{db}{b} \right|$$
$$= \frac{2}{3} C \left(\frac{Z^2}{A} \right) \frac{r_0}{\beta^2 c} \ln \frac{b_{\max}}{b_{\min}}. \tag{7.599}$$

To avoid the divergence problem, the lower limit of the impact parameterization is modeled by,

$$b_{\min} = \frac{\hbar c}{m_e \beta}$$

and the upper limit can be taken to be the ratio of the incident electron speed to the cutoff frequency (which is necessary as the electron cannot emit infinite energy). The ratio of impact parameters is,

$$\frac{b_{max}}{b_{min}} = \frac{\beta c}{\omega}\frac{m_e \beta}{\hbar c} = \frac{\beta^2 m_e}{\hbar \omega}.$$

For convenience, this will be written as,

$$\frac{b_{max}}{b_{min}} = \frac{m_e v_0^2}{\hbar \omega}$$

where v_0 is the incident electron speed and the electron rest mass is now given in units of mass rather than energy. This gives the expression for the radiated energy spectrum per unit length traversed as,

$$\left(\frac{d^2E}{\rho\, dx\, d\omega}\right)_{Rad} = \frac{2}{3} C \left(\frac{Z^2}{A}\right) \frac{r_0 c}{v_0^2} \ln \frac{m_e v_0^2}{\hbar \omega}. \quad (7.600)$$

However, as the electron does lose kinetic energy as a result of the radiative collision, it would be more appropriate to replace the v_0^2 term in the logarithm with the square of the mean of the pre- and postdeflection speeds,

$$\frac{1}{2}\left(\sqrt{\frac{2T_0}{m_e}} + \sqrt{\frac{2(T_0 - \hbar\omega)}{m_e}}\right),$$

where T_0 is the incident electron kinetic energy and $\hbar\omega$ is the energy of the bremsstrahlung photon which will be now denoted by the usual symbol, k. To change the differential from frequency to photon energy, divide through the above result with the reduced Planck's constant. Thus, one obtains a classical result for the energy spectrum (the use of $\hbar$ is only for convenience here and does not imply a quantum-mechanical basis to the result),

$$\left(\frac{d^2E}{\rho\, dx\, dk}\right)_{Rad} = \frac{C}{2}\left(\frac{Z^2}{A}\right)\frac{r_0 c}{\hbar v_0^2} \times \ln\left(\frac{\left(\sqrt{T_0} + \sqrt{T_0 - k}\right)^2}{2k}\right) \quad k \ll T_0 \quad (7.601)$$

It will be seen later that this result is markedly similar to the quantum-mechanical derivation of the Bethe–Heitler theory. Figure (7.42) shows the bremsstrahlung spectrum for 100 keV electrons in lead calculated from (7.601).

Relativistic Case: Weizsäcker–Williams (Virtual Quanta) Method

This is a semiclassical approach to calculating electron-nucleus *bremsstrahlung* performed in the reference frame of the moving electron. The nuclear electromagnetic field is thus experienced by the electron as a pulse, or virtual photon, which is Thomson

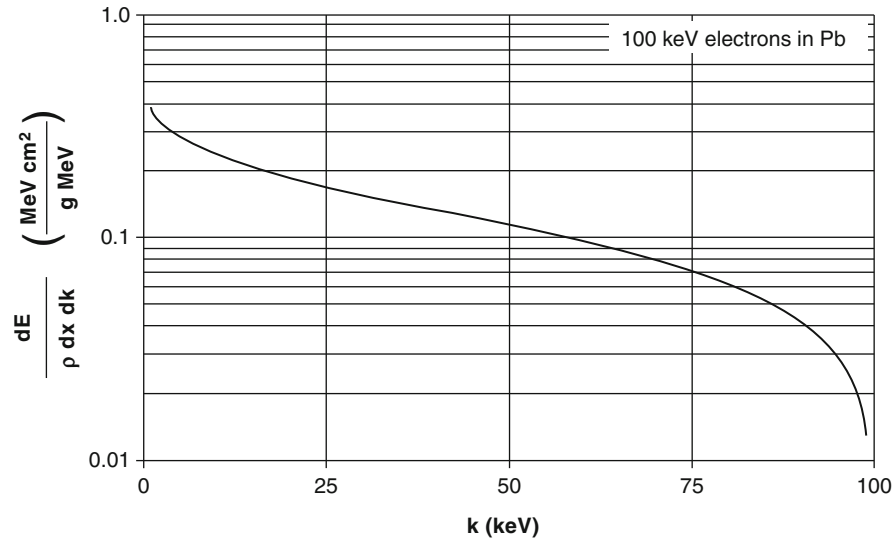

Fig. 7.42 *Bremsstrahlung* spectrum calculated from classical theory for 100 keV electrons in lead

scattered by the electron. This innovative approach is originally attributable to the independent work of von Weizsäcker and Williams, following Fermi.

In the reference frame of the electron, the nucleus with charge Ze is the "projectile." The route of the Bohr soft collision stopping power calculation is followed; recall that only the component of the nuclear electric field at the position of the electron perpendicular to the trajectory need be calculated. This is given by (7.37) except that z is replaced by Z. Thus, in this reference frame, it is the nucleus passing a stationary electron at an impact parameter b, speed v, and relativistic factor γ. The energy transported per unit area and unit frequency is given by the Poynting vector,

$$\begin{aligned} |\mathbf{P}| &= \frac{dI}{dA\, d\omega} \\ &= \sqrt{\frac{\varepsilon_0}{\mu_0}}\,|\mathbf{E}_\perp(t)|^2 \end{aligned} \tag{7.602}$$

Parseval's theorem is invoked,

$$\begin{aligned} \int_{-\infty}^{\infty} dt|\mathbf{E}_\perp(t)|^2 &= \int_{-\infty}^{\infty} d\omega|\mathbf{E}_\perp(\omega)|^2 \\ &= 2\int_0^{\infty} d\omega|\mathbf{E}_\perp(\omega)|^2 \end{aligned} \tag{7.603}$$

where a real electric field, $E_\perp(-w) = E_\perp{}^*(w)$, has been allowed for. As a result,

$$\frac{dI}{dA\, d\omega} = 2\sqrt{\frac{\varepsilon_0}{\mu_0}}\,|\mathbf{E}_\perp(\omega)|^2. \tag{7.604}$$

The Fourier transform of the electric field component is given by (7.90),

$$\frac{dI}{dA\, d\omega} = \alpha\hbar c^2\left(\frac{Z\omega}{\pi\gamma\, v^2}\right)^2 K_1^2\left(\frac{\omega b}{\gamma v}\right). \tag{7.605}$$

This is the electromagnetic energy per unit area and per unit frequency incident to the electron in its reference frame, which represents a virtual photon that can be scattered by the electron to create a *bremsstrahlung* photon. It will be assumed that this scatter is through the classical Thomson elastic process. The energy spectrum in the electron rest frame is,

$$\frac{dI}{d\omega} = \sigma_{Tho}\frac{dI}{dA\, d\omega}. \tag{7.606}$$

As the impact parameter will vary from a minimum value to infinity, note the result of (7.605) in low- and large-argument cases of the modified Bessel function,

$$\frac{dI}{dA\, d\omega} = \alpha\hbar c^2\left(\frac{Z}{\pi\, vb}\right)^2 \quad \text{for } \frac{\omega b}{\gamma v} \ll 1 \tag{7.607}$$

$$\frac{dI}{dA\, d\omega} = \frac{\alpha\hbar c^2}{2\pi}\frac{Z^2\omega}{\gamma b v^3}e^{-2\frac{\omega b}{\gamma v}} \quad \text{for } \frac{\omega b}{\gamma v} \gg 1. \tag{7.608}$$

The exponential cut-off of (7.608) allows a specification of a minimum impact parameter. On the basis of the cut-off, the maximum frequency can be approximated by $\omega_{max} \approx \gamma c/b$. As the scatter (in the electron's reference frame) is nonrelativistic, $\hbar\omega \ll m_e$, then $\gamma c/b \ll m_e/\hbar$ leading to a minimum impact parameter,

$$b_{min} = \frac{\gamma\hbar c}{m_e} \tag{7.609}$$

The power spectrum is then transformed to the laboratory reference frame in which the nucleus is at rest and the electron has a relativistic speed βc. The spectrum is the ratio of the energy to frequency and remains invariant as, for photons, the frequency and energy remain equivalent to within a factor of $\hbar$. Using the Doppler relativistic shift, the frequency in the laboratory frame is $\omega' \approx \gamma\omega$. Averaging over scatter angle (allowing for the isotropy of Thomson scatter) and approximating $\beta \approx 1$, the energy spectrum in the laboratory reference frame is,

$$\frac{dI'}{d\omega'} = \sigma_{Tho}\,\alpha\hbar c^2\left(\frac{Z\omega'}{\pi\gamma^2c^2}\right)^2 K_1^2\left(\frac{\omega' b}{\gamma^2 c}\right) \tag{7.610}$$

Following the mechanics of the derivation of the Bohr soft collision stopping power, the *bremsstrahlung* differential cross section in photon energy is,

$$\begin{aligned} \frac{d\sigma}{dk} &= \frac{2\pi}{\hbar k}\int_{b_{min}}^{\infty} db\, b\frac{dI'}{d\omega'} \\ &= \frac{2\alpha\sigma_{Tho}}{\pi}\frac{Z^2}{k}\int_{x_{min}}^{\infty} dx\, x\, K_1^2(x) \end{aligned} \tag{7.611}$$

where $x_{min} = \omega' b_{min}/\gamma^2 c$. This integral is solved for using the properties of the derivatives of the modified Bessel functions (as used in the Bohr soft collision

stopping power derivation) and recalling the exponential cutoff of (7.608), the Weizsäcker–Williams *bremsstrahlung* spectrum is thus of the form,

$$\frac{d\sigma}{dk} \approx \frac{2\alpha\sigma_{Tho}}{\pi}\frac{Z^2}{k}\left(\ln\left(\frac{1.223\gamma m_e}{k}\right) - \frac{1}{2}\right) \quad (7.612)$$

It is immediately evident that this cross section will diverge as $k \to \infty$. This corresponds to the impact parameter $b \to 0$, but this divergence is not achieved as the screening of the nucleus by atomic electrons, thus reducing its effective charge seen by the electron, has been ignored in this derivation.

7.6.3 Quantum Electron-Nuclear Bremmstrahlung: Bethe–Heitler Theory

7.6.3.1 Introduction

As the Bethe–Heitler theory of *bremsstrahlung* is based upon the Born approximation, the extent of its validity will be defined by limits of this approximation. Refinements and further extensions of the theory are necessary in order to extend beyond these restrictions. The Bethe–Heitler theory was the first relativistic quantum description of *bremsstrahlung* and, whilst being cognizant of its limitations, it is presented here because of its historical importance and the experience gained in the use of the Born approximation throughout this book. Advanced approaches to providing more accurate calculations *bremsstrahlung* cross sections can be found in Haug and Nakel (2004).

7.6.3.2 Derivation of the Triple Differential Cross Section

Interaction

The interaction to be calculated for is shown by the Feynman diagrams of Fig. 7.43.

An electron with momentum **p** and total energy E is incident to an infinitely-massive point charge Ze, which approximates the nucleus. In the first diagram, the electron interacts with the static field to reach a momentum of $\mathbf{k} + \mathbf{p}'$ and then interacts with the radiation field to emit a photon of energy k and momentum

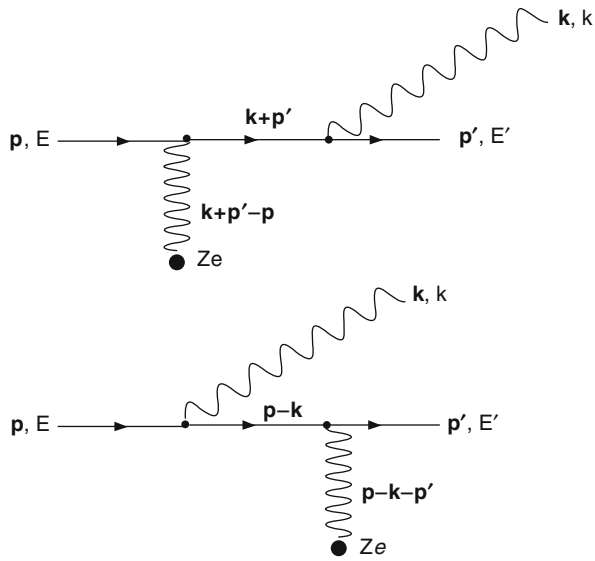

Fig. 7.43 Feynman diagrams for electron-nuclear *bremsstrahlung*

k and exit the interaction with momentum $\mathbf{p}'$ and total energy E′. In the second diagram, the electron first interacts with the radiation field to emit the photon of energy k and momentum **k** and reduce its momentum to $\mathbf{p}' - \mathbf{k}'$ before interacting with the static field and exit the interaction with momentum **p** and total energy E. The aim is to calculate the differential cross section in photon energy k, solid angle $\Omega_{p'}$ of the scattered electron and solid angle Ω_k of the emitted photon. Heitler (1984) and Bjorken and Drell (1964) derive this cross section by separately accounting for the interactions with the radiation field and with the Coulomb field of the scattering center, the former using Fermi's Golden Rule No. 1 and the latter using S-matrix theory and the Feynman propagator. Haug and Nakel (2004) instead treat the interaction with the radiation field as the perturbation, to first order, and then correct the wavefunctions of the incident and scattered electrons for the effects of the Coulomb potential of the scattering center. In order to maintain some consistency with the previous derivations of the Klein–Nishina and elastic Coulomb scatter cross sections, the derivation of the Bethe–Heitler theory will follow the Bjorken and Drell S-matrix approach using Feynman propagators. The triple differential cross section is the ratio of the transition rate and the incident electron flux,

$$d^3\sigma = \frac{\lambda_{fi}}{\phi}. \quad (7.613)$$

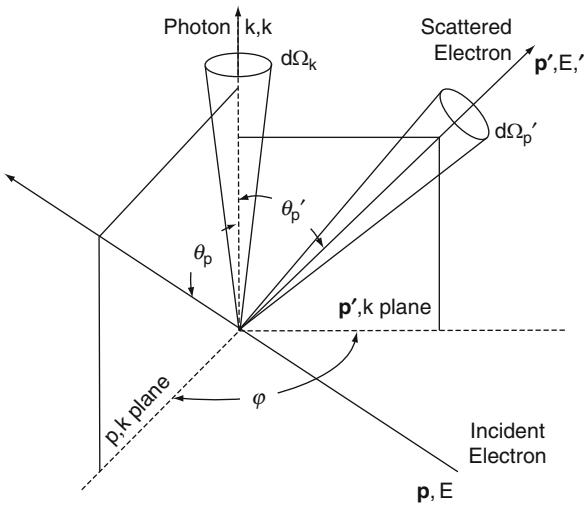

Fig. 7.44 Geometry of the *bremsstrahlung* process. The interaction occurs at the origin and angles are specified by the direction of the emitted photon

The transition rate is,

$$\lambda_{fi} = \frac{|S_{fi}|^2}{T}\rho_f \tag{7.614}$$

where T is the time duration of the interaction. The incident electron flux is,

$$\begin{aligned}\phi &= \frac{\beta c}{L^3} \\ &= \frac{pc}{EL^3}\end{aligned} \tag{7.615}$$

where L^3 is the usual volume used for normalization and ρ_f is the phase space factor, which is next calculated for.

Phase–Space Factor

The geometry of the *bremsstrahlung* process is shown in Fig. 7.44. The density of final states,

$$\rho_f\, dT' = \left(\frac{L}{2\pi\hbar c}\right)^6 d^3\mathbf{p}'\, d^3\mathbf{k} \tag{7.616}$$

where T′ is the scattered electron's kinetic energy. Expanding,

$$\begin{aligned}\rho_f\, dT' &= \left(\frac{L}{2\pi\hbar c}\right)^6 p'^2\, dp'\, d\Omega_{p'}\, k^2\, dk\, d\Omega_k \\ &= \left(\frac{L}{2\pi\hbar c}\right)^6 p'\, E'\, dT'\, d\Omega_{p'}\, k^2\, dk\, d\Omega_k.\end{aligned} \tag{7.617}$$

The density of final states is,

$$\rho_f = \left(\frac{L}{2\pi\hbar c}\right)^6 p'\, E'\, k^2\, dk\, d\Omega_k d\Omega_{p'}. \tag{7.618}$$

S-Matrix Calculation

For the graphs of Fig. 7.43, the S-matrix element is,

$$\begin{aligned}S_{fi} = e^2 \int d^4\boldsymbol{r}\, d^4\boldsymbol{\rho}\, \bar{\psi}_f(\boldsymbol{r},\boldsymbol{p}')\big\{&-i\not{A}(\boldsymbol{r};\boldsymbol{k}) i S_F(\boldsymbol{r}-\boldsymbol{\rho}) \\ &\times \left(-i\gamma^0\right)A_0^{Coul}(\boldsymbol{\rho}) + \left(-i\gamma^0\right)A_0^{Coul}(\mathbf{r}) i S_F(\boldsymbol{r}-\boldsymbol{\rho}) \\ &- i\not{A}(\boldsymbol{\rho};\boldsymbol{k})\big\}\psi_i(\boldsymbol{\rho};\boldsymbol{p}).\end{aligned} \tag{7.619}$$

The constituents of the integrand require detailed introduction. The two components within the curly brackets correspond to the two Feynman diagrams of Fig. 7.43. Because of the existence of two graphs and two vertices in each, for clarity, a four-dimensional description is used rather than that for which spatial and temporal variables are explicit. The initial and final electron wavefunctions are,

$$\psi_i(\boldsymbol{\rho};\boldsymbol{p}) = \sqrt{\frac{m_e}{EL^3}}u(\mathbf{p},s)e^{i\boldsymbol{p}\bullet\boldsymbol{\rho}} \tag{7.620}$$

$$\psi_f(r;\boldsymbol{p}') = \sqrt{\frac{m_e}{E'L^3}}u(\mathbf{p}',s')e^{i\boldsymbol{r}\bullet\boldsymbol{p}'} \tag{7.621}$$

where

$$\boldsymbol{\rho}\bullet\boldsymbol{p} \equiv \frac{\boldsymbol{\rho}\bullet\mathbf{p}}{\hbar c} - \frac{\boldsymbol{E}\tau}{\hbar} \tag{7.622}$$

and

$$\boldsymbol{r}\bullet\boldsymbol{p}' \equiv \frac{\mathbf{r}\bullet\mathbf{p}'}{\hbar c} - \frac{E't}{\hbar}. \tag{7.623}$$

The four-vector potential of the photon with four-vector momentum k_μ and 4-component polarization ε_μ is,

$$\not{A}(\boldsymbol{r};\boldsymbol{k}) = \frac{\not{\varepsilon}}{\sqrt{2k\varepsilon_0 L^3}}\left(e^{-i\boldsymbol{k}\bullet\boldsymbol{r}} + e^{-i\boldsymbol{k}\bullet\boldsymbol{r}}\right). \tag{7.624}$$

The Coulomb interaction between the projectile electron and the nucleus is,

$$A_0^{Coul}(\mathbf{r}) = -\frac{Ze}{4\pi\varepsilon_0|\mathbf{r}|}. \tag{7.625}$$

The Feynman relativistic propagator describes the electron between the two vertices and is derived by Bjorken and Drell (1964),

$$S_F(\boldsymbol{r}-\boldsymbol{\rho}) = \lim_{\varepsilon \to 0^+} \frac{1}{(2\pi)^4} \times \int d^4\boldsymbol{p} \frac{e^{-i\boldsymbol{p}\bullet(\boldsymbol{r}-\boldsymbol{\rho})}}{p^2 - m_e^2 + i\varepsilon} \times (\not{p} + m_e \mathbf{1}) \tag{7.626}$$

where $\mathbf{1}$ is the 4×4 unity matrix and, following the integrations, the S-matrix is,

$$S_{fi} = -\frac{m_e Z e^3}{2\varepsilon_0 L^3 \sqrt{2\varepsilon_0 k E E' L^3}} \frac{\delta\left(\frac{E'+k-E}{\hbar}\right)}{|\mathbf{q}|^2} \bar{u}(\mathbf{p}', s') \times \left\{ (-i\not{\varepsilon}) \frac{i}{\not{p}' + \not{k} - m_e \mathbf{1}} (-i\gamma_0) + (-i\gamma_0) \frac{i}{\not{p}' - \not{k} - m_e \mathbf{1}} (-i\not{\varepsilon}) \right\} u(\mathbf{p}, s) \tag{7.627}$$

where $\mathbf{q} = \mathbf{p}' + \mathbf{k} - \mathbf{p}$. This result can be simplified in the soft photon limit (i.e., k→0). Consider the quantities in the curly brackets. For example,

$$\frac{1}{\not{p}' + \not{k} - m_e \mathbf{1}} = \frac{\not{p}' + \not{k} - m_e \mathbf{1}}{(\not{p}' + \not{k})^2 - m_e^2 \mathbf{1}} \cong \frac{\not{p}' + \not{k} - m_e \mathbf{1}}{2\not{p}'\not{k}}. \tag{7.628}$$

Applying this (and that for the other term in the curly brackets), after considerable algebra,

$$\bar{u}(\mathbf{p}', s') \left\{ (-i\not{\varepsilon}) \frac{i}{\not{p}' + \not{k} - m_e \mathbf{1}} (-i\gamma_0) + (-i\gamma_0) \times \frac{i}{\not{p}' - \not{k} - m_e \mathbf{1}} (-i\not{\varepsilon}) \right\} u(\mathbf{p}, s) \cong -i\bar{u}(\mathbf{p}', s')\gamma_0 u(\mathbf{p}, s) \left(\frac{\hat{\boldsymbol{\varepsilon}} \bullet \mathbf{p}'}{\mathbf{k} \bullet \mathbf{p}'} + \frac{\hat{\boldsymbol{\varepsilon}} \bullet \mathbf{p}}{\mathbf{k} \bullet \mathbf{p}} \right). \tag{7.629}$$

Thus, the squared magnitude of the S-matrix is,

$$|S_{fi}|^2 = \frac{m_e^2 Z^2 e^6}{8\pi L^6 k E E' \varepsilon_0^3} \frac{T}{|\mathbf{q}|^4} \delta\left(\frac{E'+k-E}{\hbar}\right) \times |\bar{u}(\mathbf{p}', s')\gamma_0 u(\mathbf{p}, s)|^2 \left(\frac{\hat{\boldsymbol{\varepsilon}} \bullet \mathbf{p}'}{\mathbf{k} \bullet \mathbf{p}'} + \frac{\hat{\boldsymbol{\varepsilon}} \bullet \mathbf{p}}{\mathbf{k} \bullet \mathbf{p}} \right)^2 \tag{7.630}$$

Triple Differential Cross Section in the Soft Photon Limit

Combining the above and performing the usual averaging and summing over electron spins and photon polarizations, the *bremsstrahlung* triple differential cross section is,

$$\frac{d^3\sigma}{dk\, d\Omega_k\, d\Omega_{p'}} = \alpha \left(\frac{Z r_0 m_e}{2\pi} \right)^2 \left(\frac{p'}{kpq^4} \right) \times F(p, p', k; \theta_p, \theta_{p'}, \varphi) \tag{7.631}$$

where

$$F(p, p', k; \theta_p, \theta_{p'}, \varphi) = \frac{\left(4E'^2 - q^2\right) p^2 \sin^2\theta_p}{(E - p\cos\theta_p)^2} + \frac{(4E^2 - q^2) p'^2 \sin^2\theta_{p'}}{(E' - p'\cos\theta_{p'})^2} - \left(4EE' - q^2 + 2k^2\right) \times \frac{2pp' \sin\theta_p \sin\theta_{p'} \cos\varphi}{(E - p\cos\theta_p)(E' - p'\cos\theta_{p'})} + \frac{2k^2 \left(p^2 \sin^2\theta_p + p'^2 \sin^2\theta_{p'}\right)}{(E - p\cos\theta_p)(E' - p'\cos\theta_{p'})}. \tag{7.632}$$

In parallel to the soft photon limit, one applies the nonrelativistic limit in order to simplify $F(p, p', k; \theta_p, \theta_{p'}, \varphi)$ by neglecting those terms with k, p and p relative to m_e and approximating $E \approx m_e$ and $E' \approx m_e$ to give,

$$F(p, p', k; \theta_p, \theta_{p'}, \varphi) \approx 4\left(p^2 \sin^2\theta_p + p'^2 \sin^2\theta_{p'} - 2pp' \sin\theta_p \sin\theta_{p'} \cos\varphi\right). \tag{7.633}$$

The final expression for the Bethe–Heitler *bremsstrahlung* triple differential cross section in this limit is,

$$\frac{d^3\sigma}{dk\, d\Omega_k\, d\Omega_{p'}} = \alpha \left(\frac{Z r_0 m_e}{\pi} \right)^2 \left(\frac{p'}{kpq^4} \right) \times \left(p^2 \sin^2\theta_p + p'^2 \sin^2\theta_{p'} - 2pp' \sin\theta_p \sin\theta_{p'} \cos\varphi \right). \tag{7.634}$$

It will be noted that this result predicts a $1/k$ dependence of the cross section – the cross section diverges for low photon energies, a result termed the "infrared catastrophe." Bjorken and Drell note that an experimental device detecting the inelastically-scattered electrons for $k = 0$ will also detect elastically scattered electrons and that additional radiative corrections to the elastic scattering cross section (so that the contributions of *bremsstrahlung* and elastic scatter are both considered to the same order of e) will exactly cancel this $1/k$ factor. Heitler also notes this correction arising from consideration of higher orders of the calculation.

Bethe–Heitler Bremsstrahlung Differential Cross Section in Photon Energy

The differential cross section in photon energy alone is obtained by integrating the triple differential cross section over the two solid angles. Whilst a straightforward procedure, it is tedious and only the result is presented here,

$$\frac{d\sigma}{dk} = \alpha\frac{(Zr_0)^2}{k}\left(\frac{p'}{p}\right)\left\{\frac{4}{3} - 2EE'\left(\frac{p^2+p'^2}{p^2p'^2}\right) + \frac{\kappa m_e^2 E'}{p^3} + \frac{\kappa' m_e^2 E}{p'^3} - \frac{\kappa\kappa' m_e^2}{pp'} + K\left[\frac{8EE'}{3pp'} + k^2\left(\frac{E^2E'^2+p^2p'^2}{p^3p'^3}\right) + \frac{k}{2pp'}\left(\kappa\frac{EE'+p^2}{p^3} - \kappa'\frac{EE'+p'^2}{p'^3} + \frac{2kEE'}{p^2p'^2}\right)\right]\right\} \tag{7.635}$$

where

$$\kappa = 2\ln\left(\frac{E+p}{m_e}\right) \tag{7.636}$$

$$\kappa' = 2\ln\left(\frac{E'+p'}{m_e}\right) \tag{7.637}$$

$$K = 2\ln\left(\frac{EE'+pp'-m_e^2}{m_e k}\right). \tag{7.638}$$

In the nonrelativistic limit, this becomes,

$$\frac{d\sigma}{dk} = \alpha\frac{(Zr_0)^2}{k}\frac{8}{3}\ln\left(\frac{\left(\sqrt{T}+\sqrt{T-k}\right)^2}{{}_e k}\right). \tag{7.639}$$

Screening Effects

The above Bethe–Heitler result for electron-nucleus *bremsstrahlung* neglected the reduction in the nuclear Coulomb potential experienced by the electron due to the screening by atomic electrons. This can be accounted for by changing the Coulomb potential into a Yukawa type,

$$A_0^{Yuk}(\mathbf{r}) = -\left(\frac{Ze}{4\pi\varepsilon_0|\mathbf{r}|}\right)e^{-\lambda r} \tag{7.640}$$

and repeating the calculation. This introduces a $(1-F(q; Z))$ multiplicative factor into the expressions for the differential cross section, where $F(q; Z)$ is the atomic form factor.

Deviations from the Born Approximation

From Chap. 2, the Born approximation used by the Bethe–Heitler calculation is valid only if the inequalities $(\alpha Z/\beta) \ll 1$ and $(\alpha Z/\beta') \ll 1$ where β and β are the electron speeds (normalized to the speed of light) before and after the interaction, respectively, are met. Hence, the result is valid only for low-Z media or relativistic electrons. At low electron energies, it is invalid to approximate the electron wavefunctions by plane waves and Coulomb distortion must be accounted for. An approximate solution to this dilemma is to multiply the differential cross sections by the Elwert factor,

$$F_{Elw} = \left(\frac{\beta}{\beta'}\right)\frac{1-e^{-2\pi(\alpha Z/\beta)}}{1-e^{-2\pi(\alpha Z/\beta')}} \tag{7.641}$$

7.6.3.3 Further Considerations

The derivations of the Bethe–Heitler *bremsstrahlung* theory are limited by the restrictions just noted, which are particular to the low electron energies of interest to nuclear medicine. At these energies, the assumption of a plane wave for the electron wavefunction is not entirely valid as it neglects the distortion induced by the nuclear Coulomb field. It has been estimated that, in the electron kinetic energy range of 200 keV to

1 MeV (of most interest to nuclear medicine), the Bethe–Heitler calculation agrees with experiment to within ±20% (Morgan 1970).

7.6.4 Electron–Electron Bremsstrahlung

Earlier, in the discussion of classical *bremsstrahlung*, arguments were provided to show that electron–electron *bremsstrahlung* could be neglected at low energies, certainly within the classical framework. However, electron–electron *bremsstrahlung* is not an entirely negligible process. There are two significant differences between the electron-nucleus and electron–electron *bremsstrahlung* interactions. First, the recoil of the target body cannot be neglected and, second, exchange effects must be allowed for. Cross sections for electron–electron *bremsstrahlung* are derived in Haug and Nakel (2004); they show that 8 Feynman diagrams contribute to the calculation of the S-matrix element, rather than 2 for electron-nucleus *bremsstrahlung*. Hence, we will not pursue a derivation of the cross section and the interested reader is referred to that book.

It is convenient (ICRU 1984) to use dimensionless radiative energy-loss cross sections for both electron-nuclear and electron–electron *bremsstrahlung* for an incident electron with total energy, E,

$$\phi_{rad,n} = \frac{1}{\alpha r_0^2 Z^2} \int_0^{E-m_e} dk \frac{k}{E} \frac{d\sigma_n}{dk} \tag{7.642}$$

$$\phi_{rad,e} = \frac{1}{\alpha r_0^2} \int_0^{E-m_e} dk \frac{k}{E} \frac{d\sigma_e}{dk} \tag{7.643}$$

The ratio, $\phi_{rad,e}/\phi_{rad,n}$, has a value of about 0.5 at electron kinetic energies of 700 keV and vanishes at low kinetic energies.

7.6.5 Positron-Nucleus Bremsstrahlung

Positrons are repelled by the nucleus and attracted to the atomic electrons; hence, the positron *bremsstrahlung* cross section will differ from that of the electron, primarily at low kinetic energies where it is significantly less. ICRU Publication 37 summarizes calculations of the positron *bremsstrahlung* cross section and notes that a universal curve can be derived of the ratio of the dimensionless cross sections for positron to electron radiative losses, $\phi^+_{rad,n}/\phi^-_{rad,n}$, as a function of the variable $\ln T/Z^2$, where T is the electron/positron kinetic energy and Z is the atomic number of the medium, exists. Figure 7.45 presents the ratio of the positron radiative cross section to that for the electron as a function of kinetic energy for carbon.

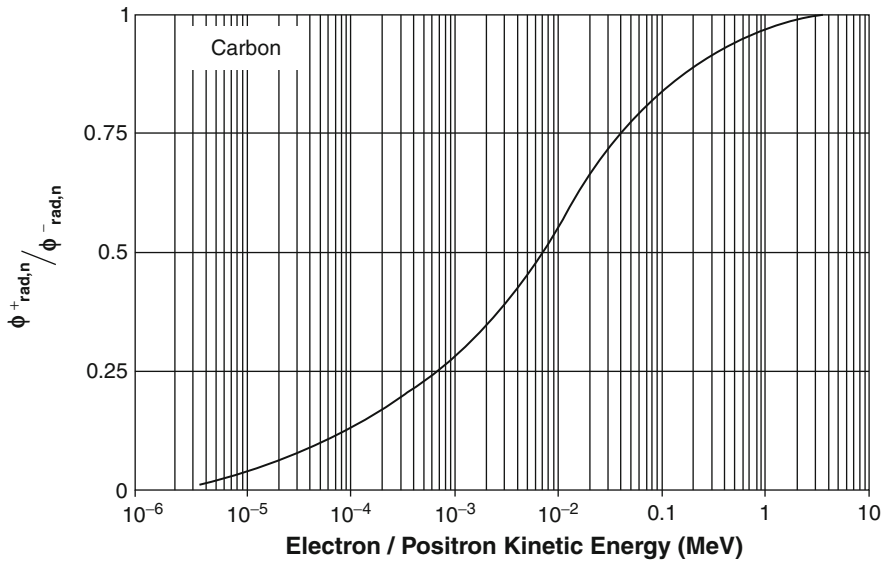

Fig. 7.45 The ratio of the positron to electron-nuclear *bremsstrahlung* cross section in carbon as a function of kinetic energy. Curve drawn from a calculation using tabulated data in ICRU Publication 37 (1984)

7.6.6 Mass Radiative Stopping Power for Electrons

Having calculated differential cross sections for electron-nuclear *bremsstrahlung*, we next evaluate the radiative stopping power. As with energy transfer as a result of collisions with atomic electrons, we can define the probability that an incident electron with kinetic energy T will emit a photon with an energy between k and k + dk is,

$$\Phi_{Rad}(T,k)dk = 4\alpha r_0^2\left(\frac{N_A Z^2}{A}\right)F(T,k;Z)\frac{dk}{k} \quad (7.644)$$

where F(E, k; Z) is a function accounting for the screening of the nucleus by the atomic electrons. The extent of screening is defined by the dimensionless parameter,

$$\zeta = 100\left(\frac{m_e}{T+m_e}\right)\left(\frac{\left(\frac{k}{T+m_e}\right)}{1-\left(\frac{k}{T+m_e}\right)}\right)Z^{-1/3}. \quad (7.645)$$

The degree of screening by the atomic electrons is an inverse function of ζ. That is, $\zeta = 0$ may be described as "complete screening" and that of $\zeta \gg 1$ as "no screening." Note that for a given photon energy k, ζ will decrease (i.e., screening increases) as the incident electron energy increases ($k_{max} = T$). For large T, the function F(T, k; Z) has the following forms for different values of ζ. For total screening, $\zeta = 0$,

$$F(T,k;Z) = \left(1+\left(1-\frac{k}{T+m_e}\right)^2 - \frac{2}{3}\left(1-\frac{k}{T+m_e}\right)\right)^2 \ln 183\, Z^{-1/3} + \frac{1}{9}\left(1-\frac{k}{m_e}\right). \quad (7.646)$$

For no screening (large ζ),

$$F(T,k;Z) = \left(1+\left(1-\frac{k}{T+m_e}\right)^2 - \frac{2}{3}\left(1-\frac{k}{T+m_e}\right)\right)^2 \times \ln\left(\frac{2(T+m_e)}{m_e}\frac{\left(1-\frac{k}{T+m_e}\right)}{\left(\frac{k}{T+m_e}\right)} - \frac{1}{2}\right). \quad (7.647)$$

The mass radiative stopping power for an electron with kinetic energy T is,

$$\frac{dE}{\rho\, dx_{Rad}} = -\frac{1}{\rho}\int_0^{T_e} dk\, k\, \Phi_{Rad}(T,k) \quad (7.648)$$

where, again, a negative sign is used to indicate that energy is lost by the particle. From the above expressions, one can write the mass collision stopping power as,

$$\frac{dE}{\rho\, dx_{Rad}} = -4\alpha r_0^2\left(\frac{N_A Z^2}{A}\right)(T+m_e) \times \ln\left(\frac{2(T+m_e)}{m_e} - \frac{1}{3}\right) \quad \text{for } m_e \ll T+m_e \ll \frac{m_e}{\alpha}Z^{-1/3} \quad (7.649)$$

or as,

$$\frac{dE}{\rho\, dx_{Rad}} = -4\alpha r_0^2\left(\frac{N_A Z^2}{A}\right)T\left(\ln\left(183Z^{-1/3}\right) + \frac{1}{18}\right) \quad \text{for } \frac{m_e}{\alpha}Z^{-1/3} \ll T+m_e. \quad (7.650)$$

The mass radiative stopping powers calculated for electrons in carbon and lead are shown as functions of electron kinetic energy in Fig. 7.46. Comparing Figures 7.15 and 7.46, it can be seen that, for a given electron energy, the mass radiative stopping power of lead exceeds that of carbon (due to the Z^2/A multiplicative factor), whereas the mass collision stopping power of carbon exceeds that of lead (as the multiplicative factor in that case is only Z/A). For the electron energies of interest to nuclear medicine in a low-Z medium such as tissue, the mass radiative stopping power is of the order of about 0.1% of the mass collision stopping power. This indicates the challenge of using *bremsstrahlung* to image the biodistribution of a β-emitting therapeutic radiopharmaceutical, as discussed later in this book. For electron energies below about 1 MeV, the lead and carbon mass radiative stopping powers slowly increase with energy, but after this energy they increase with energy in almost constant proportion.

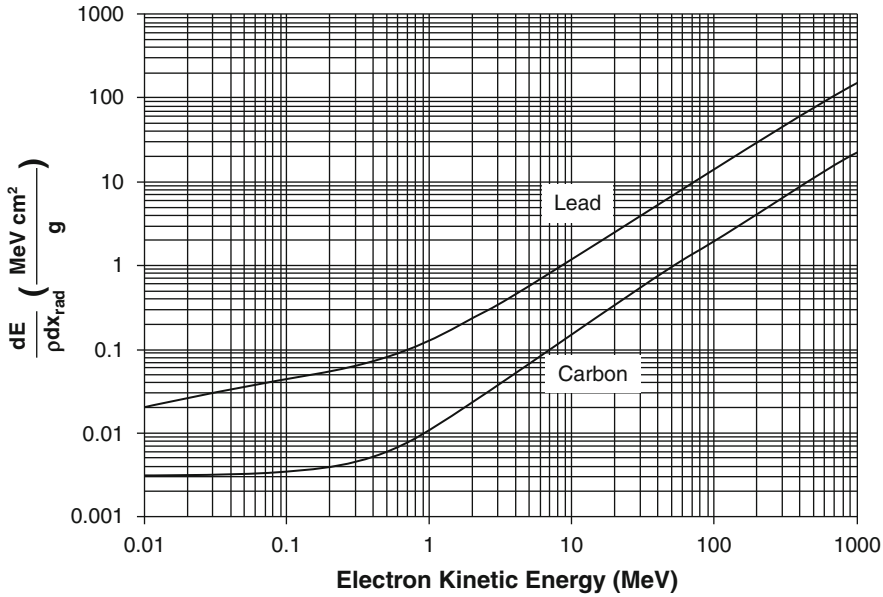

Fig. 7.46 Mass radiative stopping powers for electrons in carbon and lead

7.6.7 Radiation Length

A comparison of Figs. 7.15 and 7.46 demonstrates that the energy loss of an electron slowing down in a medium is predominantly through *bremsstrahlung* at high electron kinetic energies, $\frac{m_e}{\alpha}Z^{-1/3} \ll T + m_e$. Hence, (7.650) would provide a reasonable expression for the total energy loss rate at these electron kinetic energies. If this equation were rewritten as the ratio of the incident electron energy to a length (given in centimeter/gram), the result is,

$$\frac{dE}{\rho\, dx_{Rad}} = -4\alpha\, r_0^2\left(\frac{N_A Z^2}{A}\right)T\left(\ln\left(183Z^{-1/3}\right) + \frac{1}{18}\right) \equiv -\left|\frac{T}{X_0}\right|. \tag{7.651}$$

This length, X_0, is defined as the *radiation length*, with its reciprocal given by,

$$\frac{1}{X_0} = 4\alpha\, r_0^2\left(\frac{N_A Z^2}{A}\right) \times \left(\ln\left(183Z^{-1/3}\right) + \frac{1}{18}\right). \tag{7.652}$$

It is a constant for a given material.

7.7 Collision and Radiative Stopping Powers: A Summary

Figure 7.47 shows the collision and radiative mass stopping powers for electrons in carbon and lead along with their sum (total mass stopping power).

While the overall morphological features of the two graphs are similar, there are distinctive differences. The most important is the difference between the collision and radiative stopping powers. For carbon, an element representative of soft tissue, electron energy losses through *bremsstrahlung* exceed those through collision for kinetic energies above about 100 MeV; the energy threshold is much lower for lead at about 10 MeV. This is characterized by the *bremsstrahlung* efficiency or radiation yield.[29] In theapproximation that the energy loss of the electron in the medium is continuous as it slows down

[29]There is also a radiation yield calculation associated with positrons, although this is not considered here. Customarily, the in-flight $e^- e^+ \to 2\gamma$ is excluded from the calculation of the positron radiation yield.

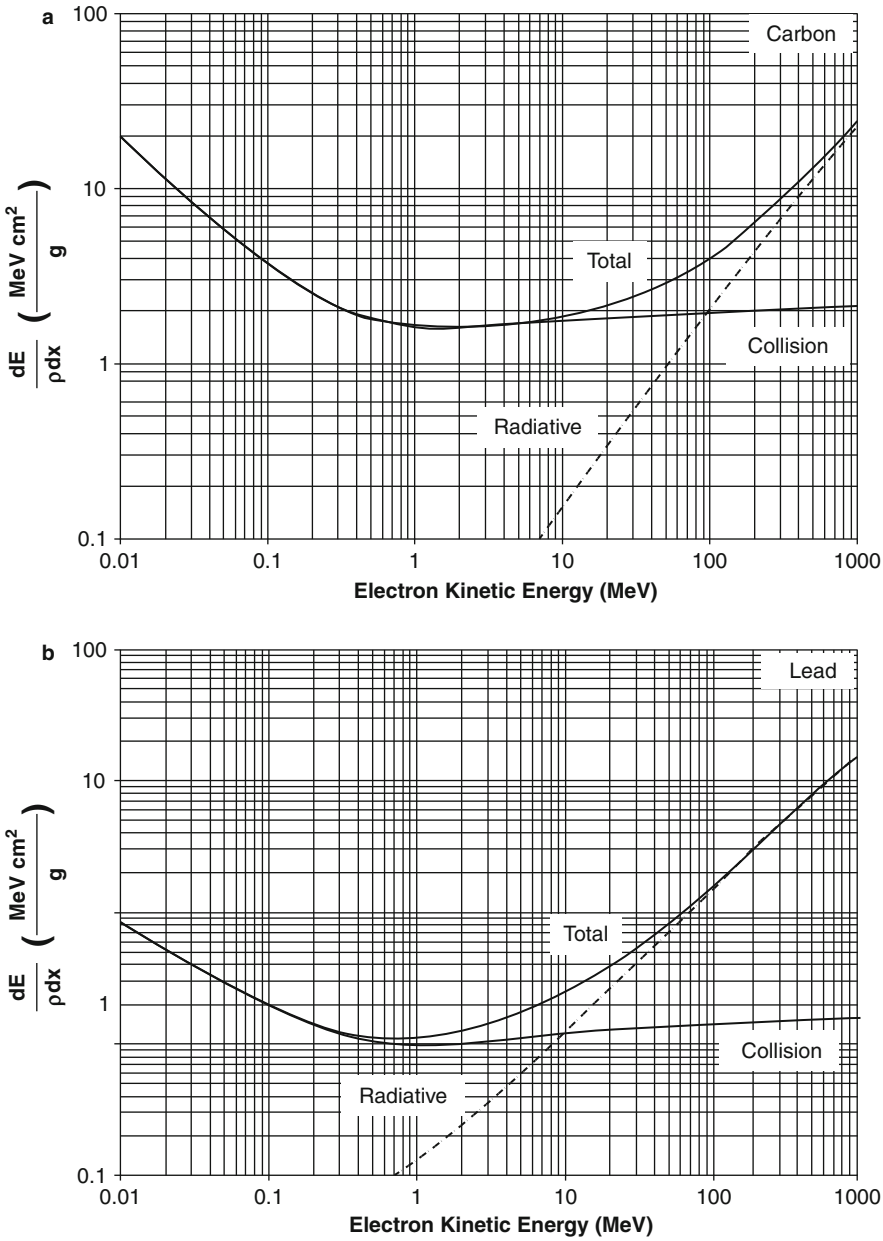

Fig. 7.47 Mass collision, radiative, and total stopping powers for electrons in carbon and lead

(the CSDA), this is, for an electron with initial kinetic energy,

$$Y(T) = \frac{1}{T}\int_0^T dT' \frac{(dE/dx)_{Rad}}{(dE/dx)_{Col} + (dE/dx)_{Rad}}. \quad (7.653)$$

Recall the fundamental features of the collision and radiative mass stopping powers: the former increases with Z and increases logarithmically with electron energy whereas the latter increases with Z^2 and increases linearly with energy. As a result, the radiation yield Y(T) will increase with electron energy and the atomic number of the medium (Fig. 7.48).

Throughout the above derivations, graphical examples of stopping powers have been provided for carbon and lead elemental media in order to display the two extremes of atomic number dependencies (carbon can

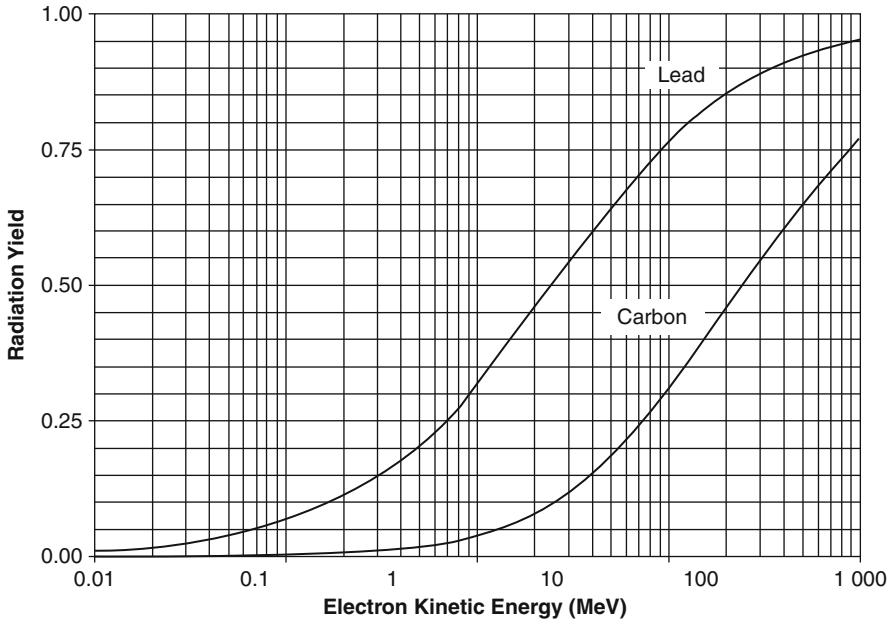

Fig. 7.48 Radiation yield Y (T) for electrons in lead and carbon

also be representative of tissue when normalized to physical density). To calculate stopping powers for compound media (such as soft tissue), Bragg's additivity rule is frequently applied. Bragg's additivity rule is an approximation in which the stopping power of a compound is given by the mass-weighted sum of the stopping powers of the atomic constituents,

$$\frac{dE}{\rho\, dx} = \sum_i w_i \frac{dE}{\rho\, dx}\bigg|_i \tag{7.654}$$

where w_i is the fraction by weight of the element.

7.8 Range of Charged Particles

7.8.1 Introduction

The range of a charged particle slowing down in a medium is, at the simplest level, the depth of penetration until its kinetic energy reaches thermal levels. However, we must recall that energy transfer to the medium is a stochastic process and, hence, the range is the expectation value of the pathlength that the particle follows until it is thermalized. The projected range is defined as the effects of multiple scattering must also be considered, especially with electron and positron projectiles. This quantity is the expectation value of the greatest penetration of the particle in the medium. A graphical comparison of the range and the projected range is provided in Fig. 7.49.

7.8.2 Continuous Slowing-Down Approximation (CSDA) Range

The CSDA range (Berger and Seltzer 1983; ICRU 1984) is similar to the concept of the pathlength described above, but neglects the effects of multiple scatter and assumes a straight-line trajectory for a particle with an initial kinetic energy T,

$$\Re_{CSDA} = \int_0^T \frac{dE}{dE/dx|_{Total}} \tag{7.655}$$

where the total stopping power is the sum of the collision and radiative stopping powers. As $dE/dx|_{Total}$ is the expectation value of the rate of energy loss, $\Re_{CSDA}$ represents an expectation value of the particle's range. For the materials and energy ranges of interest to nuclear medicine, the radiative energy loss contribution can usually be ignored. As the stopping power is relatively constant in the minimally-ionizing region and has a β^{-2} dependence at lower energies, a charged particle penetrating a medium will lose energy at near a constant rate with depth until, as

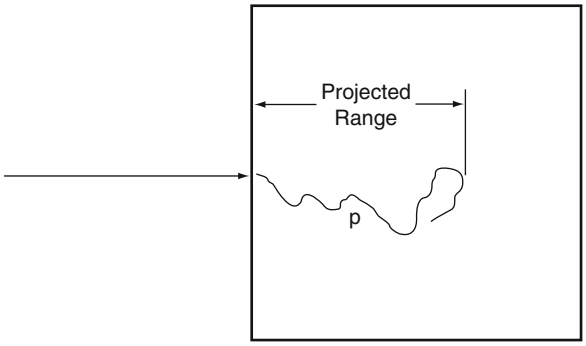

Fig. 7.49 A charged particle enters a medium from the left. The *range* (the expectation value of the pathlength p between the point where the particle enters the medium and where it is thermalized) can be tortuous, depending upon multiple scattering of the particle. The *projected range* is the depth of maximum penetration into the medium

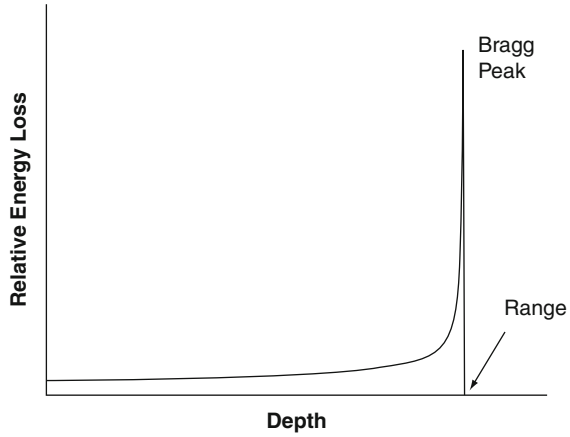

Fig. 7.50 Energy loss (deposition) as a function of depth for a heavy charged particle (e.g., proton or α particle)

it slows down beyond the minimally-ionizing region, it loses its energy at ever-an increasing rate until it has thermalized. Figure 7.50 shows the curve of relative energy deposition as a function of depth for a heavy charged particle, such as an α particle, where multiple scattering can be neglected and the particle travels very nearly along a straight line. Only near the end of its range does the relative energy loss increase from its near continuous value; this rapid increase is known as the "Bragg" peak.

Recall that, for a projectile of charge ze in a medium with atomic number Z and atomic mass number A, the collision stopping power is proportional to $(zZ/\beta A)^2$. Hence, for a given projectile and kinetic energy, the CSDA range, in gram per square centimeter, will be proportional to $(A/Z)^2$. Because of the charge and mass dependencies of the stopping power, it is possible to estimate the CSDA range in a medium of a particle of rest mass m_2 and charge z_2e knowing the CSDA range of a particle of rest mass m_1 and charge z_1e,

$$\Re_{CSDA,2} = \frac{m_1}{m_2}\left(\frac{z_1}{z_2}\right)^2 \Re_{CSDA,1} \tag{7.656}$$

The CSDA ranges of electrons and positrons will differ due to the former's use of the Møller cross section and the latter's use of the Bhabha cross section. As the collision stopping powers differ, the electron range in a medium is greater than that of a positron at lower energies and approximately equalizes at high energies Fig. 7.51 shows the CSDA range of electrons and positrons in carbon and lead as a function of kinetic energy in the range of interest to nuclear medicine applications. As shown, due to the $(A/Z)^2$ dependence, the range (in gram per square centimeter) is greater in lead than in carbon; the positron range is slightly less than that of the electron for both media and equalizes, and slightly exceeds, at higher kinetic energies.

As electrons and positrons are also subject to multiple scatter (which will be significant due to their relatively low rest masses), the $\Re_{CSDA}$ will be an approximation only of the actual range of these particles. As the spatial resolution of PET imaging will be limited by the distance between the emission of the positron and its annihilation, an evaluation of the positron range is of particular practical importance in nuclear medicine. It is most efficiently done within a Monte Carlo calculation which incorporates the stochastic nature of the electromagnetic interactions between the positron and the medium. Examples can be found in the papers by Levin and Hoffman (1997) and Champion and Le Loirec (2007).

7.8.3 Projected Range

The projected range $\bar{t}$ is the maximum perpendicular penetration of the charged aprticle into the medium and is defined as,

$$\bar{t} = \int_0^\infty dt\, t \left|\frac{dN}{dt}(t)\right| \tag{7.657}$$

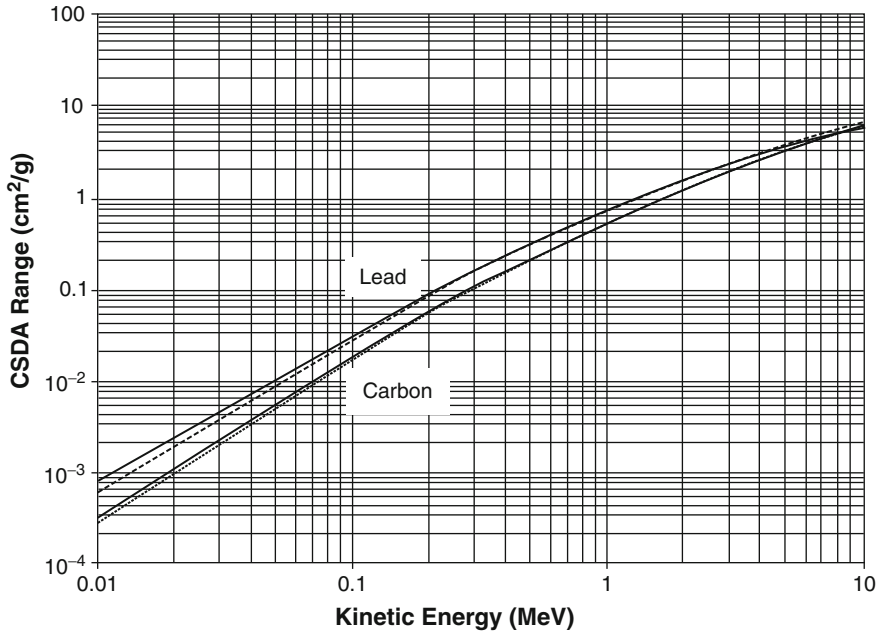

Fig. 7.51 CSDA ranges of electrons (*solid lines*) and positrons (*dashed lines*) in carbon and lead as a function of kinetic energy relevant to nuclear medicine applicatios. Curves are drawn using tabulated numerical data in ICRU Publication 37 (1984)

where $dN/dt(t)$ is the rate at which particles are stopped per unit depth and which is normalized to,

$$\int_0^\infty dt \left| \frac{dN}{dt}(t) \right| = 1. \tag{7.658}$$

The absolute value sign is a formality as the rate is negative due to the loss of particles as they stop.

7.8.4 Range Straggling

Both the CSDA and projected means of calculating the range of a charged particle penetrating a medium are expectation values of an assumed continuous energy losses of the charged particles. However, as demonstrated in Sect. 7.4, energy loss is stochastic and is described by a probability distribution function. As the range is inversely proportional to the stopping power and is also affected by multiple scatter (predominantly in the case of electrons and positrons), the range of a charged particle is also a stochastic quantity. Range straggling is a consequence of the energy loss pdf only.

7.9 Positron–Electron Annihilation

7.9.1 Introduction

The interactions of positrons with atomic electrons resulting in their annihilation and the production of photons are now considered. In terms of internal radiation dosimetry, the annihilation has a limited effect as the result is high-energy (511 keV) γ-ray pairs or triplets. The process is, of course, fundamental to PET imaging. Whereas a moving electron or α-particle will slow down to thermal equilibrium, a positron will eventually annihilate with an electron in the medium, either whilst in-flight or following thermalization. One can consider the annihilation process to be the opposite of electron–positron pair production and, using the hole theory, treat positron annihilation as the transition of an ordinary electron from a positive energy state to a negative energy state with the emission of quanta with a combined energy $\geq 2m_e$ (the inequality accounts for the contributions of any incoming kinetic energy), as shown in Fig. 7.52.

The annihilation processes results in the production of one or more γ rays in order to conserve energy and momentum; in fact up to three photons can be emitted.

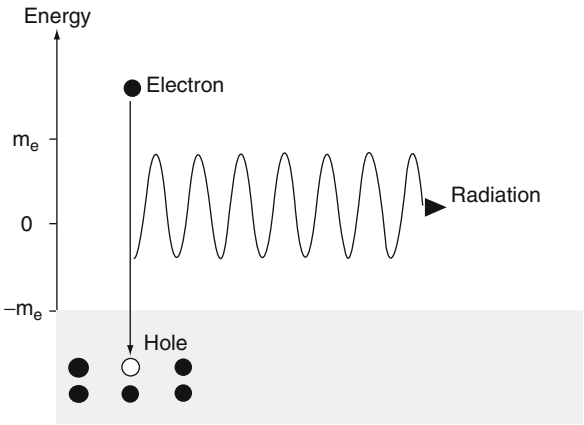

Fig. 7.52 Positron–electron annihilation described by hole theory. A positive energy electron falls into a negative energy hole with the result of radiation being emitted. This radiation will be in the form of two or more photons

For example, a single γ ray can result from the positron annihilation on a bound atomic electron such that the recoil nucleus is available for momentum conservation; γ-ray pairs are created when the positron annihilates with a free electron or is initially bound in the singlet $^1S_0$ state of positronium and γ ray triplets can be produced if the electron and positron are initially bound in the triplet $^3S_1$ state of positronium.

Figure 7.53 shows the Feynman diagrams for positron–electron pair annihilation. A comparison of these graphs with those of incoherent scatter in Chap. 6 show that they are the same if turned on their sides, allowing a similarity in the calculation of the cross section.

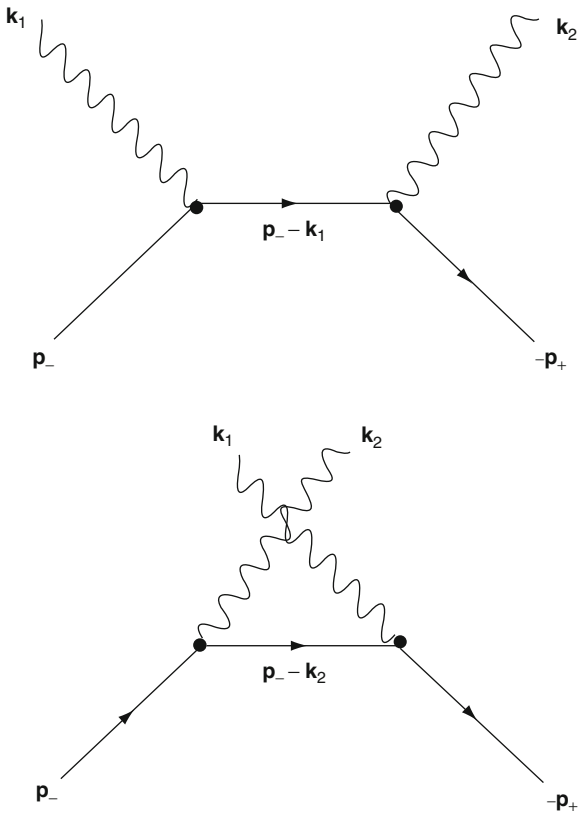

Fig. 7.53 Feynman diagrams for positron–electron annihilation

7.9.2 Annihilation Probabilities and Cross Sections

7.9.2.1 General Features

It is possible to generate estimations of the positron lifetime following emission from β decay and its annihilation in-flight within the medium. The probability of positron annihilation per unit length should obviously be proportional to the electron density of the medium,

$$\frac{d\Phi_{ann}}{dx} = \sigma\left(\frac{N_A Z}{A}\right)\rho \qquad (7.659)$$

where the constant of proportionality, σ, is the annihilation cross section. The probability of annihilation per unit time is,

$$\frac{d\Phi_{ann}}{dt} = \sigma\left(\frac{N_A Z}{A}\right)\rho\,\beta\,c. \qquad (7.660)$$

By crudely approximating the cross section by $\sigma \approx \pi r_0^2$, the probability of positron annihilation per unit length can be estimated to be 0.15 and 0.67/cm in carbon and lead, respectively. For relativistic positrons ($\beta \approx 1$), the estimated probability of in-flight annihilation per unit time is 4.5×10^9/s and 2×10^{10}/s for the same respective elements, corresponding to positron lifetimes of 220 and 50 ps.

These, of course, are relevant only for in-flight annihilation. The positron, like any other charged particle, transfers kinetic energy to the medium as it slows down to eventually thermalize to annihilate or to form a bound system with a free electron known as positronium. This

state has a finite lifetime. Due to the intrinsic spin-1/2 of the electron and positron, positronium can exist in either a singlet ($^1S_0$) or triplet ($^3S_1$) state. In order to maintain parity conservation, singlet positronium (parapositronium) will decay into two photons and triplet positronium (orthopositronium) will decay into three photons.

7.9.2.2 Positron Annihilation on a Bound Atomic Electron

Positron annihilation on a bound atomic electron can result in the emission of a single electron as the recoil nucleus is available to take up momentum and kinetic energy. The nonrelativistic calculation of this positron annihilation cross section is easily obtained from the nonrelativistic photoelectric absorption cross section for a K-shell electron,

$$\sigma_{PE} = \sigma_{Tho}\left(4\sqrt{2}\right)\alpha^4 Z^5 \left(\frac{m_e}{k}\right)^{\frac{7}{2}}$$

for a photon of energy k absorbed by K-shell electron in an atomic of atomic number Z. In the positron annihilation case, we consider from Dirac hole theory that the atomic electron following annihilation transits to a state of negative energy and momentum –**p**, where +**p** is the three-vector momentum of the incident positron. Following annihilation, a single photon of energy,

$$k = \sqrt{m_e^2 + p^2} + m_e - E_B \tag{7.661}$$

where E_B is the electron binding energy. The recoil kinetic energy of the atom is neglected. The phase space factor for the photoelectric absorption case, $(L/2\pi\hbar c)^3 m_e p_e \, d\Omega$, is replaced by that for the positron annihilation, $(L/2\pi\hbar c)^3 k^2 \, d\Omega$. The energy of the incident photon in the photoelectric absorption case is replaced by the sum of the total energy of the incident positron and the electron/positron rest mass $k \to \sqrt{p^2 + m_e^2} + m_e \approx 2m_e$, where the nonrelativistic case has been assumed in the last step. Inserting this into the $(m_e/k)^{7/2}$ factor leads to $(m_e/k)^{7/2} \approx 1/8\sqrt{2}$. Combining this and the p/m_e multiplicative factor arising from the change in phase space expressions gives the total cross section (in the nonrelativistic limit) for the annihilation of a positron with momentum p in a medium of atomic number Z on a bound atomic electron leading to a single emitted photon as,

$$\sigma_{1\gamma,K} = \frac{\sigma_{Tho}}{2}\alpha^4 Z^5 \frac{p}{m_e} \tag{7.662}$$

As with photoelectric absorption, this result displays a Z^5 dependence indicating that it will only be of importance with high-Z media and of limited concern to nuclear medicine dosimetry.

The extreme relativistic form of (7.662) and the more general form can be found in Heitler (1984).

7.9.2.3 Positron Annihilation on a Free Electron

The Feynman diagrams of Compton scatter and positron annihilation on a free electron are very similarly in their architecture and, consequently, the calculational procedures of both map closely to each other. Using 4-vectors, the S-matrix element for a positron annihilating with a free electron is, from Bjorken and Drell (1964),

$$\begin{aligned} S_{fi} = &-\frac{(2\pi)^4 \, m_e e^2}{\varepsilon_0 L^6 \sqrt{2\varepsilon_0 k_1 k_2 E_+ E_-}} \delta\left(\boldsymbol{k}_1 + \boldsymbol{k}_2 - \boldsymbol{p}_+ - \boldsymbol{p}_-\right) \\ &\times \bar{v}\left(\boldsymbol{p}_+, s_+\right) \times \left\{ (-i\not{\varepsilon}_2) \frac{i}{\not{p}_- - \not{k}_1 - m_e \mathbf{1}} (-i\not{\varepsilon}_1) \right. \\ &\left. + (-i\not{\varepsilon}_1) \frac{i}{\not{p}_- - \not{k}_2 - m_e \mathbf{1}} (-i\not{\varepsilon}_2) \right\} u(\boldsymbol{p}_-, s_-). \end{aligned} \tag{7.663}$$

This expression satisfies Bose–Einstein statistics by being symmetric under the exchange of the two photons. A long and tedious calculation is avoided in presenting the total cross section for a positron of kinetic energy T_+ annihilating with an electron at rest to produce two photons (refer to Bjorken and Drell (1964) and Heitler (1984) for details),

$$\begin{aligned} \sigma_{2\gamma} = &\left(\frac{\pi r_0^2}{\gamma + 1}\right)\left(\frac{\gamma^2 + 4\gamma + 1}{\gamma^2 - 1}\right) \\ &\times \ln\left(\gamma + \sqrt{\gamma^2 - 1}\right) - \frac{\gamma + 3}{\sqrt{\gamma^2 - 1}}\Bigg) \end{aligned} \tag{7.664}$$

where $\gamma = (T_+ + m_e)m_e$. This result predicts a diverging cross section at low energies ($\gamma \to 1$)

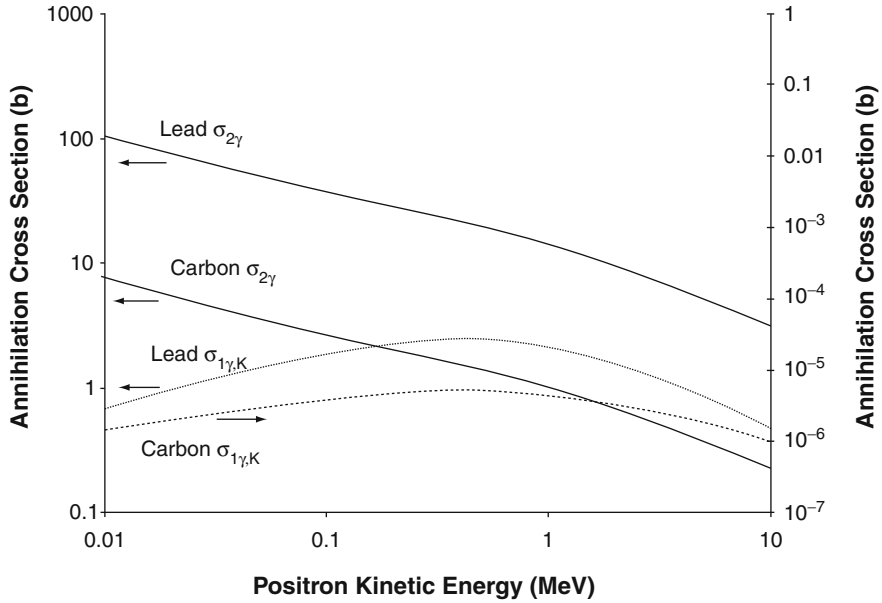

Fig. 7.54 $e^+e^- \rightarrow n\gamma$ cross sections as a function of positron kinetic energy for one- and two-photon annihilation. Note the different scale for the single-photon annihilation in carbon cross section

which is a consequence of the use of plane waves to describe the electron and positron wavefunctions (the calculation is performed in the center-of-mass system and then Lorentz-transformed to the laboratory reference frame); Coulomb wavefunctions should be used at such energies.

Figure 7.54 shows the positron annihilation cross sections per atom for one- and two-photon processes in carbon and lead as functions of the positron kinetic energy. The two-photon annihilation process cross section decreases exponentially with positron energy, thus showing that in-flight annihilation is much less probable than annihilation once the positron has slowed down towards the end of its range. On the other hand, the single-photon annihilation cross sections for both carbon and lead show maxima at positron kinetic energies of about 0.4 MeV. It is of particular interest to compare the relative magnitudes of the cross sections. The dual-photon annihilation cross sections of lead and carbon differ only by the ratio of the number of electrons available in each atom. On the other hand, the Z^5 dependence of the single-photon annihilation cross section leads to the lead cross section being about 5×10^5 times greater than that for carbon. Hence, positron annihilation in low-Z media resulting in a single photon final state is a negligible process, which is not the case for high-Z media. As a means of further comparison, Fig. 7.55 shows the ratio of the

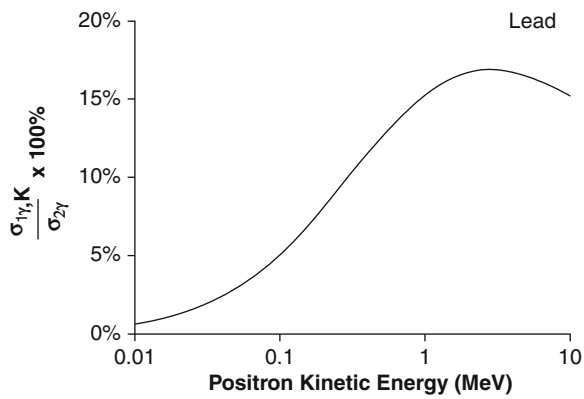

Fig. 7.55 Ratio of the single-photon annihilation cross section to that for two-photon annihilation as a function of positron energy in lead

single- to dual-photon cross sections for lead expressed as a percentage and as a function of positron kinetic energy. The largest value of the lead single-photon annihilation cross section is about 17% of the dual-photon cross section at a positron kinetic energy of about 3 MeV.

The above results show that the probability of annihilation in-flight for a fast positron is small with the result that the positron slows down (thermalizes) and is then annihilated nearly at rest. As the kinetic energy of the positron will be non-zero, although small, and

the atomic energy with which it annihilates has a finite speed, the combined kinetic energies of the two photons emitted will slightly exceed the value of $2m_e$ and will be emitted at an angle slightly different than 180°.

7.9.3 Positronium

As positron annihilation occurs predominantly at low positron energies, it is possible for the positron and an electron to form positronium, an unstable bound state similar to that of the hydrogen atom. Due to the reduced mass, the positronium Bohr radius is $2r_\infty$. The spins of the two leptons can couple to form a singlet ($^1S_0$) state or a triplet ($^3S_1$) state for antiparallel and parallel spins, respectively. Positronium is unstable. From the conservation of angular momentum, the singlet state of positronium produces two photons whereas the triplet state produces three or more. The density of electrons in (7.659), $(N_AZ/A)\rho$, is replaced by the density of the electron, calculated from its wavefunction,

$$|\psi(r=0)|^2 = \frac{1}{8\pi r_\infty^3}. \tag{7.665}$$

Equation (7.663) does not include the contribution of the triplet decay. Hence, the probability per unit time of $^1S_0$ annihilation is, including a factor-of-four to account for the combined spin directions of the electron and positron,

$$\begin{aligned}\frac{d\Phi_{ann}}{dt} &\approx 4\pi r_0^2\left(\frac{1}{8\pi r_\infty^3}\right)c \\ &\approx \frac{r_0^2 c}{2r_\infty^3}\end{aligned} \tag{7.666}$$

which is about 8×10^9/s. The probability per unit time of the triplet state annihilation can be shown to be about 1,110 times less. These estimates of positronium lifetime are, of course, *in vacuo*. In a condensed medium, the positron wavefunction can overlap those of surrounding electrons sufficiently to increase the annihilation rate.

The number of photons that the positronium can decay to will depend upon the total angular momentum of the bound system. This is a consequence of the charge conjugation operator, **C**, which exchanges a particle with its antiparticle. A system containing an equal number of particles and antiparticles (which is, by definition, electrically neutral) with total spin s and orbital angular momentum number l is an eigenstate of **C** with eigenvalue $(-1)^{l+s}$. **C** has eigenvalues of $+1$ and -1 for the singlet $^1S_0$ and triplet $^3S_1$ states of positronium, respectively. As **C** exchanges the signs of all electric charges, it will also change the direction of the electric field **E**. For a single photon, this is equivalent to $\mathbf{C}|\gamma\rangle = |\gamma\rangle$ or, for an ensemble of n photons, the eigenvalue of **C** is $(-1)^n$. Hence, as the eigenvalue of **C** is $+1$ for the $^1S_0$ state, the number of photons resulting from the annihilation of the singlet state must be even. The simplest case is $n = 2$. Similarly, as the eigenvalue of **C** is -1 for the $^3S_1$ state, the number of photons resulting from the annihilation of the triplet state must be odd. As $n = 1$ is not permissible by the conservations of momentum and energy, then $n = 3$.

References

Abramowitz M, Stegun IA (eds) (1972) Handbook of mathematical functions. Dover, New York

Ahlen SP (1980) Theoretical and experimental aspects of the energy loss of relativistic heavily ionizing particles. Rev Mod Phys 52:121–173 (erratum Rev Mod Phys 1980; 52:653)

Ammi H, Zemih R, Mammeri S, Allab M (2005) Mean excitation energies extracted from stopping power measurements of protons in polymers by using the modified Bethe-Bloch formula. Nucl Instr Meth B 230:68–72

Andreo P, Medin J, Bielajew AF (1993) Constraints of the multiple-scattering theory of Molière in Monte Carlo simulations of the transport of charged particles. Med Phys 20:1315–1325

Ashley JC, Ritchie RH, Brandt W (1972) Z_1^3 effect in the stopping power of matter for charged particles. Phys Rev B 5:2393–2397

Ashley JC, Ritchie RH, Brandt W (1973) Z_1^3-dependent stopping power and range contributions. Phys Rev B 8:2402–2408

Andersen HH, Simonsen H, Sørensen H (1969) An experimental investigation of charge-dependent deviations from the Bethe stopping power formula. Nucl Phys A 125:171–175

Barkas WH (1962) Technical Report UCRL-10292, University of California Lawrence Radiation Laboratory, August 1962.

Barkas WH, Birnbaum W, Smith FM (1956) Mass ratio method applied to the measurement of K-meson masses and the energy balance in pion decay. Phys Rev 101:778–795

Barkas WH, Dyer JN, Heckman HH (1963) Resolution of the Σ^--mass anomaly. Phys Rev Lett 11:26–28 (erratum Phys Rev Lett 1963; 11:138)

Berger MJ, Seltzer SM (1983) Stopping powers and ranges of electrons and positrons. NBSIR 82-2550-A, National Bureau of Standards, Washington, DC

Bethe HA (1953) Molière's theory of multiple scattering. Phys Rev 89:1256–1266

Bhabha HJ (1936) The scattering of positrons by electrons with exchange on Dirac's theory of the positron. Proc Royal Soc A 154:195–206

Bhabha HJ (1938) On the penetrating component of cosmic radiation. Proc Roy Soc A164:257–294

Bichsel H (1990) Barkas effect and effective charge in the theory of stopping power. Phys Rev A 41:3642–3647

Bjorken JD, Drell SD (1964) Relativistic quantum mechanics. McGraw-Hill, New York

Blunck O, Leisegang S (1951) Zum Energieverlust energiereicher Elektronen in dunnen Schichten. Z Phys 130:641–649

Briesmeister JF (2000) MCNP – A general Monte Carlo N-particle transport code, Version 4C. Report LA-13709-M, Los Alamos National Laboratory, Los Alamos

Champion C, Le Loirec C (2007) Positron follow-up in liquid water: II. Spatial and energetic study for the most important radioisotopes used in PET. Phys Med Biol 52:6605–6625

Čerenkov PA (1934) Visible emission of clean liquids by action of γ radiation. Doklady Akad Nauk SSSR 2:451

Chibani O (1998) New algorithms for the Vavilov distribution calculation and the corresponding energy loss sampling. IEEE Trans Nucl Sci 45:2288–2292

Chibani O (2002) Energy-loss straggling algorithms for Monte Carlo electron transport. Med Phys 29:2374–2383

Churchill RV, Brown JW, Verhey RF (1974) Complex variables and applications, 3rd edn. McGraw-Hill, New York

Dalgarno A (1960) The stopping powers of atoms. Proc Phys Soc (London) 76:422

Douthat DA (1975) Electron degradation spectra in helium. Radiat Res 61:1–20

Eyges L (1948) Multiple scattering with energy loss. Phys Rev 74:1534–1535

Fano U (1956) Atomic theory of electromagnetic interactions in dense materials. Phys Rev 103:1202–1218

Fano U (1964) Studies in penetration of charged particles in matter. Nuclear Science Series Report No. 39, National Academy of Sciences, Washington, DC, 1–338

Fano U, Spencer LV (1975) Quasi-scaling of electron degradation spectra. Int J Radiat Phys Chem 7:63–76

Fermi E (1940) The ionization loss of energy in gases and in condensed materials. Phys Rev 57:485–493

Fernández-Varea JM, Mayol R, Baro J, Salvat F (1993) On the theory and simulation of multiple elastic scattering of electrons. Nucl Instr Meth Phys Res B73:447–473

Fernández-Varea JM (1998) Monte Carlo simulation of the inelastic scattering of electrons and positrons using optical-data models. Rad Phys Chem 53:235–245

Feynman RP, Leighton RB, Sands M (1963) The Feynman lectures on physics. Addison-Wesley, Reading

Findlay DJS, Dusautoy AR (1980) Improvements to the Blunck-Leisegang energy loss straggling distribution. Nucl Instr Meth 174:531–533

Fowler RH (1923) Contributions to the theory of the motion of α-particles through matter. Part II. Ionizations. Proc Cambridge Philos Soc 21:531

GEANT Team (2001) GEANT Version 4.0, physics reference manual. CERN-Information Technology Division, Application Software and Databases, Geneva

Goudsmit S, Saunderson JL (1940) Multiple scattering of electrons. Phys Rev 57:24–29

Haug E, Nakel W (2004) The elementary process of bremsstrahlung. World Scientific Publishing, Singapore

Heitler W (1984) The quantum theory of radiation. Dover, New York

Hogstrom KR, Mills MD, Almond PR (1981) Electron beam dose calculations. Phys Med Biol 26:445–459

ICRU (1979) Average energy required to produce an ion pair, ICRU Report 31, International Commission on Radiation Units and Measurements, Bethesda

ICRU (1984) Stopping powers and ranges for electrons and positrons. ICRU Report 37. International Commission on Radiation Units and Measurements, Bethesda

ICRU (1993) Stopping powers and ranges for protons and alpha particles ICRU Report 49. International Commission on Radiation Units and Measurements, Bethesda

Inokuti M (1971) Inelastic collisions of fast charged particles with atoms and molecules – the Bethe theory revisited. Rev Mod Phys 43:297–347

Jackson JD (1999) Classical electrodynamics, 3rd edn. Wiley, New York

Jette D (1988) Electron dose calculation using multiple-scattering theory. A. Gaussian multiple-scattering theory. Med Phys 15:123–137

Kase KR, Nelson WR (1978) Concepts of radiation dosimetry. Pergamon, New York

Kawrakow I, Rogers DWO (2003) The EGSnrc Code System: Monte Carlo simulation of electron and photon transport. National Research Council of Canada Report PIRS-701, Ottawa

Koch HW, Motz JW (1959) Bremsstrahlung cross-section formulas and related data. Rev Mod Phys 31:920–955

Kölbig KS, Schorr B (1984) Asymptotic expansions for the Landau density and distribution functions. Comput Phys Commun 32:121–131

Landau LD (1944) On the energy loss of fast particles by ionization. J Phys USSR 8:201

Levin CS, Hoffman EJ (1997) Calculation of positron range and its effect on the fundamental limit of positron emission tomography system spatial resolution. Phys Med Biol 44:781–799

Lindhard J, Scharff M (1953) Energy loss in matter by fast particles of low charge. K Dansk Vidensk Selsk, Mat-Fys Medd 34, No. 15

Lindhard J (1976) The Barkas effect – or Z_1^3, Z_1^4-corrections to stopping of swift charged particles. Nucl Instr Meth 132:1–5

McKinley WA, Feshbach H (1948) The Coulomb scattering of relativistic electrons by nuclei. Phys Rev 74:1759–1763

McParland BJ (1989) A derivation of the electron mass scattering power for electron dose calculations. Nucl Instr Meth in Phys Res A274:592–596

McParland BJ, Cunningham JR, Woo MK (1988) Electron beam dose calculations for heterogeneous media. Med Phys 15:489–497

Massey HSW, Corben HS (1939) Elastic collisions of mesons with electrons and protons. Proc Camb Philol Soc 35: 463–473

Molière VG (1947) Theorie der Streuung schneller geladener Teilchen, I. Einzelstreuung am ambgeschirmten Coulombfield. Z Naturforschg 2a:133–145

Molière VG (1948) Theorie der Streuung schneller geladener Teilchen, II. Mehrfach-und Veilfachstreuung. Z Naturforschg 3a:78–97

Møller C (1932) Zur theorie des durchgangs schneller electronen durch materie. Ann Physik 14:531–585

Morgan SH Jr (1970) Coulomb corrections to the Bethe–Heitler cross sections for electron-nucleus bremsstrahlung. NASA Technical Note D-6038. National Aeronautics and Space Administration, Washington, DC, October 1970

Mott NF (1929) Scattering of fast electrons by atomic nuclei. Proc Roy Soc A124:425–442

Mott NF (1932) The elastic scattering of fast positrons by heavy nuclei. Proc Roy Soc A135:429

Moyal JE (1955) Theory of ionization fluctuations. Phil Mag 46:263–280

Nobel JA, Trickey SB, Sabin JR, Oddershede J (2005) Basis set limitations on the ab initio calculation of stopping cross-sections via generalized oscillator strengths. Chem Phys 209:89–94

Oppenheimer JR, Snyder H, Serber R (1940) The production of soft secondaries by mesotrons. Phys Rev 57:75–81

Pratt RH, Tseng HK, Lee CM, Kissel L, MacCallum C, Riley M (1977) Bremsstrahlung energy spectra from electrons of kinetic energy 1 keV T_1 2000 keV incident on neutral atoms 2 Z 92. At Data Nucl Data Tables 20:175

Rohrlich F, Carlson BC (1954) Positron-electron differences in energy loss and multiple scattering. Phys Rev 93:38–44

Rossi B (1952) High-energy particles. Prentice-Hall, New York

Rossi B, Greisen K (1941) Cosmic-ray theory. Rev Mod Phys 13:240–309

Rotondi A, Montagna P (1990) Fast calculation of Vavilov distribution. Nucl Instr Meth in Phys Res B47:215–223

Salvat F, Fernandéz-Varea JM, Sempau J, Mazurier J (1999) Practical aspects of Monte Carlo simulation of charged particle transport: mixed algorithms and variance reduction techniques. Radiat Environ Biophys 38:15–22

Segrè E (1977) Nuclei and particles, 2nd edn. Benjamin/Cummings, Reading

Sternheimer RM, Peierls RF (1971) General expression for the density effect for the ionization loss of charged particles. Phys Rev B 3:3681–3692

Symon KR (1948) Fluctuations in energy lost by high energy charged particles in passing through matter. Thesis, Harvard University, Cambridge

Tabata T, Ito R (1976) An improved interpolation formula for the parameter B in Molière's theory of multiple scattering. Jpn J Appl Phys 15:1583–1584

Tamm IE, Frank IM (1937) Coherent radiation of fast electrons in a medium. Doklady Akad Nauk SSR, 14:107

Van Ginneken A (2000) Edgeworth series for collision energy loss and multiple scattering. Nucl Instr Meth B160: 460–470

Vavilov PV (1957) Ionization losses of high-energy heavy particles. Sov Phys JETP 5:749–751

Sauli F (1977) Principles of operation of multiwire proportional and drift chambers. CERN Report 77–09, CERN, Geneva

Schorr B (1974) Programs for the Landau and the Vavilov distributions and the corresponding random numbers. Comput Phys Comm 7:215–224

Schorr B (1975) Numerical inversion of a class of characteristic functions. BIT Numer Math 15:94–102

Scott WT (1963) The theory of small-angle multiple scattering of fast charged particles. Rev Mod Phys 35:231–313

Seltzer SM (1991) Electron-photon Monte Carlo calculations: the ETRAN code. Appl Radiat Isot 42:917–935

Spencer LV, Fano U (1954) Energy spectrum resulting from electron slowing down. Phys Rev 93:1172–1181

Uehling EA (1954) Penetration of heavy charged particles in matter. Annu Rev Nucl Sci 4:315–350

Ziegler JF (1999) The stopping of energetic light ions in elemental matter. J Appl Phys 85:1249–1272